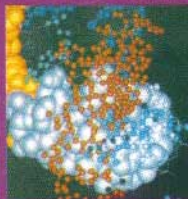
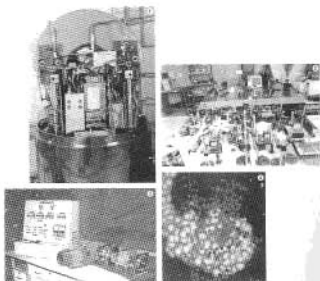


BARC

NEWSLETTER



BHABHA ATOMIC RESEARCH CENTRE

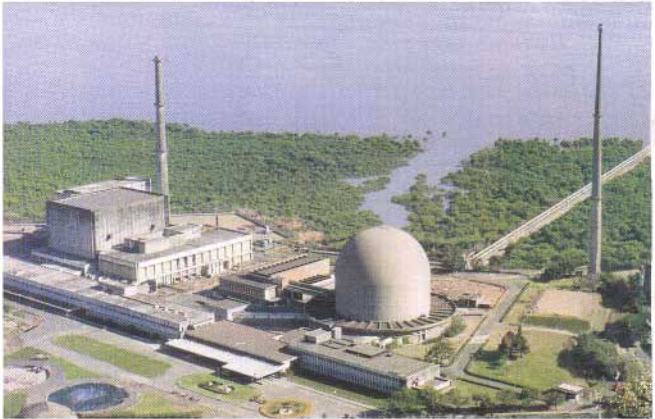


1. 180° folding magnet inside the high voltage terminal of FOTIA.
2. A view of the Magneto Optical Trap(MOT) assembly.
3. Test rig for qualification of spiral spring, rotary switchgear and potentiometer.
4. Protein molecule structure.



Government of India

BHABHA ATOMIC RESEARCH CENTRE



BARC Founder's Day Special Issue

October 2001
Issue No. 213

**DEDICATED TO THE
MEMORY OF**



Homi Jehangir Bhabha

(1909 - 1966)

**Founder & Architect of
Indian Atomic Energy Programme**

Editorial Staff

CHIEF EDITOR

Dr Vijai Kumar

MANAGING EDITOR

T.C. Balan

Computer Graphics & Layout

P.A.S. Warrior

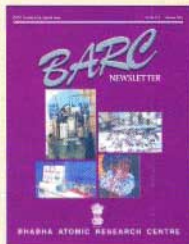
E.R. Prakashan

BARC NEWSLETTER

Founder's Day Special Issue

No 213

October 2001



on the web

Available at

URL: <http://www.barc.ernet.in>

- Small-Angle Neutron Scattering from Micellar Solutions** 1
 V.K. Aswal
Young Fellow of Indian Academy of Sciences for the period 2000-2005
- Radiation Chemical Studies on Biologically Important Molecules in Model Systems: Relevance to Biology and Medicine** 7
 Soumyakanti Adhikari
International Union of Pure and Applied Chemistry (IUPAC) prize for Young Chemists
- Geometric Phases, Foundations and Quantum Information Theory** 14
 Arun Kumar Pati
N.S. Satyamurthy Award for Young Scientists for the year 2000
- Use of Modulation Transfer Function in Determination of Focal Spot Dimensions** 19
 P.R. Vaidya
Ron Halmshaw Award for being the best paper published in the journal INSIGHT (Nondestructive Testing and Condition Monitoring) in the year 2000
- A Novel Naturally Occurring Prodigiosin Analogue with Potential DNA Targetting Property** 27
 Mahesh Subramanian and Ramesh Chander
Best Paper Prize in the International Conference on 'Natural Antioxidants and Free Radicals in Human Health and Radiation Biology' organized by Society for Free Radical Research (India/Asia) and International Society for Free Radical Research (USA)

Fluxes and Residence Time of Different Toxic and Trace Elements in Thane Creek	33
S.K. Jha et al. <i>Best Paper Award in the Second International Seminar on 'Analytical Techniques in Monitoring the Environment', December 18-20, 2000</i>	
Encapsulation, Characterization and Catalytic Properties of Uranyl Ions in Mesoporous Molecular Sieves	39
K. Vidya et al. <i>Best Oral Presentation Award by a research scholar at 15th National Symposium on Catalysis and 2nd Indo-Pacific Catalysis Symposium, January 23-25, 2001</i>	
Molecular Dynamical Simulations of the High Pressure Transformations in α Cristobalite – SiO₂	46
Nandini Garg and Surinder M. Sharma <i>Best Poster Award at the National Conference on 'Computational Materials Science (NCCMS)-2000', July 27-29, 2000</i>	
Biomedical Applications of Cell Electroporation	52
S. H. Sanghvi et al. <i>Best Poster Presentation Award in the Section of Biochemistry, Biophysics and Molecular Biology, 88th Indian Science Congress, New Delhi, January 3-7, 2001</i>	
Detection of <i>Listeria Monocytogenes</i> in Foods: Comparison of Colony Hybridization Technique with Conventional Method	56
Anu Kamat et al. <i>3rd Best Poster Paper Presentation Award in the First International Conference on 'Global Sustainable Biotech Congress 2000 A.D.', Nagpur, November 26, 2000-December 1, 2000.</i>	
Modeling of Ductile Fracture by Gurson Model	64
M.K. Samal et al. <i>One of the best papers in the poster session in 'National Conference on Computational Materials Science (NCCMS-2000)', July 27-29, 2000, organized by Materials Research Society of India, Mumbai Chapter.</i>	
Pheromones in the Management of Major Lepidopterous and Coleopterous Pests of Cotton	77
A.J. Tamhankar et al. <i>"Selected Titles" recommended by a Consortium for International Crop Protection formed by the U.S. Department of Agriculture</i>	
Emission from Charge Transfer State of Dye-Sensitized TiO₂ Nanoparticles: A New Approach to Determine the Back Electron Transfer Rate and Verification of Marcus Inverted Regime	94
Hirendra Nath Ghosh <i>Anil Kumar Bose Memorial Award for the year 2000 by the Indian National Science Academy, New Delhi.</i>	

Automation and Control: Technology Spin-Offs	101
Y.S.Mayya	
<i>DAE Technical Excellence Award for the year 1999</i>	
Determination Of $^3\text{He} / ^4\text{He}$ Ratio Using Double Focusing Mass Spectrometer	112
K.A.Jadhav et al.	
<i>Best Paper prize in 8th ISMAS Symposium on Mass Spectrometry, December 7-9, 1999, IICT, Hyderabad</i>	
ICP-MS – Improvements in Detection Limits	115
V.Nataraju et al.	
<i>Second Best Paper prize in the 8th ISMAS Symposium on Mass Spectrometry, December 7-9, 1999, IICT, Hyderabad.</i>	
Fabrication of High Density ThO_2 , $\text{ThO}_2\text{-UO}_2$ and $\text{ThO}_2 - \text{PuO}_2$ Fuel Pellets for Heavy Water Reactors	120
U. Basak et al.	
<i>Best Paper Award in the Annual Conference of Indian Nuclear Society (INSAC-2000) on "Power from Thorium : Status, Strategies and Directions", BARC, Mumbai, June 1-2, 2000.</i>	
TRISUL – The Computational Tool for Strategic Planning of Thorium Fuel Cycles	124
V. Jagannathan et al.	
<i>Best Poster Award at the Annual Conference of Indian Nuclear Society (INSAC-2000) on "Power from Thorium : Status, Strategies and Directions", BARC, Mumbai, June 1-2, 2000</i>	
Effect of Diluent on the Transport of Am(III) from Nitric Acid Medium Across A Supported Liquid Membrane (SLM) Using Dimethyl Dibutyl Tetradecyl Malonamide (DMDBTDMA) as the Carrier	132
S.Sriram and V.K.Manchanda	
<i>Young Scientist Award for the Best Oral Presentation at the 19th Conference of the Indian Council of Chemists (2000)</i>	
Positron Annihilation Studies on Radiation Crosslinked Poly(N-isopropylacrylamide) Hydrogels	138
Anjali Panda et al.	
<i>Best Paper and Presentation at Trombay Symposium on 'Radiation and Photochemistry (TSRP-2000)', BARC, January 12-17, 2000.</i>	
Studies on Voltammetric Determination of Gallium in Dilute Hydrochloric Acid at Glassy Carbon Electrode	141
Jayshree Kamat et al.	
<i>Best Oral Presentation award in the Workshop-cum-Seminar on 'Electroanalytical Chemistry and Allied Topics, ELAC 2000', BARC, November 27 to December 1, 2000</i>	

Determination of Uranium and Plutonium in Nuclear Fuel Materials by Electroanalytical Methods	143
N. Gopinath et al.	
<i>Best Poster Presentation award in the Workshop -cum-Seminar on 'Electroanalytical Chemistry and Allied Topics, ELAC 2000', BARC, November 27 to December 1, 2000</i>	
Thermal Ionisation Mass Spectrometric Analysis of Neodymium pre-separated by High Performance Liquid Chromatography	147
N.M. Raut et al.	
<i>Best Oral Presentation award in the 9th ISMAS Workshop on 'Mass Spectrometry', Goa, December 12-16, 2000</i>	
A Simple and Rapid Molecular Method for Distinguishing between Races of <i>Fusarium oxysporum</i> f.sp. <i>Cigaris</i> from India	149
A. Chakrabarti et al.	
<i>Best Presentation award at the Symposium on 'Biotechnology of Plant Protection, Banaras Hindu University, Varanasi, February 25-27, 2000</i>	
A Methodology for the Estimation of Mercury, Boron, Samarium and Cadmium by Prompt Gamma Ray Activation Analysis	154
Yogesh Scindia et al.	

Small-Angle Neutron Scattering from Micellar Solutions

V.K. Aswal

Solid State Physics Division
Bhabha Atomic Research Centre

Abstract

Micellar solutions are the suspension of the colloidal aggregate of the surfactant molecules in aqueous solutions. The structure (shape and size) and the number density of these aggregates, referred to as micelles, depend on the molecular architecture of the surfactant molecule, presence of additives, and the solution conditions, such as temperature, concentration etc. We have studied the structures of variety of micellar solutions of recent interest using the technique of small-angle neutron scattering (SANS) at BARC. These include the micellar solutions of conventional surfactants, mixed surfactants, block copolymers, and newly synthesized gemini and multi-beaded surfactants. SANS is an ideal technique for the study of micellar solutions because contrast between the micelle and the solvent can be easily varied by deuterating either one of them.

Introduction

NEUTRON SCATTERING PROVIDES AN IDEAL probe for investigating the structure and the dynamics of the materials at microscopic scale [1]. This field consists of a whole family of techniques and small-angle neutron scattering (SANS) is one of these. Unlike conventional diffraction experiments, where the structure of a material is examined at atomic resolution ($\sim 1 \text{ \AA}$), SANS is used for studying the structure of materials with a spatial resolution of $\sim 100 \text{ \AA}$. That is, SANS covers a length scale of particular interest to a number of applied problems relating to polymers, ceramics, biological systems etc. SANS has been successfully used to determine the shapes and sizes of particles dispersed in a homogeneous medium. The particle could be a macromolecule (e.g. biological molecule, polymer, micelle etc.) in a solvent, a precipitate of material *A* in a matrix of another material *B*, a microvoid in certain metal or a magnetic inhomogeneity in a non-magnetic matrix [2]. We have used the technique of SANS at BARC for investigating the structures of variety of micellar solutions. This article gives a brief survey of the results of these studies. The next section gives an introduction to the

small-angle neutron scattering. Section III gives an introduction to the micellar solution and the SANS results from the micellar solutions are given in section IV.

Small-Angle Neutron Scattering

SANS is a diffraction experiment, which involves scattering of a monochromatic beam of neutrons from the sample and measuring the scattered neutron intensity as a function of the scattering angle (Fig. 1).

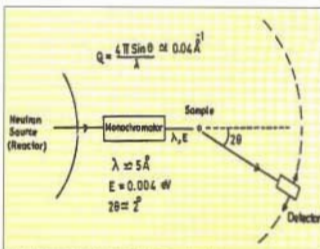


Fig. 1 Schematic details of SANS experiment

The wave vector transfer Q ($= 4\pi\sin\theta/\lambda$, where λ is the incident neutron wavelength and 2θ is the scattering angle) in these experiments is small, typically in the range of 10^{-3} to 1.0 \AA^{-1} . The wavelength of neutrons used for these experiments usually being $4 - 10 \text{ \AA}$. Since the smallest Q values occur at small scattering angles ($\sim 1^\circ$), the technique is called as small-angle neutron scattering.

In SANS experiment one measures the coherent differential scattering cross-section ($d\Sigma/d\Omega$) as a function of wave vector transfer Q . For a system of monodisperse particles, it is given by

$$\frac{d\Sigma}{d\Omega}(Q) = n(\rho_p - \rho_s)^2 V^2 P(Q) S(Q)$$

where n is the number density of the particles, ρ_p and ρ_s are, respectively, the scattering length densities of the particle and the solvent, and V is the volume of the particle. $P(Q)$ is the intraparticle structure factor and is decided by the shape and size of the particle. $S(Q)$ is the interparticle structure factor, which depends on the spatial arrangement of particles and is thereby sensitive to interparticle interactions. In case of dilute solutions, interparticle interference effects are negligible, and $S(Q) \sim 1$.

Scattered neutron intensity in the SANS experiment depends on $(\rho_p - \rho_s)^2$ - the square of the difference

between the average scattering length density of the particle and the average scattering length density of the solvent. This term is referred to as contrast factor. It is equivalent to the contrast term in optics where it is decided by the difference in the refractive indices of the particle and the solvent. Due to the fact that the scattering length is negative ($= -0.3723 \times 10^{-12} \text{ cm}$) for hydrogen and positive ($= 0.6674 \times 10^{-12} \text{ cm}$) for deuterium, SANS is ideally suited for studying the structural aspects of hydrogenous materials, such as micellar solutions. The contrast between the particle and the solvent can be easily enhanced deuterating either the particle or the solvent.

Figure 2 shows a SANS diffractometer installed at the guide hall of Dhruva reactor at BARC. Neutron beam from the guide is monochromatized by the BeO filter [3]. The average wavelength of the monochromated beam is 5.2 \AA . This beam passes through two slits S_1 ($2 \text{ cm} \times 3 \text{ cm}$) and S_2 ($1 \text{ cm} \times 1.5 \text{ cm}$) before it is incident on the sample. Distance between S_1 and S_2 is 2 m and this gives an angular divergence of $\pm 0.5^\circ$. The angular distribution of neutrons scattered by the sample is recorded using a one-dimensional position sensitive detector. The sample to detector distance is 1.85 m . The Q range of the diffractometer is $0.018 - 0.30 \text{ \AA}^{-1}$ and it is suitable for sizes in the range $10 - 150 \text{ \AA}$.

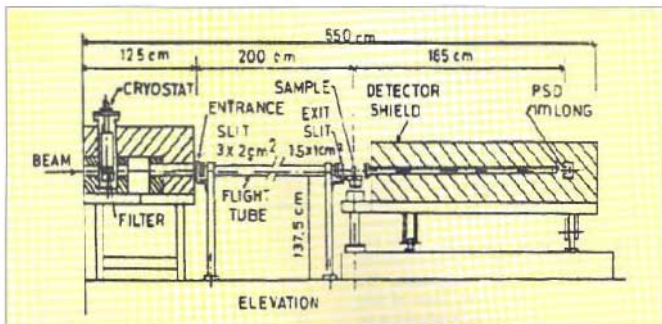


Fig. 2 A layout of SANS diffractometer at Dhruva reactor

Micellar Solutions

Micellar solutions are the suspension of the colloidal aggregates of the surfactant molecules in aqueous solutions [4]. Surfactant molecules [e.g. cetyltrimethylammonium bromide (CTAB)] consist of a polar hydrophilic head group and a long hydrophobic chain connected to the head group. The coexistence of the two opposite types of behavior (hydrophilic and hydrophobic) in the same molecule leads to the self-aggregation of the surfactant molecules in the solution. The aggregates are called as micelles. The typical size of a spherical micelle is about 50 Å and is made up of about 100 surfactant molecules. A schematic representation of a surfactant molecule and a micelle is shown in Figure 3.

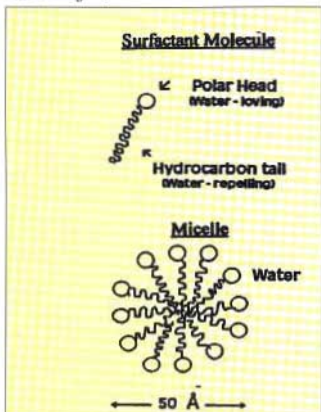


Fig.3 A schematic structure of a surfactant molecule and a micelle

The surfactant molecule is referred to as ionic or nonionic depending on whether its head group ionizes or not in the aqueous solution. For example, CTAB and sodium dodecyl sulfate (SDS) are ionic surfactants and triton x-100 is a nonionic surfactant. SANS has been used extensively to study the shapes and sizes of the micelles [5]. The strength of SANS for studying the

micellar solutions emerges from the fact that it is possible to vary the contrast between the micelle and the solvent by simply preparing the solution in D_2O instead of H_2O .

The study of micellar solutions is of interest from both the point of view of basic research and the applications [6]. The most important property of the micellar solutions is their ability to solubilize the materials that are otherwise insoluble in the water. This is relevant for many industrial and biological processes. For example, the detergency involves the removal of oil or dirt by the formation of micelles. Many colloidal solutions are stabilized by the addition of surfactant molecules, which are then adsorbed into the particle surfaces and form a protective layer against coagulation. Micellar solutions are also used in tertiary oil recovery in the petroleum industry.

Micelles are formed by the delicate balance of opposing forces: the attractive tail-tail hydrophobic interaction provides the driving force for the aggregation of surfactant molecules, while the electrostatic repulsion between the polar head groups limits the size that a micelle can attain [7]. As a result, the characteristics of micelles are easily controlled by the changes in the architecture of the surfactant molecule as well as in the solution conditions. The micelles formed are of various types, shapes and sizes, such as spherical, ellipsoidal, cylindrical or thread-like, disk-like etc. We have studied the structural aspects of variety of micellar solutions using SANS. The emphasis in these studies was to understand the reasons for the changes in the micellar shapes and sizes under the different solution conditions. In this connection, the micellar solutions of different types of surfactants, and the effect of solution conditions, such as concentration, temperature, and presence of various additives in these systems have been examined. The structures of micelles when there are two different types of surfactants in the solution have also been examined. The surfactants, which we have studied, are the conventional surfactants [8-11], mixed surfactants [12,13], block copolymers [14,15], and the newly synthesized gemini [16-22] and multi-headed surfactants [23]. In the following, results of some of the above studies are given.

Results

Structures of Ionic Micelles in Presence of Electrolytes

The ionic micelles (e.g. CTAB) are nearly spherical in pure micellar solutions. These micelles become elongated and grow in length on addition of electrolytes, such as KBr, sodium salicylate (NaSal) etc. The effect of different electrolytes is interestingly quite different. This provides one of the easiest ways for practical applications to control the properties of the micellar solutions by the addition of the electrolytes. We have used SANS to address some of the specific questions in these systems [8-11]. For example, it was not clear why CTAB or CTAC micelles grow with the addition of small quantities of KBr, but not with KCl even at high concentrations? SANS results from these systems in terms of the structures and interactions of the micelles showed that differences in micellar growth of CTAB or CTAC in presence of KCl and KBr are connected with the different counterion sizes of Cl and Br ions [8,9]. The smaller the hydrated size of the counterion, higher will be its tendency to screen the charge on the micelle, and hence the larger size of the micelles. The other example, where we have used the SANS is to understand the structures and the interactions in the viscoelastic CTAB/NaSal micellar solutions [10,11]. This system shows a striking double peak behaviour of the zero-shear viscosity as a function of NaSal concentration. It is found that beyond the first

viscosity maximum micelles behave as living polymers. In the living polymer regime, micelles break and coalesce on a time scale smaller than time scale of diffusional motion. The micelles are highly polydispersed in this regime and their length distribution is exponential. These studies further suggest that the variation in viscosity after the first viscosity maximum is connected with the change in the intermicelle interactions.

Figure 4 shows a typical SANS data from a micellar solution of 0.1 M CTAC to compare the effect of the addition of KBr and KCl [9]. The correlation peak in the data is an indication of strong repulsive interaction between the positively charged CTAC micelles. The peak usually occurs at $Q_m = 2\pi/d$, where d is the average distance between the micelles. The peak shifts to lower Q with KBr is an indication of the growth of the micelles in CTAC/KBr solutions. The broadening of the peak is due to the screening of the repulsive interaction between the micelles in the presence of the electrolyte. The same is not the case in the CTAC/KCl solutions, where the peak broadens without a significant shift in the peak position. This shows that CTAC micelles do not grow with the addition of KCl. The quantitative information about the structure and the interactions of the micelles is obtained by fitting the experimental data in terms of eq. (1) using suitable models for $P(Q)$ and $S(Q)$. The solid lines in the Figure 4 are the fit to the experimental data.

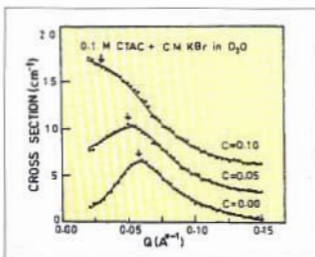
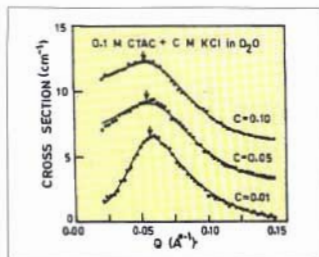


Fig 4 The comparison of SANS data from 0.1 M CTAC with KBr and KCl

Micellar Structure of Gemini Surfactants

Gemini or dimeric surfactants consist of two hydrophobic chains and two hydrophilic head groups covalently connected by a spacer. Gemini surfactants are called as the surfactants of the next generation because of the number of exceptional properties that they manifest. Additionally, the gemini format allows for expanded structural diversity in surfactant chemistry, as head groups, hydrophobic chains, spacers and counterions can be varied in search for enhanced performance. We have studied in detail the effect of (a) spacer length, (b) flexibility vs. rigidity of the spacer, (c) hydrophobicity vs. hydrophilicity of the spacer and (d) role of change of the head group from cationic to anionic on the micellar structures of gemini surfactants [16-22]. Depending on the nature of spacer and head groups, length of hydrophobic chains and spacer lengths, various types of aggregates, such as spherical, ellipsoidal, rod-like or disc-like micelles, have been observed. As an example, Figure 5 shows the SANS data from 2.5 mM micellar solutions of 16-*m*-2Na⁺ gemini surfactants for spacer length $m = 2, 4, 6$ and 10 [20]. The measurements were carried out at

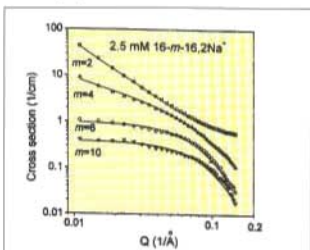


Fig.5 SANS data from micellar solutions of Gemini surfactants with different spacer lengths

enough low concentration to ensure the micellar solutions as dilute, i.e. $S(Q) \sim 1$. Fig. 2 shows the cross section ($d\Sigma/d\Omega$) and the slope of the SANS data at the low Q region ($Q < 0.05 \text{ \AA}^{-1}$) decreases as the m is increased. This suggests that micellar structures are widely different in these systems. For $m=2$ and 4, SANS distributions are straight lines in the low Q range of

0.01 to 0.05 \AA^{-1} . For $m=2$, $d\Sigma/d\Omega$ varies as $1/Q^2$ and for $m=4$, it varies as $1/Q$. These observations on Q dependence of the cross section suggest micelles are disc-like for $m=2$ and rod-like for $m=4$. The small values of $d\Sigma/d\Omega$ at low Q region for $m=6$ and 10 is an indication of smaller micelles in these systems than those for $m=2$ and 4. It is found that micelles are ellipsoidal for $m=6$ and 10.

Structural Studies of Mixed Micelles

Mixed micellization of surfactant is of practical interest as surfactants used in applications are often mixtures of homologous compounds or are contaminated by impurities. SANS studies on these systems are useful to find the composition of the mixed micelles. We have studied the structural aspects of mixed micelles with different types of surfactant molecules [12,13]. These studies include the mixed micelles of alkytrimethylammonium halides, which differ in the hydrophobic tail length or head group size [12]. SANS results show the dependence of the size, aggregation number and the interaction parameters of the mixed micelles on the molecular architecture of the mixing surfactants. It is found that the micellar parameters in mixed systems have values in between those for the single surfactant systems. Mixed micelles of CTAB and gemini surfactants produce an interesting systems [13]. As mentioned in the earlier sections, while CTAB forms nearly spherical micelles, gemini surfactants depending on the spacer length form different types of structures, such as disc-like, rod-like, and spherical. SANS studies indicate that the extent of aggregate growth and the variations of shapes of the mixed micelles could be modulated by the type and the amount of gemini surfactant present in these mixture. It is seen with the short spacer length in the gemini surfactant, the propensity of micellar growth is particularly pronounced.

Acknowledgement

I thank Dr. P.S. Goyal for his guidance and support. I am grateful to Dr. M. Ramanadham and Dr. S.K. Sikka for their encouragement and the interest in this work. I am also grateful to all the collaborators in this work for their help.

References

1. K. Skold and D.L. Price (Editors), Neutron Scattering, Parts A, B, & C, in Methods in Experimental Physics, Academic Press, 1986.
2. Proceeding of the XIth International Conference on Small-Angle Scattering, J. Appl. Cryst. 33, 421-866 (2000).
3. V.K. Aswal and P.S. Goyal, Current Science 79, 947 (2000).
4. Y. Chevalier and T. Zemb, Rep. Prog. Phys. 53, 279 (1990).
5. P.S. Goyal and V.K. Aswal, Current Science 80, 972 (2001).
6. J.M. Schnur, Science 262, 1669 (1992)
7. J.N. Israelachvili, Intermolecular and Surface Forces, Academic Press, 1992.
8. V.K. Aswal, P.S. Goyal, S.V.G. Menon and B.A. Dasannacharya, Physica B 213, 607 (1995).
9. V.K. Aswal and P.S. Goyal, Phys. Rev. E 61, 2947 (2000).
10. S.V.G. Menon, P.S. Goyal, B.A. Dasannacharya, S.K. Paranjpe, R.V. Mehta and R.V. Upadhyay, Physica B 213, 604 (1995).
11. V.K. Aswal, P.S. Goyal and P. Thyagarajan, J. Phys. Chem. B 102, 2469 (1998).
12. V.K. Aswal and P.S. Goyal, Physica B 425, 73 (1998).
13. S. De, V.K. Aswal, P.S. Goyal and S. Bhattacharya, J. Phys. Chem. B 101, 5639 (1997).
14. N. Jain, V.K. Aswal, P.S. Goyal and P. Bahadur, J. Phys. Chem. B 102, 8452 (1998).
15. V.K. Aswal, P.S. Goyal and P. Bahadur, Chem. Phys. Lett. (Submitted).
16. S. De, V.K. Aswal, P.S. Goyal and S. Bhattacharya, J. Phys. Chem. 100, 11664 (1996).
17. V.K. Aswal, S. De, P.S. Goyal, S. Bhattacharya and R.K. Heenan, Phys. Rev. E 57, 776 (1998).
18. V.K. Aswal, S. De, P.S. Goyal, S. Bhattacharya and R.K. Heenan, J. Chem. Soc., Faraday Trans. 94, 2965 (1998).
19. S. De, V.K. Aswal, P.S. Goyal and S. Bhattacharya, J. Phys. Chem. B 102, 6152 (1998).
20. V.K. Aswal, S. De, P.S. Goyal, S. Bhattacharya and R.K. Heenan, Phys. Rev. E 59, 3116 (1999).
21. S. De, V.K. Aswal, P.S. Goyal and S. Bhattacharya, Chem. Phys. Lett. 303, 295 (1999).
22. V.K. Aswal, P.S. Goyal, S. De, S. Bhattacharya, H. Amenitsch and S. Bernstorff, Chemical Physics Letter 329, 336 (2000).
23. J. Haldar, V.K. Aswal, P.S. Goyal and S. Bhattacharya Angew. Chem. Int. Ed. 40, 1228 (2001)

Dr V.K. Aswal was elected as Young Fellow of Indian Academy of Sciences for the period 2000-2005.

Radiation Chemical Studies on Biologically Important Molecules in Model Systems: Relevance to Biology and Medicine

Soumyakanti Adhikari

Radiation Chemistry & Chemical Dynamics Division
Bhabha Atomic Research Centre

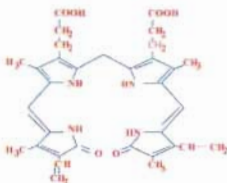
THE SUBJECT OF RADIATION CHEMISTRY DEALS with the chemical changes induced by high-energy radiations. The main effect of radiation on solutions is to produce excited states and free radicals depending on the nature of the medium and energy of radiation. By judicious choice of the medium and the scavengers one can generate the desired excited state and free radical. The techniques of pulse radiolysis and radiolysis have been employed to generate and study free radicals. Radiation chemistry in model systems including biological model systems (e.g., proteins) system may throw light on three fundamental queries:

- 1) Whether these media can provide novel catalytic environment?
- 2) Can radiation chemistry provide some information regarding the physical properties of micro droplets (e.g., size of water pool, location of the probes, etc.)?
- 3) Does the medium mimic physiological situation?

In the present study, emphasis has been given to understand free radical reactions in different environment with a variety of bio-molecules to address the aforesaid queries. While a good number of systems were covered in the award-winning thesis¹, only a brief account of a few systems are included in this brief article. The search started with the redox reaction of bilirubin (BR), a good heme model, in micelles.

Bilirubin (BR), the tetrapyrrolic bile pigment is the end product of heme catabolism.

This molecule has been chosen because other than its property of protecting Bovine Serum Albumin (BSA) from copper-mediated denaturation², it also exhibits



Structure of bilirubin [3]

antioxidant activity. Stocker et al. have shown that BR can act as antioxidant *in vivo* at a micromolar concentration and can inhibit lipid peroxidation by peroxy radicals³. Pulse radiolysis study of BR using primary radicals was initiated^{4,5} before the report by Stocker et al. Later several groups including us have taken up the issue and extensive studies have been carried out on the redox reactions of BR in aqueous homogeneous, micellar media and in presence of the carrier protein, bovine serum albumin (BSA).

The hydrated electrons react with BR four times faster⁶ as compared to that in the pure homogeneous aqueous solution. It is very interesting that the reaction of $\text{CO}_2^{\cdot -}$ with BR is not detectable in homogeneous aqueous solution under the pulse radiolysis condition. $\text{CO}_2^{\cdot -}$, a strong reducing agent with $E^\circ(\text{CO}_2^{\cdot -}) = 1.8 \text{ V}$ vs NHE and its inertness towards BR is indicative of a higher negative potential for the couple $\text{BR}^{\cdot -}/\text{BR}^-$ in aqueous medium. BR, being a highly reduced product, is much more prone to oxidation than reduction. In CTAB micellar media this reaction proceeds at an almost

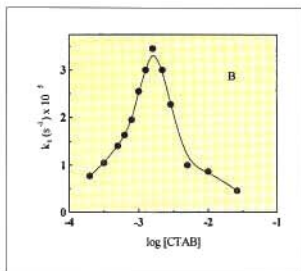
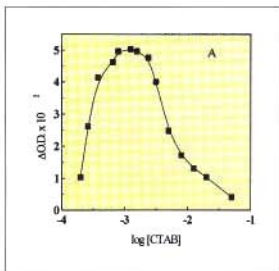


Fig.1 Dependence of (A) the yield and (B) formation rate constant of the BR^+ species on the concentration of CTAB

diffusion controlled rate⁷. The bimolecular rate constant being $5.4 \times 10^9 \text{ dm}^3\text{m}^{-3}\text{s}^{-1}$. In a plot of Δ Absorbance (at 520 nm) versus [CTAB] (Fig. 1) at constant dose and fixed BR concentration Δ Absorbance increases as [CTAB] increases but at a very high concentration of CTAB, the rate constants as well as Δ Absorbance decrease probably due to alteration in the micellar structure at a higher concentration of CTAB. The rate constant for the reaction of hydrated electrons with BR in CTAB micellar medium is more than 10 times faster as compared to that of $CO_2^{\cdot -}$ radical. This shows that these two species behave differently in this medium. Hydrated electrons can penetrate the hydrocarbon core of the micelle and attack the BR molecule dissolved in this region, whereas $CO_2^{\cdot -}$ can not.

The reaction of BR has been extended in BSA solution (the protein is used as the biological microheterogeneous medium). It has been observed that BSA protects the bound BR molecule⁸ from oxidative attack by free radicals like OH , CCl_3OO^{\cdot} , N_3^{\cdot} , etc. The competition kinetics plots can manifest the protection of BR by BSA from free radical induced damage. The equation by which the competition kinetics is explained, is as follows

$$\frac{\text{O. D.}_0}{\text{O.D.}} = \frac{k[\text{BSA}]}{k'[\text{BR}]} + 1 \quad (1)$$

where O.D.₀ and O.D. are the yields of the semi-oxidized BR species in the absence and presence of BSA. k and k' are the bimolecular rate constants for the reaction of CCl_3OO^{\cdot} radical with BSA and BR, respectively.

The open circles (Fig. 2) show the experimental points, although a straight line can not be drawn through these, comparison of these points with the calculated line (line a of Fig. 2) is sufficient to show that BR is protected to a considerable extent by BSA. At a molar ratio of 1:1, the apparent k/k' is 2.46, i.e., in the complex the reactivity of CCl_3OO^{\cdot} radical towards the BSA is more than double than that of BR bound to the protein. N_3^{\cdot} radicals react in more or less similar way to that of CCl_3OO^{\cdot} radicals with BSA-BR complex. The protection of BR from the attack of this radical is less than that in case of CCl_3OO^{\cdot} radicals (Fig. 2b and d). The calculated ratio of k and k' is 0.28 as compared with 1.78 in the complex. In the case of $Br_2^{\cdot -}$ radical induced oxidation, the observed k/k' is 2.55 whereas the calculated ratio of k and k' is 1.38 (Fig. 2c). Hence, in this case the protection is less and the lowest in the series of CCl_3OO^{\cdot} and N_3^{\cdot} radical induced oxidation.

It has been concluded that biological microheterogeneous environment can induce even negative catalytic effect for the destruction of biomolecules by different free radicals, which can otherwise complicate the situation.

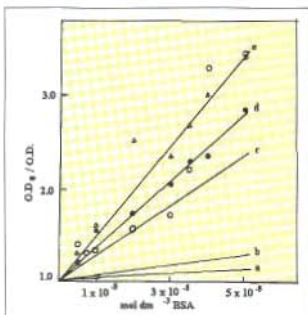


Fig. 2 Calculated and experimental competition kinetics plot for the reaction of $BR(5 \times 10^5 \text{ mol dm}^{-3})$ in the presence of varying amounts of BSA. The calculated plots: (a) CCl_4/OO radical, (b) N_2 radical, and (c) Br_2 radical reaction. The experimental plots: (d) N_2 radical, (e) Br_2 radical reaction. Open circles, for CCl_4/OO radical reaction.

To address the second point, a water-in-oil microemulsion has been used¹⁰. The microemulsion is composed of SDS/water/cyclohexane/1-pentanol. A detailed discussion on this point has been presented in a recent review article¹¹. In a microemulsion, there are two sources of hydrated electrons; one is the scavenging of excess electrons produced in the hydrocarbon phase by the water pools and the other is the direct radiolysis of water. Remarkably high lifetime (20 μs) for hydrated electrons has been obtained. In general, these are two orders of magnitude higher than those reported earlier in reverse micelles. The decay kinetics of hydrated electrons has been employed to determine the water pool size and location of the probes. The variation of hydrated electron concentration with time is given by:

$$[e_{aq}^-] = [e_{aq}^-]_0 \exp\{-(k_0 + k_2 [Q])t\} \exp\left[-\frac{n}{n} [1 - \exp\{-k_q t\}]\right] \quad \dots (2)$$

where $[e_{aq}^-]$ and $[e_{aq}^-]_0$ are the hydrated electron concentrations at time t and zero, respectively. k_0 is the first order decay rate constant of the hydrated electron in the absence of solutes, k_2 is the bimolecular rate constant for an exchange process that involves water

pool collisions, k_q is the hydrated electron decay constant in the presence of solutes and n is the average number of solutes per micelle.

At any given time t , P_0 , the probability of finding zero solute per micelle is given by

$$P_0 = \frac{\left[\frac{e_{aq}^-}{[e_{aq}^-}] \text{ in presence of solutes}\right]}{\left[\frac{e_{aq}^-}{[e_{aq}^-}] \text{ in absence of solutes}\right]} \quad (3)$$

Then following the Poisson distribution,

$$\ln P_0 = \bar{n} - [Q] / [WP] \quad (4)$$

where $[Q]$ and $[WP]$ are the concentration of the solute and water pool, respectively. Hence a plot of $\ln P_0$ versus $[Q]$ gives a measure of the water pool concentration which in turn gives the radius of the water pools, assuming these are of spherical shape. In our experiment we have measured the water core radii from the electron decay in the presence and absence of solute at a particular time window. Different solutes used for this purpose are $CuSO_4$, N,N -dimethylformamide, CCl_4 and BSA. Following the procedure described, water core radii have been determined for almost all w_s ($w_s = [\text{water}] /$

$[\text{surfactant}]$) values using different solutes as mentioned. Earlier, an empirical relation between w_0 and r as $r = 1.5 w_s$ had been proposed. In our measurements the radii of the water pool are close to $1.5 w_s$.

Further, as the absorbance of the hydrated electrons is directly proportional to the concentration of e_{aq}^- , equation [2] reduces to

$$\ln\left(\frac{A_0}{A}\right) = k_0 t + \left(\frac{[Q]}{[WP]}\right) [1 - \exp\{-k_q t\}] \quad (5)$$

where A_0 and A are the absorbances of the hydrated electrons at time 0 and time t , respectively. k_0 has been evaluated after modifying equation 4 and by plotting $\ln(A_0/A)$ versus $[Q]$, Where A_0 and A' are the absorbances of hydrated electrons at time t in the absence and presence of quenchers, respectively. As k_0 varies as $1/w_s^3$ when solute is located in the water pool and varies as $1/w_s^2$ when solute is located at the interface we have determined the location of different

solute in the microemulsion by following the decay kinetics of the hydrated electrons [Fig. 3]. It has been shown that not only k_t but bimolecular rate constants calculated from k_t for the reaction of the molecules like BSA and lysozyme (Lz) increases steadily as w_o increases in a NaLS/H₂O/cyclohexane/1-pentanol system¹². Hence it has been concluded that radiation chemistry may be employed to determine the physical parameters of a microemulsion. In addition some information regarding the reactivity of bio-molecules in a bio-mimicking environment can also be predicted. It may be mentioned that microemulsion can also be a potential catalytic medium for preparation of small mono-dispersed metal clusters¹³.

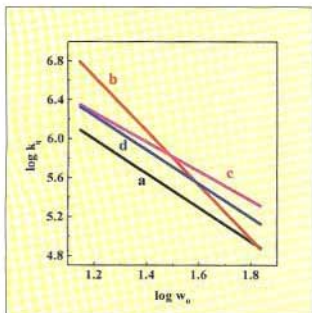


Fig. 3 Variation of $\log k_t$ with $\log w_o$ for the solutes: (a) BSA, (b) *N,N*-dimethylformamide, (c) CuSO_4 , (d) CCl_4 .

Third point is to evaluate whether the micro-heterogeneous media can really provide a bio-mimicking environment. For this purpose the aforesaid microemulsion has been chosen as the model. The exact role of β -carotene in cancer prevention is still speculative, although it is known as an ubiquitous free radical quencher, whereas retinol has drawn extensive attention for its cancer prevention activity. β -carotene is a known 'provitamin A' due to its conversion into retinol by the enzyme dioxygenase via its central or excentric cleavage. This has been demonstrated earlier by *in vivo* tests with vitamin A deficient animals. Although the enzyme is present chiefly in the intestine

and possibly in the liver, accumulation of vitamin A has been surprisingly noticed in many tissues in mice. This leads to the speculation as to whether it is possible that vitamin A may also be derived from β -carotene by some purely chemical protocol. This question has been addressed by focusing investigation on the interaction of β -carotene with reactive oxygen species in the microemulsion¹⁴. The transient absorption spectra recorded at 50 μs following the reaction of CCl_3OO radical with all *trans* β -carotene are shown in Fig. 4.

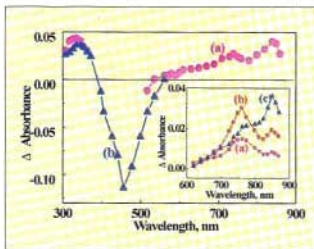


Fig. 4 Transient absorption spectra recorded from an air-saturated microemulsion ($w_o = 32$) solution containing β carotene (a) $1 \times 10^{-4} \text{ mol dm}^{-3}$, (b) $1 \times 10^{-5} \text{ mol dm}^{-3}$, $5 \times 10^{-2} \text{ mol dm}^{-3} \text{ CCl}_4$, at 50 μs after the electron pulse.

Inset: time resolved absorption spectra within a narrow wavelength region for the transients obtained from an air saturated microemulsion ($w_o = 32$) solution containing $1 \times 10^{-4} \text{ mol dm}^{-3} \beta$ carotene, $5 \times 10^{-2} \text{ mol dm}^{-3} \text{ CCl}_4$, at (a) 5; (b) 15; and (c) 80 μs after the electron pulse.

Interestingly, in addition to the bleaching spectrum, three distinct peaks were noticed. The difference in kinetics for the formation and decay of these peaks suggest that they belong to three independent species. The first formed peak at 740 nm was ascribed to an adduct of $\text{CCl}_3\text{OO}^{\cdot}$ radical and β -carotene. It is evident in the inset that even at a higher time scale (15 μs), growth of the transients continued. At a comparatively longer time scale (80 μs), when there was no CCl_3OO radical present in the solution, the peak due to the radical adduct started decreasing. However, the growth at 840 nm due to $[\beta\text{-carotene}]^{\cdot}$ continued suggesting that this is formed both by a direct route as explained above and also through the intermediate radical adduct.

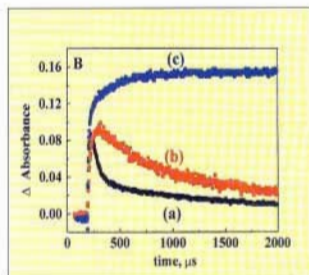
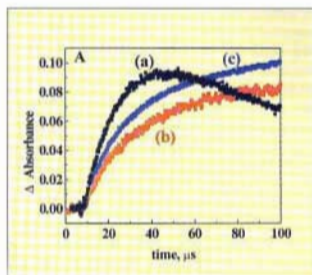


Fig 5 Absorption vs time plot for the transients obtained from an air saturated microemulsion ($w_2 = 32$) solution containing 1×10^4 mol dm⁻³ β carotene, 5×10^2 mol dm⁻³ CCl₄, (A) formation: (a) 740nm; (b) 840nm; and (c) 345 nm. (B) decay: (a) 740nm; (b) 840nm; and (c) 345 nm

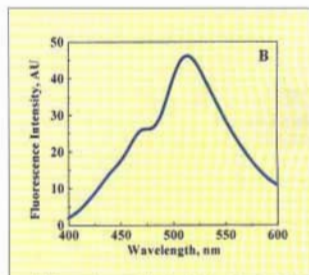
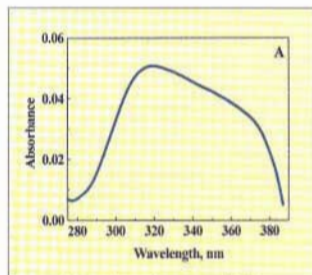


Fig 6 (A) Steady-state absorption and (B) fluorescence spectra recorded after continuous pulse irradiation of an air-saturated microemulsion ($w_2 = 32$) solution containing 5×10^4 mol dm⁻³ β carotene, 5×10^2 mol dm⁻³ CCl₄. Cumulative dose 4.8 kGy (thiocyanate dosimetry)

The most striking feature of the present study was the appearance of a new absorption band in the UV region with the maximum at 345 nm. This peak was very intense, appeared at a comparatively longer time scale and was stable upto 5 ms. The oscilloscope traces of the peak are shown in Fig. 5 (A) c and (B) c. When the solute was kept for 10 min, the solution started showing an absorption in the same region as the transient spectra, thereby indicating the formation of a stable product.

To characterize the product, radiolysis was carried out with large numbers of 50 ns pulses and the steady state-absorption and fluorescence spectra were recorded. Fig. 6 a show the steady-state absorption spectra obtained from the microemulsion solution containing 5×10^4 mol dm⁻³ β -carotene and 0.1 mol dm⁻³ CCl₄ with a total irradiation dose of 4.8 kGy. A broad spectrum beginning at 280 nm and culminating at 380 nm with the peak around 305 nm was observed.

Spectral characteristics indicated strong resemblance with those due to retinol. In order to confirm this, the product was excited at 340 nm when a strong fluorescence spectrum with a maximum at 525 nm (Fig. 6 b) was obtained. To optimize the maximum yield of retinol, pulse radiolysis was carried out with continuous pulse irradiation (total dose of 4.8 kGy according to thiocyanate dosimetry). A quantitative assay of the product formation was also carried out using standard calibration technique and at best 16-18% of retinol formation was noticed under the optimized condition. Microemulsions can be a very good model for studying bio-reactions for extrapolating the results into physiology in some cases. Our study confirmed the possibility of formation of retinol from β -C via a non-enzymatic oxidative pathway exhibiting its role as an antioxidant. This might also explain the presence of retinol in organs other than the intestine and liver as found earlier with mice. Hence, it can be concluded that in some cases the microemulsion can really mimic the physiological situation.

Future direction

Living systems are extremely complex and the final biological effects of radiation are results of complex processes occurring during and after irradiation. In order to get a clear understanding of actual processes occurring inside the living tissue it is necessary to have specific models which can provide us with information regarding specific pathways. In recent times, microemulsions are being widely used for biochemical studies. Still there is ample scope for future researchers to study oxidation reactions in microemulsions, though several studies are in progress^{18,19} in other model systems such as liposome, microsome, etc.

However, there is one area of radiation chemical research that can be of immediate help in medicinal chemistry. The importance of this area has still not been adequately understood. This field is the study of pulse radiolysis of drugs and antioxidants in aqueous solution. Many drug molecules undergo redox reactions in biological systems. These can be duplicated in pulse radiolysis studies. As a first stage, the transient species produced from the drug molecule can be made to react with other biological molecules

in solution. This will give a very good idea of some aspects of the physiology of these molecules. The next step would be the study of the reaction of these transients with living systems such as viruses and cells. Instead of giving a number of examples, we will give two single examples studied by the authors. This should adequately illustrate the importance of radiation chemistry. The molecule, 5'-azido-3'-deoxythymidine (AZT) is a derivative of thymine and is the most widely used drug in AIDS therapy. Unfortunately, the positive anti-HIV effect of the drug is often accompanied by several side effects. However, to understand the side effects, it is necessary to study the reactions of the original molecule. It has been shown²⁷ that AZT upon reacting with primary free radicals produces transient species which can destroy many important biological molecules like bilirubin, riboflavin, etc., that may have some relevance with the side effects associated with the use of this molecule in AIDS therapy.

The next example is the widely used medicine, folate, which helps in preventing cardiovascular disease and neural tube defects. Studies revealed, though speculative but perhaps one of the most provocative, new medical application of folate as a potential agent for cancer prevention. Employing pulse radiolytic kinetic measurements and biochemical assays in aqueous and liposomal media it has been shown that folate has a good antioxidant property^{28,29} that may be responsible for the anti cancer activity at least to some extent.

Acknowledgements

The author acknowledges Dr. Tulsi Mukherjee (Research Guide for the award thesis), Dr. Jai P. Mittal for excellent support and all colleagues and collaborators who have contributed to the research work in one way or the other.

References

1. S. Adhikari, Ph.D. thesis (Guide, Tulsi Mukherjee), Mumbai University, 2000
2. S. Adhikari, R. Joshi and C. Gopinathan, *Biochemica et Biophysica Acta* **1380**, 109, 1998
3. R. Stocker, Y. Yamamoto, A. F. Mc Douagh, A.N. Glazer, B.N. Ames. *Science*. **235**, 1043, 1987

4. D. J. W. Barber, J. T. Richards. *Radiat. Res.* **72**, 60, 1977
5. E. J. Land, R. W. Sloper, T. G. Truscott. *Radiat. Res.* **96**, 450, 1983
6. S. Adhikari, S. N. Guha, T. P. Balan, C. Gopinathan. *Radiat. Phys. Chem.* **43**, 503, 1994
7. S. Adhikari, S. N. Guha, and C. Gopinathan. *Int. J. Chem. Kinet.* **26**, 903, 1994
8. S. Adhikari, C. Gopinathan. *Int. J. Radiat. Biol.* **69**, 89, 1996
9. S. Adhikari, R. Joshi, C. Gopinathan. *J. Coll. and Int. Sci.* **191**, 268, 1997
10. S. Adhikari, R. Joshi, C. Gopinathan. *Int. J. Chem. Kinet.* **30**, 699, 1998
11. S. Adhikari, R. Joshi, T. Mukherjee. *J. Ind. Chem. Soc.* **78**, 75, 2001
12. R. Joshi, S. Adhikari, C. Gopinathan. *Res. Chem. Int.* **25**, 393, 1999
13. S. Kapoor, S. Adhikari, C. Gopinathan, J. P. Mittal. *Mat. Res. Bull.* **34**, 1333, 1999
14. S. Adhikari, S. Kapoor, S. Chattopadhyay, T. Mukherjee. *Biophysical Chem.* **88**, 110, 2000
15. H. Sprinz, S. Adhikari, O. Brede. *Adv. Coll. Int. Sci.* **89**, 313, 2001
16. S. Adhikari, H. Sprinz, O. Brede. *Res. Chem. Int.* **2001**, (in print)
17. R. Joshi, S. Adhikari, T. Mukherjee. *Res. Chem. Int.* **2001**, (in print)
18. R. Joshi, S. Adhikari, B. S. Patro, S. Chattopadhyay, T. Mukherjee. *Free Radical Biology & Medicine*, **30**, 1390, 2001
19. B. S. Patro, S. Adhikari, R. Joshi, T. Mukherjee, S. Chattopadhyay (communicated)

Dr Soumyakanti Adhikari is the recipient of the prestigious International Union of Pure and Applied Chemistry (IUPAC) prize for Young Chemists. This prize has been given to five chemists in a worldwide contest and he is the only Indian to receive the award for the year 2001. The award is based on his thesis entitled "Radiation chemical studies on biological and other important molecules in micelles, microemulsions and aqueous solutions", guided by Dr. Tulsī Mukherjee, Head, Radiation Chemistry & Chemical Dynamics Division, BARC. The award was conferred on Dr Adhikari on July 1, 2001, at Brisbane, Australia.

About the author ...



Dr. Soumyakanti Adhikari, after completion of his formal education from the Vistā Bharati University, Shantiniketan, West-Bengal, joined BARC Training School in 1990 (34th batch). In 1991, he joined the then Chemistry Division. Since then he has been involved in studying radiation chemistry of biologically important molecules in micro heterogeneous media. He has published several papers in reputed International journals. His recent interest is on mechanistic aspects of antioxidant activity of naturally occurring compounds.

Geometric Phases, Foundations and Quantum Information Theory

Arun Kumar Pati

Theoretical Physics Division
Bhabha Atomic Research Centre

Abstract

Twentieth century physics has witnessed many conceptual breakthroughs and discoveries, most of which started right at the beginning of the century. Starting with the development of special and general theory of relativity and quantum mechanics, there have been numerous developments in last century. Nevertheless, talking about quantum mechanics which rules entire micro-physical world, most of its foundations were laid in the early part of last millennium. Though quantum theory is one of the finest theory, its foundational aspects are not yet well understood. In spite of several difficulties, quantum theory has predicted many new effects that have been verified from time to time over many years. The author's area of research can be broadly classified into three topics of fundamental importance. One is theory of Geometric Phases, second is Foundational issues of quantum theory and third is Quantum Computation and Information theory.

Geometric Phases in Quantum Theory

THE BEAUTY OF A PHYSICAL CONCEPT LIES IN ITS simplicity with which it enters a theory and elegance with which it encompasses variety of fields. A new major discovery really took place in 1984, when Sir M. V. Berry found a geometric phase or the so called "Berry Phase" in adiabatic quantum systems. We know that all the information about a physical system is contained in the wave function. It is simply an extra phase acquired by the wave function when the parameters of the Hamiltonian are slowly changed along a closed path. It is geometric because it is local gauge invariant, does not depend on the energy eigenvalue but depends only on the geometry of the path traversed in the parameter space. It is non-integrable in nature, thereby attributing a memory to a quantum system. This is one of the profound discoveries in quantum theory in recent times. This paved the way for understanding several phenomena ranging from quantum Hall effect, fractional statistics, magnus forces in superfluidity to solar neutrinos in astrophysics.

My aim was to understand and interpret the non-adiabatic geometric phase using simplified geometric concepts like "length" and "distance" inherent to the Hilbert space and projective Hilbert space of a quantum system. Geometrically, the state is a point in the projective Hilbert space and the evolution is a curve. Our formalism uniquely brings out the manner in which the geometric phase depends on the geometry of the path. I was the first to explicitly show that the geometric phase really depends on the geometry of the path by relating it to the manifestly geometric concepts like the "length" of the curve and the "distance" function in the projective Hilbert space of the quantum system. This study provides a new understanding, interpretation and calculational tool for the non adiabatic geometric phase [1,4,5].

Subsequently, I have generalized geometric phase for non-cyclic, non-unitary and non-Schrödinger evolutions of quantum systems. A gauge potential description of generalized geometric phase was lacking. I have defined a gauge potential whose line integral yields the exact geometric phase for arbitrary

non-cyclic evolutions [9,12]. Further, I asked if the generalized geometric phase can be defined from the idea of paths. I introduced a new concept called "reference-distance" function and proved that the generalised geometric phase arises due to a basic difference between "reference-distance" and the usual "distance" function [10].

We have applied the non-adiabatic geometric phase theory in dispersive fibers and argued that it can reveal the statistics of the input light, contrary to the general belief that first order interference does not yield the statistics of the input light [8]. In Josephson junction system we have proved that the supercurrent is proportional to the "distance" function for a DC junction. We have given geometric meaning to the Cooper-pair density and relative phases and viewed Josephson effect geometrically [16].

A long standing problem in many-body system is to understand the damping of collective excitations. Recently, a many-body Fermi system has been treated in terms of a single-particle in an effective mean-field undergoing adiabatic deformation. By expressing the cyclic and non-cyclic geometric phase as time-correlation functions, we have related the geometric phases to the imaginary part of the susceptibility. Since later quantity is related to dissipation, this work provides a quantal origin of the damping in collective excitations for the first time [17]. Further, we have shown that geometric phase is related to quantum metric tensor and derived a fluctuation-correlation theorem [21].

We have developed the theory of open-path Berry phase and provided a new gauge potential whose line integral gives the Berry phase. We studied its semi-classical limit and established the connection between Hannay angle and Berry phase using adiabatic-coherent state formalism. By expressing the Berry phase as a commutator between projection operator and its differential we have studied its classical limit using Wigner formalism. Our theory provides for the first time an operational definition of Hannay angle for open path [20].

All the previous work on geometric phases has been focused on quantum systems described by pure states. If a system is in a pure state then one can associate a

wave function to it. Recently, we have generalized the concept of geometric phase for mixed states. If a quantum system has not been prepared in a definite pure state but weighted sum of various pure states with appropriate probabilities (due to our ignorance), then it is described by a mixed state. Mixed states can arise in variety of situations. If we have a composite system in an entangled state and have access to only one subsystem, then the subsystem is described by a mixed state. Using our definition of phase we define parallel transport condition for mixed state and introduce a notion of geometric phase. Further, in the special cases our definition reduces to the pure state definition of geometric phase [28].

Foundations of Quantum Theory

Natural laws look comprehensible if formulated in a simplest way with the help of fundamental constants. In special theory of relativity we have the fundamental constant c . The existence of c and principle of causality say that the maximum value of velocity for any material particle is limited by the speed of light. In quantum world also all the particles obey this universal speed limit. However, there was no known limit on the acceleration of a particle either in special relativity or in quantum theory. I have shown that by combining uncertainty principle and principle of special relativity, there exists a limit on the acceleration of a particle [2]. This fundamental limit provides understanding to several phenomena in quantum world. For example, it explains for the first time Bohr's postulate that why electrons in energy eigenstate do not radiate [3].

It was known that photon cannot be localized precisely. If one could find a localized state of photon, then there will be a violation of the special theory of relativity. Nevertheless, one can localize a photon only optimally. For an optimally localised photon the position operator has non-commuting components. I gave a new interpretation to position operator and predicted non-abelian Aharonov-Bohm effect for optimally localised photons, which can provide a direct test for the existence of photon position operator and the extent of localisability [14].

In the context of quantum Zeno effect, I have shown that continuous observation in Von Neumann type

measurement is not possible. There is a limit on the frequency of measurement coming from the geometry of the quantum state space [13]. Further, I have predicted a new effect called quantum Zeno phase effect. It says that in the limit of high frequency of measurement of some observable of the system, the development of geometric phase is inhibited. Thus, repeated observation erases the memory of a quantum system and could have implication in preserving the phase coherence of a quantum system undergoing measurement process. The quantum Zeno Phase effect has been proved using Von Neumann's projection postulate as well as a continuous measurement model [15].

There is a remarkable difference between a classical and a quantum system. For classical system the value of a physical quantity exists prior to measurement—which is an element of reality independent of anything else. However, in quantum world an element of reality is brought to existence only after measurement. Prior to a measurement only potential values of an observable exist. Einstein, Podolsky and Rosen argued that reality and locality leads to the conclusion that quantum theory is incomplete. It was John Bell who pointed out that one can put certain constraints on correlation if locality and reality criteria hold. It was found that quantum theory violates these constraints (now called Bell inequalities). I have proposed an experiment on how to test Bell's inequality for four spin-half particles using Aharonov-Gasher (AG) effect. AG effect refers to a phenomenon where a particle carrying magnetic moment is influenced by a line charge situated at a distant point. Though, locally the particle experiences no force, the wave function acquires a phase shift. The phase shift can be seen in the spin correlation measurements of two pairs of entangled particles. This correlation violates Bell's inequality [18].

Quantum Information and Computation

Recently, there has been another revolution in information processing capability that arises due to the laws of quantum mechanics. Last couple-of-years have witnessed exciting discoveries in quantum computation and information theory where linear superposition and quantum entanglement play key role in information processing. Linearity of quantum evolution gives extra

power to quantum computer and at the same time puts limitations on some basic operations. It turns out that if the classical communication channel is supplemented with quantum channel, then there are certain things possible, which cannot be done only with classical channel.

I have been working in this area for last three years. As the rule suggests, I will present those papers that have been published during my presence in India. (In my presentation for NSS memorial award of IPA 2000, I have skipped all the papers that have been published between August 1998 to August 2000 as I was abroad during that time.)

In quantum information theory entangled state play a privileged role. If we have a composite quantum system in a pure state consisting of many subsystems, then a generic pure state is in an entangled state. Entangled state is a one that cannot be written as product of individual states for the subsystems. For bipartite systems in general there always exist Schmidt decomposition for all wavefunctions such that the reduced density matrices have equal spectrum. This helps us to manipulate quantum states and to quantify entanglement of such systems. For tripartite systems this do not hold. I have provided a necessary and sufficient condition for the existence of Schmidt decomposition for tripartite systems. This shows that one can use von Neumann entropy of the partial density matrix as a measure of entanglement for such tripartite systems [30].

Another remarkable use of quantum entanglement is preparing a desired state of your choice at a remote place. Suppose, Alice's laboratory is in Mumbai and Bob's is in NewYork. Alice wants to prepare an atom in some definite state in Bob's laboratory. Instead of sending whole preparation procedure, Alice can prepare an atom of her choice in Bob's place by sending just one classical bit to Bob. I have put forward the idea of remote state preparations and remote state measurement for quantum bits (qubits) [31]. A qubit is a two-state quantum system, such as an atom, or a linear superposition of horizontal and vertical photon, or could be linear superposition of neutron spin-up and down state. It was shown that with the use of a spin-singlet state and one classical bit Alice can

remotely prepare certain class of qubits. With the same resource Alice can ask Bob to simulate any single particle measurement outcome at a remote place. This will be useful in many practical applications.

Another mysterious feature of quantum world is the interference of a single quantum particle if it is passed through a Young's double slit set-up. The quantum interference phenomena demonstrate that the particles in quantum world are not only particles but also behave like waves. This is the famous wave-particle duality in quantum theory. As Feynman has pointed out "this is the only mystery". In general if a quantum particle finds alternate possibilities then the total possibility is calculated by summing the amplitudes corresponding to each alternatives and taking its modulus. This reproduces the correct quantum interference but no body knows why it is so. The question we have asked, is it possible to observe interference between two independent, and incoherent particles after they have passed through two independent double slits or two independent Mech-Zender interferometer set-ups? We found a way to do that! We proposed a new interferometer set-up to swap the coherence from one set of interfering paths to other two paths that have no common origin, and yet they behave as if they have come through a single double-slit set-up. This phenomenon is called coherence swapping. This will open up the study of wave-particle duality from a new angle.

Our present research is an ongoing exploration of mysteries and surprises in quantum world.

References

1. Relation between "Phases" and "Distances" in Quantum Evolutions, A. K. Pati, Phys. Lett. A **159** (1991) 105.
2. On the Maximal Acceleration and Maximal Energy Loss, A. K. Pati, IL Nuovo Cimento B **107** (1992) 895.
3. A Note on Maximal Acceleration, A. K. Pati, Euro Phys. Lett. **18** (1992) 285.
4. Geometric Phase, Geometric Distance and Length of the curve in Quantum Evolution, A. K. Pati, J. Phys. A: Math & Gen. **25** (1992) L1001.
5. Interpretation of Geometric Phase via Geometric Distance and Length during cyclic evolution, A. K. Pati and A. Joshi, Phys. Rev. A, **47** (1993) 98.
6. A Geometric Meaning to the Probabilities of a Two-State Quantum systems, A. K. Pati and A. Joshi, Euro Phys. Lett. **21** (1993) 723.
7. On Phases and Length of the Curves in a Cyclic Quantum Evolution, A. K. Pati, Pramana J. of Phys. **42** (1994) 455.
8. Geometric Phases with Photon statistics and Squeezed Light for dispersive fibers, A. Joshi, A. K. Pati and A. Banerjee, Phys. Rev. A. (1994) 5131.
9. Gauge-Invariant Reference Section and Geometric Phase, A. K. Pati, J. of Phys. A: Math & Gen. **28** (1995) 2087.
10. New Derivation of the Geometric phase, A. K. Pati, Phys. Lett. A **202** (1995) 40.
11. Geometric Phase for a Finite Dimensional Hilbert Space Harmonic Oscillator, A. K. Pati and S. V. Lawande, Phys. Rev. A **51** (1995) 5012.
12. Geometric aspects of Non-Cyclic Quantum Evolutions, A. K. Pati, Phys. Rev. A **52** (1995) 2576.
13. Limit on the Frequency of Measurements in the Quantum Zeno Effect, A. K. Pati, Phys. Lett. A. **215** (1996)
14. Photon Localisation, the Pryce Operator and the Aharonov-Bohm Effect, A. K. Pati, Phys. Lett. A. **218** (1996) 5.
15. Effect of measurement on the Geometric phase during Evolution of a Quantum system, A. K. Pati and S. V. Lawande, Phys. Lett. A **223** (1996) 233.
16. Geometry of the Josephson Effect, J. S. Anandan and A. K. Pati Phys. Lett. A **231** (1997) 29.
17. Adiabatic geometric phases and Response functions, S. R. Jain and A. K. Pati, Phys. Rev. Lett. **80** (1998) 650.
18. Testing Bell's inequality using Aharonov-Casher effect, A. K. Pati, Phys. Rev. A **58** (1998) R1.
19. Geometry of the Hilbert space and the Quantum Zeno effect, A. K. Pati and S. V. Lawande, Phys. Rev. A **58** (1998) 831.
20. Adiabatic Berry Phase and Hannay angle for Open paths, A. K. Pati, Annals of Phys. **270** (1998) 178.

21. Fluctuation, time-correlation function and geometric phase, A. K. Pati, Phys. Rev. A 60 (1999) 121.
22. The issue of phase in quantum measurement theory, A. K. Pati, Acta Phys. Slovaca 49 (1999) 567.
23. Quantum superposition of multiple clones and the novel cloning machine, A. K. Pati, Phys. Rev. Lett. 83 (1999) 2849.
24. Uncertainty relation of Anandan-Aharonov and Intelligent states, A. K. Pati, Phys. Lett. A 262 (1999) 296.
25. "Assisted cloning" and "orthogonal-complementing" of an unknown state, A. K. Pati, Phys. Rev. A 61 (2000) 022308.
26. Impossibility of deleting an unknown quantum state, A. K. Pati and S. L. Braunstein, Nature 404 (2000) 164.
27. Probabilistic exact cloning and probabilistic no-signalling, A. K. Pati, Phys. Lett. A 270 (2000) 103.
28. Geometric phases for mixed states in interferometry, E. Sjöqvist, A. K. Pati, A. Ekert, J. S. Anandan, M. Ericsson, D. K. L. Oi, and V. Vedral, Phys. Rev. Lett. 85 (2000) 2845.
29. Quantum no-deletion principle, A. K. Pati and S. L. Braunstein, Curr. Sci. 79 (2000) 1161.
30. Existence of Schmidt decomposition for tripartite system, A. K. Pati, Phys. Lett. A 278 (2000) 118.
31. Minimum cbits for remote preparation and measurement of a qubit, A. K. Pati, Phys. Rev. A 63 (2001) 014302. Interference due to coherence swapping, A. K. Pati and M. Zukowski, J. Phys.-Pramana 56 (2001) 393.

Dr A.K. Pati received the N.S. Satyamurthy Award for Young Scientists for the work done during his career. The award was given by Indian Physics Association for the year 2000.

About the author ...



Dr Arun Kumar Pati of Theoretical Physics Division, BARC, was conferred the title of Honorary Research Fellow by the Senate of the University of Wales in the School of Information, Bangor, UK. He has also been selected as an Associate of Center for Philosophy and Foundations of Science (CPFS), New Delhi. Dr Pati has been working in the frontier areas of physics such as Geometric Phases, Quantum Mechanics & Quantum Computation and Information Theory. He was a member of Isaac Newton Institute of Mathematical Science, Cambridge, UK and a member of UK Quantum Computing Network. He has received "Young Physicist" award in the year 1996 from Indian Physical Society (IPS), Kolkata, for his original contribution to the theory of Geometric Phases. He has also been elected as an Associate of Indian Academy of Science (IAS), Bangalore, for the year 1998-2001.

Use of Modulation Transfer Function in Determination of Focal Spot Dimensions

P.R. Vaidya

Atomic Fuels Division
Bhabha Atomic Research Centre

Abstract

The modulation transfer function (MTF) has been used in the imaging field to evaluate fidelity of imaging systems in reproducing different spatial frequencies. It has been used for similar purpose in radiographic imaging also. As the focal spot size has an influence on the resolution of a system it should be expected to influence MTF too. Such qualitative linkage between focal spot size and MTF has been known. This paper demonstrates definitive relationship between the two which leads to a simple technique to obtain focal spot dimension from the spatial frequency at which MTF becomes zero or undergoes a minimum. This approach is applied to conventional and microfocus X-ray units. MTF curves are drawn by three different methods viz. the basic method, the FFT of line spread function (LSF) and from the derivative of the edge spread function. Results were compared with resolution (star) pattern method and were found in agreement, except with a bias towards overestimation in the case of microfocal spots when LSF method is used. The method gave lower values as compared to pin hole method for conventional units.

Introduction

THE MODULATION TRANSFER FUNCTION (MTF) is a method of describing the response of an imaging system to different spatial frequencies in the image. It is closely related to the line spread function (LSF) which is the response function of an imaging system to an impulse input. The MTF is also known as frequency response function or the optical transfer function. As the focal spot dimension is closely linked with the frequency response^(1,2), it is expected that there is a linkage between focal spot dimension and the MTF curve of a radiography system. This has been investigated in some publications^(3,4).

In the present work we have used the first zero or the first minima of the MTF curve to estimate the focal spot dimension of the industrial X-ray tubes. The method is applied to conventional (macrofocal) as well as microfocal X-ray tubes, for directional and panoramic targets. It is also verified on X-ray tubes of other

laboratories, which have reported about their focus sizes and had also provided MTF curves in their publications but have not looked for the correlation. Three different methods of drawing MTF curves were adopted and all were found to satisfy the relationship.

Theory

The frequency response function for a rectangular X-ray target with a uniform intensity was shown by Morgan⁽¹⁾ to be equal to

$$\text{FRF} = \frac{\sin \left[\pi f a \left(\frac{d_1}{d_1} + \frac{d_2}{d_2} \right) \right]}{\left[\pi f a \left(\frac{d_1}{d_1} + \frac{d_2}{d_2} \right) \right] \dots \dots \dots} \quad (1)$$

Where d_1 and d_2 are respectively source-to-object and object-to-film distances, a is the focal spot size and f is the spatial frequency. This is similar to an optical system because the Fourier transform of a slit with width a is $(\sin \pi f a / \pi f a)$, an expression identical

to eq. (1). As the Fourier transform itself is a frequency response spectrum, it can be said that the X-ray focal spot has the same effect as the slit has in an optical set-up. The value of FRF (or MTF) will be zero where frequency is such that the argument of sine function is equal to π or its multiples. Let the frequency f (at the object plane) be f_0 for that condition :

$$\text{then, } \pi f_0(d_1/d_2 + d_2) = n\pi$$

$$\text{hence } a = n [(d_1 + d_2)/d_2] 1/f_0 \dots \dots (2)$$

Conversely, it can be argued that if MTF is zero at a frequency f_0 , then f_0 must satisfy Eqn.(2). With f_0 , d_1 and d_2 being known, one can find focal spot size a . Though any value of 'n' should give the value of a , as the frequency takes higher harmonic values, the first zero ($n=1$) can be used for calculations of the focal spot. Instead of the object plane frequency, one can also use image frequency f_i for calculation. $F_i = f_0/M$ where M is the magnification factor and is equal to $(d_1+d_2)/d_2$.

$$\text{Therefore, focal spot } a = \text{focal spot } a = 1/f_i \times d_2$$

$$\dots \dots (3)$$

This can also be written as $1/f_i (M-1)$

Here f_i is the spatial frequency in the image plane when MTF is zero. This approach can be applied to determine the focal spot size of macrofocus as well as microfocus units.

MTF has a multiplicative property. In X-ray imaging application, the total MTF is composed of the MTF of the focal spot and the MTF of the film. It is given as:

$$\text{MTF (total)} = \text{MTF (film)} \times \text{MTF (focal spot)}$$

For the purpose of finding focal spot dimension we need to work with MTF (f_s) which can be found only at a magnification greater than unity. This is because the focal spot influences the transfer function only through geometric unsharpness, which occurs at a non-unity magnification. The MTF (film) is obtained from a contact image. MTF(film) does not undergo maxima or minima. Therefore the first zero or minimum observed in the MTF(total) occurs exclusively on account of MTF(f_s). Hence it is adequate to work with the MTF (total) rather than separating MTF(film) and MTF (f_s) at least for the

present purpose. This will also be shown experimentally.

Experiments and Results

Three different methods were used to get MTF curves in order to verify the proposition.

- by fundamental method of taking amplitudes of various spatial frequencies on line pattern image,
- by taking fast Fourier transform (FFT) of line spread function (LSF) obtained from a slit image.
- by obtaining edge spread function and differentiate it to get LSF : then take FFT as (ii) above.

Every time, a star pattern was imaged with identical parameters, to compare the MTF method results with those obtained by the star resolution method.⁽²⁾ In addition to the above, we tested the proposition on the MTF curves available in the published work of other researchers, where focal spot size also was available.

By the basic convention, the optical density should be converted to radiant exposure for finding the MTF and the LSF. However, we have confirmed that the dose-density relationship is strictly linear for typical industrial radiographic films and hence linearisation of density values is redundant as the amplitude axis in MTF curve is to be normalised in any case.

Fundamental method

Huttner's line resolution pattern having spatial frequencies from 0.25 lp/mm to 10 lp/mm was imaged on medium speed film at a direct enlargement ratio of $\times 2$ ($d_1 = d_2$). Conventional (macrofocus) tube, microfocus rod anode and microfocal directional target were employed. The image was scanned using Joyce-Loeble scanning microdensitometer at the slit width of 20 μ m. This slit width satisfies the Nyquist criterion of sampling rate even for the highest frequency of 10 lp/mm.

Figure 1 shows the OTF curves for the three X-ray targets employed. The phase is shown to be negative where the pattern image demonstrates reversal of optical density. (Such curves giving phase information are actually called optical transfer function rather than MTF, which displays only absolute value of the transform⁽⁶⁾.)

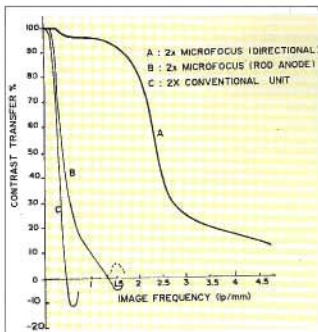


Fig.1 OTF curves generated for using various frequencies

The focal spot was calculated by the eqn. (3). Take for example, curve B for the microfocus rod anode. The frequency f_i in the image plane is 1.3 lp/mm where the curve cuts the x-axis. For the magnification of x_2 , source to object distance d_s is equal to the object to film distance d_f . Hence focal spot $a = 1/(1.35 \text{ lp/mm}) = 0.74 \text{ mm}$. The other values obtained in similar way are given in Table 1. It can be noted that the MTF curve for the microfocus directional target does not touch zero or minimum at 10 lp/mm, thereby the focal spot is smaller than 100 μm .

Table 1 : Focal Spot Size obtained by Optical Transfer Function Method

X-ray Unit	Target	KV	Focal Spot	
			By Star pattern method	By OTF method
Conventional	Directional	50	2.3 mm	2.15 mm
Microfocus	Directional	50	<87 μ	N.A
Microfocus	Rod Anode	50	0.68 mm	0.74 mm

(N.A: Till the frequency covered, MTF did not show zero or minima value beyond the scale.)

Line Spread Function Method

LSF was obtained for three different types of X-ray units by exposing a narrow slit onto a film. Slits of five different widths of 20 μm to 100 μm were employed,

which were made out of highly straight and rectangular stainless steel jaws of 4 mm thickness. Images were taken at magnifications x_1 (contact), $x_1.5$ and x_2 . Slit radiographs were scanned on the microdensitometer with a slit of 20 μm width to obtain the LSF. The scans gave LSF which were digitised and MTF was obtained by using the fast Fourier transform (FFT) programme on a personal computer using the mathematical package ORIGIN - Microcal version 4.1. A Hanning window was used for taking FFT. The Sampling interval for FFT was kept same as the interval used for digitising the curve. The digitising interval for the curve, in turn, was equal to slit width used in microdensitometer scanning. This is important for obtaining correct results because the highest frequency contained in FFT curve depends upon the sampling interval.

One of the X-ray units was of panoramic type and hence the projected focal spot was linear in shape – very narrow in one direction and long in the other. Sizes in both these directions were imaged by the slits in the direction perpendicular to the dimensions of interest. That is, the length dimension of the spot was assessed by the slit transverse to the line and width by a slit parallel to the linear dimension of the focus. Slits with different widths were employed for microfocus unit for studying the effect of slit width on the result.

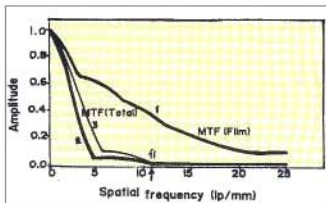


Fig.2 MTF for microfocus unit using LSF of 50 μ slit

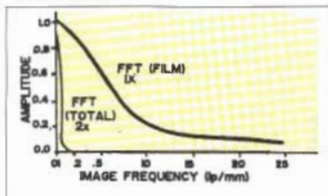
Figure 2 shows the FFT of LSF for 50 μm slit at contact (x_1) and x_2 magnifications for a microfocus unit. Contact FFT is MTF(film) whereas curve 2, at x_2 , gives MTF(total). MTF(f.s.) is obtained by dividing the curve 2 by curve 1, which is given as curve 3. As can be seen, the minimum on curve 2 and 3 occurs at the

Table 2 : Comparison of Resolution Method and MTF First Zero Method

MTF by option	X-ray unit	KV	Focal Spot data		MTF Method	
			Catalogue value	Resolution method	Slit width	Focal spot
Using slit	Conventional	45	0.4 mm	0.63 mm	100 μ	0.74 mm
	Panoramic - axial - transverse	70	0.5 mm	0.36 mm	40 μ	0.36 mm
		70	5.0 mm	3.6 mm	80 μ	See text
	Microfocus	50	>10 μ	<56 μ	20 μ	90 μ
					50 μ	90 μ
					100 μ	93 μ
Edge response	Conventional	45	0.4 mm	0.63 mm	N.A.	0.616mm σ = 0.035
	Microfocus	50	>10 μ	<56 μ	N.A.	40 μ

N.A. : Not applicable

same frequency, because the film alone has much higher response at every spatial frequency till the end. Figure 3 gives MTF curves for conventional X-ray tube (nominal focus size 0.4mm) where MTF (film) is much higher than MTF(Total) which then is not distinguishable from MTF(Ls.). These results show that there is no need to divide the curves for further work. Table 2 shows the results obtained by this method for different X-ray targets and their comparison with the focal spot size obtained by the star pattern method in the same direction.

Fig.3 MTF for conventional unit using LSF of 100 μ slit

Edge spread function route

An image trace of a knife-edge object is called edge spread function (ESF). This is similar to step a function response in electronics. It has been shown⁽⁷⁾ that ESF is nothing but summation (or integration) of the line spread functions across the edge. Therefore it is possible to acquire LSF by taking derivative of the ESF. There are certain advantages in using an edge

rather than a slit. For a given focal spot size an optimum slit width is required. The derivative of ESF yields the finest compatible slit for the given focus. An Edge has lesser inaccuracy as compared to fine slit if the placement under the beam is not very accurate. A vertical edge of highly polished surface having 4 mm thickness was exposed and MDM scan was taken. It was differentiated on a PC after digital smoothing wherever required. Figure 4(a) shows the edge trace at x2 magnification which is differentiated to get the LSF in Figure 4(b). Focal spot size for the microfocus unit then obtained from the zero as in Figure 5. The lower half of Table 2 gives the comparison of results obtained by ESF route with the resolution pattern method.

MTF curves of other authors

In order to verify the method on larger number of X-ray tubes with wider range, MTF curves available in the literature were used to find the focal spot size. This was compared with the focal spot size mentioned in the same papers. Gould and Genant⁽⁸⁾ while comparing MTF curves qualitatively with the focal spots, have measured spot sizes by pin-hole method at different locations in the X-ray beam viz. at centre, towards the anode and towards the cathode. They have also published corresponding MTF curves (for example Figure 6). Using these published curves pertaining to two different tubes, focal spot sizes were assessed by the first zero method. Results are given in Table 3, along with one other X-ray tube from K. Doi⁽⁹⁾.

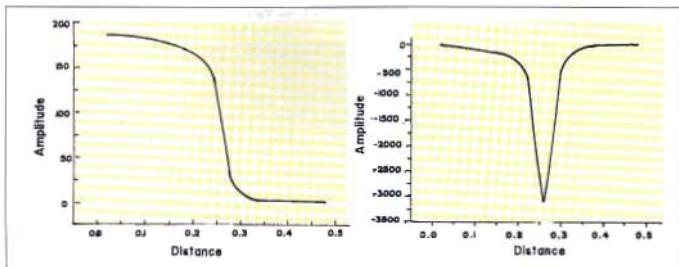


Fig 4(a) Edge trace for a microfocal unit

Fig 4(b) LSF obtained by differentiation of Fig 4(a)

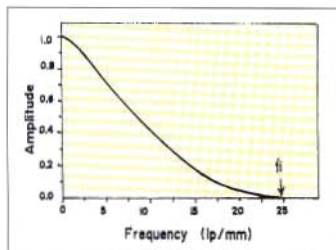


Fig 5 MTF for LSF of Fig 6

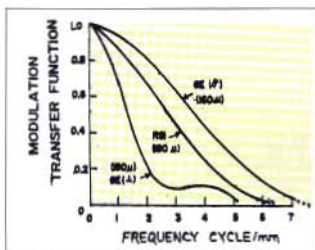


Fig 6 MTF curves for earlier published work - [see reference (3)]

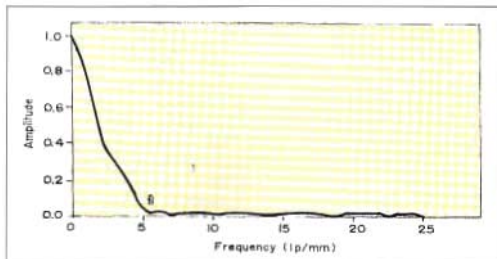


Fig 7 MTF for 40 μ slit LSF exhibiting a minimum

Table 3 : Application of MTF Method to X-ray Tubes of Other Authors

Reference No.	Tube Identification/direction	Measurement location	Authors Result		MTF method (μ)	Variation %
			Method	F.S. size (μ)		
3	GE Axial -do- -do-	Central beam	Pin hole	160	133	-17
		Cathode side	Pin hole	300	240	-20
		Anode side	Pin hole	17	Beyond scale	-
	GE Transverse	-	Catalogue	180	192	+7
	RSI Axial	Central beam	Pin hole	180	143	-20
		Cathode side	Pin hole	230	170	-26
Anode side		Pin hole	150	135	-10	
8	-	-	Catalogue value	2 mm	1.5 mm	-33

Discussion

Results from each of the four methods are discussed here separately.

The focal spot sizes found by the fundamental method of plotting MTF, using line resolution pattern of various frequencies, is in close agreement with values obtained by star resolution method. This is expected as both the approaches are based on the same principle. The frequency at which the MTF is zero is the same where the lines in the resolution pattern give blurred contrast. Both the approaches are derived from the Morgan's formula (eqn.1). The rod anode used was a panoramic target; here as well as in LSF method; panoramic targets do give variability of results. This is probably due to ring shape of such targets. The segments of equal arc lengths on the ring give increasingly smaller projected lengths, from the centre towards the edge, as seen by the slit. However, the change is not linear with the linear distance. This gives rise to a corresponding non-linear variation in radiation intensity received at the object, from across the target, thus affecting the LSF. More work is required to study the behaviour of panoramic targets as even in the star method they often give odd patterns.

The first part of the Table 2 gives FFT results of the line spread function derived from the slit images.

Agreement is very good for conventional directional targets. Even for panoramic target, the axial dimension of the spot is in excellent agreement with the star pattern value. For the transverse size of the spot, LSF was taken at only $\times 1.2$ magnification. It gave a focus size much smaller than expected. It could be due to the small magnification used; the other reason could be as discussed in 4.1. More work is required to study behaviour of panoramic targets as even in the star method they sometimes give queer patterns.

- Four different slit-widths were used (20, 50, 100, 500 μ) in the case of the microfocus unit, for obtaining the LSFs. But all have given nearly the same result of 90 μ for focus size. This value is higher than that observed by the star method. The reason for this is the broad slits. Just as a fine hole is required in the pin-hole method, a very narrow slit must be used in the case of microfocus tubes as the focal spot is too fine. An excessively broad slit has its own MTF which gets introduced in the total MTF. Ideally the MTF (focal spot) should be corrected for this contribution; it was not done here. A finer slit poses difficulties in alignment and loss in radiation intensity at the film plane. In the absence of a very fine slit LSF can be obtained by

the derivative of the edge spread function, which would automatically simulate the finest possible slit. This is seen in the next section.

The second half of the Table 2 shows the results arrived at by using the derivative of the edge spread function. It gave very good curves and results for the microfocal X-ray target (Figures 4 and 5). This supports the argument that the edge can substitute for a very fine slit. Although it is not shown in the Table, but we treated 100 μm slit as two independent edges and derived a focal spot size by that route. It showed the focal spot size to be 50 μm , close to what single edge has given.

- In the case of a conventional unit, some noise was observed on the LSF curve derived from ESF. Either the ESF or LSF were digitally smoothed to get the result. Five different combinations of smoothing operations were used. The result given in the table is average of the five with the standard deviation, which is reasonably small.

Results in Table 3 pertain to the X-ray tubes of other authors as mentioned earlier. Figure 6 gives MTF curves for one such tube. The dotted line is extrapolation done by us. The values obtained by MTF first zero method are all smaller by about 20% as compared to the pin-hole method. However, pin-hole method is known to give higher estimates. It is not known whether and what corrections the authors have applied. Their method of plotting MTF is also not known. The nature of the MTF curve for transverse direction in GE target is different in that it has a minimum as well as a zero. A Similar graph was obtained in the case of a LSF for a 50 μm slit in our laboratory for microfocal unit. It indicates a bi-modal shape of the source. This could have happened also due to contribution of the transverse dimension of the focus, if the alignment is imperfect. As the zero is distinct and follows immediately after the minima, frequency value at the zero is considered for calculations. This is only an empirical conclusion; more work is needed to sort out such behaviour.

Sometimes the MTF curve does not take zero value, but undergoes only a minima. In these cases calculation will be based on the frequency at which the minima occurs. One such example is given in the Figure 7

which is obtained from LSF of a 40 μm slit imaged by a conventional panoramic target (axial direction). Here the MTF curve does not take an exact zero value, but runs quite close to it. As the magnification used was $\times 1.5$ and f is 5.6 lp/mm, the focal spot should be $(1/5.6) \times (1/0.5)$ i.e. 0.36 mm, the value obtained also by the star method.

The presence of a minima instead of a zero could be due to many reasons. If the LSF is noisy then the high frequency component may be more in the MTF, not permitting it to vanish, where otherwise it would have been zero. The other likely source is the discrete sampling. Take for example, the dotted part in the curve B in the fig.1. The solid curve B touches zero because it is an OTF curve taking negative amplitude values also. The dotted extension is the MTF and hence takes only absolute values. As the exact frequency where it is to be zero is not the part of the sample, MTF begins to rise before touching the x-axis. This type of situation can also come when the digital transform is taken on a computer. The FFT softwares do not sample *all* the points on the curve but at discrete intervals. Then the frequency corresponding to the zero response can be missed out and MTF can rise again. But in any case, it is observed that frequency of the first minimum gives satisfactory results if a zero does not occur.

In general, dimensions obtained from nine different X-ray tubes and 17 target orientations show that the MTF method gives results reasonably close to the other methods. This method has an advantage over the method based on resolution pattern, that it can be employed even at higher X-ray energies, where thin lead strips in the resolution pattern are penetrated.

Conclusion

It is possible to find the focal spot dimension of an X-ray unit using the lowest spatial frequency at which MTF is either zero or minimum. The MTF obtained by three different methods, namely the fundamental route of imaging various spatial frequencies, taking FFT of the line spread function (LSF) and obtaining LSF by differentiating the edge spread function (ESF), generally showed similar results when compared with the results obtained by resolution test method.

However, in the case of microfocal targets, ESF method of obtaining MTF was found to give more accurate values. The method when applied to the published curves of other workers showed lower values as compared to the pin-hole method of finding the focal spot size.

Acknowledgement

The author is grateful to Mr S. Mukhopadhyay for discussions held with him, to Mr. B.P. Patil and Mr. K.N. Chandrasekharan for their help in accurate microdensitometry. He is also thankful to Mr. P.G. Kulkarni, Head, Atomic Fuels Division for the permission to publish this work.

Reference

1. R.H. Morgan, *Frequency response function*. Am. J. Roent., 88, no.1, p 175-186 (July '62)
2. P.R. Vaidya, Determination of the focal spot size of microfocal X-ray tubes by means of resolution test chart. INSIGHT, Vol. 41, No.4, April 1999.
3. Robert G. Gould, Harry K. Genant, *Qualitative and Quantitative comparison of two microfocal tube imaging systems*, Radiology 138, p.195 (1981).
4. K. Doi, K. Rossman, *Evaluation of focal spot distribution by RMS value and its effect on blood vessel imaging in angiography*, Proc. Symp. Appl. of Optical Instru in Medicine - III, SPIE Proc. Vol.47 at Palo Vardes, CA, p. 207-213 (1975).
5. Grey J.E., Treffer M., *Focal spot measurement for quality control purposes using A random object distribution*, Proc. Symp. Appl. of Optical Instru. In Medicine - IV, SPIE vol.70, Sept.1975
6. Erik Ingtestam, *Technical Note*, J. Opt. Soc. Am, 51, 1441 (1961).
7. C.E. Mees and T.H. James, *Theory of photographic process*, McMillan & Co., (1966)
8. K. Doi, *OTFs of the focal spot of X-ray tube*. Am J. Roent. 94, No.3, p. 712 (1965).

This paper was awarded the Ron Halmsbaw Award for being the best paper published in the journal INSIGHT (Nondestructive Testing and Condition Monitoring) in the year 2000.

About the author



Mr P.R. Vaidya did his B.Sc in Physics from the Gujarat University and later M.Sc in Physics from the University of Bombay. He joined the Atomic Fuels Division, BARC, in 1970 from the 13th batch of Training School. He worked on Quality Control of nuclear fuels for 2 years and then on ultrasonic testing for another 3 years. Since 1973 he has been also associated with the use of radiation in NDT by way of gamma spectrometry and radiography. He obtained Level II and Level III in radiography from the International Atomic Energy Agency (IAEA).

Mr Vaidya has equal experience in the industrial and research aspects of radiography. He has standardized radiography procedures for nuclear fuels and various systems of nuclear reactors. Real time radiography set-up configured by him in 1985 for mid-term examination of irradiated fuel of research reactor CIRUS was the first of its kind anywhere, using the industrial radiography unit. He has extensive experience in the use of micro-focus X-ray unit for industrial application and R&D purposes. Measurement of focal spot is considered a difficult problem in microfocal radiography. The accompanying paper published in the journal INSIGHT (Non destructive Testing and Condition Monitoring, Vol 42, May 2000) offer some solution to the problem. The paper has been given the R. HALMSHA W Award of the British Institute of NOT for being the best paper published in the journal INSIGHT during the year 2000, on any aspect of radiography and radiology. The work is one part of his Ph.D. dissertation. Mr Vaidya has 45 publications, including four on X-ray focal spot size measurement techniques, in national and international journals and Conferences.

A Novel Naturally Occurring Prodigiosin Analogue with Potential DNA Targetting Property

Mahesh Subramanian

Bio-Organic Division
Bhabha Atomic Research Centre

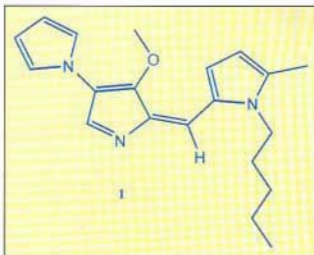
and

Ramesh Chander

Food Technology Division
Bhabha Atomic Research Centre

THERE IS A BURGEONING INTEREST IN SMALL organic molecules that are capable of binding and cleaving DNA as these can be used in the design and development of new drugs, synthetic restriction enzymes, DNA footprinting agents *etc.*^{1,2} Towards this end, the redox potential of a variety of metal ions have been exploited for the development of DNA cleaving agents.³ However, possibly the organic compounds play more important roles as they not only provide multitude binding interactions with the target DNA but also ensures the required electron transfer via their intrinsic chemical, electrochemical and photochemical properties.⁴ Some of the well-known DNA cleavers like DAPI, furamidine, bleomycin *etc.* bind preferentially to the A-T rich sequences of DNA and show mixed binding interactions at different sequences. The polypyrrole natural compounds like the tumbjamine alkaloids and the microorganism-derived pigments, prodigiosins can efficiently cleave DNA via an oxidative process. Recently, a red pigment was obtained from the *Micrococcus sp.* isolated from sterilized dehydrated shrimp. The compound possessed a novel tripyrrole structure where the third pyrrole moiety was attached to the bipyrrole nucleus through its nitrogen atom, a *N*-alkylated analogue of prodigiosin (**1**). Our interest in the compound **1** stemmed from its probable DNA targetting properties. It was envisaged that while its planer bipyrrole nucleus may bind DNA by intercalation, the ring nitrogens and

the methoxyl substituent provide hydrogen bonding sites that could contribute to groove binding mode⁵, features similar to bleomycin.^{6,7} Due to the susceptibility of polypyrroles for easy oxidation⁸, compound **1** was expected to show nuclease activity in the presence of a suitable redox active metal ion. Such activity could then be used to determine whether it interacts with DNA in a sequence-specific manner. To test our hypothesis, the DNA targeting activities of **1** were examined. It was found that **1** binds with DNA efficiently and facilitates copper-mediated DNA cleavage by a process that does not require any external reducing agent. This behavior differs from that of most of the well known DNA cleaving agents and implied that DNA may be a therapeutic locus for **1**.



Results and Discussion

DNA Binding

Compound **1** has strong absorption bands (501 and 537 nm) in the visible region that are well suited for DNA binding studies. The ability of **1** to bind DNA was determined with UV-Visible spectroscopy. As shown in Fig. 1-3, addition of poly[G-C]₂, poly[A-T]₁ and calf thymus DNA (CT-DNA) in increasing amounts to a fixed concentration of **1** (20 μM) led to gradual reductions in the intensity of both the absorption bands of free **1**. In addition, a minor red-shift (1.5-3 nm) of the bands were also noted. All these data clearly suggested efficient binding of **1** with DNA and DNA segments. More interestingly, the hypochromicity induced by binding of **1** to poly[G-C]₂ was significantly high while

those with CT-DNA and poly[A-T]₁ were similar and much less in magnitude. Based on these observations, a G-C specific binding of **1** was apparent. This was confirmed by quantitative analysis of the UV-visible data which permitted determination of the intrinsic binding constant, based on the site-exclusion model.⁴ The equilibrium binding constants (K) in respective cases were derived (Fig. 4) by titrating 20 μM of **1** with increasing amounts of CT-DNA, poly[A-T]₁ and poly[G-C]₂, added in different base pair aliquots as indicated in the Fig. 1-3. Regression analysis in all the cases showed linear fits indicative of a single mode binding of **1** with DNA. As anticipated, the K-value for G-C domain binding was 4-6 fold than those for binding with A-T domain.

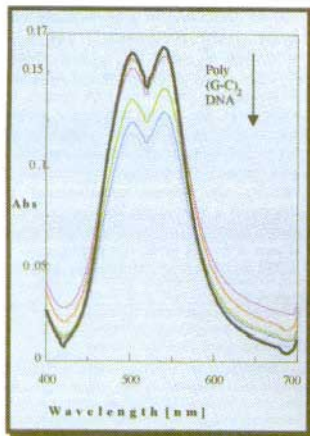


Fig. 1 Interaction of **1** with poly[G-C]₂. Increasing amounts of poly(G-C)₂ (2.5 μM aliquots) was added to 20 μM **1** in 10 mM HEPES buffer pH 7.2 in presence of 100 mM NaCl.

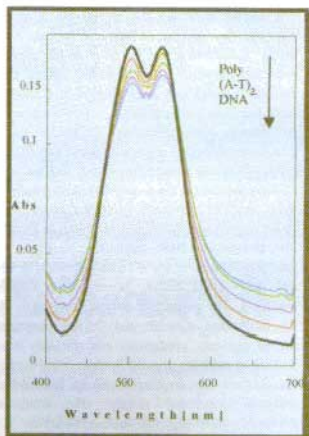


Fig. 2 Interaction of **1** with poly[A-T]₂. Increasing amounts of poly(A-T)₂ (5 μM aliquots) was added to 20 μM **1** in 10 mM HEPES buffer pH 7.2 in presence of 100 mM NaCl.

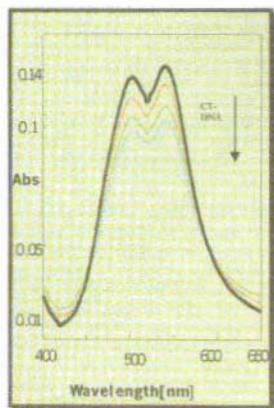


Fig. 3 Interaction of **1** with CT-DNA. Increasing amounts of CT-DNA (6 μ l aliquots) was added to 20 μ l **1** in 10 mM HEPES buffer pH 7.2 in presence of 100 mM NaCl.

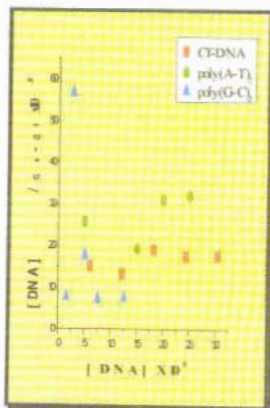


Fig. 4. Determination of the binding constant (K)

DNA	K
CT-DNA	$1.1 \times 10^4 \text{ M}^{-1}$
Poly(A-T) ₂	$1.8 \times 10^4 \text{ M}^{-1}$
Poly(G-C) ₂	$6.7 \times 10^4 \text{ M}^{-1}$

Structural basis for DNA binding

Compound **1** possesses unfused aromatic ring systems bearing cationic charge at physiological pH. The cationic property of **1** appears to be critical for its efficient binding with DNA which is also reflected from reduction of the binding constant values with increased pH (6.5 vs 8.5). The binding constant values of 10^4 M^{-1} was much lower than those of typical intercalators which show K values 10^5 - 10^7 M^{-1} .¹⁷ This argued in favour of a non-intercalative, groove binding of **1** with DNA via ion-pair interaction. Weakening of the binding with increased NaCl concentration (100-500 mM) further confirmed it. All these results were consistent with the importance of the cationic charge of **1** for its DNA binding.

Binding of **1** to DNA was also accompanied by precipitation which continued even in the presence of organic solvents (20% v/v) like DMSO and acetone.

These results were surprising as we anticipated that DNA binding would facilitate water solubility. However, in view of Rizzo's result⁸, it is tempting to speculate that **1** might show a conformational preference in binding with DNA. Thus, if the β form of **1** is the preferred binding conformation, then the pK_a of the bound compound would drop below the pH of the solution causing its precipitation.

DNA Cleavage

The ability of **1** to mediate DNA cleavage was assessed using agarose gel electrophoresis and supercoiled plasmid pBR 322 DNA (Form I). The assay were carried out in the presence of several redox active metals like Cu(II), Fe(III), Ni(II) and Zn(II). As shown in Fig. 5a, strand scission of DNA could be effected only in presence of Cu(II) (lane 3). The data in lanes 2 and 3 demonstrated that both Cu(II) and **1** were required

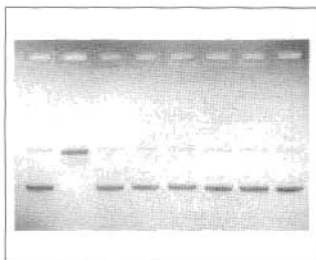


Fig. 5a Ability of different metal ions to induce DNA damage in presence of **1**. Relaxation of Form I DNA by **1** in presence of different metal ions. Reaction mixtures (20 μ L total volume) contained 200 ng of Form I DNA in 10mM HEPES buffer, pH 7.4, 75 mM NaCl and 10-volume % CH₃CN. Cleavage was carried out at 37 °C for 60 min.

Lane 1, DNA + 50 μ M Cu²⁺
 Lane 2, DNA + 50 μ M Cu²⁺-**1**
 Lane 3, DNA + 50 μ M Fe²⁺
 Lane 4, DNA + 50 μ M Fe²⁺-**1**
 Lane 5, DNA + 50 μ M Ni²⁺
 Lane 6, DNA + 50 μ M Ni²⁺-**1**
 Lane 7, DNA + 50 μ M Zn²⁺
 Lane 8, DNA + 50 μ M Zn²⁺-**1**

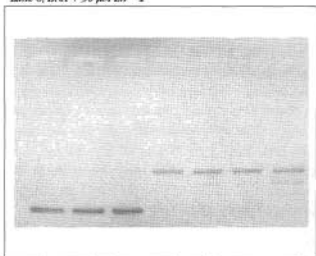


Fig. 5b. Time dependent DNA damage by cupric ion and **1**. Relaxation of supercoiled plasmid DNA (Form I) by 50 μ M Cu²⁺-**1** at 37 °C. Reaction mixtures (20 μ L total volume) contained 200 ng of Form I DNA in 10 mM HEPES buffer, pH 7.4, 75 mM NaCl and 10-volume % CH₃CN.

Lane 1, DNA + 50 μ M Cu²⁺
 Lane 2, DNA + 50 μ M **1**
 Lane 3-7, Cleavage after 0, 30, 60, 90 and 120 min incubation with 50 μ M Cu²⁺-**1**

for the cleavage. The cleavage was complete with equimolar concentration of Cu(II), while lowering the Cu(II) concentration progressively reduced the extent of DNA strand scission. Following the cleavage over a period of 30-90 min (Fig. 5b), it was observed that single strand cleavage was complete within 30 min, while significant double-strand DNA (dsDNA) cleavage appeared after ~90 min. Lanes 5-7 show all three forms of DNA which is a classical evidence of dsDNA cleavage.^{9a,c}

To gain further insight into the mechanism of the DNA cleavage especially with respect to the involvement of oxygen-derived reactive species, the experiment was also carried out in the presence of various scavengers of reactive oxygen species. Fig. 6a shows (lane 4) that the hydroxyl radical scavenger, DMSO could not prevent the DNA cleavage, indicating non-participation of this freely diffusible radical in the reaction. This was further confirmed¹² from the fact that extent of cleavage was dependent on the NaCl concentration (data not shown). Superoxide dismutase also had little effect (lane 6) on the course of the process. Thus, the superoxide radical ion was neither directly responsible for the strand scission¹² nor in reducing Cu(II).¹² Catalase, the enzyme responsible for the disproportionation of H₂O₂ completely inhibited the cleavage (lane 5). Based on these result, the cleavage was found to be oxidative wherein the intermediacy of peroxo compound could be inferred. The metal chelator EDTA could prevent the cleavage (lane 3), while sodium azide, the singlet oxygen quencher¹² had a marginal effect in preventing the DNA scission (lane 7).

All these data indicated that the Cu(II) binding by **1** is essential and that H₂O₂ is involved in mediating DNA cleavage. Mechanistically, it appears that during its interaction with Cu(II), the polypyrrole moiety of **1** gets oxidized to a π -radical cationic intermediate generating Cu(I). Since the rate constants of dimerization of bipyrrrole radical cation in water are ~10⁹ LM⁻¹s⁻¹, one fate of the intermediate derived from **1** would be its dimerization. Oxidation Cu(I) by molecular oxygen would furnish Cu(II) and superoxide radical ion, the latter producing H₂O₂ via

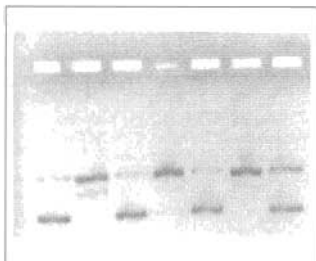


Fig. 6a Mechanism of the DNA cleavage by cupric ion and **1**. Relaxation of the Form I DNA by $50 \mu\text{M Cu}^{2+}$ -**1**. Reaction mixtures ($20 \mu\text{L}$ total volume) contained 200 ng of Form I DNA in 10 mM HEPES buffer, $\text{pH } 7.4$, 75 mM NaCl and 10 -volume% CH_3CN . Cleavage was carried out at 37°C for 60 min . Lane 1, DNA alone
Lane 2, DNA + $50 \mu\text{M Cu}^{2+}$ -**1**
Lane 3, Lane 2 + 100 mM EDTA
Lane 4, Lane 2 + 1 M DMSO
Lane 5, Lane 2 + 1000 U/ml Catalase
Lane 6, Lane 2 + 1000 U/ml SOD
Lane 7, Lane 2 + 100 mM NaCl

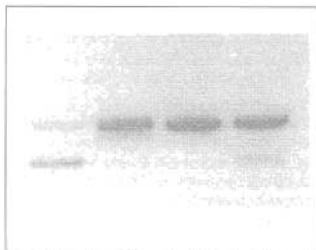


Fig. 6b Intermediacy of Cuprous Ion. Relaxation of supercoiled plasmid DNA (Form I) by $50 \mu\text{M Cu}^{2+}$ -**1** at 37°C . Reaction mixtures ($20 \mu\text{L}$ total volume) contained 200 ng of Form I DNA in 10 mM HEPES buffer, $\text{pH } 7.4$, 75 mM NaCl and 10 -volume% CH_3CN . Lane 1, DNA alone
Lane 2, DNA + $50 \mu\text{M Cu}^{2+}$ -**1**
Lane 3, lane2 + $50 \mu\text{M}$ Neocuproine
Lane 4, lane2 + $100 \mu\text{M}$ Neocuproine

disproportionation. Finally oxidation of Cu(I) with H_2O_2 would lead to a copper-oxo species that initiates the DNA cleavage as is known with prodigiosin and tambjamine.¹³ The involvement of Cu(I) was directly proved by carrying out the DNA scission experiment in presence of increasing amounts of neocuproine, a Cu(I) -specific chelator. As shown in Fig. 6b, presence of neocuproine reduced the DNA damage in a concentration dependent manner.

Considering that compounds that facilitate dsDNA cleavage are known to possess cytotoxic and anti-tumour properties, compound **1** appears to be a promising candidate as anti-cancer agent. Besides cleaving DNA without the need of any reducing agents, it induces dsDNA damage which is considered more difficult for the cells to repair than single strand cleavage. Furthermore, although a large number A-T specific DNA binders are known, designing compounds to recognize G-C sequence is more challenging. Moreover, most of the the G-C specific binding agents bind via intercalative modes. From all these perspectives, the discovery of **1** is very significant as it binds with G-C sequence of DNA via ionic interactions. Based on the results presented in this paper, compound **1** might provide unique probe of nucleic acid sequence-dependent molecular recognition.

References

1. a) Hillman, R. E.; Dandliker, P. J.; Barton, J. K. *Angew. Chem. Int. Ed. Engl.*, 1997, 36, 2714. b) Dupureur, C.; Barton, J. K. In *Comprehensive Supramolecular Chemistry*, (Ed. Lehn, J. -M.), Pergamon, New York, 1997, vol. 5, 295.
2. a) Norden, B.; Lincoln, P.; Akerman, B.; Tuite, E. In *Metal Ions in Biological Systems: Probing of Nucleic Acids by Metal Ion Complexes of Small Molecules*, (Eds. Sigel, A.; Sigel, H.), Merce Dekker, New York, 1996, vol. 33, 177. b) Sigman, D. S.; Majumder, A.; Perrin, D. M. *Chem. Rev.*, 1993, 93, 2295.
3. Wilson, W. D.; Li, Y.; Veal, J. M. *Adv. DNA Specific Reagents*, 1992, 1, 89.
4. a) Lui, S. M.; Vanderwall, D. E.; Wu, W.; Tang, X. - J.; Turner, C. J.; Kozarich, J. W.; Strubbe, J., *J. Am.*

- Chem. Soc.*, 1997, 119, 9603. b) Mao, Q.; Fulmer, P.; Lui, S. M.; Vanderwall, D. E.; Wu, W.; Tang, X. -J.; Turner, C. J.; Kozarich, J. W.; Strubbe, J., *J. Am. Chem. Soc.*, 1997, 119, 9603. and ref. cited therein.
- Patil, A. O.; Heeger, A. J.; Wudl, F., *Chem. Rev.*, 1988, 88, 183.
 - McGhee, J. D.; von Hippel, P. H., *J. Mol. Biol.*, 1974, 86, 469.
 - Hag, I.; Lincoln, P.; Sun, D.; Norden, B.; Chowdhury, B. Z.; Chairs, J. B. *J. Am. Chem. Soc.* 1995, 117, 4788.
 - Rizzo, V.; Morelli, A.; Pinciroli, V.; Scianguola, D.; D'Alessio, R., *J. Pharm. Sci.*, 1999, 88, 73.
 - a) Povirk, L. F.; Wuber, W.; Kohnlein, W.; Hutchinson, F., *Nucleic Acids Res.*, 1977, 4, 3573. b) Drak, J.; Iwasawa, N.; Danishefsky, S.; Crothers, D. M., *Proc. Natl. Acad. Sci. U.S.A.*, 1991, 88, 7464. c) Branum, M. E.; Que, L., Jr. *J. Biol. Chem.* 1999, 274, 593.
 - Lu, M.; Guo, Q.; Wink, D. J.; Kallenbach, N. R., *Nucleic Acids Res.*, 1990, 18, 3333.
 - a) Dix, T. A.; Hess, K. M.; Medina, M. A.; Sullivan, R. W.; Tilly, S. L.; Webb, T. L., *Biochemistry*, 1996, 35, 4578. (11. b) Thederahn, T. B.; Kuwabara, M. D.; Larsen, T. A.; Sigman, D. S., *J. Am. Chem. Soc.*, 1989, 111, 4941.
 - Li, Y.; Trush, M. A.; Yager, J. D., *Carcinogenesis*, 1994, 15, 1421.
 - Borah, S.; Melvin, M. Lindquist, N.; Manderville, R. A., *J. Am. Chem. Soc.*, 1998, 120, 4557-4562.

This paper was awarded the Best Paper Prize in the International Conference on 'Natural Antioxidants and Free Radicals in Human Health and Radiation Biology' organized by Society for Free Radical Research (India/Asia) and International Society for Free Radical Research (USA).

About the authors ...



Mr. Mabesh Subramanian joined the BARC Training School in 1997 (41st Batch) after completing his M. Sc. in Microbiology from M. S. University, Vadodara. Subsequently, he joined the Bio-Organic Division and has been working on naturally occurring radiomodifiers especially available from plants of Ayurvedic importance. His other interest is mechanistic studies on the interaction of bioactive compounds with various exogenous/endogenous reactive oxygen species.



Dr. Ramesh Chander joined the Food Technology Division in 1975 after graduating from the 18th Batch of BARC Training School. His work pertains to development of safe, shelf-stable meat and meat products using hurdle technology. He is also working on inhibition of lipid peroxidation in radiation processed meats by using novel natural antioxidants. His major contribution is development of Artificial Viral Envelopes for targeted intracellular delivery of peptides, enzymes, toxins and gene constructs for which he holds US and European patents.

Fluxes and Residence Time of Different Toxic and Trace Elements in Thane Creek

S. K. Jha, G. G. Pandit, S. B. Chavan and B. S. Negi

Environmental Assessment Division
Bhabha Atomic Research Centre

Introduction

TOXIC AND TRACE ELEMENTS ARE INTRODUCED into aquatic environments as a result of various processes. The sources are geological weathering, effluent discharge from industries, use of metal and metal components, leaching from dump and leaching of fertilizers, atmospheric deposition and animal excretion and the discharge of human sewage. These toxic elements tend to be trapped in creek and accumulate in sediments. Elevated concentration of trace and toxic elements such as Cu, Fe, Pb, Zn in the creek water was reported by several worker (Patel et al. 1985b; Bosale 1991; Mirajkar et al. 1995). Concentration of heavy metals in sediments usually exceeds those of overlying water by 3 to 5 orders of magnitude. There are various routes by which sediment metals reach the biota. With such high concentrations the bio availability of even a minute fraction of total sediment metals assumes considerable importance.

Toxic and trace elements enter Thane Creek from river run off and through direct industrial and sewage discharge from different discharge channels. While all toxic and trace elements are naturally present in the creek sediment it is their presence at elevated concentration, which presents a potential threat to aquatic life (Turner 1990). The present study has been carried out in a creek near Mumbai City, which is one of the most heavily populated and industrialized cities of India. The creek, known as 'Thane Creek', separates the Island City of Mumbai in the west from the mainland in the east and houses industrial area at a distance of about 25 Km north-east of Mumbai city. The bay could be considered as an estuary during southwest monsoon period (June-September, rainfall 200 cm), when the land drainage and river run-offs are considerable. During this period salinity drops down to

about 4‰. During the rest of the year the salinity is maintained in accordance with the ingress of seawater (maximum 38‰). This area is also highly Bio productive (Patel et al., 1979) and yields about 2 to 3 thousand metric tones of fish annually. This area was developed by the state Government essentially for the chemical industries towards the beginning of the sixties and at present about 25 large industries and about 300 medium and small scale units using hazardous chemicals are located out of 2000 units. The main water source for the industrial consumption is MIDC. The industrial area utilizes about 45000 m³/day of fresh water. The effluent discharge –treated and untreated amounts to 28750 m³/day i.e. 64% of the total industrial effluents generated in Thane Creek area. Except few major industries, medium and small scale industries discharge their treated or untreated effluents through the unlined surface drains to Thane Creek. In addition to this domestic sewage discharges from suburbs of Mumbai City meet the Thane Creek from the west side. In addition, atmospheric fallout from the chimneys and stack and vehicle exhausts estimated to be 22000 t/day over the city, reach the creek after washout.

In an attempt to determine the pollution history and to assess the fate of heavy metals detailed investigation has been made in core samples collected from Thane Creek.

Samples Collection, Preparation and Analysis

The entire Creek was divided into three zones as shown in Fig 1. The samples were collected using a gravity corer, its inner and outer diameters being 5.2 and 6.0

cm respectively. The length of the core collected with the help of an adjustable piston rod with silicone packing ranged from 21 to 59 cm. The gravity-coring unit was lowered as slowly as possible into the sediments to prevent lateral motion of the pressure wave created by the descent of the corer. One core each was collected from zone-1 and zone-2, whereas two core samples were collected from zone-3. The collected cores were extruded vertically and sliced at 2 cm intervals and care was taken during coring to ensure minimum disturbance of the sediment water interface. All the samples were freeze-dried, homogenized and stored for analysis.

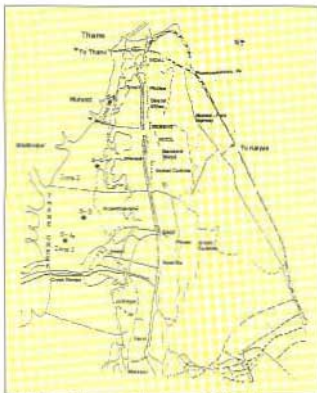


Fig.1 Map of Thane creek showing sampling locations

The determination of ^{210}Pb content is based upon the measurement of the granddaughter ^{210}Po , which is assumed to be in secular equilibrium with its parent. The basic radiochemical procedure involved successive leaching of the sediment samples with aqua regia, the residual solids were filtered off and solution was dried and converted to chloride with concentrated HCl. The final solution was taken in 0.5M HCl and Po was deposited spontaneously on a silver disc. Yield tracer ^{209}Po was added to each sample prior to acid digestion. Activities of ^{210}Po along with the ^{209}Po tracer were measured by Alpha Spectrometry using a silicon

surface barrier detector connected to a multichannel analyzer.

The determination of elemental concentration in the sediment core samples were carried out using Energy Dispersive X-ray Fluorescence (EDXRF) technique for elements Fe, Cu, Zn and Pb, which has been, described elsewhere (Jha et al., 1999b). The Mn, Cr were analyzed by AAS. The standard APHA methods were followed for analysis of toxic and trace elements in the water by AAS (APHA, 1985).

Result and Discussion

The concentration depth profile of Pb, Zn, Cu, Fe, Mn and Cr is shown in Figure 2. The surface concentration of Cr in zone 2 and zone 1 is 121-126 ppm compared to 37-71 ppm in zone 3 of Thane creek sediment compared to the average total Cr concentration in U.K. estuarine sediments (Bryan and Langston 1992) which ranges from about 32-200 ppm. Apart from slight deviation in zone-2 concentration profile values of Fe is constant throughout the entire core. The depth profile of Cu, Zn, Mn and Pb shows gradual increase in concentration as we move from bottom to the top of the core. This variation in concentration is more or less similar in trend but magnitude of variation is more in zone 2. We attribute these increases mainly to contributions to the creek sediment from industrial effluent discharge and from sewage.

The deposition of elemental flux entering the creek at different location was calculated as a product of the elemental concentration (mg/g) in each section of the core with average mass sedimentation rate ($\text{gcm}^{-2}\text{y}^{-1}$) from the respective location. If the cores extended far enough back in time beyond cultural pollution it would be possible to derive local base level concentrations for these elements and determine more recent fluxes to the sediments. For Pb the total flux is 2.5 and 1.8×10^4 $\text{gcm}^{-2}\text{y}^{-1}$ in zone 1 and zone 3 compared to 11.9×10^4 $\text{gcm}^{-2}\text{y}^{-1}$ in zone 2. Assuming that the net concentration for the bottom segments is close to the baseline concentrations, we calculated recent net fluxes for these elements. The calculated recent net fluxes above the corrected background for Pb, Zn, Cu, Cr, Mn and Fe are listed in Table-I. The values for recent net deposition rates can be compared to those for total Pb ($0.4 - 1.1$) $\times 10^3$ $\text{gcm}^{-2}\text{y}^{-1}$ and Cu of ($0.6 - 1.4$) $\times 10^3$

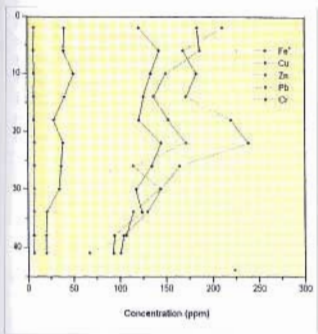


Fig.2a Concentration of trace elements in core collection from zone-1 of Thane Creek

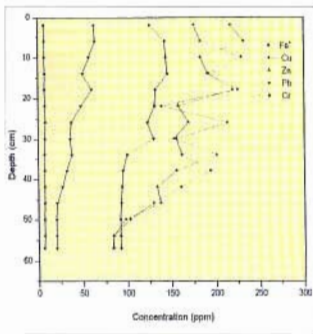


Fig. 2b Concentration of trace elements in core collected from zone-2 of Thane Creek

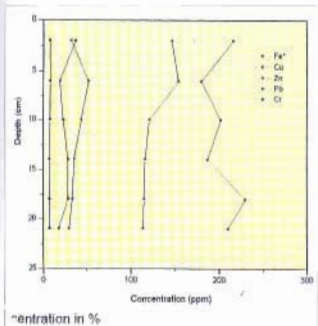


Fig.2c Concentration of trace elements in core collected from zone-3 of Thane Creek

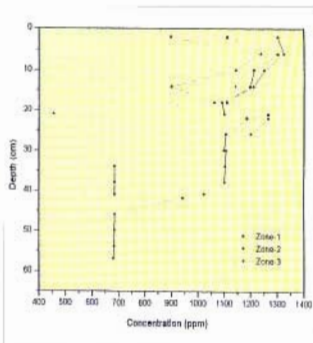


Fig.2d Concentration of Mn in core collected from different zones of Thane Creek

Table 1: Description of sampling locations along with linear and mass sedimentation rate and flux of ^{210}Pb in Thane Creek

Zone no.	Core no.	Location	Sedimentation rate		Flux of ^{210}Pb (dpm $\text{cm}^{-2} \text{y}^{-1}$)
			Linear (cm/y)	Mass ($\text{g cm}^{-2} \text{y}^{-1}$)	
Zone-1	S1	Between Airoli and Thane	0.323	0.06	0.2
Zone-2	S2	Opposite to proposed bridge	0.77	0.2	1.4
Zone-3	S3	Ghansoli	0.17	0.07	0.07
	S4	Koparkhairane	0.25	0.05	0.06

Table 2: Recent net fluxes of different elements in Thane Creek

Zone	Core	Net flux ($\mu\text{gcm}^{-2} \text{y}^{-1}$)					
		Fe	Cu	Zn	Pb	Cr	Mn
Zone-1	S-1	0.03	6.51	5.82	1.26	1.65	25.62
Zone-2	S-2	0.08	26.6	18.5	8.6	6.8	124.1
Zone-3	S-3	0.06	0.18	2.49	<1	<1	1.34

* - Value of flux in $\% \text{cm}^{-2} \text{y}^{-1}$

$\text{gcm}^{-2} \text{y}^{-1}$ obtained by Matsumot and Wong (1977) in cores of marine Fjord in New Pacific with similar sedimentation rates between 0.09 and 0.27 $\text{gcm}^{-2} \text{y}^{-1}$ and ^{210}Pb fluxes of 1.9-5.1 $\text{dpm cm}^{-2} \text{y}^{-1}$. In case of Thane creek with a sedimentation rate of 0.06-0.20 $\text{g cm}^{-2} \text{y}^{-1}$ and ^{210}Pb flux of 0.433 $\text{dpm cm}^{-2} \text{y}^{-1}$ and calculate excess flux of $(0.12-0.86) \times 10^3 \text{gcm}^{-2} \text{y}^{-1}$ indicates the highest value of net fluxes about background are observed for Pb in zone 2.

Under the assumption of constant ^{210}Pb deposition rate, constant sediment accumulation and with no post depositional migration, the sedimentation rate from vertical distribution of excess ^{210}Pb in core can be obtained (Jha et al., 1999a). Table 2 gives the description of sampling location and linear and mass sedimentation rate (Jha et al., 1996) at each location. From the table II mean ^{210}Pb flux in the surficial sediment from the core is 2 times lower than the

reported values (Lewis 1977). The mean global atmospheric ^{210}Pb is about 0.0165 $\text{Bq cm}^{-2} \text{y}^{-1}$ with a inventory of about 0.53 Bqcm^{-2} . The mean atmospheric flux of ^{210}Pb in Mumbai is about 0.025 $\text{Bq cm}^{-2} \text{y}^{-1}$ with an inventory of about 0.80 Bqcm^{-2} . Lewis shows that ^{210}Pb effectively retained by the soil and its removal is very low may result in the lower mean ^{210}Pb flux because of preferential attachment of ^{210}Pb with soil in catchment area. The variation of ^{210}Pb flux in the creek might be caused by nearby watershed.

The most meaningful comparison is obtained for the flux ratio of stable lead and radio lead F_n / F_{210} by normalizing the excess Pb fluxes to the fluxes of radio-lead, which have been corrected for decay, most differences in sedimentation processes are eliminated. Both should have behaved physically and chemically similarly. Furthermore the ^{210}Pb deposition appears to

be constant for a region and probably for a broad latitude band and indications are that atmospheric ^{210}Pb and pollutant Pb are well mixed. Thereby making ^{210}Pb as a useful tracer. Fig. 3 gives the flux ratio $F_{\text{pb}} / F_{\text{ex}210}$ in the cores from different zones. The ratio in the zone 3 might be considered close to background value reminder representing various stages of anthropogenic contribution.

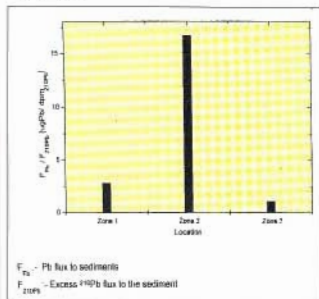


Fig.3 Comparison of ratios $F_{\text{pb}}/F_{\text{ex}210}$ for cores from different locations in Thane Creek

Analysis of toxic and trace elements abundance in the water column was carried out (Inter agency project report 1998) at three different occasions i.e. in the month of February, May and October of the same year. The variation of concentration found in these three measurement in the water samples are 56.6 and < 10 $\mu\text{g/l}$ for Pb, <178 $\mu\text{g/l}$ for Cu, 55.6 $\mu\text{g/l}$ and 6.3 $\mu\text{g/l}$ for Zn, 141 and 3 $\mu\text{g/l}$ for Cr, 117 and 5 $\mu\text{g/l}$ for Fe and 58.6 and 11 $\mu\text{g/l}$ for Mn. Total residence time in the water column were estimated (Henson and Gruendling, 1977) using the water column content divided by total flux to the sediment, iterately averaged over several residence times assuming the complete mixing of the water column. The value of residence time obtained show a low residence time for the Fe and Mn followed by Pb and Cu. Which is consistent with the assumption that particulate are main sequestering agent. A high residence time for the Cr and Zn was obtained.

Conclusion

The data clearly shows that several chemically distinct events have effected Thane creek and the timing of these events was reasonably well defined. The intensity of deposition chronology differs in three zones. The observed pattern of variation in the concentrations of Pb, Zn, Cu, Cr, Mn found greater than the sediments from non-polluted areas. The increase in the deposition rate of toxic elements above natural level may be due to local Industrial effluent discharge from Industrial belt of Thane Creek.

References

1. APHA, (1985). Standard methods for the examination of water and wastewater, Part 703, American public health association, Washington DC, 1985.
2. Bhosale U. (1991). Heavy metals pollution around the Island City of Bombay, India. Chemical Geology 90: 285-305.
3. Bryan, G.W. and Langston, W.J. (1992). Bioavailability, accumulation and effects of heavy metals in sediments with special reference to United Kingdom estuaries: a review. Environmental Pollution 76, 39-131.
4. Henson, E.B. and Gruendling, G.K. (1977). The tropic status and phosphorous loading of lake Champlain. EPA Ecological Res. Series No. EPA-600/3-77-106.
5. Lewis, D.M. (1977). The use of ^{210}Pb as a heavy metal tracer in the Susquehanna River system. Geochim. Cosmochim. Acta 41, 1557-1564.
6. Matsumoto, E. and Wong, C.S. (1977). Heavy metal sedimentation in Saanich Inlet with ^{210}Pb technique. J. Geophys. Res. 82, 5477-5481.
7. Mirajkar P., Moily R., Kulkarni V.V., Bhosale V.M. and Krishnamoorthy T.M. (1995). Preliminary studies on the distribution of heavy metals in Thane Creek ecosystem in relation to industrial effluent discharges. Proceedings of 4th National Symposium on Environment, Madras, February 1995.
8. Patel, B., Patel, S. and Balani, M.C. (1979). Biological responses of a tropical coastal ecosystem to releases from electro-nuclear

- installations. Biological implications of radionuclides released from nuclear industries (Proc. Symposium Vienna, 1979), IAEA, 335-349.
9. Patel, B., Bangera V.S., Patel S. and Balani M.C. (1985). Heavy metals in the Bombay Harbour Area. *Marine Pollution Bulletin*, 16, 22-28.
 10. Report on Inter Agency Project, Assessment and management of health and environmental risk from industries in Trans Thane Creek area (India case study), 1998.
 11. Jha S.K., Krishnamoorthy T.M. and Pandit G.G. (1997). Recent Sediment Accumulation Rate In Thane Creek Using ^{210}Pb Technique. IAEA-EM-349, pp. 158-159.
 12. Jha S.K., Krishnamoorthy, T.M., Pandit G.G., Nambi K.S.V. History of accumulation of mercury and nickel in Thane Creek, Mumbai, using ^{210}Pb dating technique. *The Science of the Total Environment* 236 (1999a), pp. 91-99.
 13. Jha S.K., Chavan S.B., Pandit G.G., Krishnamoorthy T.M. and Negi B.S. (1999b). Heavy metal geo-accumulation pattern in coastal marine sediment near Airoli region of Trans Thane Creek. *Proceedings of the Eighth National Symposium on Environment, Kalpakkam*. 26-28.
 14. Turner, DR. The chemistry of metal pollutants in water. In: Harrison RM, editor. *Pollution-Causes, effects, controls*. Cambridge: Royal Society of Chemistry, 1990:19-32.

This paper received the Best Paper Award in the Second International Seminar on 'Analytical Techniques in Monitoring the Environment', December 18-20, 2000 held at Sri Venkateswara University, Tirupati

About the authors ...



Dr. S. K. Jha joined Environmental Assessment Division (EAD), BARC, after completing his M.Sc. in Inorganic Chemistry from Patna University and after graduating through B.A.R.C. Training School in 1988. His earlier work on physico-chemical behaviour of ^{239}Pu in marine environment earned his

Pb.D. from Mumbai University. Since then, Dr Jha has carried out extensive research work on many aspects of environmental problems using Nuclear Analytical Techniques. At present, he is working on sedimentation rate, behaviour and fluxes of different pollutants affecting marine environment of Mumbai city. His field of interest also includes use of nuclear techniques for monitoring of toxic and trace elements in different environmental samples.



Dr. (Ms) G. G. Pandit joined EAD, in 1981 after graduating from 2nd batch of BARC Training School. She obtained M.Sc. (Organic Chemistry) from University of Mumbai in 1980 and Ph.D. (Sciences) from University of Mumbai in 1990 for her thesis entitled "Source

Reconciliation of Atmospheric Hydrocarbon". Her specialisation includes development and standardization of methodologies for monitoring of various organic pollutants such as volatile organic compounds (VOCs), polycyclic aromatic hydrocarbons (PAHs) and organo chlorine pesticides in the different environmental matrices. At present, she is

working on characterization and risk assessment of persistent organic pollutants (POPs) in indoor and outdoor aerosols and in coastal marine environment. Her field of interest also includes speciation of mercury in marine environment.



Ms S. B. Chavan joined EAD, in 1998 after completing her graduation in Physics from Mumbai University. She is associated with use of nuclear and related techniques (EDXRF and INAA) for the measurement of toxic and trace elements of environmental samples. At

present, she is working on geochemical peculiarities of sediments in the coastal marine environment around Mumbai city.



Dr. B. S. Negi joined BARC in 1969 after completing one year training course of Training Division. He obtained Ph.D. degree from Mumbai University in 1988. He has been associated with the development and use of nuclear and related techniques (EDXRF and INAA), systems for the measurement of toxic

and trace elements of environmental samples (air particulates, soil, fly ash, coal, etc.) and statistical analysis of the data to identify pollution sources. He is also involved in the R & D activities related to the natural and man made radionuclides in environmental samples like air filters, dry and wet deposition samples collected at various sampling stations spread all over the country and analyzed at low level radioactivity measurement laboratory of EAD. The laboratory is being upgraded under his supervision with advance system to handle new challenges in the field.

Encapsulation, Characterization and Catalytic Properties of Uranyl Ions in Mesoporous Molecular Sieves

K. Vidya, S.E. Dapurkar and P. Selvam

Department of Chemistry,
Indian Institute of Technology, Mumbai

and

S.K. Badamali, D. Kumar and N.M. Gupta

Applied Chemistry Division,
Bhabha Atomic Research Centre

Abstract

Occlusion of uranyl ions (UO_2^{2+}) in the channels of mesoporous MCM-41 and MCM-48 molecular sieves was accomplished using direct template ion-exchange method, and the samples were characterized by XRD, FT-IR, DRUV-VIS, and fluorescence spectroscopy. A shift in U=O stretching IR band ($\Delta\nu = -34\text{ cm}^{-1}$), and the appearance of broad and diffused bands in the fluorescence spectra (480–620 nm) of the UO_2^{2+} -exchanged samples indicate a definite electronic interaction of UO_2^{2+} species with the silicate ($=Si-O$) surface. This inference is corroborated by DRUV-VIS results. Calcination in air/ N_2 at 820 K resulted in the formation of well-dispersed $\alpha-U_3O_8/\alpha-U_3O_8$ moieties, accompanied by a marginal decrease in the concentration of UO_2^{2+} groups. The binding of UO_2^{2+} species to mesoporous materials framework remained intact even after calcination. The molecular sieves loaded with uranium oxide species showed appreciable activity, both for the oxidation of CO and for adsorption/decomposition of CH₃DH.

Introduction

MESOPOROUS MOLECULAR SIEVES HAVE received wide attention because of their diversified applications as shape selective catalysts, adsorbents, ion-exchangers and also in removal of heavy metal ions, radionuclides and organics from effluents [1-3]. The well defined (tunable) pore sizes and the large pore openings of these molecular sieves render them unique host materials for occlusion/anchoring of large molecules or that of reactive metal complexes in their channels. The incorporation of specific functional groups onto the walls of the channels in these molecular sieves thus

serves as an important step in heterogenizing the homogeneous catalyst systems. In consideration that uranium (i.e., uranyl ions or uranium oxides) may serve as promising oxidizing catalyst owing to its variable valence states vis-a-vis vacant *f*-orbitals [4,5], we have attempted the encapsulation of uranyl species (UO_2^{2+}) in the mesopores of hexagonal MCM-41 and cubic MCM-48 molecular sieves. The emphasis was to achieve a well-dispersed catalyst system for oxidation reactions. Earlier studies in this direction concern dispersion of uranium oxides over dense oxide supports such as Al_2O_3 , TiO_2 , SiO_2 , MgO , etc. [6].

In the present investigation, we adopted a direct template ion-exchange method [7] for the entrapment

of uranyl species (UO_2^{2+}) in the mesopores of MCM-41 and MCM-48 silicates. The samples in the as-synthesized, as-exchanged and corresponding calcined forms were characterized by various techniques such as X-ray diffraction (XRD), induced coupled plasma-atomic emission spectroscopy (ICP-AES), Fourier transform infrared spectroscopy (FT-IR), diffuse reflectance ultraviolet-visible spectroscopy (DRUV-VIS), and fluorescence spectroscopy. The catalytic performance of these materials was evaluated for model reactions, viz., oxidation of CO and adsorption/decomposition of CH_3OH over a temperature range 373–773 K.

Experimental

Synthesis of MCM-41 and MCM-48

The mesoporous MCM-41 and MCM-48 silicates were synthesized hydrothermally as per the procedure described elsewhere [8,9]. The typical gel (molar) composition was $10 \text{ SiO}_2 : 1.35(\text{CTA})_2\text{O} : 0.75(\text{TMA})_2\text{O} : 1.3\text{Na}_2\text{O} : 680\text{H}_2\text{O}$ for MCM-41, and $10\text{SiO}_2 : 3.0(\text{CTA})_2\text{O} : 2.5\text{Na}_2\text{O} : 600\text{H}_2\text{O}$ for MCM-48. The gels were crystallized in teflon-lined stainless steel autoclaves at 373 K for 1 and 3 days for MCM-41 and MCM-48, respectively. The solid products obtained were washed with distilled water several times, filtered, and dried at 353 K, and were designated as as-synthesized samples.

Preparation of UO_2^{2+} -exchanged MCM-41 and MCM-48

The entrapment of UO_2^{2+} ions in the mesoporous materials was carried out by contacting 1 g sample of as-synthesized MCM-41 or MCM-48 with 80 ml of aqueous uranyl acetate solution (0.035 molar) at a pH of 4.0, under constant stirring at 323 K. Different loadings of uranium were achieved by varying contact time, 12–54 h. A saturation loading of UO_2^{2+} ion was reached in around 20 h time using both as-synthesized MCM-41 and MCM-48. The latter, however showed a higher saturation uranium uptake (~ 53 wt % of uranium as metal) compared to MCM-41 (43 wt %). The details can be seen elsewhere [10]. For the experiments carried out in the present study, the

samples with the saturation uranium loading were utilized. The solid mass after decantation was washed repeatedly, followed by filtration and drying at 353 K for 5 h. The UO_2^{2+} -exchanged samples were calcined first in N_2 for 1–2 h and then for 6 h in air at 823 K. The effect of calcination in N_2 on the oxidation state of occluded UO_2^{2+} species was also evaluated.

Characterization

Powder XRD patterns of the ion exchanged and calcined samples were recorded in 2θ region of $1-10^\circ$ on Rigaku diffractometer using a nickel filtered $\text{Cu K}\alpha$ radiation. The scan speed and step size was $0.2^\circ \text{ min}^{-1}$ and 0.02° respectively. The diffraction patterns were also recorded in higher 2θ region ($10-60^\circ$) in order to identify the bulk uranium phases. FT-IR spectra in mid IR region were recorded on a JASCO model-610 spectrometer at a resolution of 4 cm^{-1} and using 6 wt % of a sample in a compressed KBr pellet. For each spectrum 100 scans were co-added. UV-fluorescence spectra were obtained on a Hitachi, F-4500 fluorescence spectrophotometer, using a monochromated 310 nm radiation for excitation and a UV-35 filter to cut off this radiation in emission spectrum. DRUV-VIS spectra of uranium containing samples were recorded on a Shimadzu UV-260 spectrophotometer.

The catalytic activity was determined in pulse mode using a tubular quartz reactor (8 mm o.d.) in a temperature range of 473–773 K and at ambient pressure. A catalyst charge of ca. 150 mg was loaded in the reactor in between quartz wool plugs. While the catalyst was maintained under He flow (30 ml min^{-1}), successive pulses (500 μl each) of feed mixture ($\text{CO}:\text{O}_2 = 2:1$) were introduced at a desired temperature. In the case of experiments involving methanol decomposition, reactant feed mixture was 9 vol% of methanol vapor in argon. The time interval between two pulses was around 30 min. Prior to the run, the catalyst was activated at 623 K under He and O_2 flow. A Chemito model-8510 gas chromatograph, equipped with thermal conductivity detector and Porapak-QS / Spercocarb column, was employed for on-line analysis of the reactant and product species.

Results and Discussion

XRD studies

XRD patterns of both as synthesized and UO_2^{2+} -exchanged MCM-41 showed typical reflections 100, 110, 200, and 210 in the range $2-5^\circ$, characteristic of MCM-41 [8]. Similarly, the XRD pattern of as-synthesized MCM-48 and corresponding UO_2^{2+} -exchanged sample showed two major reflections at 211 and 220, in addition to six minor reflections 321, 400, 420, 332, 422, and 431 in the range 3.5 to 5.0° , typical of MCM-48 [8]. However, a decrease in the intensity of the reflections was observed in case of UO_2^{2+} -exchanged samples [10] indicating a partial loss of crystallinity. This could be attributed to the partial hydrolysis of =Si-O-Si= linkages of the mesoporous silicate network during the exchange process. No diffraction reflections due to uranium (bulk oxide) phases were detected in the as-exchanged samples. Upon calcination, weak reflections at $d = 4.15, 3.39, 2.62, 2.07, 1.96,$ and 1.75 \AA were observed, which can be indexed for $\alpha\text{-U}_3\text{O}_8$ (JCPDS Card No. 24-1172). The formation of this uranium oxide phase may be attributed to the dehydroxylation of the uranyl oligomers, followed by oxidation. It may be noted that in addition to UO_2^{2+} ions, abundance of other hydrolysed species/oligomers such as $(\text{UO}_2)_2(\text{OH})_2^{2+}$ and $(\text{UO}_2)_3(\text{OH})_4^{2+}$ in uranyl solution has been reported

under the concentration and the pH conditions used in the present study [11,12]. The samples calcined exclusively in N_2 atmosphere indicated the formation of $\alpha\text{-U}_3\text{O}_8$ ($d = 3.43, 3.13, 2.88, 2.71, 1.92, 1.63,$ and 1.54 \AA ; JCPDS Card No. 15-4).

FT-IR studies

Typical FT-IR spectra of unloaded, UO_2^{2+} -exchanged, and UO_2^{2+} -exchanged and calcined MCM-48 are shown in Fig. 1. Corresponding data for MCM-41 are shown in Fig. 2. In the IR spectra, the absorbance values of the selected bands are reported in parentheses for a comparative evaluation of their intensities. The IR bands at ~ 2922 and 2852 cm^{-1} are typical of $\text{CTA}^+(\nu_{\text{C-H}})$ group. The major bands appearing between $1230-459 \text{ cm}^{-1}$ are attributed to various stretching ($\nu_{\text{Si-O-Si}}$) and bending ($\delta_{\text{Si-O-Si}}$) frequencies of =Si-O-Si= linkages. The band at 960 cm^{-1} is due to defect sites ($\text{=Si-O}^-\dots\text{X}^+$; where $\text{X}^+ = \text{Na}^+, \text{CTA}^+$ or H^+). All these bands are characteristic features of the MCM-41 and MCM-48 silicate framework [13]. An additional IR band appearing at $\sim 902 \text{ cm}^{-1}$ in the UO_2^{2+} -exchanged samples of MCM-48 or MCM-41 (Figs. 1b, 2b) may be attributed to $\nu_{\text{U-O}}$ stretching vibrations of uranyl species [14]. The bands appearing at $1543, 1460 \text{ cm}^{-1}$ ($\nu_{\text{O=C}}$) and 676 cm^{-1} ($\delta_{\text{O=C}}$) are characteristic of the acetate ions [15].

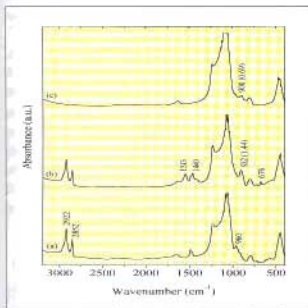


Fig. 1 FT-IR spectra of MCM-48: as-synthesized (a) UO_2^{2+} -exchanged (b), and UO_2^{2+} -exchanged and calcined (c). The values in parenthesis indicate the absorbance values.

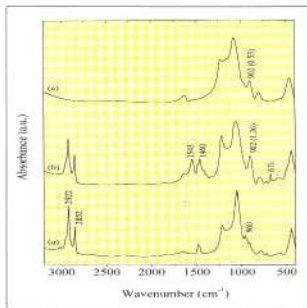


Fig. 2 FT-IR spectra of MCM-41: as-synthesized (a) UO_2^{2+} -exchanged (b), and UO_2^{2+} -exchanged and calcined (c).

As reported widely [16], the UO_2^{2+} groups are linear, and in uranyl acetate they exhibit a strong absorption band at $\sim 930 \text{ cm}^{-1}$ due to asymmetric U=O stretch; the corresponding symmetric vibration expected at $\sim 856 \text{ cm}^{-1}$ is observed only in very thick samples. It is well documented that the U=O stretching frequency in a uranyl compound changes with the ligand and a relationship exists between this frequency and the U=O bond distance [14]. A red shift of $\sim 30 \text{ cm}^{-1}$ in this band, as seen in Figs. 1b and 2b, thus indicates a perturbation of adsorbed uranyl ions, arising from their bonding (through oxygen of uranyl group) with the mesoporous framework, hence weakening the U=O bond. On calcination, these bands are seen in the nearly at the same frequencies when the acetate groups are removed completely (Figs. 1c, 2c). The intensity of 902 cm^{-1} band, however, decreases marginally on calcination (Figs. 1c, 2c), indicating that a part of UO_2^{2+} groups transform to other uranium oxides during the calcination process, as is evident from XRD data. From the relative intensities of ν_{OH} at 2922 cm^{-1} and $\nu_{\text{C=O}}$ at 906 cm^{-1} , as seen in an earlier study [10], it is evident that the attachment of UO_2^{2+} ions is accompanied with the progressive removal of CTA⁻ ions. It may thus be inferred that the anchoring of the uranyl group occurs *via* direct replacement of template ions, as is brought out in Ref. [10] in detail.

UV-Fluorescence studies

The UV-fluorescence study (Fig. 3) provides important information regarding the form in which uranium is present in the mesopores. Curves (a) and (b) present the representative fluorescence spectra of UO_2^{2+} -exchanged MCM-48 before and after calcination, respectively. For a comparison, the fluorescence spectrum of uranyl acetate is shown in inset. It gives rise to several well defined and sharp emission bands in the 470–590 nm range, which are assigned to transitions between vibrational level of first excited electronic state ($\nu' = 0$) to vibrational levels of ground electronic state ($\nu'' = 0, 1, 2, 3, 4, 5$) of uranyl ions [17]. On the other hand, UO_2^{2+} -exchanged MCM-48 shows considerably broad and overlapping emission bands between 484–620 nm (curve). Apart from that, all the band positions are shifted to higher wavelength,

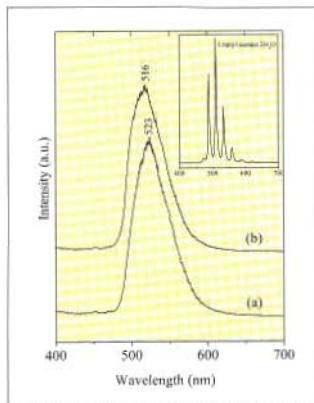


Fig. 3 Fluorescence spectra of MCM-48: UO_2^{2+} -exchanged (a) UO_2^{2+} -exchanged and calcined (b). Excitation wavelength 310 nm.

which is an indication of weakening of the uranyl (U=O) linkages. This can be envisaged to happen as a result of an interaction of UO_2^{2+} ions with the silicate ($=\text{Si}-\text{O}^-$ groups) matrix, as discussed above. A decrease in the intensity of the emission bands after calcination (Fig. 3b) is consistent with our IR data suggesting the transformation of some of the UO_2^{2+} species giving rise to non-fluorescent uranium oxides, the presence of which is also revealed by XRD data. A comparison between Figs. 3a and 3b show a small but reproducible blue shift ($\Delta\lambda = -7 \text{ nm}$) in the wavelength of the emitted radiation after calcination of the as-exchanged sample. This could be tentatively ascribed to their less constrained environment after the removal of template ions. Further, as in case of IR result, similar fluorescence behaviour was observed in the UO_2^{2+} -exchanged MCM-41 samples.

DRUV-VIS studies

The DRUV-VIS spectra of UO_2^{2+} -exchanged MCM-41 and MCM-48 are shown in curves a and c of Fig. 4,

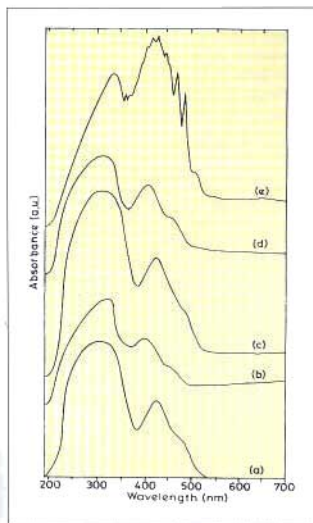


Fig. 4 DRUV-VIS spectra of: UO_2^{2+} -exchanged MCM-41 (a), UO_2^{2+} -exchanged and calcined MCM-41 (b), UO_2^{2+} -exchanged MCM-48 (c), UO_2^{2+} -exchanged and calcined MCM-48 (d), and uranyl acetate dihydrate (e).

respectively. For a comparison, the spectrum of uranyl acetate is included (curve e), which shows the characteristic structure due to electron-vibration interaction, typical of UO_2^{2+} moiety [18]. The distinct structure of the uranyl spectrum with sharp bands is ascribed to definite transitions from electronic levels coupled to $\text{O}=\text{U}=\text{O}$ vibrations [18]. The comparison of spectra of the UO_2^{2+} -exchanged sample with that of uranyl acetate reveals that the UO_2^{2+} -exchanged samples also exist in the hexavalent state in the form of UO_2^{2+} species. It is also observed that the spectra of UO_2^{2+} -exchanged samples may be attributed to the bonding of =Si-O units to linear $\text{O}=\text{U}=\text{O}$ molecules in the equatorial plane forming a uranate type of local structure, similar to an observation reported elsewhere

[18]. Figures 4b and 4d show the DRUV-VIS spectra of UO_2^{2+} -exchanged and calcined MCM-41 and MCM-48 samples. It is observed that the maximum appearing at ~ 430 nm in UO_2^{2+} -exchanged MCM-41 shifts to a shorter wavelength in the corresponding calcined sample (~ 421 nm). Similarly, a shift from ~ 430 to ~ 424 nm is observed for the UO_2^{2+} -exchanged MCM-48. It has been generally agreed that the nature of blue shift of the visible and the near infrared bands may be taken as a measure of the metal-ligand covalent bonding [19]. This hypsochromic shift seen in Figs. 4b and 4d could therefore be taken as a reflection on the stability of the UO_2^{2+} species in the mesoporous matrix due to a strong interaction between UO_2^{2+} and the =Si-O sites, as mentioned above.

Catalyst activity studies

In order to evaluate catalytic activity of the uranium containing mesoporous molecular sieves, two model reactions, viz., oxidation of CO and adsorption / decomposition of CH_3OH were chosen for study over the temperature range of 373-773 K. Typical results obtained for uranium containing (53 wt %) MCM-48 are presented here in brief.

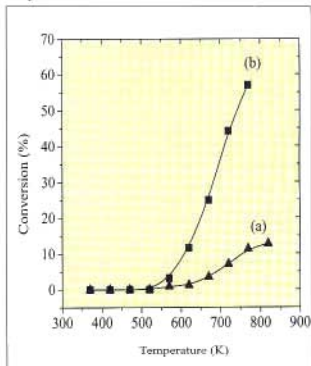


Fig. 5 Catalytic oxidation of CO over MCM-48 (a) and UO_2^{2+} -exchanged and calcined MCM-48 (b).

CO oxidation : The uranium containing MCM-48 showed considerably high catalytic activity compared to host MCM-48, as shown in data of Fig. 5. Around 60 % of CO dosed in a pulse over uranium containing MCM-48 converted to CO_2 at a temperature of 770 K (curve b), the corresponding yield over host MCM-48 being less than 10 % (curve a). Also the activity onset temperature is relatively low in the uranium containing molecular sieve. This oxidative activity can be attributed to the definite role of UO_2^{2+} ions and/or oxides for the conversion of CO to CO_2 , in agreement with the literature [20].

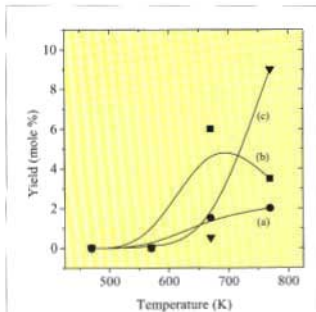


Fig. 6 Reaction products formed on exposure of methanol pulses over UO_2^{2+} -exchanged and calcined MCM-48 a) CO_2 , b) CO, and c) CH_4 .

Methanol adsorption/decomposition : A higher amount of methanol was adsorbed/reacted over uranium containing-MCM-48 compared to the host matrix. While no unreacted methanol was eluted when successive 6 to 7 pulses of methanol (14.8 μmol each) were dosed over uranium loaded sample at temperatures in range 470-770 K, about 25, 11, and 5 volume percent of methanol was eluted from each of these pulses, when introduced over MCM-48 at temperatures of 470, 570, and 770 K, respectively. The reaction products were also different. Thus, while reaction over MCM-48 predominantly gave rise to formation of dimethyl ether (~ 1.7 mol %) at temperatures above 670 K, the reaction products over

uranium containing MCM-48 were CO, CO_2 , and CH_4 . The product distribution for reaction of CH_3OH over uranium containing MCM-48 as a function of temperature is shown in Fig. 6. The difference in catalytic behavior of two samples can be attributed to the difference in the catalyst nature. In case of MCM-48, due to the presence of weakly acidic $\equiv\text{Si-OH}$ groups, the products obtained are catalyzed by an acid pathway. On the contrary, in uranium containing MCM-48, the reaction is catalyzed by an oxidative route, yielding CO, CO_2 , and CH_4 [21].

Conclusions

In the present investigation, the successful entrapment of UO_2^{2+} ions within the mesopores of MCM-41 and MCM-48 is demonstrated. MCM-48 was found to be trapping higher amount of UO_2^{2+} ions than MCM-41. Under the experimental conditions, it was observed that both MCM-41 and MCM-48 suffer a partial loss in crystallinity, even though the structure does not collapse. Both FT-IR and fluorescence studies indicated the binding of UO_2^{2+} ions onto the silicate surface, possibly *via* an interaction between $\equiv\text{Si-O}^-$ and the UO_2^{2+} ions. Upon calcination, UO_2^{2+} moieties are partly converted to uranium oxide species ($\alpha\text{-U}_2\text{O}_7/\alpha\text{-U}_2\text{O}_9$), which are dispersed within the mesoporous matrix. Further, the results of catalytic oxidation of CO and adsorption/decomposition of CH_3OH indicate that the entrapped UO_2^{2+} ions and/or oxides may serve as potential candidates for the selective oxidation reactions. Further study is in progress to corroborate these claims.

Acknowledgements

Authors thank Mr. S. Varma, Mr. B. Dhavakar, Ms. M. Anita and Ms. M.R. Pai for their help in recording FT-IR and fluorescence spectra. This work is supported by the Board of Research in Nuclear Sciences, Department of Atomic Energy, Mumbai under a Contract No. 98/37/31/BRNS/1049.

References

- Stein, B.J. Melde, R.C. Schroden, Adv. Mater. 12 (2000) 1403.

2. K. Moller, T. Bein, Chem. Mater. 10 (1998) 2950.
3. A. Corma, Chem. Rev. 97 (1997) 2373.
4. C.A. Colmenares, Prog. Solid State Chem. 15 (1984) 257.
5. Collette, V. Deremince-Mathien, Z. Gabelica, J.B. Nagy, E.G. Derouane, J.J. Verbist, J. Chem. Soc., Faraday Trans. 83 (1987) 1263.
6. H. Collette, S. Maroie, J. Riga, J.J. Verbist, Z. Gabelica, J.B. Nagy, E.G. Derouane, J. Catal. 98 (1986) 326.
7. S. Dai, Y. Shin, Y. Ju, M.C. Burleigh, J-S Lin, C.E. Barnes, Z. Xue, Adv. Mater. 11 (1999) 1226.
8. J.S. Beck, J.C. Vartuli, W.J. Roth, M.E. Leonowicz, K.D. Schmidt, C.T.-W. Chu, D.H. Olson, E.W. Sheppard, S.B. McCullen, J.B. Higgins, J.L. Schlenker, J. Amer. Chem. Soc. 114 (1992) 10834.
9. S.E. Dapurkar, S.K. Badamali, P. Selvam, Catal. Today, 68 (2001) 63.
10. K. Vidy, S.E. Dapurkar, P. Selvam, S.K. Badamali, N.M. Gupta, Microporous Mesoporous Mater. (revised).
11. C.H. Ho, D.C. Doern, Canada J. Chem. 63 (1987) 1100, and references cited therein.
12. R. Amadelli, A. Maldotti, S. Sostero, V. Carassiti, J. Chem. Soc., Faraday Trans. 87 (1991) 3267.
13. C-Y. Chen, H-X, Li, M.E. Davis, Microporous Mater. 2 (1993) 17.
14. K. Nakamoto, Infrared and Raman Spectra of Inorganic and Coordination Compounds, John Wiley & Sons, New York, 1978.
15. S.V. Ribnikar, M.S. Trtica, J. Serb. Chem. Soc. 63 (1998) 149.
16. E. Rabinowitch and R.L. Belford, "Spectroscopy and Photochemistry of Uranium Compounds", Pergamon, Oxford, 1964.
17. S. G. Schulman, "Molecular Luminescence Spectroscopy Methods and Applications: Part I", John Wiley & Sons, New York, 1985.
18. L. Sacconi, G.J. Giannoni, J. Chem. Soc. (1954) 2368.
19. C.K. Jorgensen, Prog. Inorg. Chem. 4 (1962) 73.
20. F. Nozaki, I. Inami, Bull. Chem. Soc. Jpn. 45 (1972) 3473, J.M. Tatibouet, Appl. Catal. 148 (1997) 213.

This paper received the Best Oral Presentation Award by a research scholar at 15th National Symposium on Catalysis and 2nd Indo-Pacific Catalysis Symposium, January 23-25, 2001 held at N.C.L., Pune.

About the authors ...



Narendra Mohan Gupta (Ph.D. in Chemistry, Agra University) joined BARC in 1966 through 9th batch of Training School. Since then he has contributed to a number of basic research and development related areas of catalysis, surface science and solid state chemistry. He was President of the Catalysis Society of India (1995-1997) and also served as a member of international Catalysis Congress for a term 1996-2000. He is on various important official committees of BARC and was also responsible in the organization of a number of symposia and conferences on the subjects of Catalysis and Water Chemistry.

He has more than 125 publications and 2 books to his credit. Presently, Dr Gupta is designated as Head, Applied Chemistry Division, BARC.



Darnesh Kumar (M.Sc. Chemistry, University of Mumbai) is a research scholar (DAE fellowship), working in Applied Chemistry Division since February 2000 on a project "Preparation, Characterization and Catalytic Properties of Modified Molecular Sieves".



Dr Susbanta Kumar Badamali (Ph.D. Chemistry, IIT, Mumbai) works in Applied Chemistry Division as a Dr K.S. Krishnan Research Associate-2000 (DAE-BRNS). His research interests include development of mesoporous molecular sieves for catalytic applications and host-guest chemistry.

Molecular Dynamical Simulations of the High Pressure Transformations in α Cristobalite – SiO_2

Nandini Garg and Surinder M. Sharma

High Pressure Physics Division
Bhabha Atomic Research Centre

Abstract

Static and dynamic high pressure experiments reveal that the behaviour of α -cristobalite SiO_2 , depends on the rate of stress loading. To understand this behaviour we have carried out extensive molecular dynamics simulations. The response to shock loading was simulated by raising the pressure and temperature simultaneously and instantaneously to the expected Hugoniot values. Shock simulations along the Hugoniot path of porous cristobalite revealed that alpha cristobalite transforms to a new six coordinated crystalline phase beyond 16 GPa, 1410.3 K. This transformation to the crystalline phase is very sluggish and proceeds via a disordered phase. Our simulations show that between 16 GPa and 18 GPa, even after equilibrating for a very long time, the disorder persists. On sudden release of pressure, this disordered state is retained in agreement with the experimental observations under shock conditions.

SILICA AND ITS POLYMORPHS ARE IMPORTANT geological materials found abundantly in the earth's mantle and therefore the high pressure behaviour of these compounds is of considerable importance. At low pressures, most of these minerals exist in corner linked framework structures and display a typical intrinsic behaviour of Si-O linkages. Cristobalite, the mineral of interest in the present study, is a high temperature polymorph of silica and is often found in volcanic rocks. Its idealized structure at high temperatures is cubic (β -phase) which, on lowering the temperature, completely and displacively converts into a tetragonal form (α -phase, also called low cristobalite).

High pressure behaviour of α cristobalite displays distinct differences when it is subjected to shock¹ and static² pressures. Gratz et al¹ observed that when powder specimens of α -cristobalite were shocked to 28.2 GPa, the recovered samples were almost completely amorphous. However the specimens shocked to pressures lower than 22.9 GPa retained their original structure¹. In contrast, under static high

pressures, depending on the degree of non hydrostatic stresses present, low cristobalite displays several intermediate crystalline \rightarrow crystalline phase transitions. In a hydrostatic environment it transforms from alpha to a 'stishovite like' phase at 18 GPa¹. Theoretically the high pressure behaviour of α -cristobalite has been investigated by molecular dynamics simulations (MD)^{3,4} and total energy calculations⁵. MD calculations of Tsuneyuki³ et al showed that α -cristobalite, transforms to an orthorhombic phase (Cmcm) at 16.5 GPa which further transforms to stishovite at 23 GPa. However neither of these theoretical studies imply a pressure induced amorphization of cristobalite.

To understand the atomic mechanism of some of these structural phase transformations in cristobalite under high pressure we have carried out detailed MD simulations. Our simulations are likely to be more realistic and less sensitive to MD cell dimensions as we use a large macrocell having an order of magnitude more atoms than used in the earlier MD studies. Molecular dynamical simulations (MD) presented here

were carried out using a modified¹⁰ Nose-Hoover (N, P, T) algorithm for variable cell size and shape. Equations of motion were integrated every 2 fs using Verlet's algorithm. The MD cell was considered equilibrated when the fluctuations in temperature, pressure, volume and total energy of the system were less than 0.001%. To minimize the effect of periodic boundary conditions most of the simulations were carried out using a large macrocell having 8x8x6 unit cells of α -cristobalite (4608 atoms)¹¹. The starting α -cristobalite structure ($P = 0.1$ MPa and $T = 300$ K) was obtained by equilibrating the experimentally known coordinates of this structure¹². At each temperature and pressure the system was equilibrated for ~ 40ps and the atomic coordinates, volume and pressure of the macrocell were averaged over several thousand time steps. However at pressures and temperatures where a phase transformation takes place, equilibration was carried out until the thermodynamic quantities converged.

For representing the behaviour of shocked samples, simulations were carried out at P and T corresponding to the shock Hugoniot of porous α -cristobalite. P, T along the Hugoniot were calculated using jump conditions with the initial density of the samples as 1.44 gm/cm³ which is same as in the samples used by Gratz et al¹. These simulations were carried out using the BKS¹³ pair potentials. In these simulations, the temperature and pressure were suddenly raised to the required value. Table 1 gives the summary of P and T conditions at which simulations have been carried out. Also to make a contact with the results of recovered samples after shock loading one must evaluate the effect of residual temperatures on shock release. In the absence of knowledge of these residual temperatures we arbitrarily reduced the P and T at c and d to 0.1 MPa and T = 1200 K, 1000 K, 500 K.

Table 1 Simulation conditions along the Shock Hugoniot

Shock Hugoniot	
P (GPa)	T (K)
(a)	10.0
(b)	13.4
(c)	16.3
(d)	18.1
(e)	19.9
(f)	20.9
(g)	22.4
Release	
From	To
(h) 18.1 GPa, 1542.6 K	0.1 MPa, 500 K
19.9 GPa, 1682.9 K	0.1 MPa, 1200 K
19.9 GPa, 1682.9 K	0.1 MPa, 1000 K
19.9 GPa, 1682.9 K	0.1 MPa, 500 K
Annealing	
Amorphous phase in step (h)	1000 K

Results and Discussion

As mentioned above, the shocked state was generated by sudden increase of pressures and temperatures to the values expected in the experiment. As the experiments were carried out on powder samples it is reasonable to treat the material as being under isotropic pressure. In a sense this simulation represents the effect of mean stress loading and thus ignores the effect of the deviatoric stresses if any. Even in doing so there is no way to ensure that the thermodynamic variables P and T in the simulations increase in the same manner (revelations) as in the experiments¹⁴. In this sense the present results should be taken to represent the gross features rather than the quantitative measure.

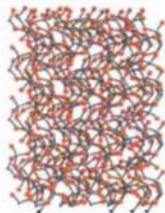
Simulations were carried out at a few representative values of pressures and temperatures listed in table 1. Below the point e ($P=16.3$ GPa, $T=1410.1$ K) the macrocell equilibrates reasonably fast and the crystalline state continues to exist in the α -phase. However at c and d , (16.3 GPa, 1410.1 K and 18.1 GPa, 1542.6 K) the α -phase evolves very slowly to the new structure. It took ~ 750 ps for the new structure to stabilize. This new crystalline structure as well as all the other equilibrated structures beyond the point e in table 1 have six Si-O coordination. However various structures differ from each other in terms of the crystalline order. Also the time taken for the final states to equilibrate reduces significantly at P, T points higher than d . For example, at 22 GPa, 1869 K equilibration could be achieved in ~ 60 ps.

The final state at 16.3 GPa, 1410.1 K had a disordered Cmcm structure despite equilibrating for a very long time. This is shown in Fig.1(a). However it was observed that on equilibrating the system well beyond 500 ps there was the emergence of a disordered stishovite like phase. This phase continues to remain disordered on release of pressure and after annealing at the residual temperatures of 500 K and 300 K. The diffraction patterns were computed for all these different thermodynamic conditions. It was observed that the disorder in the Cmcm structure at 16.3 GPa, 1410.1 K increased on release of pressure, which was indicated by a significant increase in the diffused and non Bragg like scattering observed in the computed

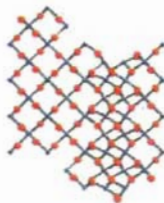
diffraction pattern. From these simulations it is evident that at these temperatures and pressures there are several phases with comparable energies. Once the structure goes into the disordered stishovite phase it is not able to attain the ordered stishovite like structure even on equilibrating for a long time. Since in shock experiments the sample is subjected to the peak pressure only for a few micro seconds, the material may not have sufficient time for the emergence of the stishovite phase. Therefore these results may be taken to correspond to the amorphous phase observed in the shock experiments. These simulations also show that on release of pressure and temperature, the disordered phase has 5.2 Si-O coordination. However it is possible that if this recovered disordered phase is annealed at a higher residual temperature, this Si-O coordination may revert to four fold.

For thermodynamic conditions beyond d (18.1 GPa, 1542.6 K), the equilibrated states display the emergence of crystalline order. Though all these phases have six Si-O coordination, the degree of frozen disorder decreases from e to g (Table 1). Figs. 1(b) and 1(c) show the results of simulations at 19.9 GPa, 1682.9 K. The equilibrated phase when projected on (100) plane shows almost perfect order. However when projected on (001) plane, one can discern the remnants of disorder. The crystalline part of this phase is 'stishovite like'. At still higher P and T (22.4 GPa, 1869.1 K) the remaining disorder reduces dramatically as shown in Fig.1(d). Here also the crystalline phase is 'stishovite like'.

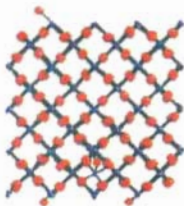
Under compression, particularly the non-bonded atoms, cannot be brought closer than some limiting value without an excessive cost in terms of energy. When the energy of compression of these distances become comparable to the cohesive energy differences between the structures, the initial structure becomes unstable. A survey of large number of materials indicate that the extreme limiting value of O...O is 2.6 Å. It is interesting to note that just before the transition, the sites at which the transformation is triggered, were those where the non bonded O...O distances were ~ 2.42 Å i.e lower than the extreme limiting distance. Therefore, our simulations show that the nucleation for the phase transformation starts at the sites where O...O distances are highly constrained.



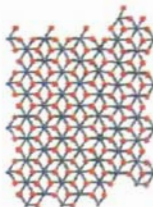
(a) [1 0 0] view at 1410 K, 16.3 GPa



(b) [0 0 1] view at 1682.9 K, 19.9 GPa

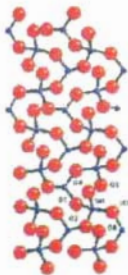


(c) [1 0 0] view at 1682.9 K, 19.9 GPa

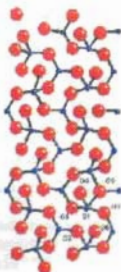


(d) [0 0 1] view at 1869.1 K, 22.4 GPa

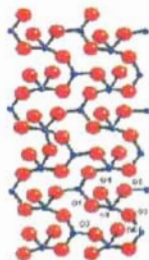
Fig.1 Structures of the new phases at different *P*, *T* along the shock Hugoniot



(a) 20 ps



(b) 22 ps



(c) 24 ps

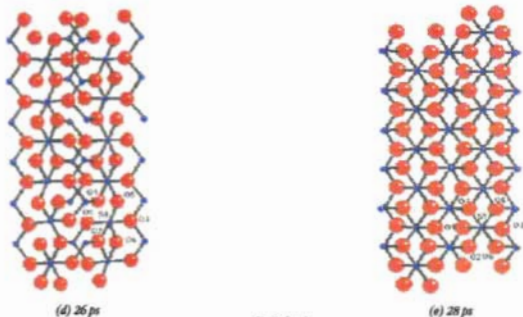


Fig.2 (a-e)

Analysis of the evolutionary history of Fig.1b, 1c and 1d shows that α -cristobalite transforms to this 'stishovite like' phase through an intermediate disordered Cmcm like phase. Fig.2 shows the structural evolution from α -phase to stishovite as predicted in our simulations. Fig. (2a) shows that at 20 ps the structure is alpha phase. One can clearly discern a bond making between S1 (silicon) and O5 (oxygen) and bond breaking between S1 and O2 22 ps (Fig.2b). After a time interval of 26 ps O2 and O6 coordinate to S1 and the structure then relaxes to almost perfect order at 28 ps. The structure is almost Cmcm at 24 ps. It was seen that after the transformation was initiated at 22.4 GPa, 1869.1 K it was over within 8 ps. These results show that no diffusion is necessary to bring about a transformation from α cristobalite to stishovite phase through the Cmcm phase. A slight local atomic rearrangement is all that is needed to cause the structural change.

Summary of the simulations at different thermodynamic conditions has been plotted in Fig.3. It is clearly seen that though beyond 16 GPa alpha phase transforms to a disordered phase, and it transforms to a stishovite like phase beyond 18 GPa. The difference in the observed and calculated pressure of amorphization may depend significantly on the pair potentials. In addition this

difference may also arise from the differences in the rate of increase of pressure and temperature in two different settings¹⁴.

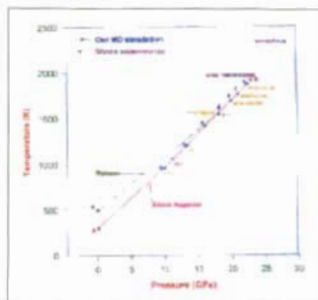


Fig. 3 Simulations were carried out at the temperatures and pressures marked (Δ) (∇) indicate the estimated P & T for the experiments¹⁴

However qualitatively we have shown that alpha cristobalite transforms to a disordered phase when subjected to sudden pressures beyond 16.3 GPa, 1410.1. It was also observed that in contrast with the

calculated behaviour of the disordered state at 18.1 GPa, 1542.6 K, the stishovite like structure at 19.9 GPa became more ordered when annealed at 1200 K, 1000 K, and 500 K after release of pressure. Calculated Bragg peaks are found to be the sharpest after annealing at 500 K. These predictions should encourage more experiments on shock loading of cristobalite to higher pressures.

Acknowledgements

Authors acknowledge many useful suggestions and discussions with Dr. S.K. Sikka.

Bibliography

1. A.J. Gratz L.D. DeLoach, T.M. Clough and W.J. Nellis. *Science*, **259**:663, 1993.
2. David C. Palmer and Larry W. Finger. *Amer. Miner.*, **79**:1, 1994.
3. Though the x-ray diffraction TEM and SEM studies suggested no amorphization below 22.9 GPa, the Raman spectra of samples shocked to 18.2 GPa and 22.9 GPa also indicated broad features.
4. Masaki Yamakata and Takehiko Yagi. Technical report, ISSP University of Tokyo, 1996.
5. S. Tsuneyuki M. Tsukada and H. Aoki. *Phys. Rev. Lett.*, **61**: 869, 1988.
6. Shinji Tsuneyuki Yoshito Matsui Hiideo Aoki and Masaru Tsukada. *Nature*, **339**:209, 1989.
7. John S. Tse and Dennis D. Klug. *J. Chem. Phys.*, **95**:9176, 1991.
8. Nitin R. Keskar and James R. Chelikowsky. *Phys. Rev. B*, **46**:1, 1992.
9. M.B. Boisen Jr. and G.V. Gibbs. *Phys. Chem. Miner.*, **20**:123, 1993.
10. S. Melchionna G. Ciccotti and B.L. Holian. *Mol. Phys.*, **78**:533, 1993
11. We made a choice of 8x8 unit cells in the basal plane to avoid bypassing the Cmc₂ phase.
12. P.J. Heany C.T. Prewitt and G.V. Gibbs, editors. *SILICA*. Miner. Soc. America, 1994.
13. B. W. H. van Beest, G. J. Kramer and R. A. van Santen, *Phys. Rev. Lett.* **64**:1955, 1990.
14. In the recovery capsule of the experiments, impact pressure is achieved through a reverberating shock wave. Only 50 % of the final pressure is achieved with the first shock wave. As we used the single shock jump conditions to simulate P and T, the temperatures used in the present simulations may be somewhat overestimated.

This paper received the Best Poster Award at the National Conference on 'Computational Materials Science (NCCMS)-2000' held during July 27-29, 2000

About the authors ...



Ms. Nandini Garg did her post graduation in Physics from Ravensbanker University, Raipur, MP, in the year 1989. She was the recipient of the university gold medal for securing 1st position in her MSc examination. She graduated from the 34th batch of BARC Training School and joined High Pressure Physics Division of BARC. Since then she has been working on high pressure phase transformations in different materials.



Dr. Surinder M Sharma joined BARC through the 19th batch of Training School. His research interests are behaviour of materials under static as well as dynamic high pressures. He was awarded the Homi Science & Technology award in 1996 and Medal of Materials Research Society of India in 1998.

Biomedical Applications of Cell Electroporation

S. H. Sanghvi, V. W. Bedekar and K. P. Mishra

Radiation Biology Division
Bhabha Atomic Research Centre

Abstract

Application of high intensity short electrical pulses to biological cells induces dramatic transient permeabilization of outer membrane presumably by implantation of micropores. This allows incorporation of drugs, enzymes, antibodies and other molecules of interest into cells providing a new pathway to cell loading for goal-oriented applications in cell biology, medicine and biotechnology. More recently, membrane electroporation has successfully been used to deliver anti-cancer drugs to certain tumor cells including those known to display drug resistance. Combined treatment of electroporation and chemotherapeutic drug to tumor cells results in enhanced killing, which holds a promise in improving cancer therapy. Electric field induced cell alignment and fusion of cells in vitro offers a novel technique to achieve efficient cell fusion, which has found application in monoclonal antibody production by hybridoma. In addition, electroporation based gene transfer has opened a new approach for genetic manipulation of a variety of biological cells. Following electroporation several protein metabolites and other small molecules have been incorporated into a recipient cell offering a potential for many biomedical applications.

Introduction

CELL ELECTROPORATION INVOLVES EXPOSURE of cells to brief high intensity electrical pulses, which produces dramatic transient increase in membrane permeability allowing entry of otherwise impermeant molecules/drugs into cell interior. This has become an important biophysical method for introduction of a variety of exogenous bioactive molecules into a number of cells. Electric field induced increased membrane permeability is generally believed to arise due to formation of micropores in the plasma membrane, which are found to reseal within seconds to minutes under controlled experimental conditions. Using human red cells, Chinese hamster ovary and ascites tumor cells, we have demonstrated that magnitude of induced membrane permeability is governed by various factors such as field parameters (e.g. voltage, pulse shape and duration etc.) cell type, suspension medium, thermal conditions during and post pulse incubations. Studies on electroporation of

normal as well as tumor cells are actively being pursued in our laboratory including combination with radiation and/or chemotherapeutic drugs. World over research is rapidly progressing on electroporation of mammalian, plant and microbial cells for fundamental understanding as well as for developing goal-directed biomedical applications. Present communication briefly describes electroporation based emerging technologies for practical applications such as electro-gene transfer, electrodeivery of anticancer drugs into target tumor cell and electroencapsulation of drugs.

Methodology and Instrumentation

A Biological Cell Electroporator designed and developed in our laboratory has been used to permeabilize mammalian cells such as erythrocytes, thymocytes, tumor cells etc., which provides exponentially decaying pulses of variable amplitudes and pulse duration. The equipment is capable of delivering pulses of variable amplitudes with pulse

durations ranging from microsecond to millisecond. A prototype of square pulse generating facility has been developed for more efficient electroporation, which is currently under testing. Moreover, design work has been undertaken to develop a biphasic pulse electroporator with operation in auto and manual modes to achieve symmetrical poration of cells for efficient tumor killing especially for *in vivo* tumor model experiments.

A prototype cell fusion set up has been assembled to investigate effects of various AC and DC field parameters on cell alignment and cell fusion. Present studies are limited to fundamental aspects of fusion of red blood cells.

Electroencapsulation

In our laboratory electroencapsulation into human red blood cells has been studied extensively, which has potential therapeutic use in delivery of radio-labelled and anticancer drugs into target organs. Encapsulation studies on electroporated mouse red cells showed that injection of loaded red cells encapsulated technetium 99m or anticancer drug, methotrexate (MTX) substantially concentrated in the liver (>70%) of mouse suggesting a possibility of organ specific targeted delivery of drugs. Results from other laboratories have shown potential of electroencapsulated inositol hexaphosphate (IHP) in red cells in improving tissue oxygenation during cardiopulmonary bypass operation in patients with respiratory problems. Another significant development in drug delivery in cardiology using loaded red cells is encapsulation of antiproliferative agent such as PG12 with the goal of reducing restenosis after blood vessel injury.

Electrogene Transfer

Membrane presents a natural barrier for the entry of foreign molecule/gene into cells. Transient permeabilization of membrane by electroporation has opened a new possibility of introducing DNA/genes into a variety of cell. Success of this method in cell transformation *in vitro* has been amply demonstrated and it has become a routine procedure in cellular and molecular biological experiments. Considerable

research has been devoted to electroporation mediated gene transfer *in vitro* and returning the manipulated cells to meet specific medical objective of correcting the defects cells / organs of patients with certain diseases. In western countries clinical trials are undergoing to ameliorate bleeding disorder by delivery of encapsulated defective factors IX and VIII in hemophilia A & B human patients.

Electrofusion Of Erythrocytes

Usually two cells can be fused when they are brought in contact by dielectrophoretic force, which aligns cells into long chains called pearl chains. This occurs when weak but continuous inhomogeneous AC electric field is applied in an appropriate medium containing the cells. After cells are aligned in tight contact a strong but brief DC pulse is applied which induces cells to fuse by the process of intermixing of electro-perforated membranes. Experiments in our laboratory have shown that for the same field conditions suspension of cells in isotonic sucrose and manitol solutions accelerated the process of chain formation and increased the percent efficiency of cell fusion. Pearl chain formation is quantitatively dependant on the AC field parameters such as frequency, voltage and resistivity of suspension medium. Figure 1 shows a typical chain of human red cells suspended in isotonic manitol exposed to AC field.



Fig.1 Human red cells suspended in manitol and subjected to AC field. Freq. : 200 kHz, Amp: 10 V p-p

Electro-Delivery Of Anticancer Drugs

Combination of electroporation and drug treatment of tumor cells called electrochemotherapy is a novel

approach for developing more effective cancer therapy. This method takes advantage of membrane permeabilization by electric pulses to facilitate the entry of anticancer drugs into the target tumor cell. Under controlled conditions it has been shown possible to electroporate tumor cell membrane making it more responsive to drug action both *in vitro* as well as *in vivo*.

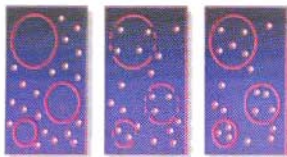


Fig.2 Schematic representation of drug and electroporation treatment to tumor cell

In particular, electroporation has been shown to facilitate uptake of bleomycin (BLM) into recipient cells in suspension and in culture cells. BLM is a chemotherapeutic drug frequently used clinically in the treatment of many solid tumors and malignant lymphomas. In clinic, therapeutic effectiveness of anti-tumor drugs is limited by the low drug uptake into tumor cells and efflux of drugs from the resistant tumor cells. Therefore, a higher dose of drugs is required to increase cytotoxicity in clinical practice for more effective cancer treatment. Researchers aim to potentiate the effect of anti-cancer drugs at low dose minimizing undesirable side effects. Electrochemotherapy allows to reduce the total dose of drugs considerably and permits larger amount of drug

to enter tumor cells producing maximum cytotoxicity. It is hoped that further active research will enable apply this technology to human cancer patients. Clinical trials using certain drugs are under progress in several western countries for treatment of specific tumor.

Future Prospects

Cell electroporation has moved from laboratory to practical applications. Electroporation research continues to witness rapid advances in fundamental understanding of the phenomenon and emergence of newer technologies for applications in biotechnology, molecular biology and medicine. *In vitro* research is directed to determine and optimize factors that increase efficiency of membrane electroporation. Medical applications, among others, are turning out especially promising. Clinical application of electroporation in cancer therapy is reaching close to patient treatment and potential feasibility has been shown in many other applications. However, development of suitable electrode applicators and electropulse generators for clinical settings remains a challenge. Research on transdermal electro-drug delivery is becoming a hot topic in systemic and skin medical research. Electro gene therapy, electro-cell-fusion, electrosterilization of food, electro drug delivery, electro-transformation of microbial cells are some of the developing technologies based on membrane electroporation. However, much remains to be understood concerning molecular mechanism of membrane permeabilization, which evidently is necessary for the success of present technologies and further new developments.

This paper was given the Best Poster Presentation Award in the Section of Biochemistry, Biophysics and Molecular Biology, 88th Indian Science Congress held at IARI Campus, New Delhi, during January 3-7, 2001.

About the authors

Dr K.P.Mishra joined Biomedical Group of BARC in 1969 after graduating through 12th Batch of BARC Training School. He obtained M.Sc. degree in Chemistry from Allahabad University in 1968 and Ph. D. from Gujarat University in 1979. His research interests involve investigations on free radical mechanism of radiation damage to biological systems employing biophysical techniques such as fluorescence, magnetic resonance techniques etc. He has extensively investigated radiobiological and biophysical aspects of radiation oxidative damage to mammalian cells and their membranes with an emphasis on fundamental mechanisms relevant to cancer radiotherapy. He has designed and developed suitable liposomes for targeted delivery of anticancer drugs and radiolabelled compounds to recipient cells/ diseased organs. In addition, Dr Mishra has made significant contributions in understanding the molecular mechanism of cell membrane electroporation employing indigenously designed and fabricated Biological Cell Electroporator. Presently, he is Head of Cellular and Free Radical Radiation Biology Section actively pursuing research on radiation and electroporation induced cytotoxicity to normal and tumor cells with a goal to understand underlying mechanism of cell killing for improving cancer radiotherapy.



Mr S. H. Sanghvi joined BARC in 1961 in Electronics Division and acquired M. Sc. degree in Physics on "Studies of quantitative electromyographic signals in muscle from diagnostic consideration" from Mumbai University in 1980. Design and development of biomedical instruments has been his major research interest. He has developed microprocessor based Electromyograph System and Magnetic Stimulator. Currently, he is involved in developing Biphasic Medical Electroporator and doing Ph. D. work on "Magnetic and Electrical field effect on cellular system to develop device for biomedical applications" under guidance of Dr. K. P. Mishra, Radiation Biology Division.



Shri V.W. Bedekar joined BARC in 1965 after completing Diploma in Radio Engineering from Bombay Technical Board, Mumbai. He is involved in supervising and maintaining radiation facilities in the laboratory. He has been associated with the design and development of Biological Cell Electroporator.

Detection of *Listeria Monocytogenes* in Foods: Comparison of Colony Hybridization Technique with Conventional Method

Anu Kamat and D. R. Bongirwar

Food Technology Division
Bhabha Atomic Research Centre

and

K.K. Ussuf

Nuclear Agriculture and Biotechnology Division
Bhabha Atomic Research Centre

Abstract

A fragment of hly A region, essential in intracellular survival of Listeria monocytogenes was labeled with ³²PdCTP by random primer labeling and used as a probe to detect L.monocytogenes present in food by colony hybridization. This detection method was compared with conventional one by screening sixty two samples of vegetables, fish and meat procured from local markets. Food samples were examined at various stages of enrichment. These food samples were transferred to nitrocellulose filters in a grid forms to detect L.monocytogenes by colony hybridization using the hlyA gene probe by employing standard procedure. L.monocytogenes was not found in any of the samples of meat and fish but in number of samples of vegetables like coriander leaves, tomatoes and cabbage it was detected ; but only after an enrichment step. The validity of the method was examined further by using other species of Listeria as well as non Listeria cultures. As compared to the conventional method of detection of L. monocytogenes ,colony hybridization was found to be less laborious and less time consuming. However, to get positive signals in autoradiogram, minimum cell concentration of 10⁶ cfu/ml was needed for both saline and fish homogenate samples. The colony hybridization technique was more sensitive than the conventional method for detection of L. monocytogenes in some vegetables. By employing both the methods the efficiency of radiation treatment in eliminating L.monocytogenes was seen in vegetables like tomatoes and coriander leaves.

LISTERIA MONOCYTOGENES IS A GRAM POSITIVE, non-sporulating foodborne pathogen. It is ubiquitous in nature. As a result, *L. monocytogenes* contamination occurs in a variety of foods, such as milk and milk products, raw meat, seafoods and vegetables (Farber and Peterkin 1991). Consumption of contaminated foods can cause severe and often fatal infection in the susceptible people (Farber and Peterkin 1991).

Therefore, this organism has been of major concern in the food industry in recent years. A routine analysis of food samples for detection of *L. monocytogenes* is an essential step in determining the quality of food. India is one of the major seafood exporting countries (MPEDA 1999) and is concerned about the presence of *L.monocytogenes* as recently, more and more importing countries examine consignments for the presence of this pathogen.

The current methodology for detection or numeration of *L. monocytogenes* usually involve primary enrichment, secondary selective enrichment, isolation on selective medium and finally confirmation of the *Listeria* by using a battery of biochemical tests which requires about 8-10 days. Also based on the biochemical tests, it is often difficult to differentiate *L. monocytogenes* from *L. innocua* or virulent strains of *L. monocytogenes* from avirulent ones. Thus, the conventional method is cumbersome, skilled and labour intensive as well as time consuming. Therefore, there is a need to develop a rapid, reliable and simple method for detection of *L. monocytogenes*. Such a test would be useful in screening at a time a number of samples. Our experience during small-scale surveillance studies for *Listeria* by employing prevalent standard methods like USFDA/PHLS (UK) in various foods is confusing. This organism was not detected in food of animal source like meat, fish and their products (Kamat and Nair 1994) but was found in some samples of ice cream and vegetables (Warke et al. 2000, Pingulkar et al. 2001)

DNA probe hybridization technique provides a specific, rapid and reliable way to identify the foodborne pathogens (Datta 1990; Notermans and Werners 1990; Walcott 1992; Bandekar et al 1995). Colony hybridization is more suitable method for screening a large number of food samples at a time. Although the polymerase chain reaction (PCR) is also reported to be a powerful technique for detection of *Listeria monocytogenes* (Almeida & Almeida, 2000), it detects both viable and non-viable cells. Practically this is less significant from food safety point of view. Considering all the above mentioned problems encountered in the conventional methods; the focus has been in the last few years on the use of recombinant DNA techniques to detect *L. monocytogenes* (Datta et al. 1987). The Food and Drug Administration (USFDA) was the first to develop a DNA probe for *L. monocytogenes* by using a virulent gene, the hemolysin and has shown that non hemolytic *L. monocytogenes* could not be detected by this probe (Datta et al 1987; Gavalchin et al 1992). Thereafter Mengaud et al (1988) cloned the *hlyA* gene in pUC18 to get pLis3 (Mengaud et al 1989) and showed its essential role in intracellular survival and therefore in virulence of *L. monocytogenes* by gene

complementation of a non hemolytic mutant (Cossart et al 1989). Using southern hybridization technique they claimed specificity of *hlyA* gene probe for *L. monocytogenes* (Mengaud et al 1988). In this study, this fact was further explored to detect *L. monocytogenes* in various foods using a simple colony hybridization (CH) technique using *hlyA* gene probe. Total sixty two samples of vegetables, fish and meat procured from local market were screened at various stages of enrichment for the presence of *L. monocytogenes* by both conventional and CH techniques. Both the methods are comparable in detecting *L. monocytogenes* and in some vegetables CH technique was observed to be more sensitive than the conventional one.

Materials and Methods

Food samples : Ten samples of fish (mackerel, Bombay duck, shrimp and golden anchovy), 44 samples of vegetables (coriander leaves, tomatoes, carrot, cabbage and beet root) and 8 meat samples were obtained from different markets in Mumbai (India). Fish and meat samples were brought to the laboratory in ice containers. Samples, in 25 g were analyzed for the presence of *L. monocytogenes* by standard procedure given in Bacteriological Analytical Manual (FDA, 1984) as well as colony hybridization.

Chlorine treatment : The fresh coriander leaves were procured from local market. These were then washed in running tap water. One set of coriander leaves was given Chlorine water (250 ppm) dip treatment for 10 min at ambient temperature. Coriander leaves of untreated and Cl₂ treated sets were air-dried and packed, (25 g) in the polyethylene bags (22 cm x 15 cm) with blotting paper padding for absorbing moisture during storage at 8-10° C.

Gamma irradiation : Chlorine water treated and untreated coriander leaves in pouches were exposed to gamma radiation at melting ice temperature at 1 kGy dose in package irradiator (Atomic Energy, Canada Limited., Canada) at the dose rate 0.06 kGy / min. (IAEA 1977). Fresh washed tomatoes packed in polyethylene bags were also irradiated at 1 kGy dose and stored at 8-10° C.

Treated coriander leaves and tomatoes were stored at 8-10° C for two weeks and were analysed by standard procedure and *bly A* gene probe method.

Bacterial cultures : Cultures of *Listeria* were obtained from Dr. Hof (Klinikum dr Stadt Mannheim, Germany) and Dr. McLauchlin (PHLS Central PublicHealth Laboratory, London, NW9 5HT U.K.) *Yersinia enterocolitica* 5692 and *Escherichia coli* 0157 : H19 were obtained from Dr. Hitchins (USFDA) and the Czechoslovak Collection of micro-organisms Brno, Czechoslovakia respectively. *Bacillus cereus* and other organisms are food isolates from our collection. pLis 3 (pUC18 containing *bly A* gene) was a kind gift from Dr. Cossart (Pasteur institute, France). Strains of all the cultures were grown in Brain Heart Infusion (BHI) broth and maintained in the same medium at refrigerating temperature.

Isolation of *Listeria monocytogenes* : For isolation of *Listeria* from food samples standard USFDA /PHLS procedures were adopted (Kamat and Nair 1994). Food samples were subjected to cold enrichment in BHI at 4-10° C followed by selective enrichment in *Listeria* Enrichment Broth (LEB) at 37° C and plating on *Listeria* Selective Agar (LSA). In case of PHLS procedures primary enrichment in 1% buffered peptone water at 30°C was followed by secondary enrichment in *Listeria* Selective Broth (LSB). The presumptive positive *Listeria* colonies from LSA plates were further identified to species level on the basis of their biochemical reactions (FDA 1984).

Inoculation of fish samples : Fresh fish was eviscerated and muscle piece was aseptically inoculated by immersing it in the saline containing 10⁸ cfu / g cells of *L.monocytogenes* (1708 &35152) at ice water temperature (Kamat and Nair, 1995). A 10% homogenate of fish was diluted in saline and calculated amounts were used for CH experiment. The respective dilutions were simultaneously plated on Standard Plate Count Agar (SPCA), incubated overnight at 37°C for enumeration of bacteria.

Preparation of ³²P labeled DNA probe : The pLis 3 plasmid containing *bly A* gene was digested by restriction enzyme EcoRI (Mengaud et al.1989) and the fragment (<1kb) containing approximately 500 bp coding region of *blyA* was separated by low melting

agarose gel electrophoresis. This fragment was, then precipitated by alcohol, labeled with ³²P by random primer labeling method, and used as a probe (Sambrook et al 1989).

DNA colony hybridization : For colony hybridization, the bacterial strains under test were grown overnight at 37°C in the BHI broth and spotted (10µl) on the agar plates. After overnight incubation at 37°C colonies of various cultures (18-20 numbers) were transferred to nitrocellulose filters (HATF.085 25, 0.45µm Millipore Corporation, Bedford, MA 01730.) in a grid form and subjected to hybridization procedure described by Sambrook et al (1989). Probes with specific activity of 5x10⁷ c p m / ml were used

In case of samples; broth samples under enrichment stages from various foods, 10 µl portions of the broth were transferred on nitrocellulose papers and processed for CH as mentioned above.

Results And Discussion

Specificity of the *blyA* gene probe : Results of colony hybridization using ³²P labeled pLis 3 with 6 standard *Listeria monocytogenes*, 5 food isolates, other *Listeria* species and non - *Listeria* organisms are show that in (Table1) all strains, hemolytic as well as non - hemolytic *L. monocytogenes*, were positive whereas all other *Listeria* species and bacteria of other genus were negative under optimum hybridization conditions. These results corroborate the findings of specificity of *blyA* gene probe observed by Mengaud et al (1988) in detection of *L.monocytogenes* by Southern hybridization. Further the essential role of *bly A* gene in intracellular survival of *L.monocytogenes* using gene complementation of a non-hemolytic mutant has been revealed (Cossart et al 1989).

Sensitivity : The results of the sensitivity of *L.monocytogenes* 35152 & 1708 strains in saline and fish homogenate show that to get positive signals in autoradiogram, the 10⁷cfu/ml were needed for both saline and fish homogenate samples. These observations coincide with the reported finding that ³²P labeled probes routinely detect approximately 10⁷ to 10⁸ bacteria (Walcott1991).

Table 1: Response of bacteria to DNA colony hybridization using *HLyA* gene probe

Organisms	Colony hybridization
<i>Listeria monocytogenes</i>	+
1708	+
5641	+
19111	+
19112	+
036	+
35152	+
<i>Listeria seeligeri</i>	+
<i>Listeria welschbimeri</i>	-
<i>Listeria innocua</i>	-
<i>Listeria monocytogenes</i> (Food isolates)	
Cdr1	+
Cps1	+
Brit4	+
Cabg5	+
Tm2	+
<i>Yersinia enterocolitica</i> 5692	-
<i>Escherichia coli</i> 0157:H 19	-
<i>Salmonella typhimurium</i>	-
<i>Pseudomonas aeruginosa</i>	-
<i>Staphylococcus aureus</i>	-
<i>Bacillus cereus</i>	-

a - +ve; positive for *blyA* probe

b - -ve; negative, no signal detected

Table 2: Screening of food samples for *L. monocytogenes* using colony hybridization and culture method

Sample	Number of samples	Incidence of <i>L. monocytogenes</i>		
		After plating on ISA	After II enrichment	
			Culture method	CH method
Fish	10	Nil ^a	Nil	Nil
Meat	8	Nil	Nil	Nil
Vegetables				
Coriander	18	Nil	9	11
Carrot	8	Nil	4	4
Cabbage	6	Nil	2	4
Beet root	2	Nil	1	1
Tomato	10	Nil	6	10

ISA - *Listeria* selective agar

a - Nil - No *Listeria monocytogenes* detected

Table 3 : Detection of *L. monocytogenes* in irradiated and unirradiated tomatoes and coriander leaves by *HlyA* gene probe and conventional method

	Sample no	GH method after enrichment	Conventional method Identified as <i>Listeria monocytogenes</i>	
			I	II
Tomato		I BHI	II LEB	
Control	2	+	+	+
Initial	1	+	+	-
	1	-	-	-
15 days	2	+	+	
	2	-	-	-
Irradiated (1kGy)	4	-	-	-
Initial	4	-	-	-
coriander leaves				
Control	3	+	+	+
Initial	2	-	+	-
15 days	2	+	+	+
	1	+	+	-
	1	+	-	-
	1	-	-	-
Cl ₂ (250ppm)				
Initial	2	+	+	+
	2	+	+	-
15 days	1	+	+	+
	2	-	-	-
	3	-	+	-
	4	+	+	-
Irradiated (1 kGy)				
Initial	5	-	-	-
15 days	5	-	-	-

L. monocytogenes detected ----- + *L. monocytogenes* not detected -----

Screening of food samples : Table 2 gives the results of comparison of CH with culture method for identification *L. monocytogenes*. None of the samples tested has shown presence of *L. monocytogenes* on direct plating on L.S.A. and both the methods required an enrichment step for a positive detection of the pathogen

Fish and meat : *Listeria monocytogenes* was not isolated from any of the 6 fresh fish and 5 meat samples tested by either the USDA/ PHLIS method or CH method. Thus, these findings support our previous reports describing the absence of *L. monocytogenes* in seafood and meat from local markets (Kamat and Nair 1994).

Vegetables : The presence of *L. monocytogenes* was detected by both the methods, in 4 out of 8 carrot samples and 1 out of 2 beet roots by both the methods. On the other hand in case of other vegetables such as coriander leaves, cabbage, and tomatoes; overall higher number of *L. monocytogenes* positive samples were found when determined using CH procedure versus the culture method. It is pertinent to mention here that many researchers have experienced the difficulty in recovering *L. monocytogenes* from food by the prevalent routine procedures. (Farber and Peterkine 1991) because foods under analysis contain large mixed microbial population which hamper recovery and identification of *L. monocytogenes*. Some reports have revealed that the presence of predominating *Listeria* species varied with the method adopted for the isolation (Pini and Gilbert 1988; Kamat and Nair 1994). A recent study demonstrated that in the enrichment broths commonly used, the growth of *L. innocua* is favoured when grown together with *L. monocytogenes* (Petran and Swanson 1993). On the other hand, CH procedure, as developed by targeting a specific gene in the pathogen, is more specific (Table 1)

Treated/ Irradiated

Tomatoes : Table 3 shows the comparative results of the detection of *L. monocytogenes* in 4 samples of unirradiated as well as irradiated tomatoes using both CH and conventional method. It can be noticed that 3

out of 4 unirradiated tomato samples showed presence of *L. monocytogenes* by CH method. However, its presence was not detected in two samples by the conventional method. On storage at 15° C for 15 days also two out of four samples showed the presence of *L. monocytogenes* when determined by CH method but not by conventional method. Also application of both the methods, did not detect the pathogen in irradiated tomatoes even after cold storage.

Coriander leaves : As can be seen from Table 3 when analysed by routine conventional method, 3 out of 5 samples of leaves (control) exhibited presence of *L. monocytogenes*. On the other hand by CH procedure all the samples including other two were also noticed to be *L. monocytogenes* positive. Higher efficacy of CH procedure in detecting *L. monocytogenes* was also observed in Chlorine water treated leaves. However, those coriander leaves which received radiation (1kGy) did not show the presence of *L. monocytogenes*.

In conclusion the present study demonstrated that detection of *L. monocytogenes* in food by CH method, using *bly A* gene probe, is a less laborious and less time consuming technique than the routine culture method. The *bly A* gene probe method was more sensitive in identifying *L. monocytogenes* in vegetables and can also be applied to other foods. The documented worldwide evidences of the presence of *L. monocytogenes* in raw vegetables and animal origin food and their association in outbreaks coupled with their ability to grow at refrigeration temperature has given rise to the concern from public health point of view (Farber and Peterkin 1991). In this background development of a sensitive detection method such as CH method is significant in assessment of quality of food for export as well for internal consumption.

Acknowledgments

The authors thank Dr. Cossart for the kind gift of pLis3 containing *bly A* gene.

References

1. Almeida PF, Almeida RCC (2000) A PCR protocol using in *l* gene as a target for specific

- detection of *Listeria monocytogenes* Food Control 1: 97-101
2. Bandekar JR , Ussuf KK, Nair PM (1995) Detection of *Salmonellae* in chicken and fish samples using DNA probe J Food Safety 15 :11-19
 3. Cossart P, Vicente MF, Mengaud J, Baquero F, Perez-Diaz, JC, Berche P(1989) Listeriolysin O is essential for virulence of *Listeria monocytogenes* : direct evidence obtained by gene complementation Infect Immun 57 :3629-3636
 4. Datta AR , Wntz BA , Hill, WE (1987) Detection of hemolytic *Listeria monocytogenes* by using DNA colony hybridization Appl Environ Microbiol 53:2256-2259
 5. Datta, AR (1990) Identification of foodborne pathogens by DNA probe hybridization techniques Dev Ind Microbiol 31 Suppl 5: 165-173
 6. Farber JM , Peterkin PI (1991) *Listeria monocytogenes*, a food borne pathogen Microbiol Rev 55: 476 -511
 7. FDA (1984) Bacteriological Analytical Manual ,6th edn. , Association of Official Analytical Chemists, Arlington, VA
 8. Gavalchin J, Landy K, Batt CA (1992) Rapid Methods for the detection of *Listeria*, In: *Molecular Approaches to Improving Food Quality and Safety*, (Bhatnagar D, Cleveland TE, eds) Van Norstand, Reinhold, N Y, pp189- 204
 9. IAEA (1977) Manual of food Irradiation Dosimetry Technical Report Series No 178 IAEA, Vienna, Austria
 10. Kamat AS ,Nair PM (1994) Incidence of *Listeria* species in Indian seafoods and meat J Food Safety 14:117-130
 11. Kamat A, Nair PM (1995) Gamma irradiation as a means to eliminate *L monocytogenes* from frozen chicken meat J Sci Food Agric 69: 515-422
 12. Mengaud J, Vicente MF , Chenevert J, Moniz-Pereira J, Geoffroy C , Gicquel- Sanzey B , Baquero F, Perez-Diaz JC, Cossart P (1988) Expression in *Escherichia coli* and sequence analysis of the listeriolysin O determinant of *Listeria monocytogenes* Infect Immun 56: 766-772
 13. Mengaud J, Vicente MF, Cossart P (1989) Transcriptional Mapping and Nucleotide sequence of the *Listeria monocytogenes* *blyA* region reveal structural features that may be involved in regulation Infect Immun 57(12) :3695-3701
 14. MPEDA (1999): The Marine Product Export Development Authority India. pp203
 15. Notermans S , Wernars K (1990) Evaluation and interpretation of data obtained with immunoassays and DNA-DNA hybridization techniques Int J Food Microbiol 11: 35-50
 16. Petran RL, Swanson KM J (1993) Simultaneous growth of *Listeria monocytogenes* and *L innocua* J Food Prot 56: 938-943
 17. Pini PN, Gilbert RJ (1988) A comparison of two procedures for the isolation of *Listeria monocytogenes* from raw chickens and soft cheese In J Food Microbiol 7: 331-337
 18. Pingulkar K, Kamat, AS ,Bongirwar DR (2001) Microbiological quality of fresh leafy vegetables, salad components and read -to -eat salads: an evidence of inhibition of *Listeria monocytogenes* in tomatoes Food Sci nutrión 52 : 15-23
 19. Sambrook J, Fritsch EF, Maniatis T (1989) *Molecular Cloning ; A Laboratory Manual* 2nd edn, Cold Spring Harbor, NY
 20. Walcott MJ (1991) DNA-based rapid methods for the detection of foodborne pathogens J Food Protect 54: 387-401
 21. Warke R, Kamat A ,Kamat M, Thomas P (2000) Incidence of pathogenic psychrotrophs in ice creams sold in some retail outlets in Mumbai, India Food Control 11:77-83

This paper received the 3rd Best Poster Paper Presentation Award in the First International Conference on 'Global Sustainable Biotech Congress 2000 A.D.', held at Nagpur University, Nagpur, during November 26, 2000-December 1, 2000.

About the authors



Dr. (Ms.) Anu S. Kamat joined Food Technology Division of BARC in 1967 after her graduation in Microbiology/Chemistry from Mumbai University. Since then, she has been involved in research on development of radiation processes for highly perishable food commodities like fish and meat. She obtained her M.Sc. and thereafter Ph.D. (Biochemistry) for her thesis entitled "Studies on Germination and Radiation Resistance of Bacterial Spores". Her research work comprises of the topics such as application of radiation technology for enhancement of shelf life of seafoods and meat, surveillance of locally available foods like seafoods, meat and meat products, vegetables and other ready to eat vegetables and dairy products for presence of newly emerged food borne pathogens like *Listeria monocytogenes* and *Yersinia enterocolitica*. Contamination of these organisms in seafoods and meat has great significance from their export point of view. She has shown that application of low dose radiation successfully eliminates them. Her field of specialization is microbial safety of food in general and irradiated food in particular. At present, she is engaged in development of combination processing treatment of radiation and High pressure to control of bacterial spores contamination at practically feasible doses. Besides this, she is associated with two IAEA projects and she is the chief investigator of one of them, viz "Studies on Microbiological Analysis of Seafoods and their Products for Export with special reference to Human Bacterial Pathogens for Improvement of Seafood Export". During her research tenure, she has attended many national/international seminars and earlier she received the best paper awards at three occasions. Based on the references of her scientific publications in national/International journals, her biography sketch has been selected for inclusion in the 15th edition, 1998 World's Who Who, published by Who's Who in America; and Marquis Who's Who.



Dr. D.R. Bongirwar obtained his B.Tech. degree in Chemical Engineering from Nagpur University in 1963. He joined 7th batch of BARC Training School and then joined the erstwhile Biochemistry & Food Technology Division, BARC. In 1976, he was awarded the doctoral degree in Engg. & Technol. by Nagpur University for his dissertation on 'Improved Dehydration Processes in Food Preservation'. At present, he is Head, Food Technology Division and Project Manager, Food Irradiator Project, BARC. Dr. Bongirwar has made significant contribution in the areas of radiation preservation of foods and design, construction and installation of radiation processing facilities, allied workshop machinery and food processing equipment. Besides designing and developing processes for food preservation

like osmotic drying, freezing drying, defatting of peanuts/soybean, solar drying technique for farmers and traders, he is vigorously pursuing programs for consumer acceptance of radiation-processed foods within the country. He has been chiefly responsible for installation of India's first radiation processing facility for processing food at BARC 1967. He is also instrumental for design, construction, installation and commissioning of country's first ever demonstration facility POTION for processing of potato, onion and other low dose products at Lalgaon in Maharashtra. Dr. Bongirwar is the recipient of Gardner's Award instituted by AFST(I) and Yezdi Award of All India Food Preserver's Association. He has extensively travelled abroad on various assignments like IAEA fellowship, Indo-German Bilateral agreement, etc, visiting the US, Germany, Canada and South-East Asian countries and participated as an expert at FAO/IAEA/WHO conference and other national/international forums representing DAE. Dr. Bongirwar is closely associated with numerous professional scientific bodies like IVS, INS, IARP, NAARRI, AFST(I) and Indian Society for Nuclear Techniques in Agriculture & Biology. He is a Fellow of Indian Institute of Chemical Engineers and Cryogenic Council. He is an examiner for Ph.D & M. Tech. Degrees of IIT, Mumbai and IIT, Kharagpur, University of Mumbai and SNET University, Mumbai. He has authored monograph on 'Food Preservation by Irradiation' and a technical document on 'Radiation Processing of Foods' as a guideline to set up a radiation processing plant. Dr. Bongirwar has more than 100 publications to his credit in national as well as international journals and are widely cited. Dr. Bongirwar is the President of AFST(I), Mumbai Chapter for the current year (2001-02).

Dr K.K. Usuf, another co-author of this paper, has left BARC.

Modeling of Ductile Fracture by Gurson Model

M.K. Samal, B.K. Dutta and H.S. Kushwaha

Reactor Safety Division

Bhabha Atomic Research Centre

Abstract

The most serious limitation of the classical fracture mechanics is the non-transferability of the specimen data to the component level. This difficulty is largely overcome by the damage mechanics, which model the drop in load carrying capacity of a material with the increase in plastic strain. Such modeling is done considering nucleation, growth and coalescence of the voids in a material following large-scale plasticity. The material constitutive model is modified to consider such phenomena. A finite element in-house BARC code MADAM has been developed based on such principle. The constitutive model introduced by Gurson and modified by Tvergaard and Needleman has been implemented in this code. The code has been tested, verified and used analysing number of fracture specimens and piping components in BARC and at MPA, Stuttgart. The Indian and German piping materials have been considered in these analyses. Some of the results obtained by this code and comparison with experimental results are presented in this paper to show the usefulness of damage mechanics in analysing real life power plant components with flaws.

Introduction

THE INFLUENCE OF CRACK TIP CONSTRAINT ON ductile-fracture resistance is of major concern in the assessment of structural integrity employing conventional fracture mechanics concepts. Constraint is a structural feature, which inhibits plastic flow and causes a higher triaxiality of stresses. Experimental results show that the conventional single-parameter criteria (such as J-integral or crack-tip opening displacement CTOD) is unable to describe ductile crack growth satisfactorily. The specimen size and geometry have a pronounced effect on the fracture resistance curve. The continuum damage mechanics is one alternative approach to solve this problem. This involves simulation of the failure process using a constitutive relationship representing microscopic rupture processes. As a result, these models (also called micro-mechanical models) are able to consider implicitly the physical effect of constraint on the fracture resistance. The crack initiation and the

propagation occur with the local degradation of the material loosing completely its load carrying capacity. This is characterized using a critical value of the void volume fraction f_c over a characteristics distance l_c . The advantage of such modeling is that the corresponding material parameters can be used for analyzing specimens and real life components of any geometry. The required micro-mechanical parameters are determined from the simple tensile tests of notched bars, metallographic study of the material, and comparison of experimental and numerical simulation curves of smooth and notched tensile specimens.

A finite element BARC code **MADAM** (**MATERIAL DAMAGE MODELING**) has been developed using the principles of damage mechanics. The Gurson-Tvergaard-Needleman material constitutive model has been incorporated. The code has been used in BARC and at MPA to analyse number of fracture specimens and piping components made up of Indian and German materials. In the following, some results are presented

to demonstrate the stress state dependency of J-resistance curves with the help of this code. The results are presented for two German materials DIN StE460 (ferritic material) and DIN X6CrNiNb 18 10 (austenitic material). The details of their properties are given in references [1] and [5]. Five different types of fracture specimens have been analyzed. These are C(T) (compact tension), SE(B) (single edged notched bend), M(T) (middle tension), SE(T) (Single Edged notched Tensile) and DE(T) (Double Edged Notched Tensile) specimens respectively. The results of a straight pipe having a 122° circumferential through-wall crack have been also presented to show the analytical capability of the code. This pipe has been tested at MPA under an internal pressure of 16 MPa and increasing bending moment. The analysis has been carried out on a super-computer at MPA as part of an Indo-German Bilateral project on 'Transferability of specimen data to component level'.

Modified Gurson Model for Ductile Tearing

Based on the work of Berg [2] (which shows that a porous medium is governed by the normality rule), Gurson [3] derived a constitutive model for materials containing either cylindrical or spherical voids.

$$\phi(\sigma_{ij}, \sigma_M, f) = \frac{\sigma_{ij}^2}{\sigma_M^2} + 2f^* q_1 \cosh\left(\frac{q_2 \sigma_{ij}^2}{2\sigma_M}\right) - \left[1 + q_3 (f^*)^2\right] = 0$$

Here $\sigma_{ij} = \left(\frac{3}{2} s_{ij} s_{ij}\right)^{\frac{1}{2}}$ is the macroscopic effective stress, $s_{ij} = \sigma_{ij} - \frac{1}{3} \sigma_M \delta_{ij}$ represents the stress deviator.

and σ_M is the flow stress of the matrix material. The above yield function reduces to von-Mises yield criterion for f equals to zero. Tvergaard [4] introduced the parameters q_1 and q_2 in order to bring the predictions of Gurson model closer to the experimental values. The function $f(f)$ was introduced by Tvergaard and Needleman [4] to model more rapid loss of material stress carrying capacity after the occurrence of voids coalescence. This function is expressed as follows.

$$f = f \quad \text{for } f < f_c$$

$$= f_c + \frac{f^* - f_c}{f_j - f_c} (f - f_c) \quad \text{for } f \geq f_c$$

The function becomes more predominant once void volume fraction f exceeds a critical value f_c . The complete loss of load carrying capacity occurs at $f=f_j$. The ultimate void volume fraction in that condition is $f_u = f(f_j) = 1/q_1$. The increase in void volume fraction is due to combined effect of void nucleation and growth. The mathematical expressions for modeling these processes can be found in reference [4].

BARC Inhouse Damage Mechanics Code 'Madam'

A finite element based computer code has been developed in BARC for structural safety analysis of power plant components. The code has been tested and verified against number of case studies and also by participating in an international benchmark round robin exercise conducted by GRSS (Germany). Some of the salient features of the code are as follows.

1. Finite element based code.
2. Considerations of 2-D (plane strain and axisymmetric) and 3-D structures.
3. Availability of 8-noded iso-parametric elements for modeling 2-D structures and 20-noded brick elements for 3-D structures.
4. Availability of 2X2 and 3X3 gauss point integrations.
5. Analytical capability of elastic, elastic-plastic and damage mechanics.
6. Use of von-mises yield criteria, Prandtl-Reuss flow rule and isotropic strain hardening for conventional elastic-plastic analysis
7. Use of Gurson constitutive model and associated flow rule for damage mechanics analysis.
8. Solution of nonlinear equilibrium condition by Rik's method (arc length method) or Newton-Raphson method depending upon the user's choice.
9. Availability of following four solvers for solution of simultaneous equations.
 - a. Active column profile solver.
 - b. Frontal Solver.

- c. Preconditioned conjugate gradient (PCG) solver.
 - d. Sparse Solver.
- Any one of these solvers can be used depending upon the user's choice.
10. Availability of routines as post-processor for computing 2-D/3-D J-integral using EDI method and critical void growth using Rice-Tracey integral.

Gurson Material Parameters for Damage Mechanics Analysis

The Gurson material parameters required for the analysis are as follows.

1. Initial void volume fraction ' f_0 '.
2. Critical void volume fraction at coalescence ' f_c '.
3. Final void volume fraction ' f_f '.
4. Void volume fraction at saturated nucleation ' f_s '.
5. Mean value of strain for nucleation ' ϵ_n ' (for strain controlled nucleation).
6. Standard deviation of strain for nucleation ' s_n '.
7. The constants q_1 , q_2 and q_3 .
8. Critical length parameter ' l_c ' (required for the analysis of cracked specimens) and
9. The ultimate modified void volume fraction at fracture ' f_u '.

The values of the parameters f_0 , f_c , f_s , ϵ_n , s_n , f_u and l_c for the present materials are determined by a hybrid methodology of metallographic study, experiment on tensile tests and subsequent numerical analysis. The values obtained for materials SE460 and X6CrNiNb are as follows.

Material	f_0	f_c	f_s	ϵ_n	s_n	f_u	q_1	q_2	q_3	f_u'	l_c
SE460	0.0025	0.021	0.02	0.3	0.1	0.19	1.5	1.0	2.25	0.566	0.11
X6CrNiNb	1e-6	0.05	0.0055	0.2	0.3	0.1	1.5	1.0	2.25	0.566	0.10

Analysis of Notched Tensile Specimens and Determination of Void Volume Fraction at Coalescence

The values of critical void volume fraction at coalescence ' f_c ' shown above have been determined by analysing a number of round notched tensile bars using code MADAM. This is a widely used practice for the determination of f_c . The nominal cross section of the grooved tensile specimens has a diameter of 18

mm and reduced diameter at groove is 10 mm. The sketch of the specimen is shown in Fig. 1. The finite element mesh of the specimen is shown in Fig. 2. The analyses have been done for two different notch radii of 4mm and 10mm. The experimental results have been taken from reference [1]. The parameter f_c has been determined focusing particularly the point of sudden drop in load-diameter contraction (ΔD) curves for both the grooved specimens. This point in the load- ΔD curve is primarily influenced by the value of f_c . A comparison of the experimental load-diameter contraction (ΔD) curve with the numerically simulated curve for both the grooved specimens are shown in Fig. 3 and Fig. 4 respectively for SE460 material. The value of f_c has been found to be 0.021 through this exercise. For the stainless steel X6CrNiNb material, the notched tensile specimens have the same dimensions except that the three notch radii of 2, 4, and 8mm have been considered. Following the similar procedure, the parameter f_c has been found out to be 0.05 for this material. A comparison of experimental and numerical analysis results of the notched tensile specimens for the stainless steel material are also shown in Figs. 5, 6 and 7 for different groove radii.

Expressions used for J-Integral Determination

The J-integral in damage mechanics analysis is generally calculated using the energy concept. The expressions for J-integral for a CT specimen, a TPB specimen and a straight pipe are given below.

For compact tension (CT) specimens

The J-integral is evaluated from the area under the load-displacement curve at a particular crack growth using ASTM standard formulae given below.

$$J = J_0 \left(1 - \frac{\gamma \Delta a}{(W - a_0)} \right) = \frac{\eta U}{B_s (W - a_0)} \left(1 - \frac{\gamma \Delta a}{(W - a_0)} \right)$$

Here U is the area under load v/s deflection curve, W is the width of the specimen, B_s is the net thickness,

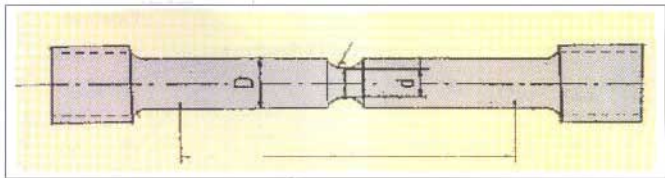


Fig. 1 A notched tensile specimen ($D=18\text{mm}$, $d=10\text{mm}$, $l_r=5D$, $r=\text{notch radius}$)

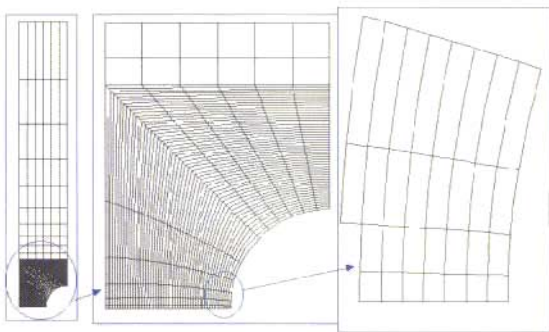


Fig. 2 Finite element mesh of the notched tensile specimen having 4mm notch radius.

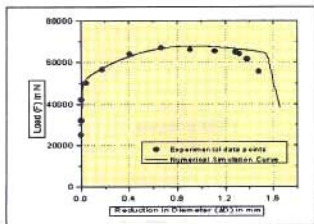


Fig. 3 Load vs reduction in diameter curve for the notched tensile specimen with 4mm notch radius

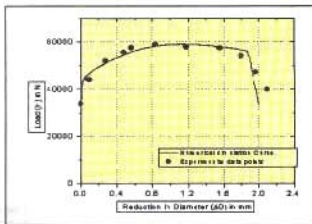


Fig. 4 Load vs reduction in diameter curve notched tensile specimen with 10 mm notch radius

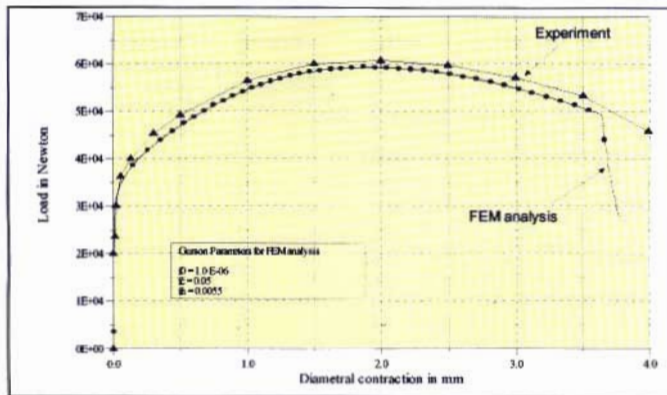


Fig. 5 Load v/s Diametral contraction curve of a notched tensile specimen of 2 mm notch radius (Material X6CrNiNb)

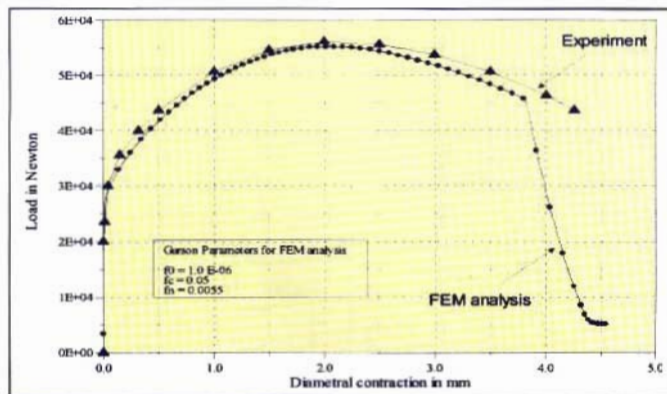


Fig. 6 Load v/s Diametral contraction curve of a notched tensile specimen of 4 mm notch radius (Material X6CrNiNb)

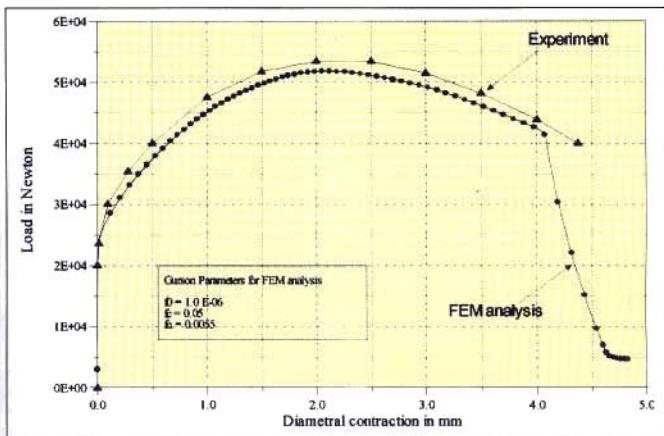


Fig. 7 Load v/s Diametral contraction curve of a notched tensile specimen of 8 mm notch radius (Material X6CrNiNb)

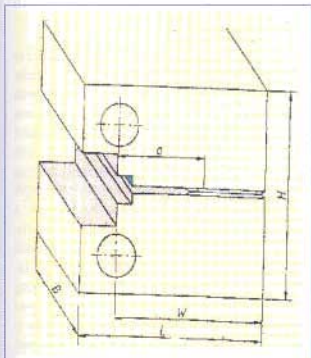


Fig. 8 A Compact Tension specimen ($W=50\text{mm}$, $a=33.25\text{mm}$, $B=25\text{mm}$, $B_n=20\text{mm}$, $H=60\text{mm}$, $L=62.5\text{mm}$, 20% side-grooved)

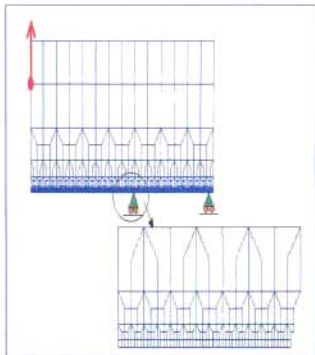


Fig. 9 Finite element mesh of a compact tension specimen

$\eta = 2 + 0.522 \cdot (1 - a/\sqrt{W})$ and $\gamma = (0.75 \cdot \eta - 1)$. (ASTM E1152)

For three-point-bend (TPB) specimen

For deep cracked specimen, the expression is same as shown above, except that the value of η is taken as 2. For other a/W specimens, the U is taken as the area under load w/s CMOD curve. In such cases, the expression for J is as follows.

$$J = \frac{\eta \cdot U}{B \cdot n \cdot (W - a_0)}$$

Where $\eta = 3.5 - 1.42 \cdot (a/W)$ where 'a' is the current crack length

For pipes with through-wall circumferential flaw under four point bending load:

$$J_{pl} = \beta \int_0^{\delta_{pl}} P \cdot d\delta_{pl}$$

Here $2P$ is the total load, δ_{pl} is the plastic deflection, $\beta = -h'(\phi) / R \cdot t \cdot h(\phi)$, R is the mean radius of pipe in mm, $h(\phi) = [\cos(\phi/4) - 0.5 \sin(\phi/2)]$, t is the thickness in mm and ϕ is the total crack angle of the through-wall circumferential crack.

Analysis of Compact Tension Specimens

All the Gurson material parameters shown above have been used in the numerical simulation of C(T) specimens having 20% side grooved. The CT specimen dimensions are in accordance with the ASTM standard. The sketch of the C(T) specimen is shown in Fig. 8. The FE analysis has been done using MADAM code with plane strain formulation. The mesh is shown in Fig. 9. The unknown critical length parameter ' l_c ' has been determined comparing the numerically simulated J_{lc} value with the experimental value. The J-integral at each load step has been calculated using the above expressions. The results are shown in Figs.10 and 11 for the material StE460. From these analyses, the critical length parameter l_c has been found out to be 0.11mm for StE460 and 0.10mm for X6CrNiNb

materials. These have been used as the crack tip mesh size in the subsequent analyses of other fracture specimens and also in the analysis of a 3-D straight pipe with circumferential crack.

Analysis of Other Fracture Specimens

A number of other fracture specimens of different geometries have been analyzed to compare their J-resistance curves. The various specimens considered are M(T), SE(T), DE(T), and SE(B). The mesh near the crack tip is similar to that of C(T) specimen shown above. Appropriate boundary conditions have been imposed for various specimens. Few sample results are presented here for demonstration. Fig. 12 and 13 show the comparison of experimental and numerical J_e curves for SE(B) specimen for StE460 and X6CrNiNb materials respectively. A similar comparison is shown in Fig. 14 for M(T) specimen having StE460 ferritic steel material. All these figures show reasonable agreement between experiments and the numerical simulations. Fig. 15 shows the comparison of all the predicted J_e curves for five fracture specimens for StE460 material. The crack tip stress triaxiality dependency of J-R curve may be seen in this figure.

Analysis Of Straight Pipe With Circumferential Flaw

To demonstrate the usefulness of damage mechanics to analyse real life power plant components, the results are presented here for a straight pipe with circumferential flaw. The straight pipe, which was tested at MPA (Stuttgart), has a 122° circumferential through-wall crack. The component is loaded with internal pressure of 16 MPa and increasing bending moment. The Gurson parameters for X6CrNiNb material shown above are used for this purpose. A simple sketch of the pipe is shown in Fig.16. The fatigue pre-crack profile is shown in Fig.17. The sketch of the experimental loading setup is shown in Fig. 18. The finite element mesh of the pipe was prepared using PATRAN software. One fourth of the pipe was analysed due to symmetry. The finite element mesh of the pipe is shown in Fig. 19. A comparison of experimental and computed results of different parameters is shown in Figs. 20(a-d).

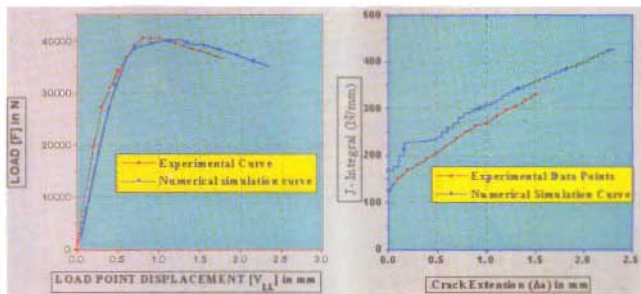


Fig.10 Comparison of experimental and computed Load v/s Load point deflection curves of a standard C(Y) specimen

Fig.11 Comparison of Experimental and computed J_c curve for material SE460 using C(T) specimen

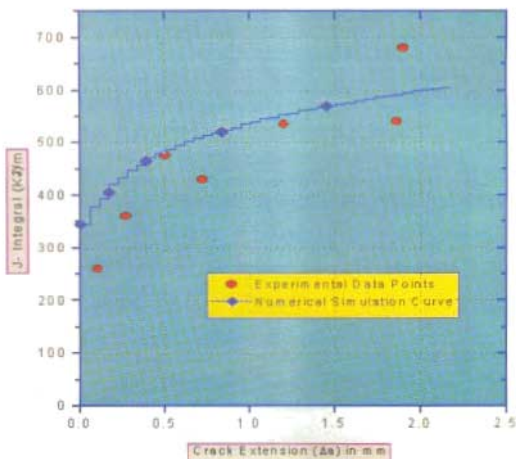


Fig.12 Comparison of Experimental and computed J_c curves for SE(B) specimen ($a/w=0.49$) for material SE460

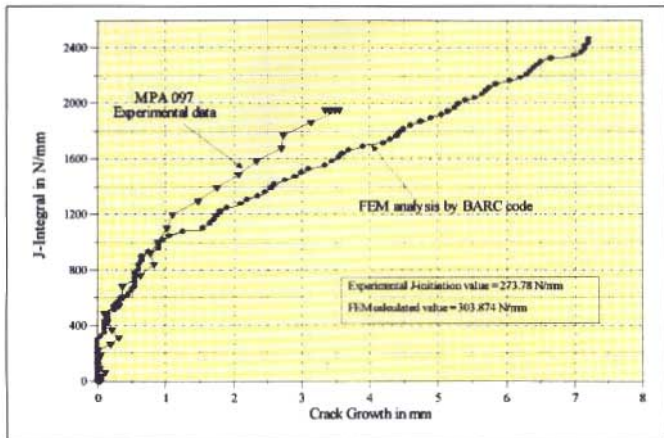


Fig. 13 Comparison of numerical and experimental J -resistance curve for a SE(B) specimen under three point bending load (Material X5CrNiNb, MPA Experiment No. ABV 097)

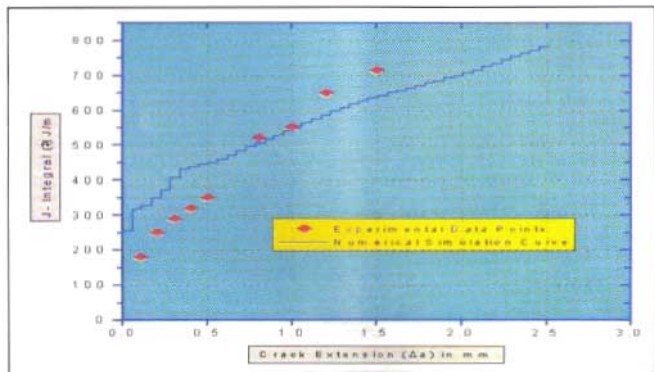


Fig. 14 Comparison of Experimental and computed J_c curves for M(T) specimen having $a/w=0.49$ for SIE460 material

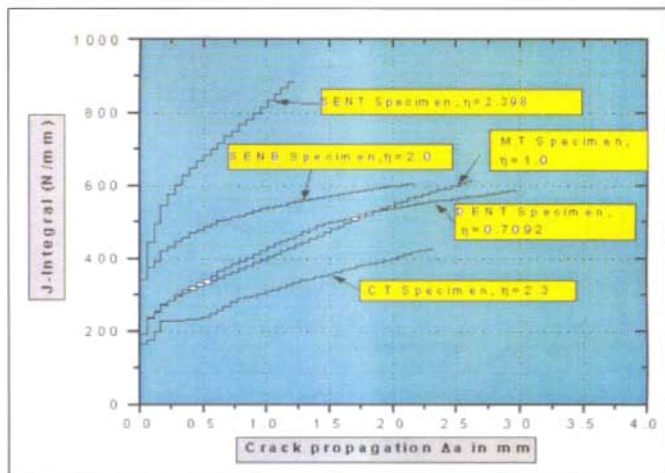


Fig.15 Comparison of J-Resistance curves for different fracture mechanics specimens for SIE460 material

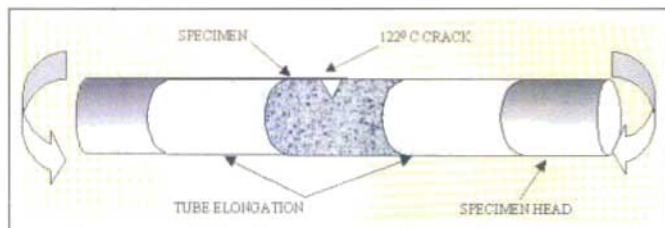


Fig.16A Sketch of the pipe specimen with 122° throughwall circumferential crack tested at MPA, Stuttgart

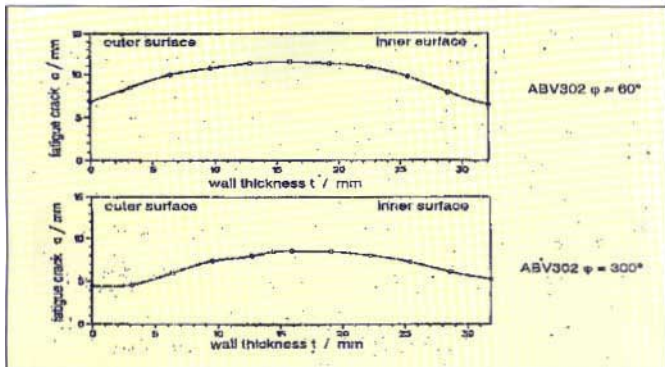


Fig.17 Fatigue crack profile of the crack front of the pipe tested at MPA, Stuttgart

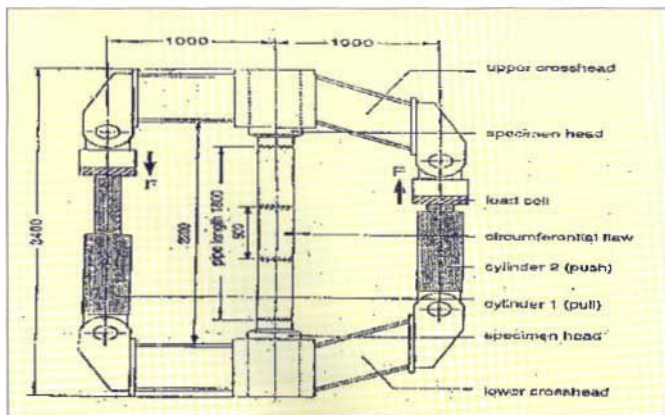


Fig.18 Sketch of the experimental setup used in the pipe fracture test under combined internal pressure and bending moment at MPA

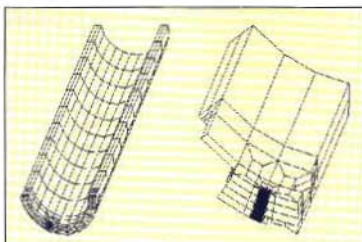
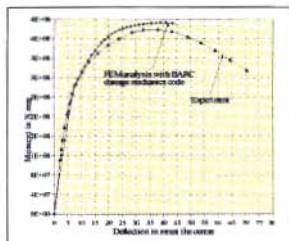
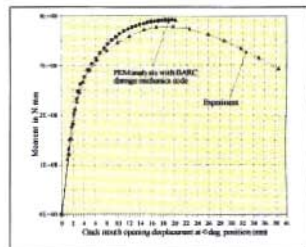


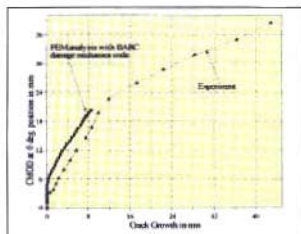
Fig.19 Finite element mesh of a straight pipe having 12° through wall circumferential crack.



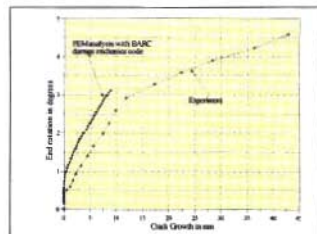
(a)



(b)



(c)



(d)

Fig. 20 Comparison of experimental *v/s* computed results for the pipe with 12° through-wall circumferential crack subjected to internal pressure and bending moment (Material X6CrNiNb MPA ABV302 Experiment)

a. Moment *v/s* deflection at center; b. Moment *v/s* CMOD; c. CMOD *v/s* crack growth; d. End rotation *v/s* crack growth

Conclusions

In the present work, the importance of damage mechanics has been shown over the classical fracture mechanics in analysing cracked components. The BARC in-house finite element code MADAM has been used for this purpose. The code has the capability of carrying out elastic, elastic-plastic and damage mechanics analysis of 2-D and 3-D components. The Gurson constitutive model has been incorporated for damage mechanics analysis. The code has been tested and verified against number of case studies and also by participating in an international round robin benchmark study conducted by GKSS (Germany). The code has been also used at MPA, Stuttgart on supercomputers for analysing number of straight pipes with flaws tested at SERC and also at MPA. Such exercise has been done as a part of an Indo-German collaborative program.

A number of grooved tensile specimens have been analysed to ascertain the Gurson material parameters for the Indian and German materials. These parameters are then used to analyse number of fracture specimens to demonstrate the dependency of J-resistance curve on the crack tip stress triaxiality condition. The results of a straight pipe with flaws under internal pressure and bending moment are presented. A close agreement between the computed and experimental data of various parameters shows the correctness of Gurson

parameters and importance of damage mechanics in analysing real life power plant components.

References

1. Brocks, W., Klingbeil, D., Kunecke, G., and Sun, D.Z., "Application of the gurson model to ductile tearing resistance", Constraint effects in Fracture, Theory and Applications: Second volume, (Eds. M. Kirk and Ad Bakker), *ASTM STP 1244*, 1995, pp. 232-252.
2. Berg, C.A., *Elastic behaviour of Solids* (Eds. M.F. Kanien et al), Mc Graw Hill Publ., 1970, pp. 171-210.
3. Gurson, A.L. "Continuum theory of ductile rupture by void nucleation and growth: Part I-Yield criteria and flow rules for porous ductile media", *J. Engg. Mat. Technology, Trans. of ASME*, Vol.9, 1977, pp.2-15.
4. Tvergaard, V. and Needleman, A., "Analysis of the cup-cone fracture in a round tensile bar", *Acta Metallurgica*, Vol 32, 1984, pp. 157-169.
5. Samal, M.K., Dutta, B.K., Kushwaha, H.S., "Three dimensional analysis of piping components using BARC damage mechanics code MADAM", Communicated for publication as BARC report, July 2001.

This paper was selected as one of the best papers in the poster session in 'National Conference on Computational Materials Science (NCCMS-2000)', July 27-29, 2000, organized by Materials Research Society of India, Mumbai Chapter.

Pheromones in the Management of Major Lepidopterous and Coleopterous Pests of Cotton

A.J. Tamhankar

Nuclear Agriculture and Biotechnology Division
Bhabha Atomic Research Centre

R.T. Gahukar

Plot :220, Reshimbag, Nagpur

and

T.P. Rajendran

Plant Protection Division,
Central Institute for Cotton Research, Nagpur

Abstract

Cotton is infested by over 30 pests belonging to lepidoptera and coleoptera. Amongst these insects, various bollworms and cotton boll weevil cause economic damage every year. In IPM, pheromones are considered to be an essential component because they are used for detecting the economic threshold levels of pest populations and for mating disruption as a direct pest suppression measure. Pheromones of major pests have been found to be effective, economic and eco-friendly in agro-ecosystems in which cotton is cultivated.

Introduction

ALL THE GROWTH STAGES OF THE COTTON suffer from insect attack and details on the economic importance of these insects; their biology, population dynamics and methods of their control, are well-documented (Frisbie, 1989; Gahukar, 1991; Matthews & Tunstall, 1994). Amongst the nearly 135 insect pests that infest cotton, economic plant damage is caused by lepidopterous and coleopterous insects. The various non-pheromonal management tactics that are employed to reduce the crop damage caused by these insects include mainly cultural and mechanical practices, releases of parasitoids and predators, use of microbial, botanical and chemical pesticides. These practices provide varying levels of efficiency of pest management in cotton and are available across the board. Since cotton is a cash-generating crop, cultivated over the last few decades,

indiscriminate use of insecticides has become widespread, in both the developed and the developing cotton growing countries. This excessive use of chemical insecticides has produced several undesirable effects including : development of resistance to insecticides; toxic residues on lint and seed; dangers to the environment, beneficial organisms and man. As a result, the concept of Integrated Pest Management [IPM] is becoming popular (Sundaramurthy & Gahukar, 1998) because it encourages the use of several components in the pest control system in a harmonious combination, which has a minimal impact on the environment.

When pheromones are used as a tool to monitor pest populations, it results in need-based use of pesticides (or any other pest management practice). As cotton cultivation is ridden with the large-scale use of insecticides, any reduction in the pesticide requirement

can make an economic impact in terms of a saving on production cost. Besides, pheromones can be used directly in the control of insects through mating disruption and can substitute for insecticide use for the suppression of populations of certain cotton pests. In cotton pest management, besides the sucking pests, the majority of insecticide usage is directed against lepidopterous and coleopterous insects that damage the fruiting bodies. This review discusses the utilization of pheromones in the management of the most damaging pest species of cotton. Some insect species occur sporadically on cotton crops and are of minor importance and utilization of their pheromones in IPM

is at a preliminary stage and therefore has been excluded from this review.

Pheromones, pheromone formulations and traps

Pheromones of several lepidopterous and coleopterous cotton pests have been identified and synthesized and only the primary references in this context are given in Table 1. Once identified, the pheromone components can be synthesized through varying alternate/improved/novel routes and this does not form the subject matter of this review. Experiments on some

Table 1. Pheromones of important insect pests of cotton.

S. No.	Insect species	Pheromone	References
1	<i>Pectinophora gossypiella</i>	*+Ph 1) Cis-7, cis-11-hexadecadienyl acetate (1) 2) Cis-7, trans-11-hexadecadienyl acetate (1) +At. - 1 & 2 in 1:1 ratio	*+Hummel et al. 1975 +Bierl et al. 1974
2	<i>Spodoptera littoralis</i>	*Ph: 1) cis-9, trans-11- tetradecadienyl acetate (35) 2) cis- 9- tetradecenyl acetate (46) 3) trans- 11- tetradecenyl acetate (9) 4) cis -11- tetradecenyl acetate (7) 5) cis- 9, cis -11- tetradecadienyl acetate (4) 6) cis- 9, trans-12- tetradecadienyl acetate (1-) +At: 1 and 6 in 1000: 1-5 ratio	*+Dunkelblum et al. 1982 Tamaki &Yushima 1974 Gampion et al. 1974
3	<i>Spodoptera litura</i>	*Ph: 1) cis-9, trans-11- tetradecadienyl acetate (5) 2) cis-9, trans-12- tetradecadienyl acetate (0.7) + At: 1 and 2 in 10: 1 ratio	*Tamaki et al. 1975 +Yashima et al. 1974 Tamaki et al. 1976
4	<i>Spodoptera exigua</i>	*Ph: 1) cis-9- tetradecenyl acetate (47.9) 2) cis-9- tetradecen-1-01 (4) 3) Tetradecenyl acetate (40.2) 4) cis-9, cis-12-tetradecadienyl acetate (6.5) 5) cis-11- hexadecenyl acetate (1.7) +At: 2, 3 and 5 in above ratio	*+Tumlinson et al. 1990 Shorey et al. 1974
5	<i>Helicoverpa armigera</i>	*Ph 1) cis-11-hexadecenal (43) 2) cis-9-hexadecenal (1-3) 3) hexadecenal (1-21) 4) cis-11-hexadecenal (1-9) 5) hexadecenal (trace) +At 1 and 2 in 100:1-10 ratio	*Nesbitt et al. 1979, 1980 +Kehat et al. 1980 Dunkelblum et al. 1980
6	<i>Heliothis virescens</i>	*Ph: 1) cis-11-Hexadecenal (81.4) 2) cis-9-hexadecenal (1.0) 3) cis-7-hexadecenal (1-3) 4) Hexadecenal (9.5) 5) cis-11-hexadecenal (3.2) 6) Tetradecenal (1.6) 7) Cis-9-tetradecenal (3. 2) +AT: 1,7,4,5in 65.1 :1.6 : 32.6 : 0.7 ratio	*Klun et al. 1980 +Ramaswamy et al. 1985 Roelofs et al. 1974 Tumlinson et al 1975 Klun et al. 1979 Teal et al. 1986

Table 1. (continued)

9	<i>Earias vittella</i>	<p>*Ph1) <i>trans</i>-10,<i>trans</i>-12-hexadecadienal (10)</p> <p>2) <i>cis</i>-11-hexadecenal (2)</p> <p>3) hexadecenal (1)</p> <p>4) octadecenal (2)</p> <p>5) <i>cis</i>-11-octadecenal (4)</p> <p>6) <i>trans</i>-10,<i>trans</i>-12-hexadecadienol (10)</p> <p>+At: 1,2 and 5 in 10:2:2 ratio</p>	<p>*+Coppedge <i>et al.</i> 1988</p> <p>Kehat <i>et al.</i> 1981</p>
10	<i>Diparopsis castanea</i>	<p>*Ph: 1) <i>trans</i>-9-11-dodecadienyl acetate (8.0)</p> <p>2) <i>cis</i>-9,11-dodecadienyl acetate (2.0)</p> <p>3) <i>trans</i>-9-dodecenyl acetate (0.5)</p> <p>4) <i>trans</i>-1-dodecenyl acetate (2.5)</p> <p>5) Dodecenyl acetate (5.0)</p> <p>+At: 1,2 and 4 in 8.0 : 2.0 : 2.5 ratio</p>	<p>*Nesbitt <i>et al.</i> 1975</p> <p>+Marks 1976</p>
11	<i>Antibonomus grandis</i>	<p>*Ph: In mixed sexes</p> <p>1) (<i>R-cis</i>)- 1- methyl -2- (1-methylethenyl) - cyclobutaneethanol (13)</p> <p>2) (<i>Z</i>)-2-(3,3-dimethylcyclohexylidene) ethenol (9)</p> <p>3) (<i>Z</i>)-(3,3-dimethylcyclohexylidene) acetaldehyde (9)</p> <p>4) (<i>E</i>)-(3,3-dimethylcyclohexylidene) acetaldehyde (1)</p> <p>**Ph: In male faecal matter 1,2,3 and 4 in 6 : 6 : 2 : 1 ratio</p> <p>+At 1,2,3 and 4 most effective in ratios of 2 : 6 : 1 : 1; 3 : 5 : 1 : 1 and 8 : 6 : 3 : 3</p>	<p>*Tumlinson <i>et al.</i> 1961</p> <p>**Hedin <i>et al.</i> 1974</p> <p>+Hardee <i>et al.</i> 1974</p> <p>Ridgway <i>et al.</i> 1990</p>

*Ph = Pheromone component's Proportion ; **Ph = Pheromone components in male ; +At = Field attraction

insects show that more than one blend of pheromone components can be attractive, as in tobacco budworm, *Heliothis virescens* (Fb.) (Vickers & Baker, 1997; Ramaswamy *et al.*, 1985; Shaver *et al.*, 1989; Hendricks & Shaver, 1990). It is also possible that any insect species may show geographical variation in this regard as is the case with pink bollworm, *Pectinophora gossypiella* (Saunders) (Flint *et al.*, 1979). However, it should be remembered that there is always a precise ratio that elicits maximum attraction, as in *P. gossypiella* (Tamhankar *et al.*, 1993), and that this ratio should always be used to obtain the best results.

Since pheromones are volatile in nature, slow release formulations have been developed so that an effective release rate is maintained over several days after application. Such pheromone formulations are commercially available for several insect pests of cotton crop (Hall *et al.*, 1980; 1992). Generally, the formulations used for monitoring are in the form of rubber septa, polyethylenesials or polyvinyl chloride

dispensers, while those for mating disruption purposes include plastic hollow fibres, plastic laminate flakes, polyethylene tube dispensers, bag dispensers etc. Some formulations are also available as emulsifiable concentrate (Downham *et al.*, 1995) or as polymeric aerosol (Kehat & Dunkelblum, 1993). The micro-encapsulated formulation is used in aqueous suspension and can be sprayed by conventional applicators, but the fibre and flake formulations require an adhesive to ensure that they stick to foliage. Polyethylene tubes have to be applied by hand individually. Sprayable formulations require less chemical and are easy to adapt to conventional practices, but their effect does not last long, whereas polyethylene tubes which can be applied by hand can be effective for months. For a long duration crop like cotton, they are eminently suitable.

Three types of pheromone traps viz., sticky, liquid and dry, are used in cotton pest management. The most widely used sticky trap in cotton is the delta trap. This trap, however, has limited trapping capacity, is not

adequate for large insects like *Helicoverpa* spp. and the scales of trapped insects and dust affect its trapping efficacy. Liquid traps have the problem of falling liquid levels due to evaporation and require careful handling. Currently, dry traps are in vogue as they are easy to handle, are rugged and have a large trapping capacity. They include the funnel trap, sleeve trap, wire cone trap, double cone trap (Texas model), automated trap etc. These traps are suitable both for monitoring and mass trapping. The rule of thumb for trap height in cotton is that for small insects like pink bollworm, traps should be 60 cm above ground level in the early season and 15 cm above the crop canopy in the late season. For large and strong flying insects like American bollworm, *Helicoverpa armigera* (Hübner), the parameters would be 1 m above ground level in the early season and 1 m above crop canopy in the late season.

Pheromones in the management of lepidopterous and coleopterous pests

Detection and monitoring

Several studies have been conducted on cotton pests to establish a quantitative relationship between the pheromone trap catches of a particular pest and the plant damage caused by it. This relationship would be used to define trap catch values that could be used to identify the economic threshold level of a pest at which control measures were necessary. For example, the correlation between pheromone trap catches and the level of egg or larval infestation were found to be highly significant in most of the major pests of cotton, such as, *H. virescens* and *Helicoverpa zea*. (Boddie) (Lopez *et al.*, 1988, 1990; Leonard *et al.*, 1989; Frisbie *et al.*, 1989), *H. armigera* (Srivastava *et al.*, 1992; Devaprasad *et al.*, 1993; Whitman & Rao, 1993), *Earias vittella* Fabricius (Qureshi & Ahmed, 1989; Naik *et al.*, 1997), *E. insulana* Boisduval (Campion *et al.*, 1981; Qureshi & Ahmed, 1989; Makkar & Kostandy, 1995); *P. gossypiella*, (Page *et al.*, 1984; Dhawan & Sidhu, 1988, Moawad, 1993) and *Antibonimus grandis grandis* Boheman (Benedict *et al.*, 1985).

Commercial advances in pheromone related monitoring and control technology have tremendous potential (Kirsch & Lingren, 1993; Cardé & Minks, 1997). However, utilization of various types of traps having varying efficacy, different dispensers and quantities of pheromone in different agro-ecosystems has resulted in variable predictive values of trap catches for any particular insect. For example, predictive values of the trap catches of pink bollworm moths ranged from 4 males/night (Dhawan & Sidhu, 1988) to as high as 22 males/night (Page *et al.*, 1984). Valuable information can be generated by conducting experiments simultaneously, using a standardised trapping protocol, in cotton growing areas. Such an effort would plug the major gaps in knowledge related to pheromone utilisation in cotton insect pest management. The data obtained could be assembled and processed together to include the local weather variables and to determine whether uniform predictive values of trap catches can be obtained for a pest, at least for the initial infestation under specified weather conditions, or there really exists a variation in this regard. Such an experiment may also help in proper

evaluation of the doubts expressed about the utility of trap catch as a predictive tool for pest infestation levels (Campion, 1994). There is also evidence to prove that exposure to sub-lethal levels of insecticides alters male sex pheromone response and female calling behaviour, at least in the case of pink bollworm (Haynes *et al.*, 1986). This may result in a delay in mating and also subsequent oviposition by females (Lingren *et al.*, 1980; Hutchison *et al.*, 1988). If this is the case, there is a need to evaluate pheromone trap catch values relating to infestation levels following insecticide application. Sequential sampling experiments may be of great value in this context since trap catch threshold levels may be exhibited after implementation of pest control measures. Most probably, because of the foregoing reasons, though pheromone traps have become an important tool for monitoring pests, their data are not easy to interpret and a lot still needs to be done to establish this methodology as a routine management practice

While the impact of weather on trap catches is routinely studied (Beasley & Adams, 1994; Tadas *et al.*,

1994; Korat & Lingappa, 1995; Adams *et al.*, 1995), not many studies have been carried out on the impact of other biotic or abiotic factors. For example, mixed cropping or mono-cropping patterns may influence pheromone-related behaviour of oligophagous insects, such as, *P. gossypiella*, *Earias* spp., and *Heliothis* spp. There is evidence that host plants or plant-odourants influence pheromone related behaviour of cotton insects (Landolt & Phillips, 1997) such as *Helicoverpa/heliothis* spp. (Raina *et al.*, 1972; Light *et al.*, 1993; Dickens *et al.*, 1990,1993), *Earias* spp. (Tamhankar, 1995), *A. grandis grandis* (Dickens, 1986) and *Trichoplusia ni* Hübner (Landolt & Heath, 1990). It appears that pure (as in monocropping systems) or altered (as in multi-cropping systems) signals may influence the pattern of trap catches. In natural settings, these major insect pests release pheromones in the presence of bioactive odourants. Traps baited with artificial lures based solely on pheromones and not properly integrated with the host ecosystem by including host odours, wherever necessary, may at times give erroneous results. A thorough evaluation of these considerations is a real need. Drapek *et al.* (1997) found that spatial patterns

of planting and wind blocking features influenced pheromone trap catches of *H. zea* and suggested the use of this information to modify pheromone trap-based predictions of *H. zea* damage. These studies need to be extended to other insects also.

Pheromone traps have been of immense value in several other areas of cotton pest management. A classic example is the tracking of cotton boll weevil, *A. grandis grandis*, as it spread to the southern parts of American continent (Whitcomb & Morengo, 1985). Pheromone traps were also used to evaluate the success of sterile backcross releases on population suppression of *H. virescens* (Laster *et al.*, 1996). Traps were successfully employed for detecting the tolerance levels to insecticides in surveys on *H. zea* during 1986-1994, for monitoring insecticide resistance in *P. gossypiella* (Haynes *et al.*, 1987) and *H. armigera* (Horowitz *et al.*, 1993), and also in an evaluation experiment of attracticide against cotton leafworm, *Spodoptera littoralis* Boisduval. Nevertheless, there are instances, as in southern Portugal, where

pheromone trapping data were affected by extraneous influences, such as predation by nocturnal avian fauna (particularly, owls) which were found feeding on the *H. armigera* male moths near pheromone traps. On the contrary, al. Meierrose *et al.* (1996) found light trap data of these moths to be more efficient and reliable.

Mass trapping/attracticide approach

The aim of mass trapping is to deploy pheromone traps in sufficient numbers over an area for an insect species to be controlled by capturing a significant proportion of pest population. In the case of Lepidoptera, varying degrees of success have been reported; a significant reduction in egg laying in *E. insulana* (McVeigh *et al.*, 1979) and *S. littoralis* (@ 5 traps/ha), (Campion *et al.*, 1980) promising control of the third generation in the case of *H. armigera* and suppression of the population below detectable levels of *P. gossypiella* moths (@ 20 traps/ha) (Mafra-Neto & Habib, 1996). However, in all these cases doubts remain about the area-wide and prolonged success, because (1) in Lepidoptera, the female sex pheromone attracts only males and then not all of them, and (2) since the males are polygamous even a small proportion of untrapped males can continue to fertilize a substantial number of females which have high egg laying potential, thereby ensuring the presence of the targeted species in that area. In the case of the boll weevil, where an aggregation pheromone is involved, mass trapping, at least at low population levels holds significant promise. A definitive field experiment on boll weevil indicated that as many as 92% of the males emerging from a population were captured with a trap density of 14 traps/ha (Lloyd *et al.*, 1983). In reality, such a trap density is not practical for high-density populations. On the contrary, with low population levels, a density of 2.5 traps/ha resulted in a high rate of elimination of boll weevils (Legget *et al.*, 1988), and such trap densities have been used in the south-eastern boll weevil eradication programme in the USA (Planer, 1988). It should, however, be remembered that difficulties involved in extensive deployment of traps in fields would always be a handicap in the mass trapping approach.

A novel pheromone use is the attracticide approach. Dean & Lingren (1982) used a series of false trails of gossypure to lead pink bollworm males to an insecticide-laced area with resultant fatality to males. This could reduce the insecticide requirement, especially as the pheromone acted like a synergist for the insecticide, because male moths became agitated and thereby more susceptible to the lethal effects of the insecticide. In Nicaragua, grandlure was used in conjunction with an early sown cotton trap crop sprayed with insecticides to control cotton boll weevil (Sterling *et al.*, 1989). It has been a practice in some parts of cotton growing countries to use pheromone sources laced with insecticide in the mating disruption method so as to inflict lethal/sublethal insecticide doses on males as they come in contact with the pheromone sources, the sublethal effect causing reduced pheromone response in survivors. Another innovation is the Boll Weevil Attract and Control Tube (BWACT) that utilizes a combination of grandlure, a feeding stimulant, and an insecticide, and was found to be three times more effective than traps alone in removing boll weevils from a local population (Villavaso *et al.*, 1998). Jansen (1994) reported an IPM strategy in which use of BWACT along with early destruction of stalks resulted in about 40% reduction in the use of insecticides aimed at boll weevil control. Large scale use of BWACT in Colombia, Brazil and Paraguay for successive years with a primary aim of prevention of establishment of boll weevil in Argentina and Bolivia has shown not only high levels of boll weevil control, but also delayed first application and minimised insecticide sprays, reduced crop damage, increased square retention and gave economic profits by way of savings in the cost of insecticides and increased fibre production. It is therefore, evident that the 'mass trapping' or 'attracticide' approach cannot be a singular method of control, but can definitely be a part of IPM strategy in cotton fields.

Mating disruption

Insecticide-based reduction of populations of various bollworms and also of the boll weevil is difficult because the larvae are inaccessible, being lodged inside the host tissue. In contrast, mating disruption is aimed at the adult stage, which is exposed throughout

its life. In the mating disruption approach, pheromone formulations are used to prevent mating of adults through mechanisms discussed in detail by Cardé & Minks (1995).

Amongst insects infesting cotton, the mating disruption technique is practiced most widely against pink bollworm. Hollow fibre formulation of pink bollworm pheromone was the first disruptant formulation to get Environment Protection Agency (EPA) registration in 1978 (Doane & Brooks, 1981). In 1981, over 40,000 hectares of cotton crop in California received hollow fibre mating disruption treatment whereby reducing plant damage and giving enhanced yields compared to conventional insecticide treatment. In 1985, twist-tie polyethylene formulation became available and thereafter these two formulations were employed continuously. Their use in an area-wide approach in Arizona during 1990-93, resulted in decreased boll damage from a pre-programme level of 23.3% - 0.0%, requiring only an occasional post-programme use of insecticides (Cardé & Minks, 1995). Further, in an IPM approach, use of pheromones in early crop season and insecticides in late crop season proved successful both in Egypt (Critchley *et al.*, 1984; Campion & Murlis, 1985; Moawad *et al.*, 1991) where the area treated increased to several thousand hectares (Russel & Radwan, 1993; El-Deeb *et al.*, 1993), and also in Pakistan (Critchley *et al.*, 1991; Ahmed & Atique, 1993; Chamberlain, 1994) with smaller losses in seed cotton yield in pheromone treated areas compared to conventional treatment. Because of these resounding successes, use of pheromone against pink bollworm is growing every year.

While it was thought in the earlier days that pheromones have to be used singly as they were species specific, their use in cotton crop protection has proved otherwise, effecting cost reductions. A hand applied twist-tie polyethylene tube pheromone formulation containing a combination of pheromones of *P. gossypiella*, *E. vittella* and *E. insulana* was used in Pakistan during 1986-89 in plot sizes ranging from 2.8 to 6.0 ha. Seasonal control was achieved using pheromone alone or together with one insecticide treatment. The level of control as well as the estimated yields achieved were comparable to five applications of insecticides (Chamberlain *et al.*, 1992). This indicated

that combined pheromone treatment could be used and that it also was effective in smaller areas. Experiments of Tamhankar and co-workers (unpublished observations) also showed that mating disruption can be achieved in plots of 100-250 sq.m., if the crop is isolated by a non-host crop or fallow land for about 100 m on all sides. Combined pheromone formulations have also proved successful in Israel (Kehat & Dunkelblum, 1993). A combined pheromone formulation of *H. armigera* and *P. gossypiella* suppressed mating of both the species for more than three months (Kehat *et al.*, 1998). They further reduced the dose of pheromone as well as number of dispensers/ha to suppress mating of individual species.

Mating/communication disruption has also been successfully attempted using the primary/secondary components or analogues in case of *Diaparopsis castaneae* Hmps. and *S. littoralis* (Bevor & Campion, 1979; Campion *et al.*, 1980; Ellis *et al.* 1980) and *S. exigua* Hübner (Mitchell *et al.* 1997). Since area-wide application is more effective in mating disruption than by individual farmers, the treatment lends itself most suitably to be used by governments or large farmers' co-operative organisations. However, there are difficulties in exploiting mating disruption on large scale. Gasagrande & Jones (1997) enumerated these problems as : unsuitable formulations, agronomic constraints, inadequate knowledge of pest biology, particularly population density fluctuations, number of generations/year and socio-economic constraints. There are also other constraints such as: interactions between different populations of a pest species, migration of males into treated fields, males attracting females for mating, the calling strategy of native females (Cardé & Minks, 1995) which can make or mar the results.

Research and Development

Semiochemicals

Host plants enhance/synergise pheromone production and the response to it in several pests of cotton such as *H. zea*, *H. virescens*, *H. armigera*, *A. grandis grandis*, (Dickens, 1986; 1989), *E. vittella* (Tamhankar, 1995) and *T. ni* (Landolt *et al.*, 1994). Reliable methods

should be developed to utilise this synergism in cotton crop protection. Female *H. armigera* moths are attracted by a steam distillate from pigeon pea plants. A mixture of six sesquiterpenes, mixed in the proportions found in the steam distillate, elicits the same behavioural responses. This is a highly promising development that needs to be exploited for use as an oviposition stimulant (Hartlieb & Rembold, 1996).

Pheromones for monitoring purposes have been explored/exploited in cotton IPM. Integration of mating disruption along with other management components has its own place in pink bollworm suppression. Several attempts have been made as in Egypt (Moawad, 1993) and in Pakistan (Chamberlain *et al.*, 1992) while integration with avoidance of insecticides needs more exploitation (Regupathy & Mahadevan, 1993). Live male *T. ni* moths attracted conspecific males and females in cotton fields (Landolt, 1995). This phenomenon should be investigated for other cotton pests also. It should also be found out if any modifications in methodology and further information on pheromone use in cotton IPM are required for further improvement.

Pheromones in cotton pest management

At times, sudden dramatic increases in pheromone trap catches occur for insects such as *Helicoverpa spp.* and *Heliothis spp.* for which local populations alone cannot account for the magnitude of these catches. A method of discriminating between local and migratory captures needs to be developed so as to forecast the likely arrival of the migrants, which come in relatively large numbers and can devastate the cotton crop, as happens in India in the case of *H. armigera*.

Auto-dissemination of entomopathogens involves the deliberate use of insects to spread entomopathogens in the insect habitat (Ignoffo & Shapiro, 1978; Yu, 1996). In this method, adult insects can be attracted to a contaminant station, where they pick up the pathogen and transfer it to the eggs, the females doing this directly and the males transferring it to the female ovipositor while mating. The neonate larvae eat the eggshell and ingest the inoculum. This is a very attractive proposition with the development of efficient methods of dispensing and it could prove to be a good

practice in cotton IPM. The initial experiments on this approach in case of non-cotton infesting as well as cotton infesting insects (Nordin *et al.*, 1991; Jackson *et al.*, 1992; Yu, 1996) using Nuclear Polyhedrosis Virus inoculum (Yu & Brown, 1997) have given promising results. The use of pheromones in conjunction with inundative releases of *Trichogramma chilonis* Ishii suppressed pink bollworm and spotted bollworm infestation to sub-economic level (Ahmad *et al.*, 1996).

Pheromone application with sterile-moth release programmes is also highly promising, as has been observed in the San Joaquin valley by the California Department of Food and Agriculture for the management of pink bollworm (Baker *et al.*, 1990). This methodology needs to be evaluated for other insects too.

It is indeed necessary to carefully evaluate whether the practice of adding insecticide to disruptant pheromone formulation will create foci for development of insecticide resistance in insects, particularly in pink bollworm against which, it has been practised for a fairly long time. The methodology is almost akin to the one used in experiments aimed at developing resistance in laboratory populations.

Based on the observations of Flint *et al.* (1977), a fundamentally different approach to mating disruption was pursued by Flint & Merkle (1983, 1984) and Flint *et al.* (1988) in which they evaluated the creation of pheromone composition imbalance by releasing only the Z, Z isomer of pink bollworm pheromone. The pheromone synthesis is generally expensive; however, current research in this area may help to bring down the cost of pheromone treatment.

Experiments to study whether there is potential for the evolution of resistance to the pheromone in the pink bollworm were generally negative (Haynes *et al.*, 1984). As the use of pheromones in pest management will undoubtedly increase, it would be prudent to monitor whether insect pests of cotton are developing resistance to pheromones. For example, genetic variation exists for the production and/or detection of pheromone compound blends in natural populations of pink bollworm (Collins & Cardé, 1985, 1990 a, b). Under such circumstances, selection may operate to

produce a strain of moths immune to disruption of communication caused by the 1:1 mixture currently used for pink bollworm. Variability in pheromone response is also possible, as described by Doane & Brooks (1980). They found that male pink bollworm would preferentially orient towards traps emitting high rates of gossypure in fields. Thus, there is an urgent need for the development of sprayable formulation, which may have season-long efficacy.

Shorey *et al.* (1996) and Shorey & Gerber (1996) evaluated 'pullers' for distributing large amounts of pheromone. This technique is eminently suitable for cotton bollworm pheromones with aldehyde components, as in this technique the pheromone chemicals are protected from oxidative degradation until they are released into air.

A field-portable electro-antennogram system used by Farbert *et al.* (1997) indicated that dispensers deployed at the edge of the crop could provide effective protection to the cotton crop from pink bollworm. Although mating disruption has proved to be an effective control strategy in cotton, improvements and optimisation in the methodology still depend largely on empirical field tests, such as: the number of pheromone releasers, the distance between them and other unknown factors including the actual aerial concentration given by a formulation, the fine scale distribution of pheromone in treated plots etc.

In the case of cotton pests, which have developed resistance to insecticides on a world-wide basis, there will be a demand for enormous utilization of bio-reactors for culturing pheromone gland cells. This is certainly a necessity because only the pheromone glands produce the full and proper blend. Minks & Gardé (1988) indicated that such blends will achieve total mating disruption with the minimum quantity of pheromones. Abernathy *et al.* (1996) reported induction of pheromone production in female *H. virescens* by topical application of a pseudo-peptide mimic of a pheromonotropic neuro-peptide. It may be possible to develop future pest suppression techniques based on the use of amphiphilic pseudo-peptides designed to bind strongly to receptors thereby continuously stimulating pheromone production so as to cause a depletion of the pool of pheromone precursors.

The discovery of Pheromone Biosynthesis Activating Neuro-peptide (PBAN) (Raina *et al.*, 1987; Raina & Menn, 1987; Ma *et al.* 1996), has the potential to lead to novel strategies of exploiting cotton plants themselves to interfere with the behaviour and ultimately the reproduction of insects, utilizing genetic engineering techniques (Keely & Hays, 1987; Menn *et al.*, 1989). It has been possible to induce pheromone production in *H. zea* females by feeding PBAN or its analogues as well as clone a synthetic PBAN gene behind polyhedron promoter of AcMNPV and a cell line infected with a recombinant baculovirus yielded pheromonotropic activity (Raina *et al.*, 1994; Vakharia *et al.*, 1995). Then a major constraint would be the delivery of the peptide to the target organism.

In a decade that ends up with increased difficulties to suppress cotton pests with the present IPM tools further work on narrowing of gaps in the present techniques of utilizing pheromones for both cotton pest monitoring as well as mass-trapping, is warranted.

Acknowledgements

A.J. Tamhankar is grateful to Dr. K. Raghu, former Head, Nuclear Agriculture Division and Dr.P.C. Kesavan, former Director, Biosciences Group, B.A.R.C., Mumbai, for useful discussions and for granting permission to publish this review.

References

1. ABERNATHY, R. L., TEAL, P. E. A., MEREDITH, J. A. and NACHMAN, R. J. (1996) Induction of pheromone production in a moth by topical application of a pseudopeptide mimic of a pheromonotropic neuropeptide. Proceedings of National Academy of Sciences, USA 93, 12621-25.
2. ADAMS, C.J., BEASLEY, C.A. AND HENNEBERRY, T.J. (1995). Effects of temperature and wind speed on pink bollworm (Lepidoptera: Gelechiidae) moth captures during spring emergence. Journal of Economic Entomology 88, 1263-70.
3. AHMAD, N., ASHAF, M., HASSAIN, T., FATIMA, B. AND NASRULLAH, A. (1996). Significance of pheromones and parasites for the control of cotton bollworms in Pakistan. Pakistan Journal of Zoology 28, 355-57.
4. AHMAD, Z. AND ATTIQUE, M.R. (1993). Control of pink bollworm with gossypure in Punjab, Pakistan. International Organization for Biological Control, West Palearctic Regional Section Bulletin 16, 141-48.
5. BAKER, T.C., STATEN, R.T. AND FLINT, H.M. (1990). Use of pink bollworm pheromone in the Southwestern United States. In Behaviour Modifying Chemicals for Insect Management: Application of Pheromones and Other Attractants (ed. by P.L. Ridgway, R.M. Silverstein and M.N. Inscoe). pp. 417-36. Marcel Decker, New York, USA.
6. BEASLEY, C.A. AND ADAMS, C.J. (1994). Relationships between environmental factors and capture time of male pink bollworm (Lepidoptera:Gelechiidae) moths in traps baited with sex pheromone. Journal of Economic Entomology 87, 986-92.
7. BEEVOR, P.S. AND CAMPION, D.G. (1979). The field use of 'inhibitory' components of lepidopterous sex pheromone and pheromone mimics. In Chemical Ecology : Odour Communication in Animals. (ed. by R.F.Ritter). pp. 313-25. Elsevier/North Holland, Amsterdam, Holland.
8. BENEDICT, J.H., URBAN, T.C., GEORGE, D.M., SEGRES, J.C., ANDERSON, D.J., McWHORTER, G.M. AND ZUMMO, G.R. (1985). Pheromone trap thresholds for management of overwintered boll weevils (Coleoptera: Curculionidae). Journal of Economic Entomology 78, 169-71.
9. BIERL, B.A., BEROZA, M., STATEN, R.T., SONNET, P.E. AND ALDER, V.E. (1974). The Pink bollworm sex attractant. Journal of Economic Entomology 67, 211-16.
10. CAMPION, D.G. (1994). Pheromones for the control of cotton pests. In. Insect Pests of Cotton (ed. by G.A. Matthews and J.P. Tunstall). pp. 505-34. CAB International, Oxon, U.K.
11. CAMPION, D.G., BETLANG, B.W., NESBITT, B.F., BEEVOR, P.S., LESTER, R. AND POPPI, R.G. (1974). Field studies of the female sex pheromone of the cotton leafworm, *Spodoptera littoralis* (Boisd.) in Cyprus. Bulletin of Entomological Research 64, 89-95.

12. CAMPION, D.G. AND MURLIS, J. (1985). Sex pheromones for the control of insect pests in developing countries. *Mededlingen van de Faculteit van Landbouwwetenschappen van de Rijksuniversiteit Gent* 50, 203-09.
13. CAMPION, D.G., MCVEIGH, L.J. AND HUNTER-JONES, P. (1981). The use of sex pheromones for the control of spiny bollworm *Earias insulana* and the American bollworm *Heliopsis armigera* in cotton growing areas of Syria. Food and Agriculture Organisation, Unpublished Report, 10 pp.
14. CAMPION, D.G., HUNTER-JONES, P., MCVEIGH, L.J., HALL, D.R., LESTER, R. AND NESBITT, B.F. (1980). Modification of the attractiveness of the Egyptian cotton leafworm, *Spodoptera littoralis* (Boisduval) (Lepidoptera: Noctuidae) by secondary pheromone components and related chemicals. *Bulletin of Entomological Research* 70, 417-34.
15. CARDÉ, R.T. AND MINKS, A.K. (1995). Control of moth pests by mating disruption: Successes and constraints. *Annual Review of Entomology* 40, 559-85.
16. CARDÉ, R.T. AND MINKS, A.K. (1997). *Insect Pheromone Research: New Directions*. Chapman & Hall, London, UK, 712 pp.
17. CASAGRANDE, E. AND JONES, O.T. (1997). Commercial exploitation of mating disruption technology: Difficulties encountered and keys to success. *International Organisation for Biological Control, West Palearctic Regional Station Bulletin*. 20, 11-17.
18. CHAMBERLAIN, D.J. (1994). Pheromones in the IPM of cotton in Pakistan. Paper presented at the Cotton Connection, Pesticide Actions Network, Hamburg, Germany, November, 25-26.
19. CHAMBERLAIN, D.J., CRITCHLEY, B.R., CAMPION, D.G., ATTIQUE, M.R., RAFIQUE, M. AND ARIF, M.I. (1992). Use of multicomponent pheromone formulation for control of cotton bollworms (Lepidoptera: Gelechiidae and Noctuidae) in Pakistan. *Bulletin of Entomological Research* 82, 449-58.
20. COLLINS, R.D. AND CARDÉ, R.T. (1985). Variation in heritability of aspects of pheromone production in the pink bollworm moth *Pectinophora gossypiella* (Lepidoptera: Gelechiidae). *Annals of Entomological Society of America* 78, 2229-34.
21. COLLINS, R.D. AND CARDÉ, R.T. (1990a). Selection for increased pheromone response in the pink bollworm *Pectinophora gossypiella* (Lepidoptera : Gelechiidae). *Behavior Genetics* 20, 325-331.
22. COLLINS, R.D. AND CARDÉ, R.T. (1990b). Selection for increased pheromone titre in the pink bollworm *Pectinophora gossypiella* (Lepidoptera: Gelechiidae). *Physiological Entomology* 15, 141-47.
23. COPPEDGE, J.R., BULL, D.L., HOUSE, V.S., RIDGWAY, R.L., BOTRELL, D.G., CORKA, CHAMBERLAIN, D.J., BEEVOR, P.S., HALL, D.R., NESBITT, B.F., CAMPION, D.G. AND ATTIQUE, M.R. 1988. Components of female sex pheromone of spotted bollworm, *Earias vittella* f. (Lepidoptera:Noctuidae) :Identification and field application in Pakistan. *J.Chem. Ecol.* 14, 929-945.
24. CRITCHLEY, B.R., CAMPION, D.G., MCVEIGH, E.M., MCVEIGH, L.J., JUSTUM, A.R., GORDON, R.F., MARRS, G.J., NASR EL-SAYED, A. AND HOSNY, M.M. (1984). Microencapsulated pheromones in cotton pest management. In: *Proceedings of British Crop Protection Conference: Pests and Diseases*. pp. 241-45. British Crop Protection Council, Croydon, Surrey, U.K.
25. CRITCHLEY, B.R., CHAMBERLAIN, D.J., CAMPION, D.G., ATTIQUE, M.R., ALI, M. AND GAFFAR, A. (1991). Integrated use of pink bollworm pheromone formulations and selected conventional insecticides for the control of the cotton pest complex in Pakistan. *Bulletin of Entomological Research* 81, 371-78.
26. DEAN, D.A. AND LINGREN, P.D. (1982). Confusing and killing cotton pests. *Agricultural Research (Washington D.C.)* 31, 4-5.
27. DEVAPRASAD, V., RAMBABU, L. AND REDDY, G.P.V. (1993). An action threshold of *Helicoverpa armigera* Hb. based on pheromone trap catches in cotton. *Indian Journal of Plant Protection* 21, 17-18.
28. DHAWAN, A.K. AND SIDHU, A.S. (1988). Correlation between the moth catch *gossypure*

- baited traps and pink bollworm incidence in F-414 Hirsutum cotton. *Indian Journal of Entomology* 50, 55-60.
29. DICKENS, J.C. (1986). Orientation of boll weevil, *Anthonomus grandis* Boh. (Coleoptera: Curculionidae) to pheromone and volatile host compounds in the laboratory. *Journal of Economic Entomology* 12, 91-98.
30. DICKENS, J.C. (1989). Green leaf volatiles enhance aggregation pheromone of boll weevil, *Anthonomus grandis*. *Entomologia Experimentalis et Applicata* 52, 191-203.
31. DICKENS, J.C., JANG, E.B., LIGHT, D.M AND ALFORD, A.R. (1990). Enhancement of insect pheromone responses by green volatiles enhance sex attractant pheromone of the tobacco budworm, *Heliothis virescens* (Lep., Noctuidae). *Naturwissenschaften* 77, 29-31.
32. DICKENS, J.C., SMITH, J.W AND LIGHT, D.M. (1993). Green leaf volatiles enhance sex attractant pheromone of the tobacco budworm, *Heliothis virescens* (Lep., Noctuidae). *Chemoecology* 4, 175-177.
33. DOANE, U., AND BROOKS, D.W. (1980). Research and development of pheromone for insect control with emphasis on pink bollworm *Pectinophora gossypiella*. In: *Proceedings of Colloquium on Management of Insect Pests*. Gainesville, Florida, USA. March, 1980.
34. DOANE, U. AND BROOKS, D.W. (1981). Research and development of pheromone for insect control with emphasis on the pink bollworm. In: *Management of Insect Pests with Semiochemicals* (ed. by E.R Mitchell). pp. 285-303. Plenum Press, New York, USA.
35. DOWNHAM, M.C.A., McVEIGH, L.J. AND MOAWAD, G.M. (1995). Field investigation of an attractiveness control technique using the sex pheromone of the Egyptian cotton leafworm, *Spodoptera littoralis* (Lepidoptera: Noctuidae). *Bulletin of Entomological Research* 85, 463-472.
36. DRAPEK, R.J., GROFT, B.A AND FISHER, G. (1977). An examination of spatial input parameters in order to improve corn earworm (Lepidoptera: Noctuidae) damage predictions for a pheromone trap catch regression model. *Pan-Pacific Entomologist* 73, 9-15.
37. DUNKELBLUM, E., GOTHILF, S. AND KEHAT, M. (1980). Identification of the sex pheromone of the cotton bollworm, *Heliothis armigera*, in Israel. *Phytoparasitica* 8, 209-11.
38. DUNKELBLUM, E., KEHAT, M., GOTHILF, S., GREENBERG, S. AND SKLARASZ, B. (1982). Optimised mixture of sex pheromona components for trapping of male *Spodoptera littoralis*, in Israel. *Phytoparasitica* 10, 21-26.
39. ELLIS, P.E., BRIMAGOMBE, L.C., McVEIGH, L.J. AND DJGNAN, A (1980). Laboratory experiments on the disruption of the mating in the Egyptian cotton leafworm, *Spodoptera littoralis* (Boisduval) (Lepidoptera: Noctuidae) by excess of female pheromone. *Bulletin of Entomological Research* 69, 673-84.
40. EL-DEEB, Y.A., EL-HAMAKY, M.A AND MOAWAD, G.M. (1993). Large scale use of pink bollworm sex pheromone formulations integrated with conventional insecticides for the control of cotton pests in Egypt. *International Organisation for Biological Control, West Palearctic Regional Section. Bulletin*. 16, 213-319.
41. FARBERT, P., KOCH, U.T., FARBERT, A., STATEN, R.T. AND CARDÉ, R.T. (1997). Pheromone concentration measured with electroantennogram in cotton fields treated with mating disruption of *Pectinophora gossypiella* (Lepidoptera: Gelechiidae). *Environmental Entomology* 26, 1105-16.
42. FLINT, H.M. AND MERKLE, J.R. (1983). Pink bollworm (Lepidoptera: Gelechiidae): Communication disruption by pheromone composition imbalance. *Journal of Economic Entomology* 76, 40-46.
43. FLINT, H.M. AND MERKLE, J.R. (1984). The pink bollworm (Lepidoptera: Gelechiidae): Alteration of male response to gossypure by release of its component Z, Z-isomer. *Journal of Economic Entomology* 77, 1099-1104.
44. FLINT, H.M., CURTICE, N.T. AND YAMAMOTO, A. (1988). Pink bollworm (Lepidoptera: Gelechiidae): Further test with (Z, Z)-isomer of gossypure. *Journal of Economic Entomology* 81, 679-83.
45. FLINT, H.M., SMITH, R.L., FOREY, D.E AND HORN, B.R. (1977). Pink bollworm: Response of

- males to (Z,Z)- and (Z,E) isomers of gossypure. *Environmental Entomology* 6, 274-75.
46. FLINT, H.M., BALASUBRAMANIAN, M., CAMPERO, J., STRICKLAND, G.R., AHMAD, Z., BARRAL, J., BARBOSA, S. AND KHALIL, A.F. (1979). Pink bollworm response of native males to ratios of (Z,Z) and (Z,E)- isomers of gossypure in several cotton growing areas of the world. *Journal of Economic Entomology* 72, 758-62.
 47. FRISBIE, R.E. (1989) *Integrated Pest Management Systems and Cotton Production*. John Wiley & Sons, London, U.K.
 48. FRISBIE, R.E., EL-ZIK, K.M. AND WILSON, L.T. (Eds.) (1989). *Integrated Pest Management Systems and Cotton Production*. Wiley Interscience, John Wiley & Sons, New York, USA.
 49. GAHUKAR, R.T. (1991). Control of cotton insect and mite pests in sub-tropical Africa : Current status and future needs. *Insect Science and its Application*. 12, 313-38.
 50. HALL, D.R., BEEVOR, P.S., LESTER, R. AND NESBITT, B.F. (1980). (E-E) -10,12-hexadecadienal: A component of the female sex pheromone of the spiny bollworm, *Earias insulana* (Boisd.) (Lepidoptera: Noctuidae). *Experientia* 36, 152-53.
 51. HALL, D.R., BEEVOR, P.S., CAMPION, D.G., CHAMBERLAIN, D.J., CORK, A., WHITE, R.D., ALMESTAR, A. AND HENNEBERRY, T.J. (1992). Nitrate esters: Novel sex pheromone components of the cotton leaf perforator, *Baculatrix thurberiella* Busck. (Lepidoptera: Lyonetiidae). *Tetrahedron Letters* 33, 4811-14.
 52. HARDEE, D.D., MCKIBBEN, G.H., RUMMEL, D.R., HUDDLESON, P.M. AND COPPEDGE, J.R. (1974). Response of bollweevils to component ratios and doses of the pheromone, *Grandlure*. *Environmental Entomology* 3, 135-138.
 53. HARTLIEB, E. AND REMBOLD, H. (1996). Behavioral response of female *Helicoverpa* (*Heliothis*) *armigera* Hb. (Lepidoptera: Noctuidae) moths to synthetic pigeon pea (*Cajanus cajan* L.) kairomone. *Journal of Chemical Ecology* 22, 821-37.
 54. HAYNES, K.F., LI, W.G. AND BAKER, T.C. (1986). Control of pink bollworm moth (Lepidoptera: Gelechiidae) with insecticides and pheromones (Attracticides): Lethal and sublethal effects. *Journal of Economic Entomology* 79, 1466-71.
 55. HAYNES, K.F., GASTON, L.K., POPE, M.M. AND BAKER, T.C. (1984). Potential for evolution of resistance to pheromone: Inter-individual and inter-populational variation in chemical communication systems of pink bollworm moth. *Journal of Chemical Ecology* 10, 1551-65.
 56. HAYNES, K.F., MILLER, T.A., SATETN, R.T., LI, W.G. AND BAKER, T.C. (1987). Pheromone trap for monitoring insecticide resistance in pink bollworm moth (Lepidoptera: Gelechiidae): A new tool for resistance management. *Environmental Entomology* 10, 84-89.
 57. HEDIN, P.A., HARDEE, D.D., THOMSON, A.C. AND GUELDER, R.C. 1974. An assessment of the life time biosynthesis potential of the male boll weevil. *Journal of Insect Physiology*. 20, 1707-1712.
 58. HENDRICKS, D.E. AND SHAVER, T.N. (1990). Persistence and performance of pheromone formulated with or without Z-11-Hexadecen-1-OC in pre-bait for trapping tobacco budworm moths. *Southwestern Entomologist* 15, 245-51.
 59. HOROWITZ, A.R., SELIGMEN, I. M., FORER, G., BAR, D. AND ISHAAYA, I. (1993). Preventive insecticidal resistance strategy in *Helicoverpa* (*Heliothis*) *armigera* (Lepidoptera: Noctuidae) in Israeli cotton. *Journal of Economic Entomology* 86, 205-12.
 60. HUMMEL, H.E., GASTON, L.K., SHOREY, H.H., KAAE, R.S., BYRNE, K.J. AND SILVERSTEIN, R.M. (1973). Clarification of the chemical status of the pink bollworm sex pheromone. *Science* 181, 873-75.
 61. HUTCHISON, W.D., BEASLEY, C.A. AND HENNEBERRY, T.J. (1988). Efficacy of selected insecticides on pink bollworm oviposition in cotton. pp.309-311. In *Proceedings of Beltwide Cotton Production Research Conference*, (ed. By T.C. Nelson), January, 3-8, 1988. New Orleans, National Cotton Council, Memphis, Tennessee, USA.
 62. IGNOFFO, C.M. AND SHAPIRO, M. (1978). Characteristics of baculovirus preparations processed from living and dead larvae. *Journal of Economic Entomology* 71, 186-88.

63. JACKSON, D.M., BROWN, G.C., NORDIN, G.I. AND JOHNSON, D.W. (1992). Auto-dissemination of a baculovirus for management of tobacco budworms (Lepidoptera:Noctuidae) on tobacco. *Journal of Economic Entomology*, 88, 710-719.
64. JANSEN, H.G. (1994). Integrated cotton production in Nicaragua. Paper presented at the Cotton Connection, Pesticide Actions Network, Hamburg, Germany, November 25-26, 1994.
65. KEELEY, L.L. AND HAYES, T.K. (1987). Speculations for biotechnology applications for insect neuroendocrine research. *Insect Biotechnology*, 17, 639-51.
66. KEHAT, M. AND DUNKELBLUM, E. (1993). Sex pheromones: Achievements in monitoring and mating disruption of cotton pests in Israel. *Archives of Insect Biochemistry and Physiology* 22, 425-31.
67. KEHAT, M., ANSHELEVICH, L., GORDON, D., HAREL, M. AND DUNKELBLUM, E. (1998). Evaluation of Shin-Etsu twist-tie rope dispensers by the mating table technique for disrupting mating of the cotton budworm, *Helicoverpa armigera* (Lepidoptera:Noctuidae) and the pink bollworm, *Pectinophora gossypiella* (Lepidoptera: Gelechiidae). *Bulletin of Entomological Research* 88, 141-48.
68. KEHAT, M., GOTHILF, S., DUNKELBLUM, M. AND GREENBERG, G. (1981). Captures of *Earias insulana* males in water traps and dry funnel traps baited with synthetic pheromone and virgin females. *Phytoparasitica* 9, 149-151.
69. KEHAT, M., GOTHILF, S., DUNKELBLUM, E. AND GREENBERG, S. (1980). Field valuation of female sex pheromone components of the cotton bollworm, *Heliothis armigera*. *Entomologia Experimentalis et Applicata* 27, 188-93.
70. KIRSCH, P. AND LINGREN, B. (1993). Commercial advancement of pheromone related monitoring and control technology. *International Organisation for Biological Control, West Palearctic Regional Station Bulletin*, 16, 121-27.
71. KLUN, J.A., PLIMMER, J.R., BIERL-LEONHERDT, B.A., SPARKS, A.N., AND CHAPMAN, O.L. (1979). Trace chemicals: The essence of sexual communication system in *Heliothis* species. *Science* 204, 1328.
72. KLUN, J.A., PLIMMER, J.R., BIERL-LEONHERDT, B.A., SPARKS, A.N., PRIMIANI, M., CHAPMAN, O.L., LEE, J.K. AND LEPONE, G. (1980). Sex pheromone chemistry of female corn earworm moth, *Heliothis zea*. *Journal of Chemical Ecology* 6, 165-75.
73. KORAT, D.M. AND LINGAPPA, S. (1995). Influence of weather factors on the pheromone trap catches of cotton bollworm moths. *Indian Journal of Plant Protection* 23, 188-90.
74. LANDOLT, P.J. AND HEATH, R.R. (1990). Sexual role reversal in male-finding strategies of the cabbage looper moth. *Science* 249, 1026-28.
75. LANDOLT, P.J. AND PHILLIPS, T.W. (1997). Host plant influences on sex pheromone behaviour of phytophagous insects. *Annual Review of Entomology* 42, 371-391.
76. LANDOLT, P.J., HEATH, R.R., MILLER, J.G., DAVIS-HERNANDEZ, K.M., DUEBEN, B.D. AND WARD, K.E. (1994). Effects of host plant, *Gossypium hirsutum* L., on sexual attraction of cabbage looper moth, *Trichoplusia ni* (Hübner) (Lepidoptera: Noctuidae). *Journal of Chemical Ecology* 20, 2959-74. LASTER, M.L., HARDEE, D. D. AND SCHNEIDER, J.C. (1996). *Heliothis virescens* (Lepidoptera: Noctuidae): Influence of sterile backcross releases on suppression. *Southwestern Entomologist* 21, 433-44.
77. LEGGET, J.E., DICKERSON, W.A. AND LLOYD, E.P. (1988). Suppressing low level boll weevil populations with traps: Influence of trap placement, grandlure concentration and population levels. *Southwestern Entomologist* 13, 205-16.
78. LEONARD, B.R., GRAVES, J.B., BURRIS, E., PAVLOFF, A.H. AND CHURCH, J. (1989). *Heliothis* spp. (Lepidoptera: Noctuidae) captures in pheromone traps: Species composition and response to oviposition in cotton. *Journal of Economic Entomology* 82, 574-79.
79. LIGHT, D.M., FLATH, R.A., BUTTERY, R.G., ZALOM, F.G., AND RICE, R.E. 1993. Host plant green-leaf volatiles synergize the synthetic sex pheromones of the corn earworm and codling moth (Lepidoptera). *Chemoecology* 4, 145-52.
80. LINGREN, P.D., BURTON, J., SHELTON, W. AND RAULSTON, J.R. (1980). Night vision goggles : For

- design, evaluation and comparative efficiency determination of a pheromone trap for capturing live adult male pink bollworm. *Journal of Economic Entomology* 73, 622-30.
81. LLOYD, E.P., McKIBBEN, G.H., LEGGET, J.E. AND HARTSTACK, A.W. (1983). Pheromone for survey, detection and control. In *Cotton Insect Management with Special Reference to Boll Weevil*. (ed. by R.L. Ridgway, E.P. Lloyd and W.H. Cross). pp. 179-205. Agriculture Handbook No. 589. United States Department of Agriculture, Agricultural Research Service, Washington, USA.
 82. LOPEZ, J.D. Jr., GOODENOUGH, J.L. AND HENDRICKS, D.E. (1988). Evaluation of two pheromone dispensers in combination with plastic and wire cone traps for tobacco budworm (*Lepidoptera:Noctuidae*). *Journal of Economic Entomology* 81, 1750-53.
 83. LOPEZ, J.D. Jr., SHAVER, T.N. AND GOODENOUGH, J.L. (1990). Multispecies trapping of *Helicoverpa* (*Heliothis*)*zea*, *Spodoptera frugiperda*, *Psuedaletia unipuncta* and *Agrotis ipsilon* (*Lepidoptera: Noctuidae*). *Journal of Chemical Ecology* 16, 3479-89.
 84. MA, P.W.K., ROELOLOFS, W.L. AND JURENKA, R.A. (1996). Characterisation of PBAN and PBAN-encoding neuropeptides in the central nervous system of the corn earworm, *Helicoverpa zea*. *Journal of Insect Physiology* 42, 257-66.
 85. MAFRA-NETO AND HABIB, M. (1996). Evidence that mass trapping suppresses pink bollworm populations in cotton fields. *Entomologia Experimentalis et Applicata* 81, 315-23.
 86. MAKAR, A.W. AND KOSTANDY, S.N. (1995). Relationship between spiny bollworm males attracted to pheromone traps and larval infestation in cotton bolls. *Annals of Agricultural Science, Moshtohor B* 33, NM1529-38.
 87. MARKS. (1976). Field studies with the synthetic sex pheromone and inhibition of the red bollworm, *Diparopsis castanea* Hmps. (*Lepidoptera:Noctuidae*) in Malawi. *Bulletin of Entomological Research*. 66, 279-300.
 88. MATTHEWS, C.A. AND TUNSTALL, J.P. (1994). *Insect Pests of Cotton*. CAB International, London, U.K.593 pp.
 89. McWEIGH, L.J., PATON, E.M. AND HALL, D.R. (1979). Factors affecting the performance of pheromone traps for male *Spodoptera littoralis*. In *Proceedings of British Crop Protection Conference: Pests and Diseases*, pp. 409-19. British Pest Control, Croydon, Surrey, U.K.
 90. MEIERROSE, C., MELISSE, M., NESKAKIS, A., WAGNER, L. AND WIEDIGER, J. (1996). The use of photovoltaic insect traps for the establishment of a forecast system against noctuid pests in south Portugal. *Mededlingen Faculteit Landbouwkundige en Toegepaste Biologische Wetenschappen Universiteit Gent* 61 (3A), 773-76.
 91. MENN, J.J., KING, E.G. AND COLEMAN, R.J. (1989) Future control strategies for *Heliothis* in cotton. In *Pest Management in cotton* (ed. by M.B.Green and D.J.de Lyon). pp. 101-121. Ellis Harwood Ltd, Chichester, U.K.
 92. MINKS, A.K. AND CARDÉ, R.T. (1988). Disruption of pheromone communication in moths: Is the natural blend really most efficacious? *Entomologia Experimentalis & Applicata* 49, 25-36.
 93. MITCHELL, E.R., KEHAT, M., TINGLE, F.C. AND Mc LAUGHLIN, R. (1997). Suppression of mating by beet armyworm (*Noctuidae:Lepidoptera*) in cotton with pheromone. *Journal of Agricultural Entomology* 14, 17-28.
 94. MOAWAD, G.M. (1993). Commercial use of pink bollworm (*Pectinophora gossypiella*) pheromone in Egypt. *International Organisation for Biological Control, West Palearctic Regional Section Bulletin*. 16, 175.
 95. MOAWAD, G.M., KHIR, A.A., ZAKI, M., CRITCHLEY, B.R., McVEIGH, J. AND CAMPION, D.G. (1991). Large scale use of hollow fibre and micro-encapsulated pink bollworm pheromone formulation integrated with conventional insecticides for the control of cotton pest complex in Egypt. *Tropical Pest Management* 37, 10-16.
 96. NAIK, M.L., LINGAPPA, S., HIREMATH, I.G. AND SHIVANNA, B.K. (1997). Pheromone trap to monitor adult spotted bollworm, *Earias vitella* (F.) on cotton. *Mysore Journal of Agricultural Sciences* 31, 33-35.

97. NESBITT, B.F., BEEVOR, P.S., COLE, R.A., LESTER, R. AND POPPI, R.G. (1975) The isolation and identification of the female sex pheromone of the red bollworm moth, *Diparopsis castanea*. *Journal of Insect Physiology* 21, 1091-98.
98. NESBITT, B.F., BEEVOR, P.S., HALL, D.R. AND LESTER, R. (1979). Female sex pheromone components of the cotton bollworm, *Heliothis armigera*. *Journal of Insect Physiology* 25, 535-41.
99. NESBITT, B.F., BEEVOR, P.S., HALL, D.R. AND LESTER, R. (1980). (Z)-9-hexadecenal: A minor component of the female sex pheromone of *Heliothis armigera* (Hubner). (Lepidoptera:Noctuidae). *Entomologia Experimentalis et Applicata* 27, 306-311.
100. NORDIN, G.L., BROWN, G.C. AND JACKSON, D.M. (1991) Trans-ovum transmission of two nuclear polyhedrosis viruses (Baculoviridae) by adult tobacco budworm and viral persistence on tobacco budworm and viral persistence on tobacco foliage. *Transactions of Kentucky Academy of Sciences*. 52, 33-39.
101. PAGE, F.D. MODNII, M.P. AND STONE, M.E. (1984). Use of pheromone trap catches to predict damage by pink bollworm larvae in cotton. In: *Proceedings of Fourth Australian Applied Entomological Research Conference, Adelaide, Pest Control: Recent Advancements and Future Prospects*. pp.68-73. South Australian Government Printers, Adelaide, Australia.
102. PLANER, F.R. (1988). Southeast boll weevil eradication programme. In: *Proceedings of the 1988 Beltwide Cotton Production Research Conference*, pp. 239-40. New Orleans, January 3-8, 1988. Cotton Council of America, Memphis, USA.
103. POPE, M.M., GASTON, L.K. AND BAKER, T.C. (1984). Composition, quantification and periodicity of sex pheromone volatiles from individual *Heliothis zea* females. *Journal of Insect Physiology* 30, 943-45.
104. QURESHI, Z.A. AND AHMED, N. (1989). Efficacy of sex pheromones for the control of three bollworms of cotton. *Journal of Applied Entomology* 10, 386-89.
105. RAINA, A.K. AND MENN, J.J. (1987). Endocrine regulations of pheromone production in Lepidoptera. In: *Pheromone Biochemistry* (ed. by G.D. Brestwich and G.J. Blomquist). pp. 159-74. Academic Press, Orlando, Florida, USA.
106. RAINA, A.K., KINGAN, T.G. AND MATTOO, A.K. (1972). Chemical signals from host plants and sexual behaviour in a moth. *Science* 255, 592-594.
107. RAINA, A.K., RAFAELI, A. AND KINGAN, T.G. (1994). heromonotropic activity of orally administered PBAN analogues in *Helicoverpa zea*. *Journal of Insect Physiology*. 40, 393-397.
108. RAINA, A.K., JAFFES, H., KLUN, J.A., RIDGWAY, R.L., AND HAYES, D.K. (1987). Characteristics of a neurohormone that control sex pheromone production in *Heliothis zea*. *Journal of Insect Physiology* 33, 809-14.
109. RAMASWAMY, S.B., RANDLE, D.A. AND MA, W.K. (1985). Field evaluation of the sex pheromone components of *Heliothis virescens* (Lepidoptera: Noctuidae) in cone traps. *Environmental Entomology* 14, 293-96.
110. REGUPATHY, A. AND MAHADEVAN, N.R. (1993). Management of pink bollworm of cotton through gossypure and insecticides. *Indian Journal of Plant Protection* 21, 230-33.
111. RIDGWAY, R.L., INSCOE, M.N. AND DICKERSON, W.A. (1990). Roll of boll weevil pheromone in pest management. In *Behaviour Modifying Chemicals for Insect Management* (ed. by R.L. Ridgeway, R.M. Silverstein and M.N. Inscoe). pp. 437-71. Marcel Dekker, New York, USA.
112. ROELOFS, W.L., HILL, A.S., CARDÉ, R.T. AND BAKER, T.C. (1974). Sex pheromone components of the tobacco budworm moth, *Heliothis virescens*. *Life Sciences* 14, 1555-62.
113. RUSSELL, R.A. AND RADWAN, S.M. (1993). Modelling pink bollworm mating disruption in Egyptian cotton. *International Organization for Biological Control, West Palearctic Regional Section Bulletin* 16, 268-75.
114. SHAVER, T.N., HENDRICKS, D.E. AND LOPEZ, J.D. Jr. (1989). Influence of Z11-hexadecen-1-ol on field performance of *Heliothis virescens* pheromone in PVC dispenser as evidenced by trap

- capture. *Journal of Chemical Ecology* 15, 1637-45.
115. SHOREY, H.H. AND GERBER, R.G. (1996). Disruption of pheromone communication through the use of puffers for control of beet armyworm (Lepidoptera: Noctuidae) in tomatoes. *Environmental Entomology* 25, 1401-05.
 116. SHOREY, H.H., SISK, C.B. AND GERBER, R.G. (1996). Widely separated pheromone release sites for disruption of sex pheromone communication in five species of lepidoptera. *Environmental Entomology* 25, 446-51.
 117. SHOREY, H.H., SUMMERS, C.G., SISK, C.B. AND GERBER, R.G. (1994). Disruption of pheromone communication in *Spodoptera exigua* (Lepidoptera: Noctuidae) in tomatoes, alfalfa and cotton. *Environmental Entomology* 23, 1529-33.
 118. SRIVASTAVA, C.P., PIMBERT, M.P. AND REED, W. (1992). Monitoring of *Helicoverpa* (*Heliothis*) *armigera* (Hübner) moths with light and its pheromone trap in India. *Insect Science and its Application* 13, 205-10.
 119. STERLING, W.C., WILSON, L.T., GUTIERREZ, A.P., RUMMEL, D.R., PHILLIPS J.R., STONE, N.D. AND BENEDICT, J.H. (1989). Strategies and tactics for managing insects and mites. In *International Pest Management Systems and Cotton Production*. pp. 267-325. John Wiley & Sons Inc. New York, USA.
 120. SUNDARAMURTHY, V.T. AND GAHUKAR, R.T. (1998). Integrated management of cotton insect pests in India. *Outlook on Agriculture* 27,247-55.
 121. TADAS, P.L., SARNAIK, D.N., KENE, H.K. AND SATPUTE, U.S. (1994). Effect of weather parameters on monitoring of cotton bollworms with pheromone traps. *PKV Research Journal* 18(1), 87-90.
 122. TAMHANKAR, A.J. (1995). Sex pheromone gland and calling behaviour of female spiny bollworm *Earias insulana* (Boisduval). *Entomon* 20, 1-4.
 123. TAMHANKAR, A.J., RAJENDRAN, T.P., BHAMBURKAR, M.W. AND HARWALKAR, M.R. (1993). Optimum pheromone blend for pink bollworm males: Evaluation with two experimental designs. *International Journal of Pest Management* 39, 111-12.
 124. TAMAKI, Y. AND YUSHIMA, T. (1974). Sex pheromone of the cotton leafworm, *Spodoptera litoralis*. *Journal of Insect Physiology* 20, 1005-14.
 125. TAMAKI, Y., NOGUCHI, H. AND YUSHIMA, T. (1973). Sex pheromone of *Spodoptera litura* (F.) (Lepidoptera: Noctuidae): Isolation, identification and synthesis. *Applied Entomology and Zoology* 8, 200-203.
 126. TAMAKI, Y., OSHAWA, T., YUSHIMA, T. AND NOGUCHI, H. (1976). Sexpheromone and related components secreted by virgin females of *Spodoptera litura* (F.) Japanese Journal of Applied Entomology and Zoology 20, 81-88.
 127. TEAL, P.E.A., TUMULINSON, J.H. AND HEATH, R. (1986). Chemical and behavioural analysis of volatile sex pheromone components released by calling *Heliothis virescens* (F.) females (Lepidoptera: Noctuidae). *Journal of Chemical Ecology* 12, 107-26.
 128. TEAL, P.E.A., TUMULINSON, J.H., McLAUGHLIN, J.R., HEATH, R. AND RUSH, R.A. (1984). (Z)-11-hexadecen-1-ol: a behaviour modifying chemical present in the pheromone gland of female *Heliothis zea* (Lepidoptera: Noctuidae). *Canadian Entomologist* 116, 777-79.
 129. TUMLINSON, J.H., HARDEE, D.D., GUELDER, R.C., THOMPSON, A.C., HEDIN, P.A. AND MINYARD, J.P. (1961). Sex pheromones produced by male boll produced by male boll weevil: Isolation, identification and synthesis. *Science* 166, 1010-12.
 130. TUMLINSON, J.H., MITCHELL, E.R. AND YU, H.S. (1990). Analysis and field evaluation of volatile blend emitted by calling virgin females of beet armyworm moth *Spodoptera exigua* (Hübner). *Journal of Chemical Ecology* 16, 3411-23.
 131. TUMLINSON, J.H., HENDRICKS, D.E., MITCHELL, E.R., DOOLITTLE, R.E. AND BRENNAN, M.M. (1975). Isolation, identification and synthesis of the sex pheromone of the tobacco budworm. *Journal of Chemical Ecology* 1, 203-14.
 132. VAKHARIA, V.N., RAINA, A.K., KINGAN, T.G., 1995. Synthetic pheromone biosynthesis activating neuropeptide gene expressed in a baculovirus expression system. *Insect Biochemistry and Molecular Biology* 25,583-89.

133. VETTER, R.S AND BAKER, T.C. (1984). Behavioural responses of male *Heliothis zea* moths in sustained flight tunnels to combination of four compounds identified from female sex pheromone gland. *Journal of Chemical Ecology* 10, 193-202.
134. VICKERS, N.J. AND BAKER, T.C. (1997). Chemical communication in *Heliothine* moths. VII. Correlation between diminished responses to point-source plumes and single filaments similarly tainted with a behavioural antagonist. *Journal of Comparative Physiology A. Sensory Neural and Behavioural Physiology* 180, 523-36.
135. VILLAVASO, E.J., MCGOVERN, M.L. AND WAGNER, T.L. (1998). Efficacy of bait sticks versus pheromone traps for removing boll weevils (*Coleoptera: Curculionidae*) from released populations. *Journal of Economic Entomology* 91, 637-40.
136. WHITMAN, J.A. AND RAO, G.V.K. (1993). Pheromone trapping in south Asia: Review and requirements. *Bulletin OILB/SROP* 16,149-56.
137. WHITCOMB, W.H. AND MORENGO, R.M. (1985). Use of pheromones in the boll weevil detection and control programme in Paraguay. *Florida Entomologist* 69, 153-56.
138. YU, Z. (1996). Auto-dissemination of a baculovirus for suppression of beet armyworm, *Spodoptera exigua* Hübner (Lepidoptera: Noctuidae). M.S. thesis, University of Kentucky, Lexington, USA.
139. YU, Z AND BROWN, G.C.(1997). Auto-dissemination of a beet armyworm (Lepidoptera:Noctuidae) baculovirus under laboratory conditions. *Journal of Economic Entomology*. 90, 1187-94.
140. YUSHIMA, T., TAMAKI, Y., KAMANO, S. AND OYAMA, M. (1974). Field evaluation of a synthetic sex pheromone, lidur, as an attractant for males of *Spodoptera litura* (F.) (Lepidoptera: Noctuidae). *Applied Entomology and Zoology* 9, 147-52.

This paper is a review which has appeared amongst "Selected Titles" recommended by a Consortium for International Crop Protection formed by the U.S. Department of Agriculture

About the author



Dr A.J. Tambankar did his M.Sc. (Agriculture) from Nagpur University and Ph.D. from MPKV. He is currently heading the Pheromone and SIT group of Nuclear Agriculture and Biotechnology Division, BARC. He has published several papers in national and international journals on the subject of insect sex pheromones and sterile insect technique.

Emission from Charge Transfer State of Dye-Sensitized TiO₂ Nanoparticles: A New Approach to Determine the Back Electron Transfer Rate and Verification of Marcus Inverted Regime

Hirendra Nath Ghosh

Radiation Chemistry & Chemical Dynamics Division
Bhabha Atomic Research Centre

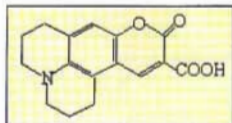
Introduction

ELECTRON TRANSFER (ET) BETWEEN molecular adsorbates and semiconductor nanoparticles has been a subject of intense research interests for many years. The understanding of this fundamental process is essential for the application of semiconductor nanoparticle materials in photography, solar energy conversion, waste degradation, and nano-scale devices. For example, photoelectrochemical solar cells based on dye-sensitized nanocrystalline TiO₂ thin films have received much attention in recent years because of their potential applications as a cost effective alternative to silicon based cells. Gratzel's group reported that solar cells based on Ru(dcbpy)₂(NCS)₂ [dcbpy=(4,4'-Dicarboxy-2,2'-Bipyridine)] (or Ru N3) sensitized nanocrystalline TiO₂ thin films could achieve a solar to electric power conversion efficiency of about 10%. The high conversion efficiency can be attributed to high solar energy harvesting by the sensitizer and high photon to current conversion efficiency. A high photon to current conversion efficiency requires a fast electron injection rate from the sensitizer to the semiconductor and a much slower back electron transfer rate to the sensitizer.

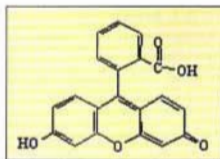
It is very important to understand the forward and backward electron transfer processes, especially their

dynamics in semiconductor nanoparticles and suitable adsorbates. So far most of the electron transfer dynamics have involved dye molecules as the adsorbates. In many of these studies the dye molecules are excited using suitable wavelength of light and dynamics of electron transfer is measured by their transient absorption or fluorescence decay and consequently electron transfer rate constants have been measured from these analyses. Back electron transfer rates have been also measured by monitoring the bleach recovery of the ground state absorption of the dyes. Recently, femtosecond mid-IR spectroscopy has been used to study the interfacial ET processes by directly monitoring the injected electrons in the semiconductor nanoparticles and also by observing the vibrational spectral changes of the adsorbates. IR studies mostly eliminate the spectral overlap problems that hinder the estimation of ET dynamics in the visible region. This approach is favored for small adsorbates such as SCN⁻ and Fe(CN)₆⁴⁻ which have been used to study the back electron transfer dynamics.

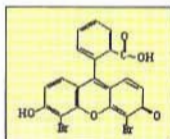
In the present article it is discussed that in the case of coumarin-343 and xanthene dyes (Fluorescein (FL), Di-bromo Fluorescein (DBF), Fluorescein Isothiocyanate (FITC), 5(6) Carboxy Fluorescein (5,6 CF) and Eosin Yellowish (EY)) (Scheme 1) when



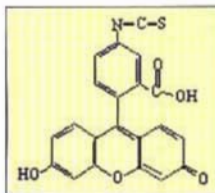
Coumarin 343



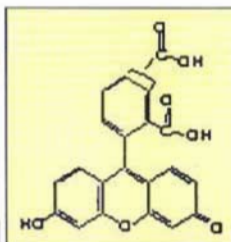
Fluorescein



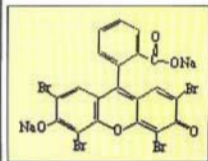
Di-bromo Fluorescein



Fluorescein Isothiocyanate



5(6)Carboxy Fluorescein



Eosin Yellowish

Scheme 1

adsorbed on the TiO_2 nanoparticle surface, a good portion of the molecules form charge transfer complex. On excitation of the above systems two processes take place simultaneously. First adsorbed dye molecules go to the excited state and then inject electron into the conduction band of the nanoparticle. Second, when the photons excite the charge transfer complex, electron injection takes place directly to the conduction band of the nanoparticle rather than via the excited state of the dye molecules. Back electron transfer dynamics have been measured by monitoring the bleach recovery dynamics using time-resolved picosecond spectroscopy. When the electron comes back in the case of charge-separated species of CT complex from the nanoparticle to the dye molecule, a low quantum yield CT emission has been observed in the dye-nanoparticle systems. Measuring the decay of the CT emission by picosecond time-resolved

fluorescence spectroscopy we get the dynamics of back electron transfer reaction from nanoparticle to the dye molecule.

Experimental

Time-resolved absorption and emission measurements were carried out using a picosecond laser pump-probe spectrometer and a time-resolved fluorescence spectrometer. Nanometer-size TiO_2 was prepared by controlled hydrolysis of titanium(IV) tetraisopropoxide in water.

Results & Discussion

a) Assignment of charge transfer absorption and emission spectra:

To study the dye sensitized electron transfer reaction in the excited state, it is very important to know the type

of interaction of the dye molecules when they adsorb on the nanoparticle surface. Shown in Fig.1, the steady-state optical absorption spectra of fluorescein in water and in TiO_2 colloidal solution. On addition of TiO_2 nanoparticle, the optical density of the dye increases dramatically and goes broad and red shifted. Fig. 1a, Fig. 1b and Fig 1c show the optical absorption spectra of the dye in water, in ZrO_2 colloid and TiO_2 colloid.

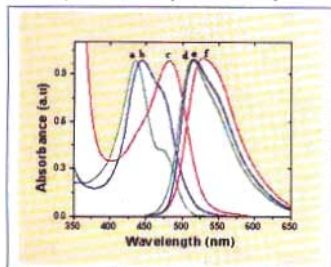
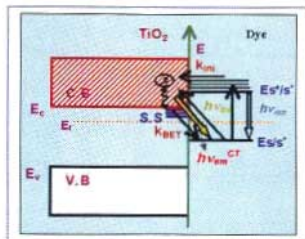


Fig. 1 Normalized (A) Optical absorption spectra of fluorescein dye (a) in water, (b) in ZrO_2 colloid, and (c) in TiO_2 colloid; and (B) Emission spectra of fluorescein dye (d) in water, (e) in ZrO_2 colloid, and (f) in TiO_2 colloid.

It is seen from Figure 1 that the optical absorption of the dye goes little red shifted as it is adsorbed on ZrO_2 surface. Here we have chosen ZrO_2 nanoparticles because it is non-injecting surface ($E_g = 5.2$ eV) for these dyes and can see the optical behavior of the dyes in the nanoparticle surface. The above results indicate that on adsorption of the dye molecule on TiO_2 nanoparticle surface, a new ligand to metal charge transfer (CT) band is formed.



The experimental observation can be explained in the following manner. When the dye molecules get adsorbed on the surface, a fraction of the dye molecules get just adsorbed on the surface of the nanoparticle and the rest goes for charge transfer interaction and gives a charge transfer (CT) complex. Formation of charge transfer complex has been observed in all the dye molecules studied when they get adsorbed on TiO_2 nanoparticle surface. Fig. 1d, shows the emission spectra of fluorescein dye in water at pH



Scheme II: Mechanistic scheme showing the electron injection and back electron transfer processes on Dye-sensitized semiconductor nanoparticle. E_c and E_v are the valence and conduction band, E_s and S are the fermi energy level and surface states, E_{s^*} and S^* are ground and excited state redox potential, k_{inj} and k_{BET} are electron injection and back electron transfer rate, $h\nu_{exc}$ and $h\nu_{em}$ excitation and emission.

2.8 peaking at 515 nm ($\phi = 0.072$). Fig. 1e shows the emission spectra of fluorescein dye in ZrO_2 colloid at pH 2.8 peaking at 518 nm ($\phi = 0.068$). To see the effect of the emission spectra of the dye, non-injecting ZrO_2 surface was chosen. The shift in emission spectra can be attributed to the electronic effect of the nanoparticle surface. But, when the dye is adsorbed on TiO_2 surface, it gives a lower quantum yield red-shifted broader emission spectra (Fig.1f) ($\phi = 0.048$) peaking at 530 nm with a broad shoulder at 545 nm. This emission is attributed to the combination of dye emission, which does not inject electron in the TiO_2 nanoparticle and the charge transfer (CT) emission. Similar type of lower quantum yield with broad and red-shifted emission spectra has been observed for coumarin 343 and in other xanthene dyes. On excitation, the photon excites the free dye molecule adsorbed on the surface and also the CT complex of the dye- TiO_2 nanoparticle. Some of the adsorbed dye molecules, which get excited, inject electrons into the conduction band of the nanoparticle while some does not inject. The dyes, which do not inject, give emission. On the other hand, excitation of the charge transfer complex goes for charge separation, which leads to direct injection to the conduction band of the nanoparticle instead of via excited state of the dye. On recombination of the charge separated CT complex, the electron comes back to the parent cation. As a result, it

gives charge transfer emission. A schematic diagram is given in Scheme II to show the excitation, injection, back electron transfer, charge transfer emission of the above dye-nanoparticle systems.

b) Assignment of transient absorption spectra:

Transient absorption spectra in the pico-second time domain in the visible region (500-900 nm) have been carried out for all the dye-sensitized TiO₂ nanoparticles using 532 nm picosecond laser pulses. Figure 2 shows the transient absorption spectra of C-343 sensitized TiO₂ nanoparticle. In this experiment a transient peak at 635 nm with a shoulder at 580 nm is assigned to the cation radical of C-343 and a broad positive feature in the spectral region 700-900 nm is observed which is attributed to the conduction band electrons in the nanoparticles. The band at 635 nm shows decay (Fig. 2 inset) and is due to the back reaction involving recapture of the conduction band electrons by the C-343 cation radicals. The decay of the observed signal can be fitted by a multiexponential function with time constants of 190 ps and >5 ns.

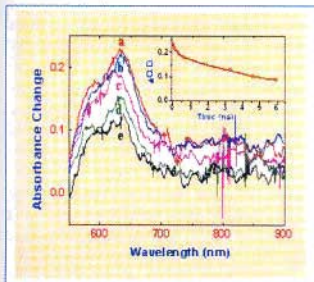


Fig. 2 Transient absorption spectra of coumarin 343 sensitized TiO₂ colloid in water at (a) 35 ps, (b) 130 ps, (c) 660 ps, (d) 1.98 ns, and (e) 3.4 ns after 532 nm excitation. [Inset: Kinetic decay trace of C-343 cation radical at 630 nm]

We have also carried out transient absorption studies for all the xanthene dyes sensitized TiO₂ nanoparticles. Fig. 3 shows the transient absorption spectra of 5(6) Carboxy Fluorescein (56 CF) sensitized TiO₂ in the spectral region 500-550 nm peaking at 520nm

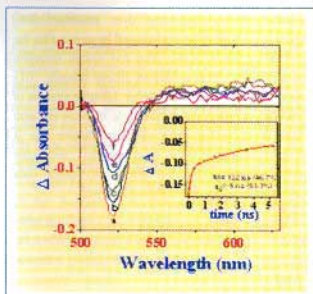
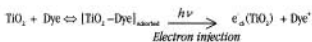
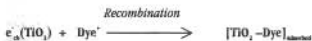


Fig.3 Transient absorption spectra of 5(6)-carboxy fluorescein sensitized TiO₂ nanoparticle in water at (a) 0, (b) 33, (c) 66, (d) 330ps (e) 1.98 and (f) 3.2 ns after excitation at 532 nm. [Inset: Kinetic trace of the bleach recovery at 520 nm].

nanoparticle in water. In this experiment a bleach peak and a broad positive feature in the spectral region 550-800 nm are observed. The bleach peak appears due to disappearance of the ground state of the dye-TiO₂ complex, on excitation by the laser pulse. The broad spectral absorption in the 550-800 nm region is attributed to the conduction band electrons in the nanoparticle. The reactions can be depicted in the following scheme.



where, Dye⁺ is the cation radical of the dye and e_{cb}⁻ is the conduction band electron in TiO₂ nanoparticle. However, the bleach at 520 nm recovers (Fig 3 Inset) and is due to the back reaction involving recapture of the conduction band electrons by 56 CF cation radical. The recombination reaction was found to be multiexponential process with time constants of 122 ps and > 5 ns.



c) Time-resolved fluorescence measurements:

In the present report we are going to demonstrate that dynamics of back electron transfer reaction for

coumarin 343 and xanthene dyes sensitised TiO₂ nanoparticle can also be investigated by monitoring the red shifted emission band. The red shifted emission band has been characterized as charge transfer (CT) emission band as described earlier. Lifetime analysis of the CT emission gives the exact rate of back electron transfer reaction. The back electron transfer rate is also cross-checked by a complimentary technique namely picosecond transient absorption studies. Data from both the techniques matched very well.

After electron injection, recombination reaction takes place for the charge separated CT complex. When the recombination takes place a charge transfer emission is observed.

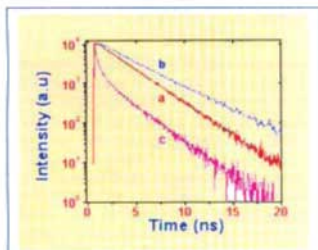


Fig. 4 Single photon counting studies of (a) 5(6)-carboxy fluorescein in water, (b) 5(6) carboxy-fluorescein sensitized ZrO₂ colloid in water, and (c) 5(6)-carboxy fluorescein sensitized TiO₂ colloid in water emission after 445 nm excitation.

Shown in Figure 4 are the typical emission decay traces for 56 CF in water, 56 CF sensitized ZrO₂ nanoparticle and 56 CF sensitized TiO₂ nanoparticle in water. 56 CF in water gives single exponential decay with lifetime of 2.6 ns. To compare the excited state lifetime of 56 CF dye on nanoparticle surface, ZrO₂ was chosen because the chemical nature of ZrO₂ surface is very similar to that of TiO₂ nanoparticle and the conduction band is very high in energy ($E_c = 5.2$ eV). Thus, electron injection is not possible although the dye is adsorbed

on the surface. The fluorescence lifetime of 56 CF on ZrO₂ surface is found to be 2.8 ns. On the other hand, 56 CF sensitized TiO₂ nanoparticle gives low quantum yield emission band. The emission decay of the band at 550 nm was fitted by a multi-exponential function with lifetimes of 129 ps (77.5%), 573 ps (14.4%) and 2.35 ns (8.1%). The first two decay components are attributed to the back electron transfer rate constants and the long component is assigned to the radiative life time of 56 CF adsorbed on TiO₂ surface, which does not inject electron in the conduction band. It is to be noted that the faster component of back electron transfer reaction measured by picosecond spectroscopy is found to be very close to the values measured by picosecond time-resolved fluorescence measurements. The most important point is that time-resolved fluorescence measurements can also be used to study the back electron dynamics of dye-sensitized TiO₂ nanoparticle systems.

d) Back electron transfer reaction and marcus inverted regime:

Both classical and quantum mechanical theories of electron transfer (ET) predicts that ET rates should ultimately decrease with increasing thermodynamic driving force ($-\Delta G^\circ$). The back electron transfer rate (k_{bet}) can be given as

$$k_{\text{BET}} = \left(\frac{2\pi}{\hbar} \right) |H_{AB}|^2 \frac{1}{\sqrt{4\pi\lambda kT}} \exp \left\{ -\frac{(\Delta G^\circ + \lambda)^2}{4\lambda kT} \right\}$$

where λ is the total reorganization energy, H_{ab} is the coupling element, ΔG° is the overall free energy of reaction = ($E_c - E_{\text{ox}} +$), E_c is the potential of electrons in the conduction band of the semiconductor (-0.52V), $E_{\text{ox}} +$ is the redox potential of the adsorbed dye (Scheme II). The prediction of "inverted" rate behavior has convincingly demonstrated in many organic, inorganic/organometallic and biological redox processes in both liquid and frozen homogeneous solution but not many reports are available for nanoparticle surface. In the present observation we have demonstrated the inverted behavior for the back electron transfer reaction of xanthene dye sensitized TiO₂ nanoparticle system. The free-energy ($-\Delta G^\circ$) has

been calculated from E_{ct} of the charge-transfer (CT) complex on the nanoparticle surface. In the present investigation E_{ct} is being calculated from the crossing point of charge-transfer excitation and emission spectra and is shown. Figure 5 is the plot of back electron transfer rate (k_{et}) vs E_{ct} . It has been observed that with increasing E_{ct} , rate of back electron transfer (k_{et}) decreases.

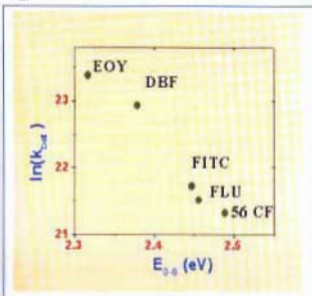


Fig. 5 Plot of $\ln(k_{et})$ versus the driving force (E_{ct}) for back electron transfer to the cation radical of the dyes. E_{ct} is the linear function of $-\Delta G$.

The observed trend of decreasing back electron transfer rate (k_{et}) with increasing driving force would be consistent with Marcus inverted region behavior if the electronic coupling does not vary considerably in these different xanthene dyes. Since all these xanthene dyes have same anchoring group to TiO_2 , and similar π^* electron donating orbital, we think that the substitution to the benzene ring should not change the electron coupling much. We have attributed the observed trend to the Marcus inverted region kinetic behavior. A more detailed analysis in the future would quantify the variation of the coupling strength in these different *xanthene dye sensitized TiO_2 CT complexes. Our ongoing experiments are carried out to find out the back electron transfer dynamics of charge transfer complex in different solvent, changing their polarity and temperature. These measurements will help us to determine many electron transfer parameters for the heterogeneous electron transfer reaction, which have not been determined so far.

Conclusions

Pico-second transient absorption and time-resolved emission spectroscopy have been used to study photoinduced electron transfer dynamics in coumarin and xanthene dye sensitized TiO_2 nanoparticles in aqueous solution. On excitation with laser pulse a bleach has been observed for xanthene/ TiO_2 systems and cation peak for C-343/ TiO_2 and a broad electron absorption (550-800 nm) in the nanoparticle have been found for all the dye sensitized TiO_2 nanoparticle systems. The dynamics of the injected electrons have been measured by monitoring the bleach recovery rate at the bleach peak and also monitoring the cation peak in the transient absorption spectra. The electron injection times are found to be pulse limited but the subsequent back ET is found to be a multi-exponential process.

On excitation of the xanthene dye sensitized TiO_2 nanoparticle systems, electron injection takes place in two different ways. Electron injection to the conduction band of TiO_2 nanoparticle can take place through the excited state of the dye. The other mechanism is through direct injection to the conduction band on excitation of the charge transfer complex. When the recombination reaction takes place, charge transfer (CT) emission has been observed for all the dye sensitized nanoparticle systems. Monitoring the CT emission, the back ET rate has been determined. We have also found that back ET rate for the xanthene dye sensitized TiO_2 CT complex decreases as the relative driving force increases. Assuming a negligible change in the electronic coupling, our results provide the evidence for the Marcus inverted region kinetics behavior for an interfacial ET process. Our ongoing experiments are carried out in different dye-nanoparticle CT complexes to find out the back ET dynamics on heterogeneous surface by changing the polarity and temperature of the media. These measurements will help us to determine many electron transfer parameters for the heterogeneous electron transfer reactions and also lead to new insights of the Marcus inverted region interfacial ET kinetics.

References

1. Ghosh, H.N.J. *Phys. Chem. B* 1999, 103, 10382.
2. Ramakrishna, G.; Ghosh, H.N.J. *Phys. Chem. B* 2001, 105, 7000.

Acknowledgements

I would like to thank Mr. G. Ramakrishna for pursue many experiments and fruitful suggestions and Dr. A.V. Sapre, Dr. T. Mukherjee and Dr. J.P. Mittal for their constant encouragements

Dr. Harendra Nath Ghosh was awarded the prestigious Anil Kumar Bose Memorial Award for the year 2000 by the Indian National Science Academy, New Delhi. Dr. Ghosh had won the prestigious INSA Young Scientist Award for the year 1998. The present award is given to an INSA Young Scientist awardee for the best output during the year after the INSA Young Scientist Award.

About the author ...



After obtaining his M.Sc. in Chemistry from IIT, Kharagpur, in 1989, Dr. Ghosh joined Chemistry Division, BARC, in 1990, through BARC Training School Course (33rd batch). He obtained his Ph.D. degree in 1996 from Bombay University for his work on fast photophysical and photochemical processes in liquid and microheterogeneous media. He did his post-doctoral studies, for the period of 1997-98, with Prof Tim Lian at the Chemistry Department of Emory University, Atlanta, USA, on femtosecond interfacial electron transfer dynamics, using Infrared spectroscopic detection. Dr. Ghosh was awarded the "INSA Young Scientist Medal" in 1998 for his outstanding Ph. D. work. He has also received the prestigious "Anil Kumar Bose Memorial Award" in 2000 for the best output during the year after the INSA Young Scientist Award by the Indian National Science Academy, New Delhi. Recently, he is involved in developing Femtosecond laser spectrometer detecting in both visible and infrared region. His current research interests include ultrafast interfacial electron transfer and electron solvation dynamics in microheterogeneous media.

Automation and Control: Technology Spin-Offs

Y.S.Mayya

Control Instrumentation Division
Bhabha Atomic Research Centre

Introduction

THIS ARTICLE REVIEWS SOME OF THE significant spin-off technologies developed or being developed by BARC during the last decade in the area of automation & control. These projects represent consolidation and extension of the pioneering developments carried-out by BARC over the previous few decades. The article covers development of control systems for the Giant Metre-wave Radio Telescopes (GMRT), vehicle mounted trackers, airborne tracking & stabilisation systems, traction control systems, real-time networks and land navigation systems. The applications span a wide area and include scientific research, industry, defence and transportation sectors. The underlying technology of computer hardware and software, used to realise these systems is changing rapidly requiring constant re-skilling. This has also increased user expectations in terms of performance, miniaturisation, autonomy, maintainability and reliability. Purpose-built microcontrollers and DSPs make it possible now to realise hard-real time applications using computers-which-until now were monopolised by hardware intensive solutions. Motor controllers, inverter and converter control applications fall in this category.

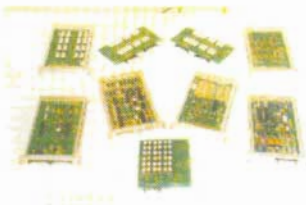
In the following paragraphs, we look at the above developments from the perspective of technological challenges they pose and the opportunities they offer.

Servo control systems for Giant Metre-wave Radio Telescopes (GMRT)

Giant Metre-wave Radio Telescope, near Pune, is a front line research facility for astronomy and



GMRT Telescope array

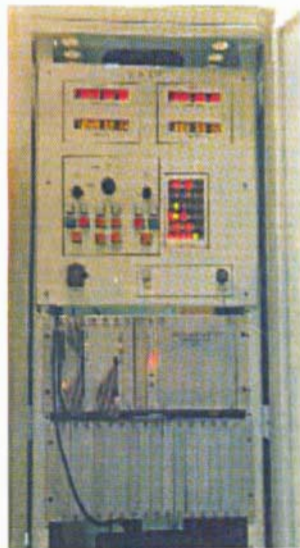


Electronic Circuit cards used in GMRT Servo

astrophysics aimed at studying phenomena, such as, sun, stellar flares, pulsars, quasars, radio galaxies and origin and evolution of the universe. GMRT consists of 30 fully steerable, 45 m. diameter parabolic dishes arranged at the centre and 3 arms of a Y shaped array. Twelve telescopes are located within the 1 km X 1 km array centre and six each along the three arms of a Y shaped configuration extending to about 14 km from

the array centre. The dish is mounted on a Elevation over Azimuth mount.

The challenges in the design and development of servo control system for such a large telescope array were manifold. The telescopes are operated remotely and largely unmanned. Hence safety of the structure under gusty winds is a primary concern and must be ensured by the system autonomously. In addition to meeting the servo performance specifications, the design accommodates maintainability using remote diagnostics, fail-safe operation without degrading availability and high degree of configurability. Cost was of overriding concern. Realising these objectives, computer based station servo computers along with thyristor drive amplifiers were developed indigenously and progressively commissioned during 90's.



GMRT Control cabinet



GMRT Motor drive cabinets

An 8086 uP based Servo Control Computer located at the base of each telescope facilitates co-ordinated program tracking of stars by all the telescopes in the array as per the target trajectory information periodically sent by a central computer. Each axis is driven by two numbers of 6 HP DC servo motors in counter-torque arrangement and are powered by SCR power amplifiers. The control topology adheres to the classical three loop cascade: the outer position loop, followed by speed loop and current loops. The servo system guarantees pointing and tracking accuracy of 1 mRad. The control system implements operational/safety interlocks, type I/ Type II position loop servo, antenna angle and status displays, manual positioning & slew modes of operation and two-way communication with central computer. The servo performance specifications are, tracking error of 1 arc minute @ 40 kmph wind, angle display resolution of 10", slew rates of 30°/ min and precision tracking rates of 150'/min for Az.

Antenna Control Systems for the FALCON and PTA projects of DRDO

The FALCON and PTA programs of DRDO provided challenging technology development opportunities in the area of real-time embedded control systems. As part of this program, a family of vehicle mounted antenna control systems were developed during the 90's, applying modern techniques and tools for dynamic modelling and simulation, software engineering and modelling etc. The systems evolved progressively, incorporating changes and new



requirements in successive models as the result of experience gained during flight trials.

These vehicle mounted antenna control systems are designed to track the airborne vehicles NISHANT and LAKHSHA. The technology is indigenously designed and developed and has been successfully demonstrated during various flight trials.



The NISHANT Remotely Piloted Vehicle (RPV) is used for battlefield reconnaissance and is required to be tracked from launch to recovery from a ground based

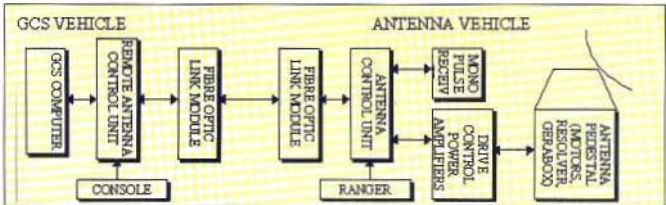
antenna vehicle. The antenna is a vehicle mounted, 6' dia, continuously steerable Az-only mount, fan beam antenna, with tracking speeds of $20^\circ/\text{sec}$, tracking acceleration of $20^\circ/\text{sec}^2$ and tracking accuracy of 0.1° . The computer based Antenna Control system incorporates anti back-lash drives, PWM amplifiers, cascade control loops with torque, speed and position control. Control system is interfaced to the ranging system and performs range dependent sector scanning if target is lost while tracking. The target is tracked from a Ground control system (GCS) vehicle through a Remote Antenna Control Unit (RACU) which is linked to the base unit through optical fibre links.

PTA is used for training ship or land based missile or gun crew in weapon engagement. PTA is to be tracked by vehicle or ship mounted, continuously steerable Az only mount antennas, with speed of $30^\circ/\text{sec}$ and tracking acceleration of $20^\circ/\text{sec}^2$ and tracking accuracy of 0.5° . The system incorporates auto-track, scan, manual positioning and slew modes of operation in LOCAL and REMOTE control regimes.

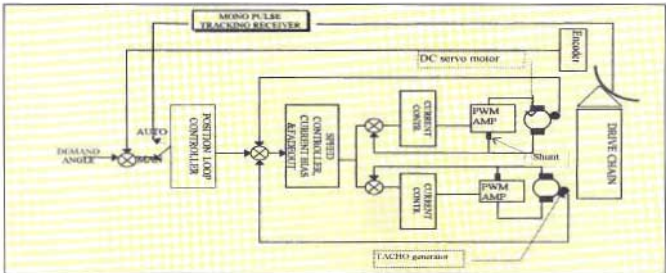
The systems are based on 80286 processor, and are designed for JSS 55555 qualification. The software was developed as per ESA software engineering standards. Software analysis and design was carried-out using Object Modelling Technique (OMT) methodology. This provided deeper insights in to the art of applying OO methods to real-time applications. The systematic approach to software development and documentation yielded rich dividends during the subsequent upgrades to the software.

Real-time Networks

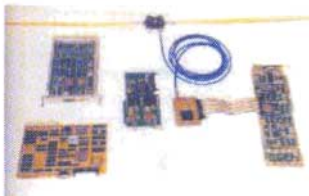
Real-time networks form the back-bone of any distributed control system. High throughput, deterministic response-times even under varying load conditions, robust protocols and media level redundancy are the defining characteristics of these networks. In order to support the integration of distributed control systems in nuclear power plants, ddevelopment of real-time Local Area Networks based on IEEE 802.4 Token Bus Media Access Protocol was undertaken during the early 90's. As part of this development 80186 based network controller cards for



Falcon ACU and RACU



ACU console & control loops



VME, ISA bus systems among others, dual redundant carrier-band modem cards, 802.2 LLC software, network drivers and APIs for pSOS, DOS and WINDOWS environments were developed and deployed.

This technology was transferred to ECIL Hyderabad, and this forms the back-bone of the distributed Programmable Logic Controllers supplied by them for use in Kaiga and Rajasthan atomic power stations. Reactor regulating System and Boiler pressure & level control systems in these reactors also employ this technology.

MIL-STD-1553B Data Bus

This avionics standard integration network forms the back-bone of many of the ongoing projects for defence applications. A new development initiative was launched with an aim to master all aspects of this technology. Development and testing facilities were created and a variety of interface cards and software components were realised as part of this activity.

Microprocessor-based Traction Control System for Thyristorised AC Locomotives

A collaborative technology development / demonstration initiative of DOE, RDSO and BARC, this effort was targeted to retrofit the large number of tap-changer AC locomotives of Indian Railways by thyristor based power converters and microprocessor based controls. The loco is propelled by six numbers of ~700 HP, separately excited DC motors, each of which is powered by a thyristor converter which is made-up of two half bridges connected in sequence. The field

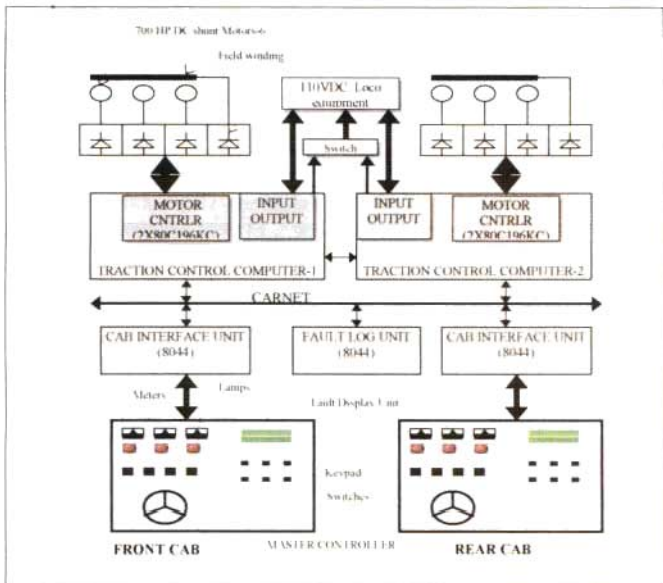
windings of three motors of one group are connected in series and is powered by a separate converter.

The challenges of developing the complex, state-of-the-art traction control system lay in many fronts- the hard-real-time constraints imposed by thyristor firing pulse control, the EMI environment of high current, high voltage switching devices, the unforgiving hot and dusty environment of a locomotive.



The system has a distributed architecture with multiple micro computers (80286 based supervisory controller, dual 80C196KC based motor controller and 8044 RUP1 based communication controllers) integrated around CARNET network and features dual redundancy. The loco is controlled by two Traction Control Computers configured in Master /Slave fashion. The control system integrates loop and logic control with fault logging and status monitoring. It incorporates computer triggered phase angle control of the armature and field converters, armature and field current control in three regimes (constant torque, constant power, constant Ia/If), dynamic brake control, two step sequence control, slip/slide detection and control, software based loco interlocks and extensive fault logging and annunciation capability. Specially designed hardware accommodates the harsh environment of an Electric locomotive.

The control loops and loco logic are programmed using a purpose-built function block programming language called Block Control Language. BCL was a significant spin-off technology in it-self, impacting development of software for reliable control applications.

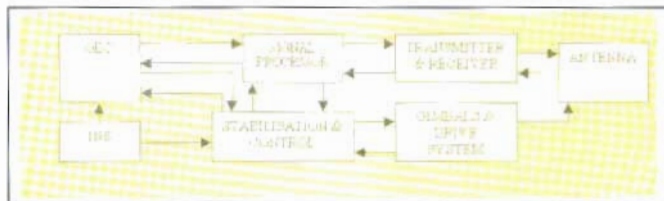
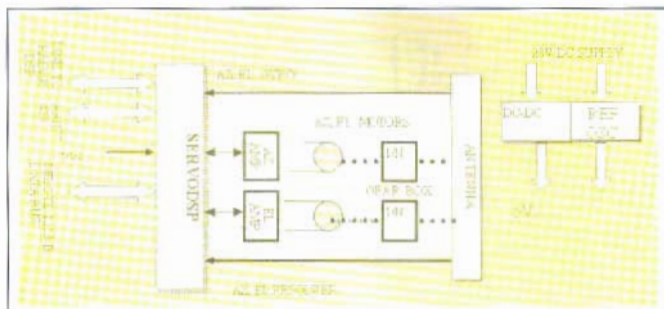


Stabilisation & Tracking Antenna Control Systems for Air-borne Applications

The ongoing development of airborne tracking and stabilisation systems represent an important extension of our activities. In these applications, while tracking a target, the control system must also stabilise the antenna in space against vehicle's rotational disturbances in pitch, roll and yaw. The servo system must reject disturbances induced by vehicle vibrations and linear accelerations. The large linear accelerations in all directions make demands on mass balancing and motor torque. The complexity is compounded by the constraints of space, weight, power dissipation, heating and servicing constraints.

Inertial sensors such as rate gyros and IMUs are used to stabilise the antenna using either feedback or feed-forward compensation schemes. The antenna is mounted on two degrees-of-freedom gimbal mechanism and target tracking is achieved by steering the antenna so as to minimise monopulse tracking errors. The tracker provides real-time updates on measured target positions and rates which are then used in the vehicle guidance loops.

The demanding real-time computations require a high performance control engine. This provided opportunities to employ floating point SHARC DSP for the control task. The evolution of control strategy and prediction of performance is aided by modelling and simulation studies.



DSP based controller and system block diagram

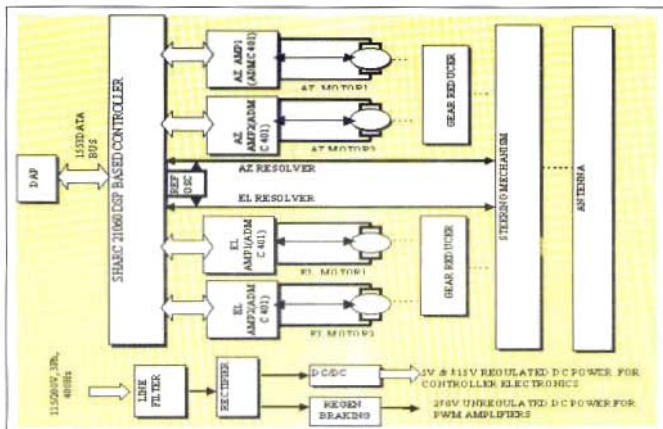
Antenna Platform Unit for Air-borne Multi-mode Radar

Efforts are underway for indigenous development a high performance Antenna Platform Unit for an airborne multi-mode Radar. This is a highly multi-disciplinary venture requiring expertise in the area of control systems, inertial systems, modelling & simulation, motor drives, Mil-1553, real-time embedded system hardware & software and mechanical design.

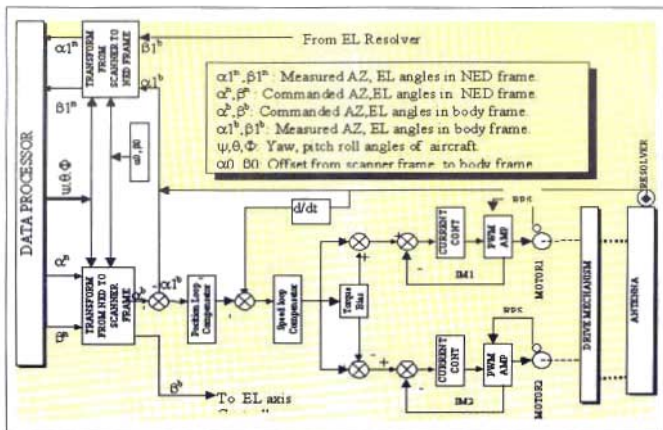
The 650 mm dia. flat plate antenna is scanned by the APL in Azimuth and Elevation planes as per the scan pattern commanded by the external Data processor. The command angles are updated by the Data processor at 200 Hz rate via. 1553B data bus. The

measured antenna angles and errors are to be reported back to DAP at 200 Hz rate. The antenna should be stabilised in space air-craft body attitudes & rates (roll, pitch & yaw rates). The commanded angles are in the North-East-Down (NED) frame- these have to be converted by APL to the scanner frame and then used for positioning the antenna. For this purpose, the instantaneous aircraft body attitudes (roll, pitch and yaw angles) are used. Additionally, the APL is designed to function within specifications under increased load caused by aircraft accelerations. It should also reject linear acceleration body disturbances.

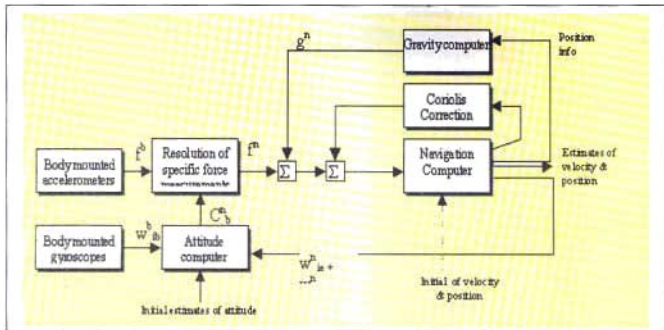
The APL consists of two axis gimbal driven by brush-less AC servo motors and gear reducers. Each axis is driven by two motors arranged in counter torque mode which eliminates the effect of gear back-lash. Each of



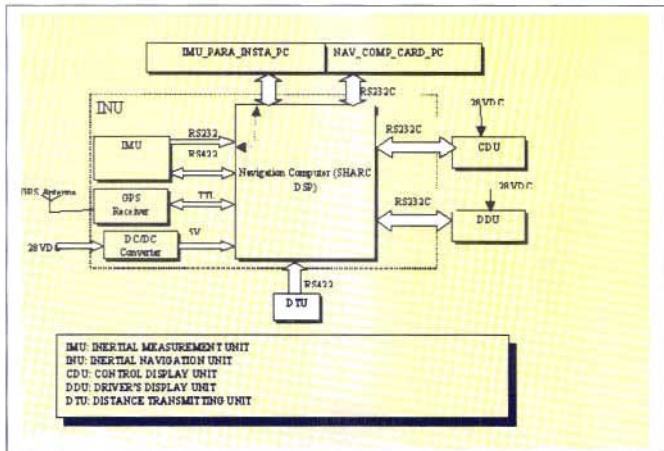
API controller block diagram



API control loops



Navigation frame mechanisation



ALNS hardware block diagram

the four motors is driven by a four quadrant power amplifier. Quick deceleration of the load is made possible due to the regenerative braking supported by the four quadrant operation. Regenerative braking is also brought in to play under powered off conditions, to arrest the antenna from gaining high accelerations.

The command input to the power amplifiers is generated by the APL controller which is a SHARC DSP based system with hosts the control software. The motor power amplifier is being developed using modern motor control DSPs for 3 phase IGBT bridge control. Motor mounted resolvers are used as rotor position sensors for realising sinusoidal commutation of the brush less AC motor. The position of the antenna is measured along AZ and EL planes by a pair of high precision resolvers coupled to the respective load axes. The APL controller receives commands from and sends responses to the DAP via the MIL-STD-1553B data bus.

Fibre-optic Gyro based Land Navigation System (GLNS) for Battle-tanks

This development is targeted to meet defence needs for advanced land navigation systems for use in battle tanks. The system is required to provide a position accuracy of 1% of distance travelled and heading accuracy of 1°. The design of the ALNS is based around an Inertial Measurement Unit (IMU) consisting of a triad of 0.1°/hour fibre optic gyros (FOG) and 500 µg accelerometers. A SHARC-21060 DSP based navigation computer performs in real-time, attitude computation, specific resolution and navigation computations.

While inertial navigation provides good short term accuracy and is autonomous, the errors in the long term grow unbounded when sensor and alignment errors are considered. For this purpose, the ALNS integrates a distance transmitting unit (DTU) and GPS receiver for improving the long-term navigation accuracy.

The navigation computer provides an estimate of the vehicle position in LAT, LONG, Height co-ordinates of the reference ellipsoid. These are in turn converted in to UTM and MGRS co-ordinates and presented to the user.

The user interacts with the ALNS from a DDU (Driver's Display Unit) and CDU (Control Display Unit). The DDU facilitates viewing of the vehicle heading, bearing to destination and the vehicle position. The CDU provides an interface to the commander for performing various functions such as self and destination navigation, way-point and route planning, gyro compassing, calibration and testing.

Conclusion

The various project activities outlined above have also resulted in the creation and consolidation of expertise in various areas such as digital/ analog hardware design, DSP, motor controllers, computer networks, real-time software modelling & design using object modelling techniques, establishment of software engineering practices with documentation, development of real-time kernels, modelling & simulation of dynamic systems, antenna and motion control systems and inertial navigation.

Mr Y.S. Mayya was conferred the DAE Technical Excellence Award for the year 1999 for his meritorious contributions to the area of automation and control systems.

About the author ...

Mr Y.S. Mayya graduated in Electronics and Communication Engineering from Karnataka Regional Eng. College in 1979. He joined Reactor Control Division, BARC in 1980 through the 23rd batch of BARC Training School in Electronics discipline. He is currently heading the Distributed Automation and Control Section of Control Instrumentation Division.

His main interests include real-time embedded systems, computer networks and dynamic modelling and simulation of control systems. He has contributed to the development of step-track systems for INTELSAT Earth stations, antenna control systems for Master Control Facility at Hassan, Giant Metre-wave Radio Telescopes at Pune and tracking systems for FALCON and PTA programs of DRDO. His efforts in the development of Token bus networks, MIL-STD-1553 data bus and distributed systems have resulted in the realisation and deployment of many distributed data acquisition and control systems in nuclear power plants and other facilities of the department. He is currently involved in development of two types of airborne tracking and stabilisation systems, advanced land navigation system and servo control system for MACE telescopes.

Determination Of $^3\text{He} / ^4\text{He}$ Ratio Using Double Focusing Mass Spectrometer

K.A.Jadhav, N.Padma, K.K.B.Nair and V.V.K.Rama Rao

Technical Physics and Prototype Engineering Division
Bhabha Atomic Research Centre

Introduction

THE DETERMINATION OF ABUNDANCE OF helium in Natural gas samples has been of great interest in the geological applications. A few Natural gas samples, from ONGC/ SRBC/ Chennai have been analysed for their total helium content using an indigenously designed and built Double Focusing Mass Spectrometer (DFMS)¹, which is capable of a resolving power upto 6000. However, the geologists and the geophysicists are also interested in $^3\text{He} / ^4\text{He}$ ratio in these samples, in order to identify the source of Helium gas collected along with the Natural Gas from the fields. In this context, an experiment was conducted to determine the percentage of ^3He in Natural Helium (which is about 0.00013% or 1.3 ppm) commercially available in pressurised cylinders. The details of the experiment are presented in this paper.

Determination of $^3\text{He} / ^4\text{He}$ Ratio

A single focusing mass spectrometer can be used to determine the ratio of $^3\text{He} / ^4\text{He}$ in atmosphere. Though the small peak of 3 a.m.u. can be measured using these instruments, the main problem will be due to the isobaric interference of ^3He by residual HD and H_2 molecules in gas source mass spectrometers. A mass resolution of about 800 is required to resolve these peaks. Hence this work was carried on using the DFMS, indigenously developed in TP&PED, BARC.

Procedure of Analysis

The resolution of the instrument was adjusted to the required value, by opening the adjustable source slit.

This also increased the sensitivity thus helping in the detection of the small peak of ^3He . A Natural He sample, taken from the commercial He cylinder of 99.9% purity, was fed into the mass spectrometer and tuned for ^3He peak. The intensity of the peak was measured on a Cary vibrating reed electrometer amplifier, which can be operated at three resistance values - $10^3\Omega$, $10^5\Omega$ and $10^{11}\Omega$ i.e., at three different conversion gains of 10^8 A/Volt , 10^9 A/Volt and 10^{11} A/Volt . The signal strength of ^3He was raised to the maximum, to about 16V at $10^5\Omega$, by increasing the source pressure under reduced pumping speed condition to about 6×10^{-6} torr, and operating the multiplier at a gain of 10^7 at a suitable voltage. Under the same operating conditions, the mass spectrometer was tuned for ^4He and the signal detected was about 20 mV when the Cary was operated at $10^{11}\Omega$ range. The ratio of the intensity of the two peaks was found to be about 1.3×10^{-4} which is the true ratio. Since the sample was of high purity, presence of H_2 was negligible and the peaks corresponding to those of Hydrogen (namely HD and H_2), due to the residual gas in the source, were not detected and there was no interference from these.

Problems Faced

While tuning the mass spectrometer near about 3 a.m.u., two peaks were detected, one was around mass number 3 and the other, which was a broad peak of much lower intensity, located near about 3.3 a.m.u. Since there is no mass indication available in our DFMS, the mass numbers could only be inferred from the measured values of the magnetic field and the

radius of curvature. To identify which of these two are really due to ^4He and also the magnetic field for ^3He peak exactly, a sample of pure ^3He was introduced and the field value at which the peak due to the ^3He sample occurs, was noted. With the Natural He sample, one of the two peaks around 3 a.m.u., was found to be at the same field value while the other was at a higher value, whose mass number was calculated from the field data to be around 3.3 a.m.u.. Also this peak was found to be much broader than the other peaks. It was suspected that while tuning for mass number 3, the highly intense peak of ^3He must have been striking the walls of the chamber and a part of the scattered beam must be giving rise to the spurious peak at 3.3 a.m.u. To confirm this, different gas samples like N_2 and Ar were introduced into the mass spectrometer raising the main peaks at 28 and 40 respectively to very high intensity, in the same manner as said earlier. Spurious peaks, which were very broad, at unexpected mass numbers around 24 and 33.68 for N_2 and Ar (i.e. for the major peaks at 28 and 40) respectively were found to occur and the ratio of the mass numbers of the spurious peak to the major peak was found to be the same in each case, thus supporting the view point that it could be due to the scattered ions.

Determination of He Concentration

A few samples of Natural Gas, from ONGC, were analysed, to determine the concentration of He present in the sample. For these measurements, initially a standard He sample of known concentration was prepared by injecting the known quantity of Helium taken through gas tight syringes, into a glass bottle of

known volume. The He standard sample was introduced into the mass spectrometer by opening the variable leak valve to a suitable level, and the peak height of ^4He was noted. The Natural Gas sample, collected from the petroleum wells, over water in a bottle, was transferred to another glass bottle, suitable to be introduced into the mass spectrometer. The height of ^4He peak rising due to the presence of Helium in the sample, for the same position of the leak valve opening was noted and compared to that obtained with the standard sample and the unknown concentration was determined.

Conclusions

The ratio of $^3\text{He} / ^4\text{He}$ (1.3 ppm) in Natural Helium sample, could be measured using the double focusing mass spectrometer. Analysis of a few Natural Gas samples, from ONGC, was carried out to determine the percentage of Helium present in these samples. To measure the $^3\text{He} / ^4\text{He}$ ratio in these samples, it is necessary to introduce the samples in the form of pure helium into the mass spectrometer so that a detectable ion current of ^3He could be obtained.

Acknowledgement

The authors wish to thank Dr.V.C.Sahni, Head, TP&PED, for his keen interest and encouragement shown in this work.

Reference

1. B.S.Prahalada Rao et al., Proceedings of 5th National Symposium on Mass Spectrometry, 1991, 1-14.

About the authors ...

Mr K.A. Jadhav graduated in Physics from Pune University. He joined Mass Spectrometry Section, BARC in the year 1978. He has made remarkable contributions to the development of electron impact and thermal ionisation source for high mass isotope ratio mass spectrometry. Currently, he is working on double focussing mass spectrometer and octopole experimental set up for R and D.



Ms. N. Padma did her M.Sc. (Physics) from University of Madras and joined the 32nd batch of BARC Training School in 1989. She has been working on the development of double focussing mass spectrometers, different types of ion sources and ion optics for ICPMS and TMS. She has initiated computer simulation techniques for study of ion optical designs and utilized it for design optimisation. She is currently working on evaluation and optimisation of isotopic ratio mass spectrometers.

Mr K.K.B. Nair joined BARC in 1965 and was working in TPPED, BARC, until his superannuation in 1998. He has been instrumental in the development of DFMS and the related sample introduction systems and has taken active part in the development of different types of mass spectrometers, viz. helium leak detectors and TMS.



Mr V.V.K. Rama Rao heads the Mass Spectrometry Section in TPPED, BARC, since 1992. He did his M. Sc. (Tech.) in Applied Physics with instrumentation as the special subject from Andhra University in 1963 and M. Tech. (Elect. Engg.) from IIT, Bombay in 1965. He joined TPPED, BARC, in 1965 and has contributed to the design and development of all mass spectrometers indigenously built in the Division, viz., low mass range general purpose mass spectrometers for gas analysis, helium leak detectors, isotope ratio mass spectrometers for Li and N, QMAS, large multicollector mass spectrometers for nuclear materials (both solid and gas samples) and the ICP-MS. He has about 50 publications to his credit. He is a founder member of several professional societies.

ICP-MS – Improvements in Detection Limits

V.Nataraju, D.Ramanathan, V.C.Sahni, V.V.K.RamaRao, P.Raju and S.R.Halbe

Technical Physics & Prototype Engineering Division
Bhabha Atomic Research Centre

Introduction

As REPORTED EARLIER [1,2], TP&PED, BARC had developed a prototype Inductively Coupled Plasma Mass Spectrometer as a Department of Science and Technology sponsored project. Here we report on some of the developments directed to improve the performance of our instrument to reach detection limits at ppb levels.

Instrumentation

The basic mounting design of the instrument remains unchanged i.e., a three stage system with the plasma-sampler/skimmer interface region as first stage, the ion optics located in the second stage and the quadrupole-detector in the third stage. Fig. 1 gives a schematic and Fig. 2 gives a photograph of the system. The following design changes/improvements have been incorporated.

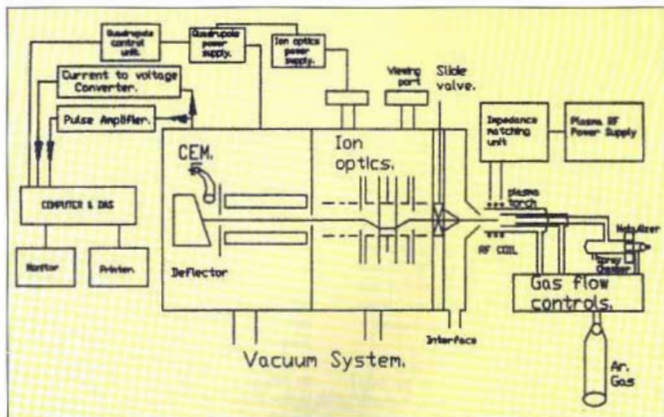


Fig. 1 Schematic of the system



Fig. 2 Photograph of the system

i) **First Interface region** : The first stage interface flange has been modified by enlarging the pumping channel dimensions and also having two additional pumping channels (instead of one before). The higher conductance resulting from this modification, enables ions to reach the second stage in larger numbers. The present dimensions of each channel are 16mm X 8mm. This new interface region is being pumped by two 300 l/min rotary pumps in parallel, to provide a speed of 600l/min. Care has been taken to ensure good surface finish to the sampler cone to minimise the peripheral leakage. The previously used sampler with 0.7 mm diameter aperture, 10mm length was replaced by one with 0.8 mm aperture diameter and 11mm length while skimmer cone of 0.7 mm aperture diameter is still in use.

ii) The diameter of differential pumping aperture (DPA), between second and third stages has been increased from 2mm to 4 mm. Though this increases the gas load in the third stage, the pressure (5×10^{-6} Torr) is still adequate for the safe operation of the Quadrupole Mass Analyser (QMA) and the Channel Electron Multiplier (CEM).

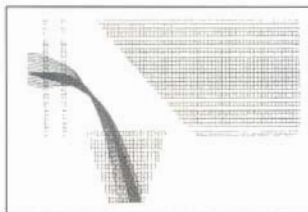


Fig.3 Deflector / Faraday cup - Multiplier assembly

iii) A new deflector / Faraday cup (FC) subsystem, has been incorporated in place of the existing deflector assembly in the collector region. The CEM is mounted at 90° to the axis of the system, as shown in Fig. 3. In the deflector mode, the FC is disconnected from the ion current amplifier and a suitable voltage is applied to it for deflecting the ion beam from quadrupole towards the CEM. Alternately the FC enables the monitoring of the ion beam exiting from the QMA. This arrangement helps in determining the Gain-Voltage characteristics of

the CEM. Fig. 3 also shows the trajectories traced by the SIMION3D version 6.0

iv) A peristaltic pump (Miclins, India) has been introduced in the sample introduction system to provide a uniform feed rate of sample solution to the nebuliser and hence the plasma.

v) The overall alignment of the system from the plasma torch to the collector assembly has been improved by checking it with a fine laser pointer.

Performance

The improved interface flange has brought down the 1st stage pressure. This pressure drop necessitated the increase in sampler length from 10mm to 11mm to provide an optimum skimming distance. The enlarged DPA has helped in increasing the intensity of the ion beam entering the QMA. These changes along with the

introduction of the peristaltic pump, have progressively enabled us to bring down the detection limits for Cesium and Silver solution samples to about ~ 1 ppb level in the analog mode of operation (figs. 4a & 4b). The detection capability of the instrument for other samples viz., Arsenic, Yttrium, Silver and Indium has been found to be in 1-10 ppb range. The working of this equipment has been established at this level of performance and has been checked by routinely operating with standard solutions. It is now being readied for analytical applications with the help of outside users. Figure 5 shows a spectrum of the mixture of elements in 25ppb concentration range. Other laboratory made standards in mass range of 60-160 amu are being analysed to check instrument repeatability, regularly.

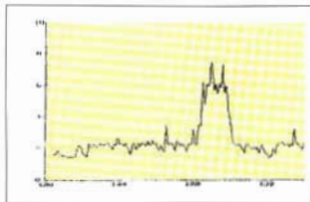


Fig.4a. Cs 1 ppb

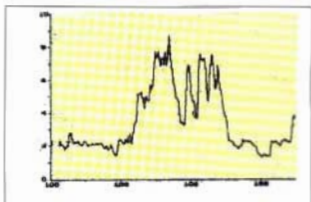


Fig.4b. Ag 1ppb

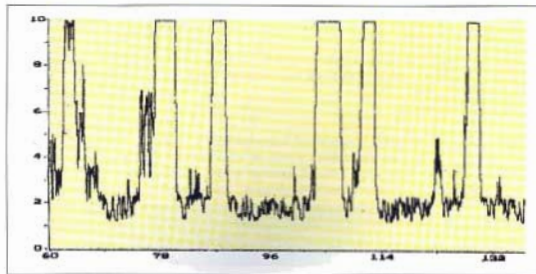


Fig. 5 Mixture of As, Y, Ag, In & Cs

The gain of the CEM (KBL20RS) at $-2100V$, estimated using the new deflector / Faraday cup, is 5×10^7 . These measurements were done by nebulising CsI solution and measuring the resulting current recorded on the faraday cup. Presently, efforts are on to switch over to the pulse counting operation.

Conclusions

The detection capabilities of our instrument have been considerably improved after incorporating the modifications in the design of some of the subsystems. Detection limits at ppb level for different elements have been achieved, in the analog mode of operation of the multiplier. These are expected to improve further in the pulse counting mode of operation of the multiplier.

Acknowledgements

The authors wish to thank the staff of MSS and MFAS for providing all the help in carrying out the

modifications, Ms. Madhumita Goswami for her help in preparing the laboratory standards and Mr. Amit Bhutani, a trainee student from IIT, Mumbai for simulating the ion trajectories using SIMION.

References

1. V.Nataraju et al., Proceedings of 7th NSMS 1996, p. 527
2. A.N.Garud et al., 8th ISMAS Workshop on Mass Spectrometry, 1997, p.58

Addendum : Since this paper was presented in December 1999, some problems encountered by way of high R.F. pickup at the collector have been reduced effectively and the pulse counting mode of operation has been made operational.

This paper was awarded the Second Best Paper prize in the 8th ISMAS Symposium on Mass Spectrometry, during December 7-9, 1999, held at IIT, Hyderabad.

About the authors ...

Mr. V. Nataraju did his M.Sc (Physics) from Andhra University and joined the 31st batch of BARC Training School in 1987. He has been working in the Mass Spectrometry Section of TPPED since 1988 and has been associated with the Development Project of ICP-MS since its inception. He has worked on computer simulation studies of ion optics of Mass Spectrometers, and used it for design optimisation in the ICP-MS. Currently, he is also working on the indigenous development of quadrupole Mass Filters.



Dr. Devaki Ramanathan did her B.Sc. (Physics) from Madras University and joined the sixth batch of BARC Training School in 1962. She joined TPPED in 1963 and worked on Ultra High Vacuum techniques and instrumentation. She obtained her M.Sc. in 1973 from Bombay University on Field Emission Microscopy and obtained her Ph.D. from Pune University in 1983 on Field Ion Microscopy. Currently, she is working in the mass spectrometry section on the indigenous development of ICP-MS. She has co-authored a number of papers in national and international journals, including a paper in the prestigious

journal 'Nature'.

Dr. V.C. Sabni is currently the Director, Physics Group, BARC. After his B.Sc. (Hons.) (Physics) from Delhi University, he joined the 8th batch of BARC Training School. He stood first in his batch. His first R & D work was in Condensed Matter Physics. He did his M.Sc. (Applied Mathematics) in 1968 and Ph.D. (Physics) in 1973 - both from Bombay University. His academic distinctions included the coveted INSA Young Scientist's medal in 1974, Visiting fellowship at Centre for Chemical Physics, Ontario, Canada (1981-82), INSA-USSR Academy Exchange fellowship (1987) and INSA-Royal Society (UK) Exchange Fellowship (1993). Dr. Sabni has published over 250 scientific papers, co-authored the book 'Dynamics of Perfect Crystals' and co-edited a book 'Developments in Theoretical Physics'. He was Head, TPPED, BARC, from 1996 to Aug. 2001 and has been intimately associated with the indigenous developments of UHV-based surface instrumentation, mass spectrometers and other analytical instruments.



Mr V.V.K. Rama Rao heads the Mass Spectrometry Section in TPPED, BARC since 1992. He did his M. Sc. (Tech.) in Applied Physics with instrumentation as the special subject from Andhra University in 1963 and M. Tech (Elect. Engg.) from IIT, Bombay in 1965. He joined TPPED, BARC in 1965 and has contributed to the design and development of all mass spectrometers developed in the Division, viz. Low mass range general purpose mass spectrometers for gas analysis, He leak detectors, isotope ratio mass spectrometers for L_1 and N_2 QMAs, large multicollector mass spectrometers for nuclear materials (both solid and gas samples) and the ICP-MS. He has about 50 publications to his credit. He is a founder member of several professional societies.

Mr. P. Raju did his B.E. (Mech.) from Osmania University and joined Mass Spectrometry Section, TPPED, BARC in 1991. He has been intimately associated with the design, fabrication and assembly of all the mass spectrometers developed in the Division.



Mr S.R. Halbe is in charge of the Mechanical Fabrication & Assembly Sectional Activity in TPPED, BARC. His group is primarily responsible for the design, development and prototype manufacture of a number of innovative components and devices required for ultra high vacuum based analytical instruments - a major programme of the Division. Technologies of two components developed by him were transferred to industry for commercialisation.

Fabrication of High Density ThO_2 , ThO_2 - UO_2 and ThO_2 - PuO_2 Fuel Pellets for Heavy Water Reactors

U. Basak, M.R. Nair, R. Ramachandran and S. Majumdar

Radiometallurgy Division
Bhabha Atomic Research Centre

Introduction

ThO_2 - PuO_2 ($\leq 4\%$) AND ThO_2 - U^{235}O_2 ($\leq 4\%$) are being considered as fuels for the proposed advanced heavy water reactor (AHWR). ThO_2 , UO_2 and PuO_2 are iso-structural (FCC, CaF₂ type), mutually solid soluble and have similar physical and thermodynamic properties. Fabrication procedures of thorium and thorium based fuels are also similar to that of UO_2 and $(\text{U,Pu})\text{O}_2$ fuels. However, ThO_2 is a perfectly stoichiometric compound with very high melting point and hence it is difficult to sinter to high density ($\geq 95\%$ TD) even at reasonably high temperature (≤ 1973 K) without any sintering aids. MgO , CaO , Nb_2O_5 , etc. act as effective sintering aids for obtaining high density pellets at relatively lower sintering temperature^{1,2}. Even among the additives, Nb_2O_5 is found to be the most effective for high densification ($\geq 95\%$ TD) at sintering temperature ≤ 1773 K in reducing atmosphere.

A modified flow sheet developed for the fabrication of ThO_2 pellets starting with thorium oxide powder containing high sulphur content is also discussed in the paper.

Fabrication of High Density Pellets

High density ThO_2 , ThO_2 - UO_2 and ThO_2 - PuO_2 pellets are fabricated by powder metallurgical route consisting of milling of MgO (~500 ppm) doped ThO_2 powder, pre-compaction & granulation followed by high temperature (≤ 1973 K) sintering in reducing atmosphere. The conventional process flow sheet for the fabrication of high density ThO_2 , ThO_2 - UO_2 and ThO_2 - PuO_2 fuel pellets is shown in Figure 1.

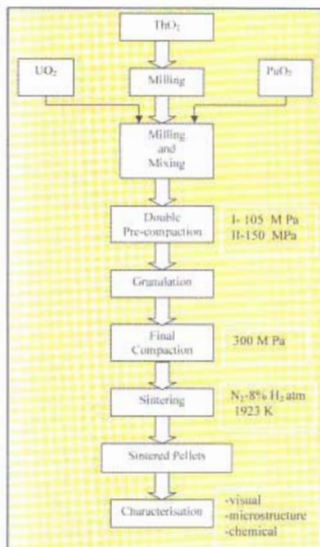


Fig. 1 Conventional flowsheet for the fabrication of ThO_2 , Th_2UO_7 and $(\text{Th,Pu})\text{O}_2$ pellets.

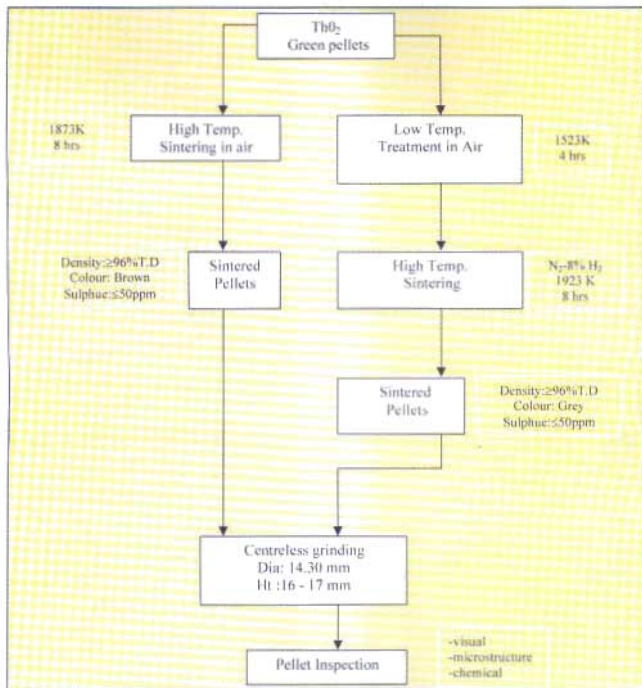


Fig. 2 Modified portion of the process flowsheet for high density pellet fabrication from ThO_2 powder containing high sulphur

A few lots of MgO doped ThO_2 powder (Qty : 2.5 t) supplied by M/s. Indian Rare Earths Ltd. contained very high sulphur impurities (800–1200 ppm). Though high sulphur impurity in ThO_2 powder did not affect either the powder sinterability or pellet fabricability but considerable amount of sulphur (400 - 700 ppm) remained in the sintered ThO_2 pellets as Th–O–S compound even after high temperature sintering under

$N_2-8\%H_2$ atmosphere⁶⁰. This caused shattering of sintered and centreless ground pellets during air drying process at 473–523 K before encapsulation. Hence experimental studies were undertaken in order to fabricate high density ThO_2 pellets of acceptable sulphur impurity starting with powder containing high sulphur. These included (a) re-calcination of as received ThO_2 powders before further processing,



Fig. 3a TBO pellets with high sulphur shattered during drying

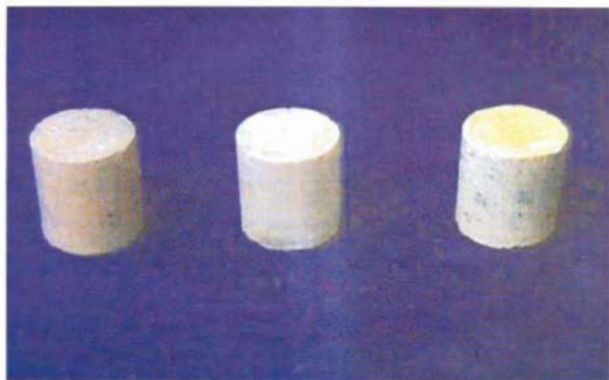


Fig. 3b Accepted TBO pellets fabricated by modified fabrication route

(b) high temperature (≥ 1873 K) sintering of pellets in air, (c) low temperature (≤ 1523 K) treatment of pellets in air followed by high temperature (≥ 1923 K) sintering in $N_2 - 8\%H_2$ atmosphere, (d) low temperature (≤ 1573 K) oxidative sintering using Nb_2O_5 dopant. Based on these investigations and keeping in view of easy adaptation of the modified process in the conventional process flow sheet for the fabrication of high density pellets, two alternative processes viz. (1) high temperature sintering in air and (2) low temperature treatment in air followed by high temperature sintering in reducing atmosphere were finalized for the fabrication of high density ThO_2 pellets with acceptable sulphur content (~ 50 ppm). The process modification incorporated in the conventional flow sheet is shown in Figure 2. Air pre-sintering of green ThO_2 pellets at 1523 K brought down the sulphur content within acceptable limit. However high density ($\geq 95\%TD$) was achieved only after the sintering of these pellets either in $N_2 - 8\%H_2$ atmosphere at ≥ 1923 K or in air at ≥ 1873 K. Figure 3a shows the typical photograph of the high

sulphur containing pellets which shattered during drying process before encapsulation and Figure 3b shows photograph of good pellets obtained after incorporating the modifications in the process flow sheet.

Conclusion

A modified flow sheet for fabrication of high density ThO_2 pellets for PHWR, starting with thorium oxide powder containing high sulphur impurity has been developed. Already 2.5 tons of high density ThO_2 pellets fabricated by this modified process have been supplied to Nuclear Fuel Complex, Hyderabad for use in five new PHWRs.

References

1. U. Basak, M.Sc(Tech) Thesis, University of Bombay, 1988
2. P. Balakrishna et al, *Jl. Nuclear Materials* 160(1988) 88-94
3. Shigeru Yamagishi and Yoshihisa Takahasi, *Jl. Nuclear Science & Technology*, 26(10), Oct. 1989 pp 939 - 947.

This paper received the Best Paper Award in the Annual Conference of Indian Nuclear Society (INSAC-2000) on "Power from Thorium : Status, Strategies and Directions", held at BARC, Mumbai, during June 1-2, 2000.

About the authors ...



Mr U. Basak joined the 21st batch of BARC Training School in 1977 after graduating in Metallurgical Engineering from Jadavpur University, Calcutta. He obtained M.Sc(Tech) from University of Mumbai in 1988. In Radiometallurgy Division, he has 23 years of work experience in the fabrication and characterisation of Uranium, Plutonium and Thorium based ceramic nuclear fuels.



Mr S. Majumdar, Head, Radiometallurgy Division, BARC, is a Metallurgical Engineer from the University of Calcutta(1967) and joined BARC through the 11th batch of Training School. He is working in the Radiometallurgy Division since 1968. His research interest include development, fabrication, characterisation and property evaluation of Plutonium, Thorium and U^{233} based fuels both for thermal and fast reactors.



Mr M.R. Nair joined Radiometallurgy Division, BARC, in 1973 after graduation from University of Kerala. He completed AMIE in Metallurgical Engineering in 1978 and got elected as Member of Institution of Engineers(MIE) in 1990. He has got 28 years of experience in the development and fabrication of UO_2 , PuO_2 and TbO_2 based nuclear ceramic fuels.

Mr R. Ramachandran is a Metallurgical Engineer from IIT, Chennai, and joined Radiometallurgy Division through 10th batch of BARC Training School in 1967. His field of specialization includes development and fabrication of oxide nuclear fuels.

TRISUL – The Computational Tool for Strategic Planning of Thorium Fuel Cycles

V. Jagannathan, R. P. Jain and R. Karthikeyan

Theoretical Physics Division
Bhabha Atomic Research Centre

Abstract

A computer code called TRISUL for Thorium Reactor Investigations with Segregated Uranium Loading has been developed. TRISUL code is a hexagonal finite difference few group diffusion theory code. It has a built-in thermal hydraulics module to calculate coolant void formation along the fuel channel height. TRISUL code caters to the design and analysis of a new reactor concept called, 'A Thorium Breeder Reactor' (ATBR). In this reactor concept, the seed zone can be enriched uranium, or futuristically, it can be plutonium or ^{235}U seed in thorium or in depleted uranium. The unique feature of ATBR concept is that the equilibrium core considers loading of 50 to 60% natural TbO_2 fuel by weight, with no seed material in them. The thorium rods, after irradiation for one fuel cycle, are integrated with seed fuel rods. In situ production of ^{235}U is adequate to attain a discharge burnup comparable to or even more than that of the seed fuel.

For the thorium fuel clusters, cross sections are prescribed as a function of neutron fluence as well as the absolute flux history pertaining to a given location. The cross sections for the integrated fuel cluster, depends on the accumulated ^{235}U in thorium rods during its first fuel cycle irradiation. Thus the starting irradiation history of thorium rods is carried forward, as the integrated fuel cluster is shuffled from one location to another in every fuel cycle. TRISUL code incorporates a semi-automatic refueling scheme to facilitate optimization studies for designing the refueling pattern for a given seed fuel type, reload batch size and the corresponding cycle length. For the types of seed and batch size considered, it is seen that the cycle length varies from 10 to as long as 22 months. The longer cycle length is particularly useful in a closed fuel cycle option which would need a sizeable time for out of pile fuel handling, i.e., reprocessing, prior cooling time and re-fabrication. Although the ATBR is a conceptual reactor, the physics analysis of such a reactor concept is helpful to identify a realistic and optimum option to be followed for an effective use of thorium. The results of the TRISUL analyses can serve as the basis for long term planning of fuel cycle strategies to maximize the fission nuclear power from the natural resources of uranium and thorium.

Introduction

A NEW REACTOR CONCEPT CALLED 'A THORIUM Breeder Reactor' (ATBR) has been evolved based on certain physics design principles [1-6]. The design parameters of the ATBR core are given in the references 1-6. Some salient characteristics are given here for ready reference. Table-1a describes the core design parameters. The unique feature of ATBR design is the possibility to load natural thorium, 50 to 60% by weight, with no external feed enrichment. Along with every new batch of seeded fuel one batch of seedless thorium rod clusters are also

loaded. In situ production of ^{235}U in one fuel cycle is adequate for these thorium rods to become like regular fuel rods. These clusters after one cycle irradiation are integrated with the seed fuel rod clusters in the subsequent fuel cycle. Thus the ATBR core consists of two types of fuel clusters viz., natural thorium cluster (Fig. 1) and the two ring clusters of fresh seed fuel rods which are integrated with the one-cycle-irradiated thorium cluster (Fig.2). The seed fuel can be of different types. The details of seed fuel design with seed materials enriched UO_2 , (eUO_2) , PuO_2 in ThO_2 and $^{235}\text{UO}_2$ in ThO_2 are described in Table-1b. A typical optimized refueling pattern for a 5-batch core with 72

assemblies per batch is shown in Fig.3. The study of the ATBR concept required the development of a special calculation tool called 'TRISUL' whose acronym is derived from Thorium Reactor Investigations with

Segregated Uranium Loading. We will describe in this paper the potential of TRISUL code as a tool for strategic planning of thorium fuel cycles.

Table-1a : ATBR core design parameters

Reactor Power	600 Mwe / 1875 MWth
No. of batches	3 / 4 / 5
No. of fuel assemblies per batch	72 / 90 / 120
No. of Seedless Thoria Rods	91 / 109 / 145
No. of Seed + Irradiated fuel Assemblies	360 / 360 / 360

Table-1b : Description of seed materials

Parameter	Seed Fuel Type					
	eUO ₂		PuO ₂ in ThO ₂		²³⁵ UO ₂ in ThO ₂	
	Enriched U		Reprocessed Pu		Reprocessed U	
Seed	Inner	Outer	Inner	Outer	Inner	Outer
Fuel Clad ID/OD (mm)	10/11.4	10/11.4	10/11.4	9/10.4	10/11.4	10/11.4
No. of Fuel Rods	24	30	24	30	24	30
Seed Content (Wt. %)	6%	5%	20%	14%	6%	5%
	²³⁵ U	²³⁵ U	PuO ₂ in ThO ₂	PuO ₂ in ThO ₂	UO ₂ in ThO ₂	UO ₂ in ThO ₂
Fissile fraction	1.0		0.745		0.941	
Hexagonal Pitch (cm)	30.5		30		29.5	
Cycle length (EFPD)	330 / 390 / 510		390 / 480 / 660		330 / 390 / 510	

Note: 30 irradiated ThO₂ rods of ID/OD 12.6/14 mm is considered in the outermost ring surrounding the seed zone for all fuel types.

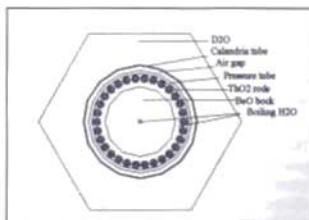


Fig.1 ATBR - 30 natural ThO₂ rods fuel cluster

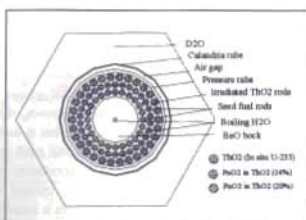


Fig.2 ATBR - (54 seed + 30 irradiated ThO₂) fuel cluster

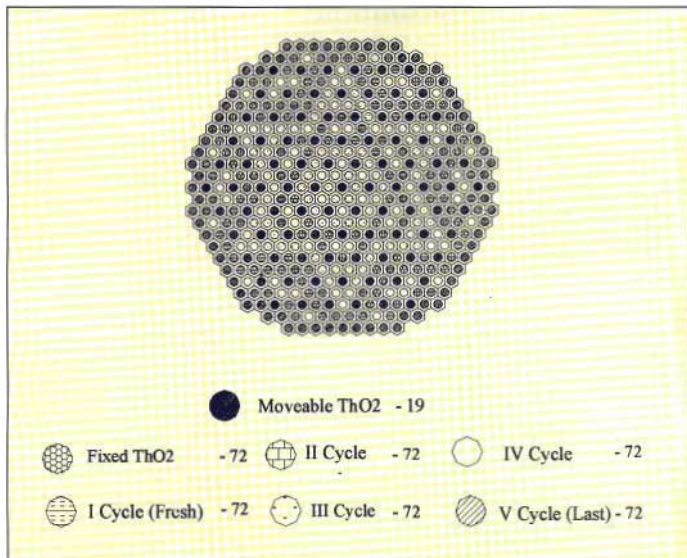


Fig. 3 ATBR equilibrium core: Typical core loading pattern 360 (seed + irradiated ThO₂) clusters + 91 ThO₂ fuel clusters

Salient Features of TRISUL Code

Neutronics and thermal hydraulics model

The neutronics model of TRISUL code is solution of few group diffusion theory equations in hexagonal geometry. The method of center-mesh finite difference with hexagonal or triangular right prismatic meshes is used. Presently TRISUL considers a single hexagonal mesh per fuel assembly radially. Since D₂O is considered as moderator and reflector, finite difference method of solution with a hexagonal mesh size of 30 cm is found to be sufficiently accurate. A thermal hydraulics model similar to that of Tarapur BWR simulator code COMETG [7] is used to calculate coolant axial void distribution in

each fuel channel. The phenomenon of sub-cooled boiling is calculated by Levy's model [8], flow quality which is different from heat equilibrium quality is calculated by Zuber-Findlay model [9], and the void-quality correlation is as per Ref. 10. Detailed pressure drop calculations are not done. A tentative flow-power correlation is used.

TRISUL uses a two group lattice parameter base generated by CLUB [11] module of PHANTOM code system [12]. Cross sections for thorium clusters depend on effective one group absolute flux level in fuel, irradiation time in days, coolant void and temperature state. For (seed + irradiated thorium rods) cluster, cross sections depend on thorium rod flux history or accumulated fluence

in thoria rods during their first fuel cycle, cluster burnup in MWD/T, coolant void, and other temperature states. The absolute flux level is not known a priori. They are therefore iteratively updated starting with some guess value. Saturated xenon and Doppler feedback effects are considered in every spatial mesh.

Additional capabilities of TRISUL code

TRISUL code models the equilibrium core following a batch mode of refueling. Normally one-sixth core is simulated with rotational symmetry. Identical number of fuel assemblies is present corresponding to every fuel cycle batch. Locations of natural thoria clusters are fixed. A semi-automatic refueling scheme is used. In this scheme, the burnups are arranged in ascending order and the fuel assembly movement from cycle to cycle follow this order number. The fuel cycle follow-up must be repeated a few times to converged burnup and power profiles.

Output from TRISUL analysis

The TRISUL output consists of k_{eff} , three dimensional flux, power, burnup and void distributions as a function of cycle burnup. Fig.4 gives the typical k_{eff} variation during a fuel cycle as computed for the three types of seeds described in Table-1b. Fig.5a and 5b give the radial plot of typical epithermal and thermal flux profiles in axial plane 15 at the beginning of a fuel

cycle. Figs. 6a and 6b give the same at the end of cycle. There are regular dips seen in the epithermal flux distribution at the locations of thoria clusters. Thermal flux peaks at these locations. It is interesting to observe that the flux and hence the power distributions are intrinsically maintained flat by optimum refueling pattern. The k_{eff} also remains close to unity and flat for a cycle duration of as long as 660 days. These features are typical of ATBR design concept. Heavy metal composition in each fuel batch, seed inventory in fresh charge and seed output in discharged fuel are computed by TRISUL. Fig.7 gives these results for the three types of seed materials with 120 assemblies per batch. Different fuel management strategies can be inter-compared by comparing the discharge burnups and the net seed output to input ratios.

Other types of TRISUL simulations

TRISUL code can evaluate the worth of moveable thoria clusters and the worth of reactivity devices located at the inter-channel space in D.O moderator [see the accompanying paper presented at this conference, Ref. [13]. Reactivity loads due to fuel, moderator and coolant temperatures, coolant void, saturated xenon and reactivity effect due to full conversion of ^{235}Pa to ^{235}U can all be estimated using the appropriate database generated by PHANTOM. More details of TRISUL code is being brought out in a BARC report.

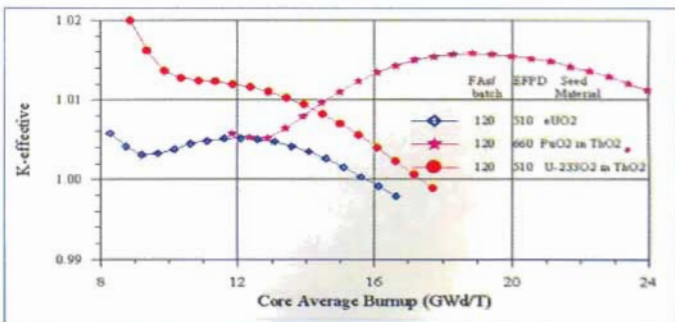


Fig.4 Comparison of k_{eff} vs cycle burnup for three batch fueling

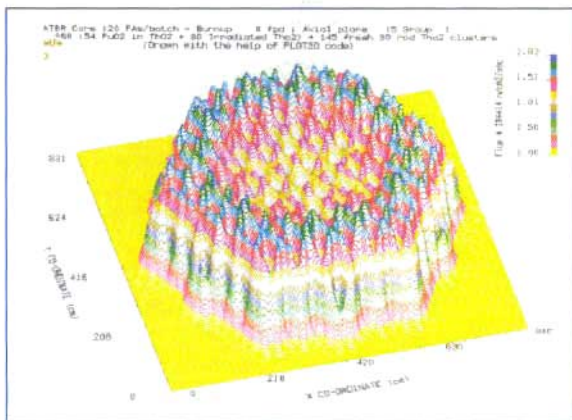


Fig. 5a Radial epithermal flux distribution at beginning of cycle (typical)

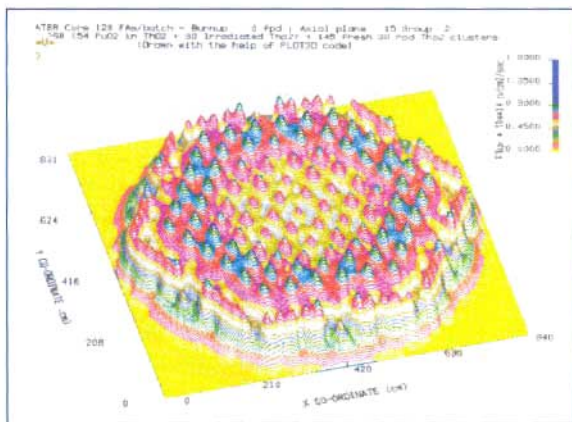


Fig.5b Radial thermal flux distribution at beginning of cycle (typical)

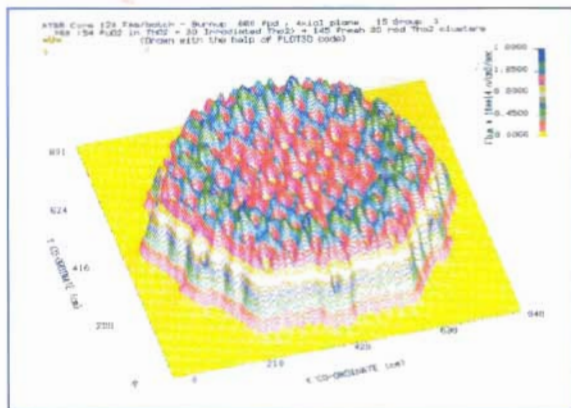


Fig.6a Radial epithermal flux distribution at end of cycle (typical)

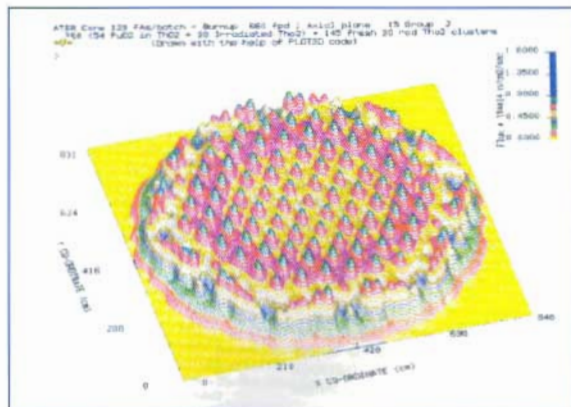


Fig.6b Radial thermal flux distribution at end of cycle (typical)

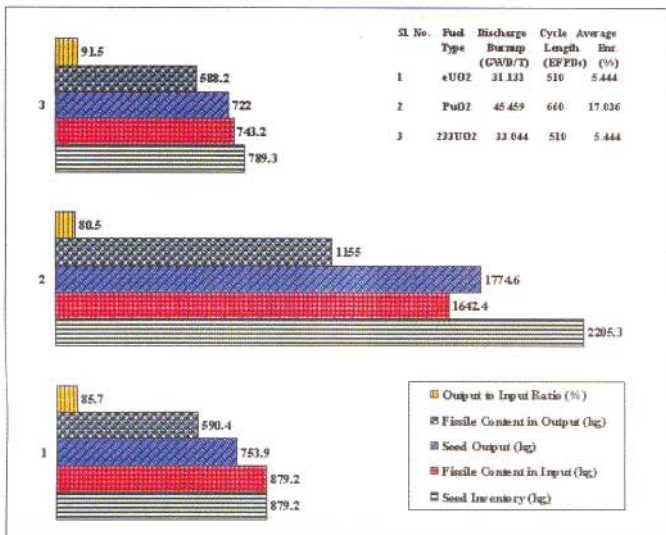


Fig.7 ATBR - Comparison of seed input / output for various types of fuel (120 EAs/batch)

Conclusions

TRISUL code is specially developed for the ATBR (A Thorium Breeder Reactor) core analysis. Though the studies pertain to a conceptual reactor, the analyses are useful in evolving optimum fuel management strategies for Th-U-Pu fuel cycles in future thermal power reactor design.

References

1. V. Jagannathan, R. P. Jain, P. D. Krishnani, G. Ushadevi and R. Karthikeyan, 'An Optimal U-Th Mix Reactor to Maximize Fission Nuclear Power', p. 323 Proc. of The International Conference on The Physics of Nuclear Science

- and Technology, Oct. 5-8, 1998, The Radisson Hotel, Islandia, Long Island, New York.
2. V. Jagannathan and S. V. Lawande, 'A Thorium Breeder Concept for Optimal Energy Extraction from Uranium and Thorium', paper presented at IAEA TCM on 'Fuel Cycle Options in LWRs & HWRS', at Victoria, Canada, p.231, IAEA-TECDOC-1122, April, 28-May 1, 1998.
3. V. Jagannathan, Usha Pal, R. Karthikeyan, S. Ganesan, R. P. Jain, and S. U. Kamat, 'ATBR - A Thorium Breeder Reactor Concept for An Early Induction of Thorium in An Enriched Uranium Reactor', original accepted and revised paper communicated to the Journal of Nuclear Technology, 2000.
4. V. Jagannathan, Usha Pal, R. Karthikeyan, S. Ganesan, R. P. Jain and S. U. Kamat, 'ATBR - A Thorium Breeder Reactor Concept for An Early

- Induction of Thorium*, Report B.A.R.C./1999/E/017, 1999.
- V. Jagannathan, 'ATBR - A Thorium Breeder Reactor Concept for Early Induction of Thorium with no Feed Enrichment', published as a feature article in B.A.R.C. Newsletter 187, August 1999.
 - V. Jagannathan, Usha Pal and R. Karthikeyan, 'A Search into the Optimal U-Pu-Tb Fuel Cycle Options for the Next Millennium,' paper presented at PHYSOR' 2000 Int. Conference - ANS International Topical Meeting on 'Advances in Reactor Physics and Mathematics and Computation into the Next Millennium', May 7-11, 2000, Pittsburgh, Pennsylvania, U.S.A.
 - S. R. Dwivedi, V. Jagannathan, P. Mohanakrishnan, K. R. Srinivasan And B. P. Rastogi, 'Core Followup Studies of The Tarapur Reactors With The Three Dimensional BWR Simulator COMETG,' B.A.R.C.-864, (1976).
 - S. Levy, GEAP-5157, General Electric Company (1966).
 - N. Zuber And J. A. Findlay, GEAP-4572, General Electric Company (1964).
 - N. Zuber et al., GEAP-4517 General Electric Company (1967).
 - P. D. Krishnani, *Ann. Nucl. Energy*, 9, 255 (1982).
 - V. Jagannathan, R. P. Jain, Vinod Kumar, H. C. Gupta And P. D. Krishnani, 'A Diffusion Iterative Model for Simulation of Reactivity Devices in Pressurized Heavy Water Reactors,' *Nucl. Sci. and Eng.*, 104, 222 (1990).
 - V. Jagannathan, R. P. Jain and R. Karthikeyan, 'Physics Design of Control and Instrumentation System for ATBR - A Thorium Breeder Reactor,' paper presented to this Conference INSAC'2000, June, 2000.
 - V. Jagannathan, 'TRISUL - A Code For Thorium Reactor Investigations with Segregated Uranium Loading', B.A.R.C. External report under preparation, 2000.

This paper presented at the Annual Conference of Indian Nuclear Society, Mumbai (INSAC-2000) on "Power from Thorium - Status, Strategies and Directions", June 1-2, 2000, held at the Multipurpose Hall, BARC Training School Hostel, Anusaktinagar, Mumbai, won the Best Poster Award

About the authors ...



Dr V. Jagannathan, BSc, Physics, Madras University, 1971; PhD, Mathematics, Bombay University, 1988. He is currently Head of Light Water Reactors Physics Section in Theoretical Physics Division, BARC. He was deputed to Italy as IAEA fellow from May 1977 to Oct. 1978. He is responsible for qualification of multigroup nuclear data libraries, development of physics and thermal-hydraulic design codes for boiling water reactors (BWRs), pressurized water reactors (PWRs), VVERs, and pressurized heavy water reactors (PHWRs) and study of optimal uranium-thorium fuel cycles. He had participated in the International Atomic Energy Agency (IAEA) Co-ordinated Research Program (CRP) on incore fuel management code package validation for each of the aforementioned types of thermal power reactors between 1988 and 1994. The evolution of a new reactor concept called 'A Thorium Breeder Reactor' is an outcome of the experience gained from the aforementioned studies.



Mr R. P. Jain, MSc, Mathematics, Agra University, 1968, is working in Reactor Design Section in Theoretical Physics Division. He has developed and validated computer codes for fuel management of BWRs, PHWRs, PWRs, and VVERs and has been using them for design and analysis of thermal reactors.



Mr R. Karthikeyan, BSc, Physics, Madras University, 1992; MSc Physics, Hyderabad Central University, 1995, is working in Light Water Reactors Physics Section in Theoretical Physics Division. His background includes analysis of thermal reactor benchmarks using multigroup nuclear data cross-section sets and design evaluations for uranium-thorium based reactors.

Effect of Diluent on the Transport of Am(III) from Nitric Acid Medium Across A Supported Liquid Membrane (SLM) Using Dimethyl Dibutyl Tetradecyl Malonamide (DMDBTDMA) as the Carrier

S.Sriram and V.K.Manchanda
Radiochemistry Division
Bhabha Atomic Research Centre

Abstract

The effect of diluents like n-dodecane, n-hexane, c-hexane, toluene, 1,2 dichloroethane, diethylbenzene, decalin and nitrobenzene on the extraction of Am(III) and it's transport from nitric acid medium across a supported liquid membrane (SLM) using DMDBTDMA as the extractant/carrier has been investigated. The distribution ratio of Am(III) displayed a good empirical correlation with some of the parameters based on the physico-chemical properties of the diluents. The experimental data for Am(III) transport were quantitatively described by rate transport equations.

Introduction

LONG LIVED ALPHA EMITTING RADIONUCLIDES present in aqueous raffinate waste streams generated after Pu recovery operation in the PUREX process have been of great environmental concern. Partitioning of actinides from such acidic waste solutions using solvent extraction and extraction chromatography has been studied extensively over the past two decades [1-4]. Facilitated transport of metal ions through a supported liquid membrane (SLM) has great potential for the separation of radionuclides especially from waste solutions with a low metal content [5]. In liquid membrane based separation technique, the extraction, stripping and regeneration operations could be combined in a single stage. Additional advantages of this technique are low cost, low energy consumption and minimum solvent inventory. Flat sheet SLM seems to represent a convenient means for the systematic study of the effect of various parameters on flux and cation selectivity in

liquid membranes. Studies on flat sheet SLM also enables one to predict whether the hollowfibre system can be used to carry out similar separations in continuous flow operations [6].

Among the various reagents used in solvent extraction (SE) and extraction chromatography (EC), CMPO (octyl(phenyl)-N,N-diisobutyl carbamoyl methyl phosphine oxide) and Dimethyldibutyltetradecyl-1,3-malonamide (DMDBTDMA) have been preferred for actinide partitioning because of their ability to efficiently extract tri, tetra, and hexa valent actinide ions from acidic waste solutions [1,7]. The main advantages of DMDBTDMA over the organophosphorous bifunctional extractants like CMPO are: a) ease of synthesis b) complete incinerability and c) innocuous radiolytic and chemical degradation products (namely carboxylic acids and aliphatic amines) [7].

Focus of the present studies is to evaluate the effect of diluent on the extraction and transport of Am(III) using DMDBDTMA as the extractant. An attempt has been made to empirically correlate the distribution ratio of Am with various physico-chemical properties of the diluents. Thus for the first time, a model for the distribution ratio of Am(III) employing a diamide in several diluents has been established. The results obtained in the SLM experiments have been used to verify a physico-chemical model proposed previously by our group [8].

Experimental

DMDBDTMA was synthesised and purified in our laboratory by a previously reported procedure [7]. Commercially available hydrophobic polypropylene (PP) membrane of pore size : 0.57 μm , porosity : 84%, and thickness : 112 μm were used in all the experiments. Effective membrane area (computed from the geometrical area and membrane porosity) was found to be 4.12 cm^2 .

The supported liquid membrane studies were carried out by using a pyrex glass cell consisting of two compartments viz. the feed side of 25 mL separated by a strip side of 10 mL. The feed and strip solutions were mechanically stirred at ~700 r.p.m using a magnetic stirrer at ambient temperature ($24 \pm 1^\circ\text{C}$) to suppress concentration polarisation conditions at the membrane interfaces and in the bulk of the solutions. Membrane permeabilities were determined by assaying the samples from both the feed as well as the strip side radiometrically at a regular interval.

In case of liquid liquid extraction experiments, equal volumes of ^{241}Am tracer in aqueous phase of desired composition and pre-equilibrated 0.6 M DMDBDTMA dissolved in a diluent were agitated in a 15 mL glass stoppered tube for an hour at $25 \pm 0.1^\circ\text{C}$. After centrifugation, aliquots from both the phases were withdrawn for radioassay. The distribution ratio (K_d), defined as the ratio of Am concentration in organic phase to that in the aqueous phase was determined.

Transport Equation

A model describing the transport mechanism which consists of a diffusion process through a feed aqueous

diffusion film, fast reaction kinetics at feed-membrane and membrane-strip interfaces, and rate determining diffusion through the membrane itself was derived previously for Am(III) transport from a feed solution of 3.0 M HNO₃ across a SLM containing DMDBDTMA in *n*-dodecane as carrier and using 0.01M HNO₃ as the strippant [8]. The equation used for the determination of permeability coefficient is :

$$P = \frac{K_d}{\left[\frac{K_d \left(\frac{da}{Da} \right) + \left(\frac{d\sigma\tau}{Do} \right) \right]} \quad (1)$$

where P is the permeability coefficient, K_d is the distribution ratio, D_a is the aqueous diffusion coefficient of Am(NO₃)₃, D_s is the membrane diffusion coefficient of Am(NO₃)₃, A_s complex, d_s is the thickness of aqueous stagnant film, d_m is the membrane thickness and τ is the tortuosity factor which is required to convert membrane thickness to effective diffusion path length in the membrane phase. Substituting R_s and R_m as the aqueous and membrane diffusion resistance parameters in equation (1).

$$P = \frac{K_d}{[R_s R_m + R_m]} \quad (2)$$

When transport is controlled by membrane diffusion resistance term i.e

$\left[\frac{K_d \frac{da}{Da} \ll \frac{d\sigma\tau}{Do} \right]$, then equation (1) reduces to

$$P = \frac{K_d D_o}{d\sigma\tau} \quad (3)$$

In the present work an attempt was made to obtain D_s using Wilke - Chang, Scheibel and Ratcliff equations which are based on hydrodynamic / absolute rate theory and Stokes-Einstein and Eyring's equations [9]. The permeability coefficient can be obtained experimentally by using following equation [5]:

$$\ln \left(\frac{[M]_t}{[M]_0} \right) = - (QV) P x t \quad (4)$$

where [M]_t and [M]₀ are the concentration of the metal ion (M) in aqueous feed at time t and initial metal ion concentration (at t = 0) respectively. Q = A x ϵ where A is the geometrical area and ϵ is the porosity.

V is the aqueous feed volume (in mL). The above equation was only applicable when carrier was not saturated and flux was linearly decreasing with time suggesting its validity in experiments where metal ion tracers are used. An excellent agreement was observed in our earlier work on P values of Am^{3+} -3M HNO_3 | 0.6M DMDBTMA – *n*-dodecane | 0.01M HNO_3 system obtained experimentally using equation (4) and those computed using equation (3) [8].

Results And Discussion

Effect of diluent on the extraction of Am(III)

The membrane carrier (extractant) and solvent (diluent) may influence the transport of metal ion through SLM in many different ways. As per equation 3, the distribution ratio (K_d) and the membrane diffusion coefficient (D_m) are the two major carrier and solvent dependent factors affecting the transport rate of metal ion.

To understand the effect of diluent on extraction of Am(III) from 3.0 M HNO_3 medium, its distribution ratio (K_d) was determined using varying extractant concentrations (0.1M – 1M DMDBTMA) in several diluents. The K_d (Am) for various diluents varied in the order nitrobenzene > *n*-dodecane > *n*-hexane > 1,2 dichloroethane (DCE) > decalin > *c*-hexane > diethylbenzene (DEB) > toluene. The plot of $\log K_d$ versus [DMDBTMA] resulted in slope values in the range 3 ± 0.3 thereby indicating the following extraction equilibria for Am extraction:



(where A is DMDBTMA)

Novel empirical correlations between K_d and diluent properties

Linear Solvation Energy Relationship (LSER) has been proposed for the correlation of physico-chemical properties of diluents with solution processes like solubility, distribution of a solute between two immiscible liquids, free energy and enthalpy of equilibria, etc. Selected properties of the diluents utilised in the present work are obtained from literature [10,11].

A multiparameter approach of the general form

$$A = a + bB + cC + dD + \dots \quad (6)$$

where a, b, c, d are solvent-independent but process dependent coefficients. Latter three of these being the indicators of the sensitivity of the solvent parameters B, C and D [12].

In the present paper, an attempt has been made to correlate the experimentally observed K_d with various solvent parameters based on linear solvation energy relationship models proposed by Schmidt, Swain, Koppel-Palm as well as by using combinations of various other diluent parameters, using a Fortran program for multi-dimensional linear fit [10-12]. The computation involved the Stepwise Multiple Linear Regression (SMLR), to meet desired statistical criteria with respect to correlation coefficient (r^2) and standard deviation (σ) [13]. Neither of the three models (mentioned above) could be successfully employed for correlating K_d (Am) with the solvent parameters.

Further correlations were attempted using the two, three and four parameter approaches with various diluent properties given in the literature [10,11]. The best correlations in each of these approaches along with correlation coefficient (r^2) and standard deviation (S.D) have been summarised in Table 1. The best correlation of $r^2=0.9327$ in case of the two parameter approach was obtained using parameter Y defined as $[Y = (\epsilon - 1) / (\epsilon + 2)]$, where ϵ is the dielectric constant) and DP (Schmidt diluent parameter). In case of the three parameter approach, the best correlation of $r^2 = 0.9466$ was obtained using the functions Y, DP and viscosity (η). r^2 value of 0.9869 and SD of 0.0067 was obtained in case of the four parameter approach utilising the diluent properties Y, DP, η and E_s^* (the normalised Dimroth and Reichardt's polarity index).

An attempt was also made to utilise equation (i) of the 4 parameter approach (see Table 1) to predict the K_d values in case of some other diluents not included for calculating a, b, c and d values. The results given in Table 2 show excellent correlation between the predicted and the experimentally observed K_d values for

Table 1: Correlation with statistical validity obtained using various approaches**(a) 2 parameter approach**

Correlation	r^2	Standard deviation
(i) $\log K_d = 2.67 Y - 0.31 DP - 0.47$	0.9327	0.1123
(ii) $\log K_d = 2.44 Y - 0.58 \delta + 4.23$	0.8196	0.2120

(b) 3 parameter approach

Correlation	r^2	Standard deviation
(i) $\log K_d = 2.65 Y - 0.30 DP - 1.54 P - 0.145$	0.9361	0.1264
(ii) $\log K_d = 3.17 Y - 0.28 DP - 1.30 E_1^A - 0.56$	0.9419	0.1205
(iii) $\log K_d = 2.88 Y - 0.33 DP - 0.07 \eta - 0.45$	0.9466	0.1125

(c) 4 parameter approach

Correlation	r^2	Standard deviation
(i) $\log K_d = 4.41 Y - 0.29 DP - 0.15 \eta - 3.34 E_1^A - 0.667$	0.9869	0.0067

Table 2: Comparison of K_d values obtained experimentally and from equation (i) of the four parameter approach (Table 3)

Diluent	Expected K_d	Experimental K_d
<i>n</i> -decane	3.89	3.45
xylene	0.60	0.58
benzene	0.33	0.38
chloroform	0.35	0.31
dichloromethane	1.72	1.53

Table 3: Comparison of P_{am} (in cm/sec) obtained experimentally and computed using D_e values obtained from Wilke Chang, Scheibel and Ratcliff equations in eqn. (3)Feed : ^{241}Am in 3.0 M HNO_3 ; Carrier: 0.6M DMDBDTMA and Strip : 1M Oxalic acid

Diluent	$P_{\text{WilkeChang}}$	P_{Scheibel}	P_{Ratcliff}	$P_{\text{Experimental}}$
<i>n</i> -dodecane	1.80×10^{-4}	1.87×10^{-4}	1.75×10^{-4}	1.80×10^{-4}
toluene	0.73×10^{-4}	0.78×10^{-4}	0.84×10^{-4}	0.90×10^{-4}
<i>n</i> -hexane	1.80×10^{-4}	2.12×10^{-4}	2.20×10^{-4}	1.63×10^{-4}
<i>c</i> -hexane	0.54×10^{-4}	0.62×10^{-4}	0.66×10^{-4}	0.76×10^{-4}
DCE	1.99×10^{-4}	1.93×10^{-4}	2.14×10^{-4}	1.80×10^{-4}
nitrobenzene	2.60×10^{-4}	2.48×10^{-4}	2.62×10^{-4}	2.41×10^{-4}
decalin	0.50×10^{-4}	0.50×10^{-4}	0.50×10^{-4}	0.62×10^{-4}
DEB	0.65×10^{-4}	0.66×10^{-4}	0.66×10^{-4}	0.71×10^{-4}

n-decane, xylene, benzene, chloroform and dichloromethane.

Effect of diluent on Am(III) transport

The membrane diffusion coefficients (D_m) for all the diluents used in the present work were calculated using the Wilke-Chang, Schiebel and Ratcliff equations reported in literature [9]. The D_m values obtained in all the three cases for each diluent were in reasonable agreement thereby suggesting little difference in the various models.

To determine the tortuosity of the membrane being used, permeabilities were measured through membrane laminates (prepared by laminating a number of membranes) of pore size 0.57 μm . This was done by immersing each membrane separately into the carrier solution and then pressing them together. The figure of americium permeability vs. reciprocal membrane thickness gives a linear plot, thus indicating that under the present conditions, the metal ion transport is membrane diffusion limited. The slope of the straight line obtained is given as $K_0 D_m / \tau$ (eqn. 3). The tortuosity value of 2.4 obtained using experimentally observed K_0 (4.46 at 0.6 M DMBDMDMA) and computed D_m (average of three different models mentioned above) was used to calculate the P_{∞} values.

P_{∞} was also determined experimentally using a feed solution of ^{241}Am in 3.0 M HNO_3 , strip of 1.0 M oxalic acid and 0.6 M DMBDMDMA as extractant in various diluents as the carrier. P_{∞} varied as nitrobenzene > *n*-dodecane > DCE > *n*-hexane > toluene > *c*-hexane > DEB > decalin (Table 3). An excellent agreement observed between the experimental and computed P_{∞} values has been reported previously by our group for Am transport across an SLM using 0.6M DMBDMDMA in *n*-dodecane as carrier [8]. Table 3 gives a comparison between experimentally obtained P value using (0.6M DMBDMDMA in various diluents as carrier) and those obtained from equation 3. A reasonable agreement in P_{∞} was observed in all cases suggesting the validity of the derived physico-chemical model equation. In case of nitrobenzene, the P_{∞} decreased to more than half of its initial value in about 6 hours time. This instability could be explained on the

basis of higher surface tension of nitrobenzene (46.34 dynes/cm) as compared to that of the critical surface tension of PP (~35 dynes/cm) [8].

Conclusions

Extraction of Am(III) by DMBDMDMA in various diluents, from 3.0 M HNO_3 , varied in the order nitrobenzene > *n*-dodecane > *n*-hexane > DCE > decalin > *c*-hexane > DEB > toluene. The best empirical correlation for variation in distribution of Am(III) with diluents was observed with the four parameter approach involving diluent properties like Schmidt's diluent parameter, dielectric constant, viscosity and the normalised Dimroth and Reichardt's polarity index. It was possible to accurately predict the K_0 (Am) for various other diluents by using this approach. The results of the permeation experiments through the SLM confirmed the validity of the physico-chemical model derived previously employing factors like distribution coefficient, diffusion coefficient as well as thickness of diffusion layer in both aqueous and membrane phase along with tortuosity.

References

1. W.W.Schulz and E.P.Horwitz; *Sep. Sci. and Technol.*, 1988, 23(12&13), 1191-1210.
2. C.Musikas; *Sep. Sci. Technol.*, *Sep. Sci. and Technol.*, 1988, 23(12&13), 1211-1226.
3. J.N.Mathur, M.S.Murali, R.H.Iyer, A.Ramanujam, P.S.Dhami, V.Gopalkrishnan, L.P.Badheka and A.Banerji; *Nuclear Technology*, 1995, 109, 216-225.
4. P.K.Mohapatra, S.Sriram, V.K.Manchanda and L.P.Badheka; *Sep. Sci. Technol.*, 2000, 35(1), 39-55.
5. P.R.Danesi; *Sep. Sci. Technol.*, 1984-85, 19, 857-894.
6. R.M.Izzat, J.D.Lamb and R.L.Brueening; *Sep. Sci. Technol.*, 1988, 23, 1645-1658.
7. C.Madic and M.J.Hudson; Report No. EUR 18038 EN; European Commission on Nuclear Science and Technology, Luxembourg, 1998.
8. S.Sriram, P.K.Mohapatra, A.K.Pandey, V.K.Manchanda and L.P.Badheka; *J. Memb. Sci.*, 2000, 177, 163-175.

9. J.C.Charpentier, (T.B.Drew, G.R.Cokelet, J.W.Hoopes Jr., and T.Vermeulin, Eds.); Academic press: London Volume -11, Chapter -1, 1981.
10. Y.Marcus; *Chem. Soc. Rev.*, 1993, 409-416.
11. D.R.Lide; Ed.; CRC press: Boca Raton, IO, 1999-2000.
12. R.A.Bartsch, E.Jeon, W.Walkowiak and W.Apostoluk; *J. Membr. Sci.* 1999, 159, 123-131.
13. C.Daniel and F.S.Wood; John Wiley & Sons: New York, 1980.

Mr S. Sriram was awarded the "Young Scientist Award" for the Best Oral Presentation at the 19th Conference of the Indian Council of Chemists (2000), Shimoga, India.

About the authors ...



After obtaining his M.Sc. (Analytical Chemistry) from Mumbai University, Mr S. Sriram joined Radiochemistry Division, BARC, in 1996 as Junior Research Fellow under the B.A.R.C. - Mumbai University Collaboration Scheme for Ph.D (Chemistry). His main area of research includes the studies on liquid-liquid extraction, synthesis and characterisation of solid actinide complexes, extraction chromatography and liquid membrane based separation of actinides and fission products using novel extractants like *N,N'*dialkyl amides and substituted malonamides relevant from the nuclear fuel reprocessing and waste management point of view. Mr S. Sriram has to his credit over 27 publications in leading national / international journals and conferences/ symposia.



Dr V.K. Manchanda joined the Radiochemistry Division, B.A.R.C. in 1969 after graduating from Delhi University and from 12th batch of Training School, BARC. He was awarded Ph.D. by Bombay University in 1975 and he carried out Post-Doctoral work at UTEP, Texas, U.S.A. as Fulbright Scholar (1985-87). He was recognised as Ph.D Guide in Chemistry by Bombay University in 1993. He is at present Head, Actinide Chemistry Section, Radiochemistry Division, BARC. Dr Manchanda has made original contributions in the following areas: i) Thermodynamics and kinetics of complexes of macrocyclic ligands with lanthanides and actinides, ii) Physico-chemical studies on actinide complexes, iii) Novel extractants of actinides and iv) Chemical Quality Control of Pu based fuels. He has over 300 publications in various international journals and (National/International) conferences.

Positron Annihilation Studies on Radiation Crosslinked Poly(N-isopropylacrylamide) Hydrogels

Anjali Panda, R. N. Acharya, A. Goswami and S. B. Manohar

Radiochemistry Division
Bhabha Atomic Research Centre

S. Sabharwal

Radiation Technology Development Section
Bhabha Atomic Research Centre

and

H.S. Sodaye

Department of Chemical Engineering
Indian Institute of Technology, Powai

Abstract

The microstructure of temperature sensitive poly(N-isopropylacrylamide) (PNIPAAm) hydrogels prepared by gamma-irradiation has been studied using Positron Annihilation Spectroscopy. The effect of water content of hydrogels on the lifetime and intensity of o-Ps in PNIPAAm was investigated. An attempt has been made to correlate the observed positron lifetime with the microstructure changes taking place in the polymer during swelling.

Introduction

POLY(N-ISOPROPYLACRYLAMIDE) (PNIPAAm) IS a thermally reversible hydrogel that exhibits a lower critical solution temperature (LCST) around 34°C in aqueous solutions and may find applications in areas such as controlled drug delivery devices, recyclable absorbents and as actuators [1]. Radiation crosslinked hydrogels have been reported to swell/deswell at much faster rate compared to conventionally produced gels probably due to different microstructure of these gels. Therefore, a study of their microstructure is of importance to equilibrium dynamic swelling behaviour. Positron annihilation spectroscopy (PAS) has emerged as a powerful technique to explore microscopic structure of polymers

due its selectivity to probe the free-volume in the polymer. The probing entity ortho-positronium (o-Ps), which is a bound state of electron and positron having their spins parallel, is stabilised in the free-volume, and its life-time (τ_2) has been found to be proportional to the free-volume hole size [2]. While the o-Ps lifetime can give information about the free-volume hole size, its intensity (I₂) may yield information about free-volume concentration. In the present work PNIPAAm hydrogel synthesized by γ -irradiation have been studied using PAS to characterise its microstructure.

Experimental

PNIPAAm gels were prepared from 20 wt. % NIPAAm monomer solution by γ -irradiation, using a ⁶⁰Co

radiation source having a dose rate of $1.3 \text{ kGy}\cdot\text{hr}^{-1}$. The samples obtained were cut into thin circular disks and purified by repeated swelling/deswelling cycles. The gel pieces were swollen in water to reach equilibrium and subsequently deswelled at a higher temperature ($> \text{LCST}$) resulting in gel with different water content. The positron source $^{22}\text{NaCl}$ deposited on 0.3 mil aluminium foil was sandwiched between the two pieces of gels and the whole of this assembly was wrapped in parafilm to avoid any water loss during the measurement. Lifetime measurements were carried out using a lifetime spectrometer that had a resolution of 285 ps. The data were analysed using PATFIT code for evaluating the *o*-Ps lifetime values.

Results and Discussion

The *o*-Ps lifetime (τ_2) and intensity (I_2) are plotted against the polymer weight content in Fig. 1. Representation error on τ_2 and I_2 are shown in one point and the lines are eye guides only in the figure.

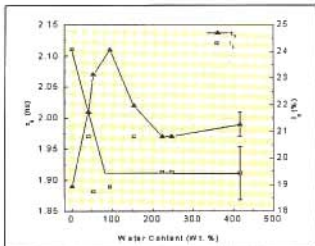


Fig. 1 Variation of τ_2 and I_2 as a function of water content of NIPAAm hydrogel

It is evident from the graph that as the water content of the polymer increases, the *o*-Ps life time (τ_2) increases from 1.89 ns to ~2.1 ns at ~94 wt. % water indicating an increase in the free volume hole size due to incorporation of water. On the other hand, the *o*-Ps intensity (I_2) decreases linearly with water content from 24% before reaching a constant value of about 19% at 94-wt.% of water. The proportional increase in τ_2 with water content up to <94% water indicates a destruction of hydrogen bonds between PNIPAAm chains, and the polar water molecules probably exist as a plasticizer below 94-wt. % water. This increases the mobility of the polymer chains increasing the free-volume hole size. Further increase in the water content leads to decrease in the τ_2 , that approaches the lifetime observed in the pure water (1.9 ns).

Acknowledgements

Dr. Anjali Panda, Research Associate, is grateful to CSIR, New Delhi, for providing financial assistance for this work.

References

- Gehrke S. H. in, "Advances In Polymer Science", Dusek K. (Ed.), Springer Verlag, Berlin, 1993, p. 83.
- Schrader D. M. and Jean Y. C. (ed.), "Positron and Positronium Chemistry", Elsevier, Amsterdam, 1988.

This paper was adjudged as the Best Paper and Presentation at Trombay Symposium on 'Radiation and Photochemistry (TSRP 2000)', held at BARC during January 12-17, 2000.

About the authors ...

her credit.

Dr. Anjali Panda (now known as Dr. Anjali Acharya) obtained her Master's and Ph. D. degrees in Chemistry from Utkal University, Bhubaneswar. She joined as a Research Associate in Radiochemistry Division, BARC, under CSIR scheme. Now she is working as a K.S. Krishnan Research Associate in Radiation Technology Development Section (RTDS), BARC. Her research interest is "synthesis, characterization and applications of stimuli sensitive hydrogels". Other areas of interest are studies on positron annihilation spectroscopy and pulse radiolysis technique. She has about 20 publications to



about 50 publications to his credit.

Dr. R.N. Acharya obtained M.Sc. in Chemistry from Utkal University, Bhubaneswar. After graduating from 37th batch of BARC Training School, he joined Radiochemistry Division, BARC, in 1994. Since then, he is engaged in research and development work on conventional, k_0 , and prompt gamma-ray neutron activation analysis. The other areas of interest are trace element speciation, nuclear reactions and positron annihilation studies. He obtained his Ph.D. degree in science from University of Mumbai in 2000. Currently he is pursuing his postdoctoral studies at Dalhousie University, Halifax, Canada. He has



Dr. A. Goswami obtained M.Sc. in Inorganic Chemistry in 1978 from Burdwan University, Burdwan. After graduating from BARC Training School in 1979, he joined Radiochemistry Division, BARC. Since then he has been working in the field of nuclear chemistry. His areas of research include studies on nuclear reactions, positron annihilation studies, and prompt gamma-ray neutron activation analysis. He has many publications to his credit.



Dr. S.B. Manobar obtained his Master's degree in Chemistry from the University of Pune in 1965. He joined Radiochemistry Division, BARC, through the BARC Training School and is at present Head, Radiochemistry Division. His areas of research are nuclear fission, nuclear reaction, nuclear spectroscopy, radiochemical separations, neutron activation analysis, nuclear probes, radioactivity in the environment, and development of non-destructive assay (NDA) techniques. He has 70 papers in international journals and more than 100 papers in symposia to his credit. He has authored a book "Experiments in Radiochemistry" and has edited the symposium proceedings NUGAR 95 and NUGAR 99. Dr. Manobar was involved in an IAEA intercomparison measurements of radionuclides in grass samples collected after Chernobyl accident. In this connection, he attended the IAEA consultants meeting at Cadarach, France, during 15-17 July, 1987. Dr. Manobar is a Ph.D. Guide for Mumbai University. He is a member of many scientific associations and President (elect) of Indian Association of Nuclear Chemists and Allied Scientist (IANCAS).

Dr. S. Sabharwal after graduating from 22nd batch of BARC Training School joined BARC in 1979. Presently, he is Head, Radiation Technology Development Section (RTDS), Isotope Group. His research interests are industrial radiation processing, radiation effects on polymeric materials, synthesis, characterization and applications of stimuli sensitive hydrogels and radiation processing of natural polymer. He has more than 75 publications to his credit.

Dr. H.S. Sodaye obtained his Master's in Chemistry from University of Mumbai. Then he worked as a DAE research fellow in Radiochemistry Division, BARC, and obtained his Ph.D. degree from University of Mumbai in 1998. After working as a research scholar in IIT, Mumbai, for a period of one year, he joined BARC as a K.S. Krishnan Research Associate. Now, he is working in Desalination Division (DD), BARC. His research interests are positron annihilation studies and studies on membranes.

Studies on Voltammetric Determination of Gallium in Dilute Hydrochloric Acid at Glassy Carbon Electrode

Jayshree Kamar, N. Gopinath, H.S. Sharma and S. K. Aggarwal

Fuel Chemistry Division
Bhabha Atomic Research Centre

DETERMINATION OF GALLIUM BY ANODIC Stripping Voltammetry (ASV) [1] and Adsorptive Voltammetry at mercury electrode [2- 4] have been carried out in the past at trace and sub-trace concentrations.

It is known that alkali metals form complex salt of the form $Ga_n[Fe(CN)_6]_n$ with ferrocyanide ions in hydrochloric acid solution of pH 2 to 3. It was thought that determination of excess $K_3[Fe(CN)_6]$ by voltammetry can serve as an indirect method for the determination of gallium [5]. With this objective, Linear Scan Voltammograms (LSV) of potassium ferrocyanide were studied employing Glassy Carbon (GC) disc (2mm dia) electrode. The electrode was scanned in the positive direction from -200 to 800 mV vs Saturated Calomel Electrode (SCE) at a scan rate of 50 mV/s and 10 mV/s in Stationary Electrode Voltammetric (SEV) and Rotating Disk Voltammetric (RDV) (1600 rpm) modes, respectively. To get reproducible results, the electrode was initially polished metallographically with 0.05 μ m alumina slurry and resurfaced after each experiment.

The anodic peak currents (I_p) were observed to increase linearly with concentrations of $K_3[Fe(CN)_6]$. Also, in RDV I_p was found to be five times of the corresponding SEV (Fig.1). Based on these observations, experiments with gallium were carried out in RDV mode. In these experiments, the concentration of $K_3[Fe(CN)_6]$ (0.1mM) and the cell volume (50 mL of 0.005M HCL) was maintained constant and the amount of gallium was varied. A plot

of decrease in I_p of $K_3[Fe(CN)_6]$ due to complexation by gallium Vs the amount of gallium was found to give a straight line with a good correlation coefficient (Fig.2).

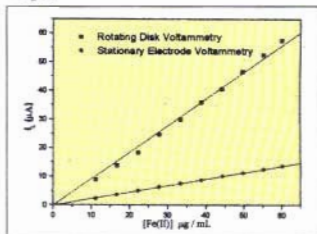


Fig.1 Plot of [Fe(II)] Vs I_p in SEV and RDV

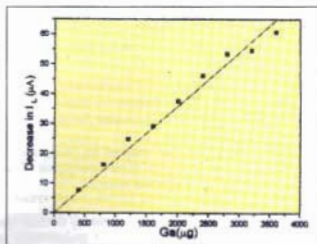


Fig.2 Effect of gallium on I_p of $K_3[Fe(CN)_6]$

Table: Ga Determination. Hydrodynamic Voltammetry, 1600 rpm, 2mm dia GCE

S.No	Aliquot Volume (μL)	I_p (μA)	Amount (μg)	Conc. (mg/g)
1a	300	5.58	500	1.66
1b	1500	23.58	2113	1.41
1c	2000	37.57	3367	1.63
2a	300	5.58	449	1.50
2b	500	8.73	703	1.41
3a	750	15.36	1189	1.58
3b	1000	18.83	1456	1.46
4a	300	5.7	446	1.49
4b	400	7.9	618	1.54
4c	500	9.5	744	1.49
Mean Conc. 1.52 ± 0.09 (rsd : 6%)				
Expected Ga conc.: 1.57 mg/g				

For the determination of gallium, similar experiments were carried out with known and unknown sample solutions and the corresponding I_p of $K_3[Fe(CN)_6]$ were measured. From the decrease in I_p of $K_3[Fe(CN)_6]$ in presence of known and unknown gallium samples, the amount of gallium in the unknown sample solution was calculated by ratio method. Table -1 presents the

results obtained from four different sets of experiments carried out on different days. As can be seen, the values were found to be within the experimental limits of error.

Acknowledgment

The authors wish to thank Dr.V.Venugopal, Head, Fuel Chemistry Division and Shri. D.S.C. Purushotham, Director, Nuclear Fuels Group for their interest and encouragement in this work.

References

1. J.Wang, Stripping Analysis : rinciples, Instrumentation and Applications, VCH Publishers, Deerfield Beach, FL, 1985.
2. J.Wang, Am. Lab., 17(5) (1985) 41.
3. Pablo Cofre and Karin Brink, Talanta 39 (2) (1992) 137.
4. Gaston East and Pablo Cofre, Talanta 40 (8) (1993) 1273.
5. I. M. Kolthof Etal, Treatise On Anal. Chemistry Part II, Vol. II, Page 37, Inter Science, New York (1962)

This paper won the Best Oral Presentation award in the Workshop-cum-Seminar on 'Electroanalytical Chemistry and Allied Topics, ELAC 2000' held at BARC from November 27 to December 1, 2000

About the authors ...



Ms J.V. Kamat has been working in the field of quality control of nuclear fuels for the last twenty years. She has been actively involved in developing various sensitive electroanalytical techniques for different applications in the nuclear fuel cycle.



Mr N. Gopinath has been working in the field of quality control of nuclear fuels for the last 24 years. He has been actively involved in developing and employing various electroanalytical techniques for different applications in the nuclear fuel cycle.



Dr H.S. Sharma obtained his Ph.D. from University of Allahabad in 1976 and joined BARC in 1977. He is currently involved in the development of voltammetric methodology for trace elemental analyses in various types of nuclear fuel materials.



Dr S.K. Aggarwal is the Head of the Mass Spectrometry Section, Fuel Chemistry Division, BARC. He has been working in the area of atomic mass spectrometry since 1973. Besides, he has been involved in electroanalytical chemistry since 1994. He is the recipient of several Medals of Honour. He has visited many countries in connection with scientific activities / meetings.

Determination of Uranium and Plutonium in Nuclear Fuel Materials by Electroanalytical Methods

N. Gopinath, J.V. Kamat, N. B. Khedekar, K.V. Lohithakshan, P. D. Mithapara, P.R. Nair, B.N. Patil, M. Renuka, Keshav Chander, H.S. Sharma, M. Xavier and S.K. Aggrwal

Fuel Chemistry Division
Bhabha Atomic Research Centre

ELECTROANALYTICAL METHODS, POTENTIOMETRY, Biamperometry and Coulometry are normally employed for the determination of U and Pu in various nuclear fuel materials such as UO_2 , PuO_2 , $(U,Pu)O_2$, $(U,Pu)C$, (UO_2+PuO_2+C) , UC, PuC etc.. Results of high accuracy and precision are required for the purpose of Chemical Quality Assurance of fuels, because an accurate knowledge of fissile content is an important and stringent requirement in the nuclear fuel. The electroanalytical methods have been adopted due to the fact that actinides ions, especially, U and Pu exist in multiple oxidation states in solution and are interconvertible. Electroanalytical methods are simple in operation, compatible for automation in a radioactive laboratory and can provide requisite level of accuracy and precision at milligram levels. Besides, instrumentation involved in potentiometry and biamperometry is inexpensive and indigenous.

Several redox methods have been developed and modified in our laboratory in the past for the determination of U and Pu in nuclear fuels. Uranium determination in uranium bearing fuels is carried out by well known modified Davies and Gray [1,2] method, which involves reduction of U(VI) to U(IV) by Fe(II) in >10 M phosphoric acid medium. Excess of Fe(II) is selectively oxidised and U(IV) is titrated with standard potassium dichromate, after dilution with dilute sulphuric acid. Potentiometric method is employed for detecting the end-point of the titration. This method is versatile in the sense that plutonium, if present, along with uranium, does not interfere. However, because of the difficulty of plutonium

recovery from analytical waste in phosphate medium, its application is preferred for uranium determination in uranium based fuel materials. An alternate method, developed in our laboratory [3] for uranium determination in plutonium bearing fuel materials is based on the reduction of U(VI) to U(IV) by $TiCl_3$ in 6-7 M H_2SO_4 , excess Ti(III) is destroyed by HNO_3 and U(IV) is titrated with standard $K_2Cr_2O_7$, using ferric ion as intermediate. The end-point is detected using Biamperometry.

Modified Drummond and Grant method [4] is routinely employed for the determination of Pu in diverse matrices of fuel samples. The method involves oxidation of Pu to Pu(VI) with argentic oxide in 1 M H_2SO_4 . The excess of argentic oxide is selectively reduced with sulphamic acid. In the next step, Pu(VI) is reduced to Pu(IV)/Pu(III) by adding a known amount of standardised Fe(II). The excess of Fe(II) is titrated with dichromate to a potentiometric or biamperometric end point.

In potentiometry, Saturated Calomel Electrode (SCE) is used as a reference electrode and a platinum wire as an indicator electrode for sensing the potential of the redox couples undergoing redox change. A digital Potentiometer directly monitors the potential of the redox couple. In biamperometric method, two identical platinum wire, embedded in a glass tube, sense the electrolysis current in the cell. Amperometer, having facilities for applying a suitable potential across the two platinum electrodes and different Current ranges, is employed for monitoring the electrolysis current. In order to achieve higher

accuracy and precision, addition of the reagents is done on weight basis.

Quantitative dissolution of the sample is an essential requirement for accurate determination. In actual practice, a weight solid (200-500 mg) sample is dissolved in a suitable solvent medium. UO_2 samples are dissolved in nitric acid and PuO_2 in conc. HNO_3 containing 0.05 M HF. Mixed carbide fuel samples are dissolved in conc. HNO_3 + conc. H_2SO_4 mixture (1:1), by direct dissolution procedure [5]. Dissolution of Pu bearing fuel samples is carried out in Glove Boxes. After the dissolution, the solution is quantitatively transferred to preweighed volumetric

flasks and is taken to another glove box for aliquoting. Quantity of U and Pu is normally in the 3-5 mg range in each aliquot. Analysis of these aliquots for Pu or U are carried out in afumehood by the above mentioned methods.

During the fabrication of FBTR fuel, a large number of samples of the finished product sintered $(U,Pu)C$, as well as starting material, UO_2 , PuO_2 , $(U,Pu)O_2$, (UO_2+PuO_2+C) , UC and PuC etc. have been analyzed for Pu and U. Typical U and Pu results obtained in a series of thirty FBTR Fuel samples are shown in figs. 1 and 2 respectively.

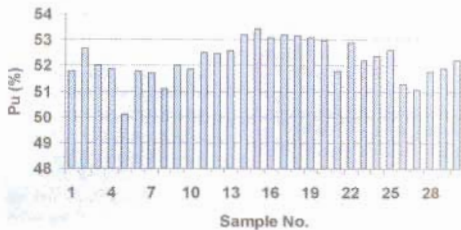


Fig.1

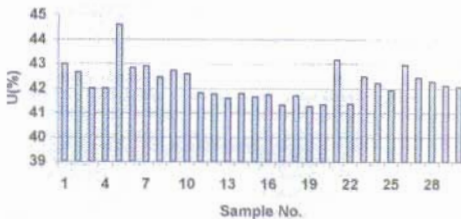


Fig.2

Distribution of U & Pu in Sintered (U,Pu)C samples of FBTR fuel

Redox chemistry involved in these methods is not only interesting but also exciting. All these aspects with an emphasis on the interference of the impurities present in the dissolved solution, reliability of the methods for routine U, Pu determination, shall be discussed.

Acknowledgements

Authors thank Dr. V. Venugopal, Head Fuel Chemistry Division and Shri D.S.C. Purushotham, Director, Nuclear Fuels Group, BARC, for their keen interest in this work.

References

1. W. Davies and W. Gray, *Talanta* 11, 1203 (1964)
2. M. John, S.Vaidyanathan, P.Venkataraman and P.R. Natarajan, convention of chemists, Bangalore (1976) and *BARC Report/1-634* (1981)
3. P.R. Nair, K.V. Lohithakshan, M. Xavier, S.G. Marathe, and H.C. Jain , " Determination of Uranium and Plutonium in Plutonium Based Fuels by Sequential Amperometric Titration" *J. Radioanal. Nucl. Chem. Articles*, 122,19 (1988)
4. C.L.Rao, G.M.Nair, N.P. Singh, M.V.Ramaniah and N.Srinivasan, *Anal. Chem.* 234,126(1971)
5. Keshav Chander, B. N. Patil, J.V. Kamat, N.B. Khedekar, R.B.Manolkar, and S.G.Marathe, *Direct Dissolution of Nuclear Materials for Chemical Quality Control*, *Nucl.Technol*, 78, 69 (1987)

This paper won the Best Poster Presentation award in the Workshop -cum-Seminar on 'Electroanalytical Chemistry and Allied Topics, ELAC 2000' held at BARC from November 27 to December 1, 2000

About the authors ...



Mr N. Gopinath has been working in the field of quality control of nuclear fuels for the last 24 years. He has been actively involved in developing and employing various electroanalytical techniques for different applications in the nuclear fuel cycle.



Ms J.V. Kamat has been working in the field of quality control of nuclear fuels for the last twenty years. She has been actively involved in developing various sensitive electroanalytical techniques for different applications in the nuclear fuel cycle.



Mr N.B. Khedekar joined BARC in 1980. Since then, he has been working in the field of chemical quality control of various kinds of nuclear fuel material.



Dr K.V. Lohithakshan joined BARC in 1981. He obtained M.Sc. and Ph.D. degrees from Mumbai University in the years 1990 and 2000 respectively in the field of solvent extraction studies of actinides. Presently, he is involved in the chemical quality control of nuclear fuels.



Mr P.D. Mithapara has been working in the field of solvent extraction studies of actinides since 1970. Presently he is involved in the quality control of nuclear fuel materials.



Mr P.R.Nair joined BARC in 1976. Since then, he has been actively involved in the area of chemical quality control of nuclear fuels.



Mr B.N. Patil joined the BARC in 1971. Since then, he has been actively involved in the area of chemical quality control of nuclear fuel materials.



Ms M. Renuka joined BARC in 1994. she is involved in the field of quality control of nuclear fuels.



Dr Kesava Chander joined BARC in 1967. since then, he has been actively involved in the quality control of nuclear fuels. He has developed and standardized many simple electroanalytical methods for the determination of Pu, U and Tb in a variety of samples. He obtained his Ph.D. degree from Bombay University in 1992.



Dr H.S. Sharma obtained his Ph.D. from University of Allahabad in 1976 and joined BARC in 1977. He is currently involved in the development of voltammetric methodology for trace elemental analyses in various types of nuclear fuel materials.



Ms Mary Xavier is a graduate from 15th batch of BARC Training School. She is responsible for introducing the simple bipotentiometric methodology for determination of uranium and plutonium in nuclear fuel samples. Presently, she is looking after the work pertaining to the quality control of nuclear fuels.



Dr S.K. Aggarwal is the Head of the Mass Spectrometry Section, Fuel Chemistry Division, BARC. He has been working in the area of atomic mass spectrometry since 1973. besides, he has been involved in electroanalytical chemistry since 1994. He is the recipient of several Medals of Honour. He has visited many countries in connection with scientific activities / meetings.

Thermal Ionisation Mass Spectrometric Analysis of Neodymium pre-separated by High Performance Liquid Chromatography

N. M. Raut, P. G. Jaison and S. K. Aggarwal

Fuel Chemistry Division
Bhabha Atomic Research Centre

ISOTOPIC COMPOSITION AND CONCENTRATION OF Nd are important for the determination of burn-up of nuclear fuel and also for geochronological studies using Sm-Nd couple. It involves three steps; (i) separation of lanthanides from the major matrix, (ii) purification of Nd from other lanthanides and (iii) mass spectrometric analysis of purified fraction. Several methods e.g. solvent extraction, chromatographic separation on anion and cation exchanger resin etc. are available for matrix separation. But separation of Nd from other lanthanides is a difficult task due to their similar chemical behaviour. Isobaric overlaps like Sm-144, Sm-148, Sm-150 and Ce-142 hamper the accurate determination of isotopic composition Nd by Thermal Ionisation Mass Spectrometry (TIMS) and therefore, an extensive chemical separation is required. High Performance Liquid Chromatography (HPLC), a promising separation method, offers the potential to resolve all the lanthanides in a short time. Keeping above aims in mind, a fast and efficient method for separation of different lanthanides using HPLC was investigated. Reverse phase dynamically modified ion exchange chromatography was selected for carrying out the studies because of its ability to alter the ion-exchange capacity and selectivity rapidly. Hydrophobic anion like camphor sulphonate was tested as a modifier for C-18 reversed phase column and α -hydroxy isobutyric acid (α -HIBA) was used as eluent. Arsenazo (III), a specific complexing agent for lanthanides, was used as the post-column derivatising agent during development of separation method. A

diode array detector was employed for monitoring the eluted lanthanides at a wavelength of 615 nm. Under the chromatographic conditions, the retention times of separated lanthanides were recorded and used for programming in the fraction collector. The use of arsenazo(III) was eliminated while collecting the fractions for mass spectrometric analysis. A synthetic mixture of Ce, Nd and Sm in 1:1:1 proportion (by weight) was prepared and separated by HPLC. The Nd fraction collected contained the organic components i. e. the eluent and the modifier used in chromatographic separation. The application of this Nd fraction along with the organic part on filament used in the ion source of TIMS suppresses the yield of Nd⁺ ions. Hence the collected fraction was pre-treated with concentrated HNO₃ and H₂O₂ and evaporated to dryness. This was repeated 4 to 5 times to destroy the organic part. The fraction free from organic matter was concentrated and analysed by TIMS using a double filament assembly. The isotope ratio measurements were done at temperatures corresponding to 4.5A and 2.5A for ionisation and vaporisation filaments, respectively. No isobaric interferences were present at 142 (Ce), 144 (Sm), 148 (Sm) and 150 (Sm) as was evident from the absence of peaks at m/z 140 (Ce⁺) and at m/z 147, 152 (Sm⁺). Results of isotopic composition of separated Nd fraction were compared with those of natural Nd and were in good agreement. Thus it is possible to determine the accurate isotopic composition of Nd from a mixture of lanthanides by TIMS and the developed HPLC procedure for separation.

This paper won the Best Oral Presentation award in the 9th ISMAS Workshop on 'Mass Spectrometry', held at NIO, Goa, during December 12-16, 2000.

About the authors ...

Mr N. M. Raut completed M. Sc. in Analytical Chemistry from Mumbai University in 1998. He joined BARC in January 1999 as a Junior Research Fellow under the Mumbai University - DAE collaborative programme. Presently, he is working in the Mass Spectrometry Section of Fuel Chemistry Division for his Ph.D. with Dr. S. K. Aggarwal. His research field includes the physico-chemical studies for determination of trace elements using HPLC and Mass Spectrometry.



Mr P.G. Jaison has obtained M.Sc. in Chemistry from Cochin University of Science and Technology in 1997. He joined Fuel Chemistry Division, BARC, through the 41st batch of Training School in 1998. Presently, he is working on HPLC and inorganic mass spectrometry.



Dr S.K. Aggarwal is the Head of the Mass Spectrometry Section, Fuel Chemistry Division, BARC. He has been working in the area of atomic mass spectrometry since 1973. Besides, he has been involved in electroanalytical chemistry since 1994. He is the recipient of several Medals of Honour. He has visited many countries in connection with scientific activities / meetings.

A Simple and Rapid Molecular Method for Distinguishing between Races of *Fusarium oxysporum* f.sp. *Ciceris* from India

A. Chakrabarti, P.K. Mukherjee, P. Sherkhane and N.B.K. Murthy

Nuclear Agriculture and Biotechnology Division
Bhabha Atomic Research Centre

Abstract

A simple, rapid and reliable method for studying the variability and identification of races of the chickpea wilt pathogen Fusarium oxysporum f.sp. ciceris (FOC) is described here. The method involves selective amplification of the intergenic spacer (IGS) region of the nuclear ribosomal DNA, and restriction digestion with a set of enzymes. RFLP analysis of the amplified IGS region of four isolates of FOC representing four races from India (Race1 - Patancheru; Race2 - Kanpur; Race3 - Gurdaspur; Race 4- Jabalpur.) was carried-out with various restriction enzymes. All the enzymes gave similar restriction pattern for race 1 and race 4, which was distinctly different from race 2 or race 3. The present finding indicates that race 1 and race 4 are either the same or very closely related to each other. It is suggested that amplification of the IGS region and digestion with restriction enzymes could be used to study polymorphism in FOC, and to identify the races existing in India.

Introduction

FUSARIUM OXYSPORUM SCHL.-FR. F.SP. CICERIS (Padwick) Mauts & Sato, which incites wilt, is one of the major pathogens of chickpea (*Cicer arietinum* L.) worldwide, especially in the Indian subcontinent and the Mediterranean basin [1, 2]. The best available method for control of fusarium wilt is the cultivation of resistant chickpea varieties [3]. However, the existence of several physiological races of the pathogen makes it complicated to contain this disease through resistance breeding. Seven races of this pathogen have so far been reported. Races 1-4 from India; 0, 1, 5, 6 from California and Spain; 1 and 6 from Morocco and 0 from Tunisia [4,5,6]. Race 1 has further been subdivided into three sub-groups viz. 1A, 1B and 1C [6]. Of these races, race 1A, 2 through 6 cause typical fusarial wilt and necrosis, whereas, races 0, 1B and 1C induce yellowing syndrome in absence of

wilting [6]. The races are conventionally identified by inoculation of a set of 10 differential varieties [3]. This method of race identification is expensive, time consuming (at least 40 days) and may be influenced by variability inherent in the experimental system [7,8,9]. In this regard, a rapid molecular method, therefore, would be advantageous over conventional techniques of race identification.

Using RAPD/AFLP analysis, Kelley *et al.* [10,11] could differentiate between the two groups/pathotypes inducing either wilt or yellowing symptoms. No polymorphism in the mitochondrial DNA was detected among the seven races studied by Perez-Artes *et al.* [12]. To our knowledge, there is no molecular method available that could distinguish between the wilt-inducing races of this pathogen. RFLP analysis of the nuclear ribosomal DNA (rDNA) was useful in demonstrating species-specific differences in to xin-

producing *Fusarium* spp. [13]. The present paper reports on the genetic variability within wilt-causing pathotype of *F. oxysporum* f.sp. *ciceris* using molecular methods based on the variability in the rDNA region. The usefulness of this method in studying the polymorphism in the wilt-inciting isolates of FOC and the rapid race identification has been discussed.

Materials and Methods

Fungal isolates

Four isolates of *F. oxysporum* f.sp. *ciceris*, representing four races from India were collected from the International Crops Research Institute for the Semi-Arid Tropics, Patancheru. Race 1 was originally isolated from Hyderabad, 2 from Kanpur, 3 from Gurdaspur and 4 from Jabalpur. The cultures were multiplied and maintained on potato dextrose medium.

Isolation of genomic DNA

High molecular weight genomic DNA from *Fusarium* mycelium grown in potato dextrose broth for 3 days, were isolated using a method described by Kim *et al* [14]. Briefly, the mycelium was harvested on Whatman no. 1 filter papers, washed thoroughly and ground in liquid nitrogen. Five ml of extraction buffer (100 mM NaCl, 10 mM Tris, 1 mM Na₂EDTA, pH 8) containing 1.0 % SDS and 0.5% β -mercaptoethanol was added to 2 g of ground mycelium taken in 50 mL Sorvall centrifuge tubes and mixed thoroughly. The mixture was incubated at room temperature for 30 minutes and extracted twice with equal volume of phenol/ chloroform/ isoamyl alcohol (25:24:1) and twice with chloroform/ isoamyl alcohol. DNA was precipitated with two volume of ice-cold ethanol, spooled, washed with 70% ethanol and dissolved in TE buffer (10 mM Tris, 1 mM Na₂EDTA, pH 8).

PCR-amplification and restriction analysis

Amplification of the IGS region was performed using the primer pair CLN 12 (CTGAAGCCTCTAAGTCAG) and CNS1 (GAGACAAGCATATGACTACTG) designed by Apple and Gordon [15] for *Fusarium oxysporum* with priming sites at the 3' end of the 28S gene and 5' end of the 18S gene respectively. The amplification mix

contained 0.5 μ M primer, 10ng DNA, 0.1mM of each of the dNTPs in 1X reaction buffer containing 1.5 mM MgCl₂ (supplied by manufacturer). After initial melting at 95°C for 5min, temperature was held at 68°C and 1U of *Taq* polymerase (Bangalore Genei, India) was added per 25 μ l final volume of reaction mix. This was followed by 30 cycles of amplification with the following parameters: annealing at 55°C for 1min, extension at 72°C for 2min, melting at 94°C and a final extension of 10 min at 72°C. The amplified products were extracted twice with chloroform/isoamylalcohol (24:1), ethanol precipitated, washed with 70% ethanol and dissolved in TE. The products thus purified were digested completely with *Eco*RI, *Bam*HI, *Hind*III, *Pst*I, *Sac*I (New England Biolabs), *Taq*I (Boehringer mannheim), *Alu*I and *Sau*3A I (Bangalore Genei, India) as per manufacturers' instructions and size separated on 1.5% agarose gels in 1X TBE buffer.

Results and Discussion

Our earlier experiments on RFLP analysis using *Neurospora crassa* rDNA as probe indicated the presence of a variable *Eco*RI site. Amplification of the ITS region followed by *Eco*RI digestion did not produce any variability and combining these two we could locate the variable *Eco*RI site on the IGS region.

Using the primer pair CLN 12 and CNS 1, we could amplify the IGS region from all the 4 races, the approximate size being 2.6kb (2.4 for Race 2) (Fig. 1). Digestion of the amplified IGS region with *Eco*RI produced similar bands for both Race 1 and Race 4 (one 1.9 and another 0.7kb). But individual and distinctive banding pattern were observed for both Race 2 (1.9 and 0.5 kb) and Race 3 (2.2 and 0.4 kb) (Fig. 1). This conclusively proved that the variability in the restriction patterns observed in Southern hybridization with rDNA repeat unit from *N. crassa* was indeed due to variability of the *Eco*RI site within the IGS region. When variability within the IGS region was further studied using *Hind*III, *Bam*HI and *Sac*I, none of them did restrict the amplified fragment indicating absence of these sites within IGS region in all the four races. However, *Pst*I was found to have one site only in case of Race 3 (2.0 and 0.6 kb fragment) (Fig. 1). When tetrabase cutters (*Alu*I, *Taq*I and *Sau*

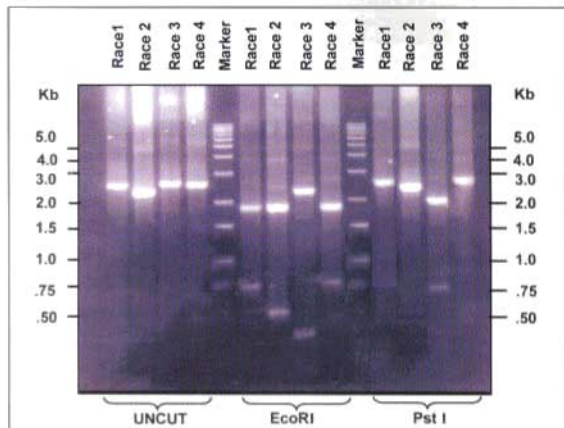


Fig.1 PCR amplified IGS region and its *EcoRI* and *PstI* restriction patterns of four races of FOC

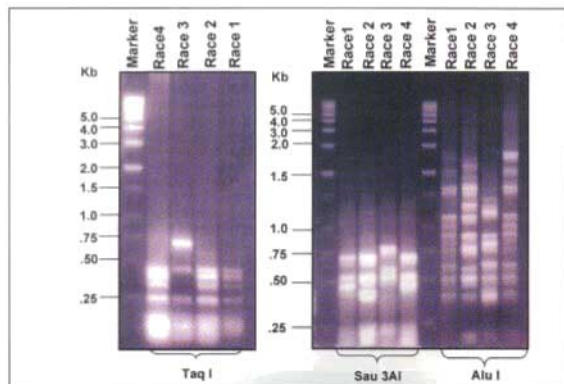


Fig.2 Restriction pattern of the PCR amplified IGS region of four races of FOC with *TaqI*, *AluI* and *Sau 3AI*

3A I) were used number of restriction fragments were produced. But in each case Race 1 and 4 had similar profile where as that for Race 2 and 3 were always different from each other and rest all (Fig. 2).

F. oxysporum f.sp. *ciceris* races were originally classified based on wilt reaction on 10 differential lines [4]. The disease reaction was scored based on percent wilting (resistant 0-20%, moderately susceptible 21-50%, and susceptible >51% wilt). While Races 1, 2 and 3 could be clearly identified based on distinct reactions (either resistant or susceptible) on two differential lines, race 4 was designated based on reaction on only one differential line i.e., CPS-1, and the reaction was "moderately susceptible" as compared to "resistant" for race 1. This observation is indicative of relatedness of race 1 to race 4. The data obtained in the present experiment also indicate that races 1 and 4 are identical with respect to restriction pattern of the IGS region of the rDNA. However, race 1/4 is distinctly different from race 2 and race 3, which are different from each other. The present investigation indicates that the wilt-causing races of *F. oxysporum* f.sp. *ciceris* are genetically distinct, and polymorphism can be studied in the wilt causing pathotype using the variability in the IGS region. We also suggest that after further verification with more representative isolates, it could be possible to develop a simple, rapid and reliable method of race identification in FOC by amplifying the IGS region and restriction digestion of the same with appropriate restriction enzyme(s).

Acknowledgement

The authors thank Dr. M.P. Haware, ICRISAT Asia Center, Patancheru, for the *Fusarium oxysporum* f.sp. *ciceris* isolates.

References

- Haware M.P. Fusarium wilt and other important diseases of chickpea in the mediterranean area. *Opt Mediterr Sem* 1990; 9: 61-64
- Nene Y.L. and Reddy M.V., in *The chickpea* (eds Saxena M.C. and Singh K.B.), Oxon: CAB International, 1987, pp. 233-70.
- Haware, M.P., Nene, Y.L., Pundir, R.P.S. and Narayana Rao J., *Field Crops Res.*, 1992, 30, 147-154.
- Haware, M.P. and Nene, Y.L., *Plant Dis.*, 1982, 66, 809-810.
- Jimenez-Diaz, R.M., Trapero-Casas, A. and Cabrera de la Colina J., in *Vascular wilt diseases of plants* (eds Tjamos E.C. and Beckman C.), Springer-Verlag, Berlin, 1989, H28, pp. 515-520.
- Jimenez-Diaz, R.M., Alcalá-Jimenez, A., Hervás, A. and Traperocas J.L., *Hod. Rosl. Aklim. Nasn. (Special Edition)*, 1993, 37, 87-94.
- Alcalá-Jimenez, A.R., Trapero-Casas, J.L. and Jimenez-Diaz, R.M., in *Resumenes. VI Congreso Latino-Americano de Fitopatología*, Torremolinos, Spain, 1992, pp. 39.
- Bhatti, M.A. and Kraft, J.M., *Plant Dis.*, 1992, 76, 50-54.
- Bhatti, M.A. and Kraft, J.M., *Plant Dis.*, 1992, 76, 1259-62.
- Kelly, A., Alcalá-Jimenez, A.R. and Bainbridge, B.W., in *Modern assays for plant pathogenic fungi- Identification, detection and quantification* (eds Schots, A., Dewey, F.M. and Oliver, R.P.), Oxon: CAB International, 1994, pp. 75-82.
- Kelly, A., Alcalá-Jimenez, A.R., Bainbridge, B.W., Heale, J.B., Perez-Artes, E. and Jimenez-Diaz, R.M., *Phytopath.*, 1994, 84, 1294-1298.
- Per-Artes, E., Roncero, M.I.G. and Jimenez-Diaz, R.M., *J. Phytopath.*, 1995, 143, 105-109.
- Lodolo, E.J., Van Zyl, W.H. and Rabie, G.J., *Mycol. Res.*, 1992, 97, 345-46.
- Kim, D.H., Martyn, R.D. and Magill, C.W., *Phytoparasitica*, 1991, 19, 211-213.
- Appel, D.J. and Gordon, T.R., *Mol. Plant-Microbe Interactions*, 1996, 9, 125-138.

About the authors ...

Mr Apratim Chakrabarti, M.Sc., is from 41st batch of BARC Training School. He won the Homi Bhabha award for Biology-Radiobiology discipline in his batch, and is working in the Plant Cell Culture Technology Section of Nuclear Agriculture and Biotechnology Division (NABTD).



Dr P.K. Mukherjee, M.Sc., completed his Ph.D. as a Dr K.S. Krishnan IAR research fellow. He is working in the Plant Pathology and Pesticide Residues Section of NABTD, on the biocontrol mechanisms of plant diseases. He was awarded the "Pran Vohra Award" for agricultural sciences 1998-99 by the Indian Sciences Congress Association.



Mr P.D. Sberbkane, B.Sc. (Microbiology), joined BARC in 1997. He is working in the Plant Pathology and Pesticide Residues Section of NABTD.



Dr N.B.K. Murthy, M.Sc., Ph.D., is the Head of Plant Pathology and Pesticide Residues Section, NABTD. His specialization is in the field of pesticide residues. He has several publications in national and international journals to his credit.



Dr A.J. Tambankar did his M.Sc. (Agriculture) from Nagpur University and Ph.D. from MPKV. He is currently heading the Pheromone and SIT group of Nuclear Agriculture and Biotechnology Division, BARC. He has published several papers in national and international journals on the subject of insect sex pheromones and sterile insect technique.

A Methodology for the Estimation of Mercury, Boron, Samarium and Cadmium by Prompt Gamma Ray Activation Analysis

Yogesh Scindia, A.V.R. Reddy, A.G.C. Nair, A. Goswami, R.N. Acharya,

K.Sudarshan and S.B. Manohar

Radiochemistry Division

Bhabha Atomic Research Centre

Abstract

Prompt Gamma ray Neutron Activation Analysis (PGNAA) is an effective analysis technique especially for lighter elements like boron, hydrogen, nitrogen and some rare earth elements. A PGNAA system was set up making use of the guided neutron beam facility at the Dhruva Reactor for the first time in BARC. A method to estimate high neutron absorbing elements like Hg, B, Sm and Cd which eliminates the variations in neutron flux and geometric efficiency is discussed.

Introduction

PGNAA TECHNIQUE IS BASED ON THE RADIATIVE capture of neutron by the nucleus. It is a unique non-destructive technique complementary to the conventional Neutron Activation Analysis. It is widely used for many elements, which are normally not amenable to NAA [1]. Its sensitivities for elements like B, Hg, Sm, Cd and Gd are superior due to their higher neutron absorption cross section. Routine assay of these elements is carried out by standard comparison technique. This calls for double irradiation and therefore requires corrections for the irreproducible parameters like neutron flux and detection efficiency mainly due to the variation in the sample geometry, self attenuation of the neutron flux. In the present approach, the sample containing elements of interest is intimately mixed with known amount of standard (ammonium chloride) and irradiated. This obviates the need for separate irradiation of the standard. In the present work, a methodology based on calibration curve of the element of interest, corrected by the count rate of ^{36}Cl as standard is reported.

Experimental

The thermal guided beam facility in 100 MW Dhruva reactor, BARC, Trombay was used for the PGNAA work. The neutron beam is transported through the guided beam tube to about 30 meters away from the reactor core. An experimental set up has been arranged for PGNAA using this guided beam. The dimensions of the beam are 2.5 cm x 10 cm. The detector was surrounded by 30 cm thick lead bricks as shielding material for reducing the gamma ray background. The γ -ray detector was located at about 40 cm distance from the sample and was at 90° with respect to the beam direction. A lead collimator of 3 cm dia and 30 cm length was used in front of the detector to collimate the gamma rays coming from the sample.

Elements in their appropriate chemical form (wherever possible the chloride salt) weighing in the range of 100-500 mg were mixed thoroughly with known amount of NH_4Cl and wrapped in a thin Teflon tape. They were exposed to the neutron beam for sufficiently long time. A 22% HPGe detector connected to a PC

based 8k MCA was used for assay of prompt gamma rays. The resolution of the detector is 2.4 keV at 1332 keV. The MCA has been calibrated in the energy region of 0.1 to 8.5 MeV using the delayed gamma rays from ^{152}Eu and ^{60}Co , and prompt gamma rays from ^{35}Cl . A second order polynomial was used for the energy calibration. Photo peak areas under the corresponding gamma lines of ^{35}Cl (1951 keV), boron (478 keV), mercury (368 keV), samarium (333 keV) and cadmium (558 keV) were determined by analysing the gamma ray spectra using the software developed in Electronics Division, Bhabha Atomic Research Centre. The count rate per mg of 1951 keV gamma ray from ^{35}Cl in a sample was taken as standard and count rate/mg of ^{35}Cl for other samples were normalised to this value. The same normalisation factors were applied to the count rate per mg of the element of interest.

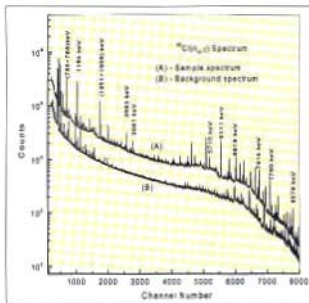


Fig.1 A typical prompt gamma ray spectrum of NH_4Cl

Results and Discussions

Fig.1 shows a typical gamma-ray spectrum of NH_4Cl with the background. The delayed gamma-rays from ^{152}Eu and the prompt gamma-rays from ^{35}Cl and ^{90}Tl were used for efficiency calibration. The absolute efficiencies were determined for low energy region (i.e., upto 1500 keV) using ^{152}Eu source. The relative efficiency plot from 500 to 9000 KeV obtained from the prompt gamma-rays of ^{35}Cl and ^{90}Tl were normalized with absolute values from ^{152}Eu . The details

of efficiency fitting are given elsewhere [2]. The absolute efficiency plot is shown in Fig.2.

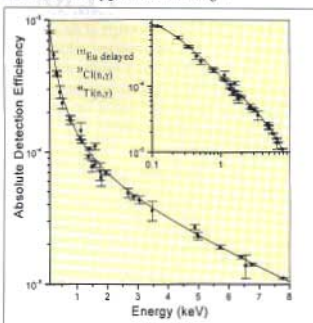


Fig. 2. Absolute efficiency curve of the PGNA system

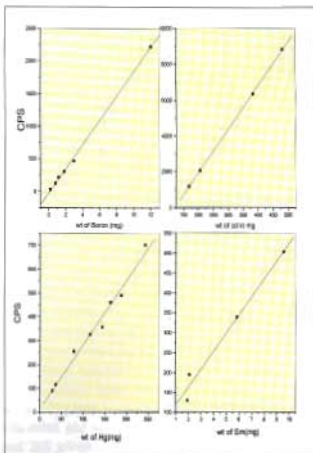


Fig. 3 Sensitivity plot of B, Cd, Hg and Sn

Fig. 3 shows the plot of the normalised count rate plotted as a function of the elemental weight for the above mentioned elements. Good linearity between the normalised count rate versus weight of the element is observed with correlation coefficient values ranging from 0.999 - 0.99 for the entire weight range studied. The linearity of the CPS Vs weight over the wide range shows the feasibility of this method for determining concentrations in unknown samples over this wide range.

References

1. G. L. Molnar, Zs. Revay, R. L. Paul, R. M. Linderstram, *J Radioanal. Nucl. Chem.* **234**, 21 (1998).
2. K. Sudarshan, A.G.C. Nair, R.N. Acharya, Y.M. Scindia, A.V.R. Reddy, S.B. Manohar and A. Goswami, *Nucl. Instr. and Meth. A* **457** (2001) 180.

SF₆ Gas Handling System for FOTIA at BARC

S.K.Gupta, R.V. Patkar, P. Singh, E. Shallom, A. Agarwal, S. Santra, Rajesh Kumar,
S.P. Sarode, P.J. Raut and B.K. Jain

Nuclear Physics Division
Bhabha Atomic Research Centre

and

S.V. Gogate, R.R. Patankar, M.G. Andhansare, A.C. Tikku and M.G. Khadilkar

Reactor Services and Maintenance Division
Bhabha Atomic Research Centre

Introduction

A N INDIGENOUSLY BUILT FOTIA FACILITY HAS recently been commissioned at BARC. It involved designing, procurement, fabrication, testing, installation and commissioning of a 6 MV Folded Tandem Ion Accelerator (FOTIA) (Fig.1), by utilizing a large part of the existing equipment such as the pressure tank, the storage tank, the equipotential rings, the high voltage dome and the accelerator room of the old 5.5 MV Van-de-Graaff accelerator at the Nuclear Physics Division, BARC.

The construction of the FOTIA involved development of state-of-the-art technologies for several important components like dipole magnets, high voltage generator, SF₆ gas handling system, vacuum systems, magnetic and electrostatic lenses, computer control system, etc [1]. A new accelerator facility of this type would have costed around 18 crore rupees to the department. However, due to availability of the expertise at BARC and utilization of infrastructure from the earlier Van-de-Graaff accelerator, it was possible to set up the facility in a cost effective way at about 3-4 crore rupees. The FOTIA has capability of delivering accelerated light and heavy ion beams up to A=40 and beam energy up to 66 MeV. These accelerated beams will be used both for research in basic and applied science in the fields of nuclear physics, astrophysics, material science, accelerator mass spectrometry, atomic spectroscopy, etc.

The high voltage column section of the FOTIA was tested and a voltage of 3.4 MV was achieved on the terminal with N₂+CO₂ gas mixture filled in the accelerator tank at a pressure of 98 psig [2]. The terminal voltage would exceed 6 MV with SF₆ gas, as its dielectric breakdown strength is more than 2 times that of the N₂+CO₂ mixture at this pressure. A SF₆ gas handling system was designed, fabricated, installed [3] for FOTIA and has been used extensively for high voltage operation. In this paper, some of the salient features of the gas handling system are discussed.

Objective of Using SF₆ Gas in FOTIA

The FOTIA is an electrostatic accelerator in which terminal is raised to a maximum voltage of 6 MV whereas the accelerator tank is at ground potential. While the lower portion of the terminal has coaxial cylindrical geometry, the upper portion has spherical geometry. The coaxial cylindrical geometry is formed between cylindrical surfaces of the high voltage dome and the accelerator tank. Similarly coaxial spherical geometry is formed between spherical top end of the high voltage terminal and the accelerator tank. The typical voltage gradients between dome and the accelerating tank at the terminal voltage of 6 MV, for cylindrical and spherical geometries, are 134 kV/cm and 205 kV/cm respectively. These voltage gradients could be withstood by using N₂+CO₂ gas mixture as insulating medium only if accelerator tank pressure is

**FOLDED
TANDEM
ION
ACCELERATOR,
B.A.R.C.**



Fig.1 Perspective view of Folded Tandem Ion Accelerator (FOITA)

maintained at about 240 psig. In FOTIA, since compressed geometry accelerating tubes are used which have a safe maximum operating gas pressure of 120 psig, achieving 6 MV at the terminal with N_2+CO_2 mixture would not be possible. Hence, an insulating medium of higher dielectric strength was mandatory. Design calculations indicated that SF_6 is the suitable insulating gas medium for this requirement. In addition to its excellent dielectric properties, SF_6 has good chemical stability, thermal properties and is nontoxic.

Properties of the SF_6 gas

Chemical and electrical properties

Under normal conditions SF_6 gas is chemically inert, stable and least reactive. It can be heated up to a temperature of 500°C in quartz containers without any decomposition. The electrical discharges, however, can cause decomposition of SF_6 gas. Under the influence of an electric arc a portion of the SF_6 gas is dissociated into its atomic constituents.



This reaction is reversible. After the discharge, the dissociation products may recombine to form the original molecule. Both solid and gaseous products such as SOF_2 , SO_2F_2 , SOF_4 , SF_4 can result from these secondary reactions. These products are not harmful in the absence of moisture. However, they hydrolyze in the presence of moisture and form highly corrosive acids like HF.

Up to 150°C, materials such as metals, ceramics, glass, rubber and cast resins, normally used in the accelerator systems, are stable in SF_6 environment. Pure SF_6 is chemically inert and does not cause corrosion. However, in the presence of moisture, the primary and secondary decomposition products of SF_6 form corrosive electrolytes which may attack and cause damage resulting in operational failure of various devices. As it is practically impossible to avoid formation of SF_6 decomposition products corrosion of devices can be largely eliminated by the careful exclusion of moisture and selection of suitable materials.

The excellent electrical insulating properties of SF_6 are attributable to its strong electron affinity (electro

negativity). SF_6 has a dielectric constant of 1.002 at 20°C.

Physical and thermal properties of SF_6

The SF_6 is a colorless, odourless non-toxic and non-inflammable gas with a molecular weight of 146.05 and is about 5 times heavier than air. Some of its physical properties, used in the system design, are as follows:

Gas density (20°C)	: 6.07 gm/litre
Thermal Conductivity	: 1.3×10^{-4} W/cm k
Heat transfer coefficient (1 bar, 2m /sec flow rate)	: 30 W/m ² k
Specific Heat (25°C)	: 97.26 J/mol k

Details of the SF_6 Gas Handling System

In view of the above mentioned electrical properties it was decided to use SF_6 gas as the insulating medium and a SF_6 gas handling system [3] was designed, fabricated, installed and commissioned at FOTIA. It consists of an oil free compressor, a centrifugal blower, a heat exchanger, dust filters, dryers and a vacuum pump etc. The schematic diagram of the SF_6 gas handling system is shown in Fig. 2.

It has been designed to achieve the following objectives:

1. Transfer of SF_6 gas from cylinders to the storage tank.
2. Transfer of SF_6 gas from the storage tank to the accelerator tank before starting the accelerator.
3. Transfer of SF_6 gas from the accelerator tank to the storage tank for repair/maintenance work.
4. Recirculation of SF_6 gas during the accelerator operation for removal of moisture, decomposition products and cooling of various devices in high voltage terminal and accelerator tank area.

Detailed heat transfer calculations were done to arrive at the recirculation flow in order to remove the total heat load of about 20 kW from the system and to ensure that high voltage terminal, which is having a maximum heat load of about 5 kW, is maintained within the permissible temperature limit of 50°C.

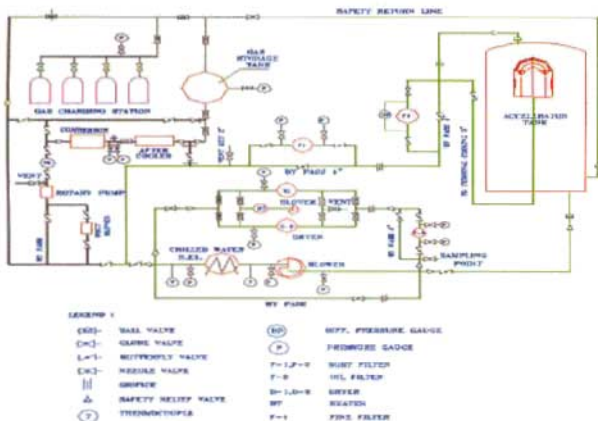


Fig.2 Schematic flow sheet of SF₆ gas handling system

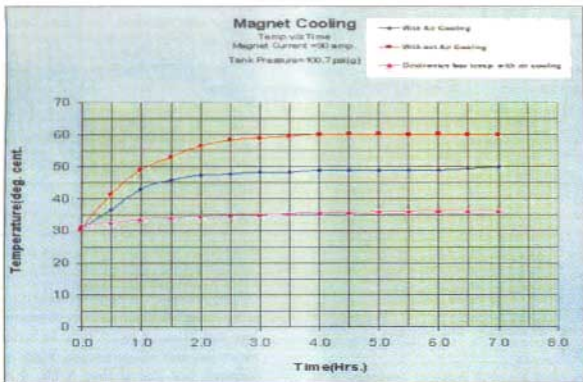


Fig. 3 Variation of temperature of the 180 folding magnet coils and its surrounding area with and without forced cooling.

(Fig 3). It was estimated that a total flow rate of 5000 lpm, at an operating pressure of 6.3 kg/cm^2 of SF_6 , is required to remove the above heat load. A blower with suitable capacity (7000 lpm) was designed, fabricated and installed in the system. Out of the total flow of 7000 lpm passing through the chilled water heat exchanger, 5000 lpm goes into the accelerator tank and 2000 lpm is used to cool the motor of the blower. It was also estimated that a total head of 5538 mm of water column, for SF_6 gas at pressure of 6.3 kg/cm^2 , is required to maintain the above mentioned flow rate in the main circuit.



Fig. 4 180° - folding magnet inside the high voltage terminal

From the main recirculation circuit 1000 lpm of gas is diverted to the terminal section inside the accelerator tank for adequate cooling of the components [4] like 180°-folding magnet, 100 amp power supply, controllers for strippers, Faraday cup and ion pump etc. installed inside the dome (Fig. 4) and 4000 lpm is directly blown on to the high voltage column section for the removal of break down products generated due to high voltage corona discharges. A globe valve is provided in the gas line to regulate and control the gas flow into the terminal. The system has been tested with

$\text{N}_2 + \text{CO}_2$ gas mixture as insulating gas at 100 psig for terminal voltages of up to 3.4 MV and found satisfactory.

An air compressor having capacity of 110 CFM, rated for a maximum discharge pressure of 125 psig and a suction pressure of 1 atm, is used. It is a non lubricating type, vertical double acting, single stage compressor (de-rated for SF_6 application). The compressor is used for transferring the gas from cylinders to the storage tank and also from the storage tank to the accelerator tank and vice versa.

The recirculating blower is a centrifugal blower designed for a flow rate of 7000 lpm at 6.3 kg/cm^2 with an equivalent discharge head of 150 mm water column at a pressure of 1 atm of air.

Heat exchanger is a shell & tube type with single pass on shell side and ten passes on tube side. It has gas on shell side and chilled water on the tube side. The heat exchanger is designed to remove a heat load of 20 kW and has a transfer area of 13.4 m^2 . The gas (at 31°C) when passed through the heat exchanger gets cooled to 25°C .

A vertical vessel twin column activated alumina filled dryer is used for removing the moisture and breakdown products. Activation of alumina balls is done by passing pre-heated air at 150°C through the alumina bed.

Coarse and fine filters are provided to make sure that dust free SF_6 gas is circulated through the accelerator column. Coarse filters are pleated bag type suitable for filtering dust particles of sizes above 1.0 micron. A fine filter assembly has been incorporated in the gas line at the entry of the accelerator tank. Fine filter is a cartridge type and has four borosilicate glass fiber cartridges mounted inside a SS housing and is suitable for filtering dust particles of size above 0.1 micron.

Safety Features of the SF_6 Gas Handling System

The gas storage and accelerator tanks of the old 5.5 MV Van-de-Graaff accelerator are used in the FOTIA. The operating pressure in the Van-de-Graaff accelerator was 225 psig. In FOTIA, SF_6 gas operating pressure will be 80 psig. The ultrasonic and "In-situ"

Discussion

The gas handling system of FOTIA is in continuous use and its performance is satisfactory. During the beam trials it was found necessary to introduce an additional filter at the entrance of the accelerator tank, which assured a dust free recirculation of the gas through high voltage column section thereby reducing the number of sparks substantially. However, incorporation of the additional filter has resulted in reduction of re-circulating flow.

The FOTIA has now been commissioned by accelerating beams of ^{12}C up to terminal voltages of 3.2 MV. In a typical experiment beams were characterized by measuring the Rutherford Back Scattering from several targets and the energies were found to be in

agreement with the terminal voltages and field values in the analyzing magnet

References

1. P. Singh, Indian J. Pure & Appl. Phys. **35**, 172 (1997).
2. P. Singh et al, Proc. DAE Symp. on Nucl. Phys. **B42**, 366 (1999).
3. S.K. Gupta et al., Proc. 4th National Symp. on Phys. and Tech. Part. Acc. & their Applications (PATPAA-96), 1996, Calcutta.
4. V. Bhasin, K.K. Vaze, H.S. Kushwaha & Anil Kakodkar-private communication.
5. B.K. Shah et al., AFD/ Report No. 25 (1997).

This paper received the 2nd Prize in the Poster Presentation Category during the DAE Nuclear Physics Symposium held during December 26-31, 1999 at Chandigarh.

About the authors ...



Mr S.K. Gupta, B.E (Electrical Engg.) from 28th batch of BARC Training School, is an accelerator technologist. He has been working in the 14 UD BARC-TIFR Pelletron Accelerator and has expertise in SF₆ gas handling and ultra high vacuum systems. He has been working for FOTIA Project since its inception. He has developed many beam line components used for an accelerator. He has been working as Operation-in-charge, Pelletron Accelerator Facility, TIFR, and presently, he is Officer-in-charge of the FOTIA facility at the Nuclear Physics Division, BARC.



Dr. Pitamber Singh joined the Nuclear Physics Division, BARC, in 1976 after graduating from 19th batch of the BARC Training School. He received his Ph.D in physics from Mumbai University in 1983. Dr Singh spent one year at the Max-Planck Institute fuer Kernphysik, Heidelberg, Germany, and has visited several European accelerator labs. In addition to building a 2 MV Tandem Accelerator at BARC, he has made an outstanding contribution in setting up the 6 MV Folded Tandem Ion accelerator (FOTIA) facility at BARC.

Recently, he has been selected as a member of the "National Academy of Sciences, India" for his outstanding contributions towards indigenous development of the accelerator technology in the country and nuclear reaction studies using heavy ion beams from particle accelerators. He has participated in an experiment at LNL, Legnaro, Italy, performed to study the role of fission dynamics in formation of Super Heavy Elements (SHE). He is co-author of more than 160 scientific publications. Presently, he is Head of FOTIA Section of the Nuclear Physics Division.



Mr Arun Agarwal joined the Nuclear Physics Division in 1994 after graduating from 37th batch of the BARC Training School. He has been working for FOTIA Project since its inception. He has made outstanding contributions towards design of gas handling system and structural design and analysis of high voltage column of FOTIA.



Mr S. Santra joined the Nuclear Physics Division in 1994 after graduating from 37th batch of the BARC Training School. He has been working for FOTIA Project since its inception. He has made outstanding contributions towards Beam Optics calculations, Design of several electrostatic and magnetic dipole and quadrupole magnets for FOTIA. He has also been involved in Nuclear Physics experiments using Pelletron Accelerator.

Mr Rajesh Kumar, B.Tech. (Electrical Engg.) from 38th batch of BARC Training School has been associated with FOTIA since joining BARC. He has been working for design of high voltage column and high voltage charging System of FOTIA Project.

Mr S.P. Sarode joined FOTIA project in April 1994 after passing Diploma in Electrical Engineering from Govt. Polytechnic, Jalgaon, in 1992.



Mr P.J. Raut joined TPPED for Magneto-Hydro-Dynamic (MHD) generator project in October 1981. After completion of this project he was transferred to GAT, Indore, for SRS/INDUS-1 project and then later on, he joined FOTIA project at NP. He is working for gas handling system and ultra high vacuum system of FOTIA.



Mr S.V. Gogate joined Reactor Group in BARC in February 1967. He was responsible for the fabrication and installation of piping for most of the systems of Dhruba reactor. Presently, he is responsible for fabrication and installation of reactor components for Critical Facility for AHW 6 500 MWe PHWR reactors and modified Apsara Reactor. He has coordinated for execution of FOTIA gas handling system.



Mr R.R. Patankar joined Reactor Group in BARC in May 1976. He was responsible for the fabrication and assembly of guide tubes & installation, commissioning of overhead cranes & compressor for Dhruba Reactor. He has performed all quality related tests for FOTIA gas handling System. Presently, he is In-charge of Quality Assurance Section for Dhruba Group.



Mr Mohan G. Andhansare, B.E. (Mechanical) joined fuel handling group of Dhruba reactor after graduation from 16th batch of BARC Training School. He has designed and erected shielding flask of "On Power" fuelling machine and later erected and commissioned on power fuelling machine. He has designed and fabricated a buggy for handling of isotopes from "On Power" tray rod and other irradiated samples and a pool site inspection facility for inspection of irradiated fuel assemblies of Dhruba. He has designed and erected SF6 gas handling system of FOTIA project. Since 1997, he is working with Reactor

Engineering Division on design of components and review of design related activities of Advanced Heavy Reactor.



Mr A.C. Tikku, B.E. (Electrical Engg.) joined Reactor Operations Group, BARC, in August 1968 after graduating from 11th batch of the Training School. He was responsible for design, installation and commissioning of fresh and irradiated fuel storage for Dhruba reactor. In 1990, he lead a team which successfully designed, developed and commissioned "On-Power operation of Dhruba tray-rods" for production of radioisotopes. Since 1999, he is holding the charge of Head, Research Reactor Services Division (RRSD), BARC.

Influence of Neutronic Parameters on the Stability of the Advanced Heavy Water Reactor

A.K. Nayak, P.K. Vijayan and D. Saha
Reactor Engineering Division
Bhabha Atomic Research Centre

Abstract

The influence of neutronic parameters on the stability behaviour of the Advanced Heavy Water Reactor has been investigated analytically. The analytical model considers homogeneous two-phase flow, a point kinetics model for the neutron dynamics and a lumped heat transfer model for the fuel dynamics. Further, to study the out-of-phase instability in the boiling channels of the reactor, a coupled multi point kinetics model was also applied. The results indicate that both Type I and Type II density-wave instabilities can occur in the reactor in both in-phase and out-of-phase mode of oscillations in the boiling channels of the reactor. The stability of the reactor is found to increase with increase in negative void reactivity coefficient or decrease in fuel time constant unlike that observed previously in vessel type BWRs. Decay ratio map was predicted considering the effects of channel power, channel inlet subcooling, feed water temperature and channel exit quality, which are useful for the design of the reactor.

Introduction

THIS STUDY FOCUSES ON THE STABILITY BEHAVIOUR OF THE ADVANCED HEAVY WATER REACTOR (AHWR) being designed IN India. This is a 750 MWth pressure tube type heavy water moderated and light water cooled Boiling Water Reactor. The reactor is designed for natural circulation core cooling during start-up, power raising, normal operating condition and accidental conditions. This necessitates large tall risers (or outlet feeders) to achieve required natural circulation flow rate, which in turn, may cause larger two-phase pressure drop in the riser portions than in the single-phase portion of the reactor coolant system composed of the downcomers, header, inlet feeders, and the single-phase portion of the core. Dominance of two-phase pressure drop may induce thermohydraulic instabilities in the reactor as observed in our previous studies (Nayak et al., 1998). Such thermohydraulic oscillations may induce reactivity oscillations through the void-reactivity coupling. A recent review by March-Leuba and Rey (1993) suggests that there are several incidents of such coupled neutronic-thermohydraulic instabilities in operating BWRs in the past. Special attention has been drawn to this topic after oscillations were observed in the La Salle 2 (US NRC, 1988) and Coarso plants (Gialdi et al., 1985). Since then many investigators have attempted to model and understand the instabilities in the above reactors by both time domain (Takigawa, et al., 1987, Muto, et al., 1990, Araya, et al., 1991) and frequency domain analysis codes (March-Leuba, 1990, Rao et al., 1995). March-Leuba and Blakeman (1991) were the first to show that the dominance of in-phase or out-of-phase oscillations in a BWR depends on whether the gain of the neutronic feedback or the inlet flow feedback is more predominant. Hashimoto (1993) showed that the

occurrence of out-of-phase mode oscillations in a BWR depends on the subcriticality and void reactivity feed back. Uehiro et al. (1996) showed that the interactions among the channels due to neutron diffusion influence the out-of-phase oscillations.

The above studies clarified that the BWR instability is a complex phenomenon which depends on the state of the thermal hydraulic behaviour of the system, neutronic feed back effects due to the void, fuel temperature and fuel time constant. Looking at the geometry of the AHWR (Fig. 1), it can be seen that the reactor contains many parallel channels which are connected between the steam drum and the header with equal number of outlet feeders and inlet feeders respectively. With such long feeder pipes, the period of density-wave oscillation is expected to be very much longer than that of a conventional vessel type BWR. It is of interest to investigate the effects of neutron and fuel dynamics on such low frequency thermohydraulic oscillations occurring in the parallel channels of the AHWR. Further to this, the effect of delayed neutrons on the coupled neutronic-thermohydraulic instabilities of such a reactor will be investigated here. In addition, the decay ratio maps for the reactor will be predicted considering various operating conditions, which will be useful in the reactor design.

For this purpose, the theoretical model developed previously (Nayak, et. al. 2000) was used. This solves the linearised conservation equations of mass, momentum and energy and the equation of state for the fluid, assuming homogeneous two-phase flow along with a point kinetics model for the neutron dynamics and a lumped heat transfer model for the fuel thermal dynamics. In addition, the model considers the thermohydraulic interactions of parallel multiple channels with the inlet and outlet feeders together with the external loop (i.e. downcomers). The characteristic equation has been derived and the stability behaviour for in-phase and out-of-phase mode of oscillations were investigated from the roots of the characteristic equation.

Primary Heat Transport (PHT) System of the AHWR

The schematic of the PHT System of the AHWR is shown in Fig. 1. As shown in the figure, the PHT system contains many parallel channels (408 numbers) which are connected between the header and the steam drums (four numbers) by an equal number of inlet and outlet feeders respectively. Each steam drum is connected to the header by four downcomers. The channels have inside diameter of 120 mm and contain fuel bundles consisting of 52 number of fuel rods and 8 number of water rods. The outer diameter of fuel rod is 11.2 mm and that of the water rod is 6 mm. There are six spacers located in the fuel bundles and they are separated by equal distances along the length of fuel. The active fuel length is about 3.5 m and the height of the loop above the core is about 30 m. The inside diameter of inlet feeders is about 97 mm and that of the outlet feeders is about 122 mm. The steam drums have a length of 10 m and inside diameter of 3 m and are kept horizontal. During normal operating condition the steam drum pressure is maintained at 70 bar. This is a typical design configuration of the AHWR considered in the present analysis. Boiling takes place in the core and the two-phase mixture leaving the core is separated into steam and water in the steam drum. The separated steam flows into the turbine and an equal mass rate of feed water enters the steam drum. The coolant circulation in the PHT system takes place by natural circulation.

Analytical Model

The analytical model consists of (i) a thermohydraulic stability model, (ii) a point kinetics or a coupled multipoint kinetics model and (iii) a lumped fuel heat transfer model. The thermohydraulic stability model assumes the flow to be incompressible and Boussinesq approximation to be valid for variation of density with temperature in the single-phase region of the loop. Also it assumes that in the two-phase region the flow is homogeneous, $\partial p / \partial t$ in energy conservation equation is neglected, two-phases are in thermo-dynamic equilibrium, axial uniform heat flux profile

(Nayak et. al., 1998), heat losses in the loop pipings are neglected, carry-over and carry-under in the steam drum are neglected and mixing of feed water in the steam drum is complete (i.e. no thermal stratification).

With these assumptions the conservation equations of mass, momentum and energy for one-dimensional two-phase flow are given by

$$A \frac{\partial \rho}{\partial t} + \frac{\partial w}{\partial z} = 0, \quad (1)$$

$$\frac{1}{A} \frac{\partial w}{\partial t} + \frac{1}{A'} \frac{\partial}{\partial z} (w'v) + \frac{g}{v} + \frac{f}{2DA'} (w'v) + \frac{\partial p}{\partial z} = 0, \quad (2)$$

$$\rho A \frac{\partial h}{\partial t} + w \frac{\partial h}{\partial z} = \begin{cases} q_s A & \text{heated region,} \\ 0 & \text{unheated region.} \end{cases} \quad (3)$$

The equation of state in the two-phase region is given by

$$\rho = f(p, h). \quad (4)$$

The frictional pressure drop in the two-phase region was estimated using the Baroczy (1966) correlation. The local pressure drop due to bends, restrictions and spacers was estimated as

$$\Delta p_s = Kw^2 / 2\rho A^2. \quad (5)$$

The governing equations are linearised by superimposing small perturbations of w' , h' , p' , v' and q_s' over steady state values where

$$w' = \bar{w}(z)\epsilon e^{st}; \quad h' = \bar{h}(z)\epsilon e^{st}; \quad p' = \bar{p}(z)\epsilon e^{st}; \quad v' = \bar{v}(z)\epsilon e^{st}; \quad q_s' = \bar{q}_s \epsilon e^{st}. \quad (6)$$

In Eq. (6) ϵ is a small quantity and \bar{w} , \bar{h} , \bar{p} , \bar{v} and \bar{q}_s are the averages of perturbed flow rate, enthalpy, pressure, specific volume and heat added/unit volume to the coolant respectively and s is the stability parameter. Substituting them in the conservation equations, the solution of the perturbed equations for various segments of the loop can be obtained by integration as follows.

In the single-phase heated region,

$$w' = w_{ss}' = \text{constant}, \quad (7)$$

$$h' = \frac{1}{\rho_{ss,sp} s} \left[-\frac{q_{h,ss} w'}{w_{ss}} + q_s' \right] \left[1 - e^{-\tau_{sp} s} \right], \quad (8)$$

$$-\Delta p_{sp}' = \left[\frac{s}{A} + \frac{f w_{ss}}{\rho_{ss,sp} D A^2} \right] w' L_{sp} - \frac{g \sigma}{C_p s} \left[-\frac{q_{h,ss} w'}{w_{ss}} + q_s' \right] \left[L_{sp} + \frac{w_{ss}}{\rho_{ss,sp} A s} (e^{-\tau_{sp} s} - 1) \right], \quad (9)$$

$$\text{where } \tau_{sp} = (\rho_{ss,sp} A L_{sp} / w_{ss}). \quad (10)$$

In the adiabatic single-phase region, the perturbed equations for flow rate, enthalpy and pressure drop can be obtained from Eqs. (7) to (9) respectively by substituting $q_{h,ss}$ and q_s' to be zero.

In the two-phase heated region,

$$w' = w_{sp}' + \frac{As}{v_{ss,sp}^2} \frac{v_{sp}}{h_{sp}} \left[\frac{P}{r_1} (e^{\gamma_1 t_c} - e^{\gamma_1 t_w}) + \frac{Q}{r_2} (e^{\gamma_2 t_c} - e^{\gamma_2 t_w}) \right], \quad (11)$$

$$h' = [P e^{\gamma_1 t_c} + Q e^{\gamma_2 t_c}], \quad (12)$$

$$\begin{aligned}
 -\Delta p' &= \left[\frac{s}{A} + \frac{fw_{ss}v_{ss,sp}}{DA^2} \right] \times \\
 & \left[w'_{sp} L_{sp} + \frac{Asv_{fs}}{v_{ss,sp}^2 h_{fs}} \left\{ \frac{P}{r_1} \left[\frac{1}{r_1} (e^{\gamma_{1c}} - e^{\gamma_{1sp}}) - e^{\gamma_{1sp}} L_{sp} \right] + \left\{ \frac{Q}{r_2} \left[\frac{1}{r_2} (e^{\gamma_{2c}} - e^{\gamma_{2sp}}) - e^{\gamma_{2sp}} L_{sp} \right] \right\} \right\} \right] + \\
 (v_{fs} / h_{fs}) & \left[\frac{fw_{ss}^2}{2DA^2} - \frac{g}{v_{ss,sp}^2} + \frac{2w_{ss}s}{Av_{ss}} \right] \left[\frac{P}{r_1} (e^{\gamma_{1c}} - e^{\gamma_{1sp}}) + \frac{Q}{r_2} (e^{\gamma_{2c}} - e^{\gamma_{2sp}}) \right] + \frac{w_{ss}^2 v_{fs}}{A^2 h_{fs}} \times \\
 & \left[P(e^{\gamma_{1c}} - e^{\gamma_{1sp}}) + Q(e^{\gamma_{2c}} - e^{\gamma_{2sp}}) \right].
 \end{aligned} \tag{13}$$

$$\text{where } P = [-h'_{sp}(r_2 + As\rho_f / w_{ss}) - q_{h,ss}Aw'_{sp} / w_{ss}^2 + q'_h A / w_{ss}] / (r_1 - r_2)e^{\gamma_{1sp}}, \tag{14}$$

$$Q = (h'_{sp} - Pe^{\gamma_{1sp}}) / e^{\gamma_{1sp}}, \tag{15}$$

$$r_{1,2} = [-C_1 \pm (C_1^2 - 4C_2)^{0.5}] / 2, \tag{16}$$

$$C_1 = As / v_{ss,sp} w_{ss}, \tag{17}$$

$$C_2 = (q_{h,ss} / v_{ss,sp}^2) \chi A^2 s / w_{ss}^2 (v_{fs} / h_{fs}), \tag{18}$$

and h'_{sp} is the perturbed enthalpy at the inlet of boiling region of the channel which can be estimated from Eq. (8).

In the adiabatic two-phase region

$$w' = w'_m + (w_{ss} / v_{ss}) \chi (v_{fs} / h_{fs}) h'_m [1 - e^{-\tau_L}], \tag{19}$$

$$h' = h'_m e^{-\tau_L}, \tag{20}$$

$$-\Delta p' = \left[\frac{s}{A} + \frac{fw_{ss}v_{ss}}{DA^2} \right] \left[w'_m L + \frac{w_{ss}v_{fs}}{v_{ss}h_{fs}} h'_m \left\{ L + \frac{w_{ss}v_{ss}}{As} \left\{ e^{-\tau_L} - 1 \right\} \right\} \right] - \frac{v_{fs}}{h_{fs}}$$

$$\left[\frac{fw_{ss}^2}{2DA^2} - \frac{g}{v_{ss}^2} + \frac{2w_{ss}s}{Av_{ss}} \right] \left\{ e^{-\tau_L} - 1 \right\} h'_m \frac{w_{ss}v_{ss}}{As} + \frac{w_{ss}^2 v_{fs}}{A^2 h_{fs}} \left\{ e^{-\tau_L} - 1 \right\} h'_m. \tag{21}$$

$$\text{where } \tau_L = (\rho_m AL / w_{ss}). \tag{22}$$

Similarly, the perturbed pressure drop due to bends, orifices, spacers and other restrictions in various regions are given by,

$$\text{in the single-phase region, } \Delta p'_{i,sp} = (K_{sp} / \rho A^2) w_{ss} w'_m, \tag{23}$$

$$\text{in the two-phase region, } \Delta p'_{i,sp} = (K_{sp} / 2A^2) \left[w_{ss}^2 h'_m (v_{fs} / h_{fs}) + 2w_{ss}v_{ss}w'_m \right]. \tag{24}$$

The perturbed heat added/unit volume of coolant (q'_h) that appears in the above calculation depends on the neutron and fuel dynamics which are estimated as discussed below.

Neutron kinetics

The point kinetics approximation is adopted for the neutron field dynamics as given by

$$\frac{dn(t)}{dt} = \frac{k(t)(1-\beta) - 1}{l} n(t) + \sum_{m=1}^6 \lambda_m C_m(t), \quad (25)$$

$$\frac{dC_m(t)}{dt} = \frac{k(t)\beta_m n(t)}{l} - \lambda_m C_m(t), \quad (26)$$

Eqs. (25) and (26) are linearised by perturbing over the steady state as discussed in section 3 and the perturbed equations can be easily solved after eliminating the steady state conditions to obtain

$$\frac{n'}{n_{ss}} = \frac{k'}{ls + \sum_{m=1}^6 \frac{s\beta_m}{s + \lambda_m}}, \quad (27)$$

where n' is the perturbed neutron density and k' is the perturbed reactivity which is related to the void reactivity coefficient and Doppler coefficient as

$$k' = C_v \gamma'_{sv} + C_D T'_{f,av}. \quad (28)$$

In Eq. (28) γ'_{sv} and $T'_{f,av}$ are the perturbed void fraction and fuel temperature respectively averaged over the heated channel length. They can be estimated from the coolant density and the fuel heat transfer equations as discussed below.

Fuel heat transfer model

Assuming only radial heat transfer, the fuel heat transfer equation can be written as

$$m_f C_f \frac{dT_{f,av}}{dt} = Q(t) - H_f a_f (T_{f,av}(t) - T_{sat}), \quad (29)$$

where m_f is the mass of fuel rods; C_f is the specific heat capacity of fuel; H_f is an effective heat transfer coefficient; $Q(t)$ is the heat generation rate in the fuel rods; $T_{f,av}(t)$ is the length average fuel temperature; a_f is the heat transfer area of fuel rods and T_{sat} is the coolant saturation temperature.

Perturbing Eq. (29) over the steady state for $T_{f,av}(t)$ and $Q(t)$ and canceling the steady state terms, we get

$$T'_{f,av} (m_f C_f s + H_f a_f) = Q', \quad (30)$$

where Q' is the perturbed heat generation rate in the fuel rod.

Applying the heat balance equation for the heat transfer from fuel to coolant

$$H_f a_f (T_{f,av} - T_{sat}) = q_h A_c L_c. \quad (31)$$

Perturbing Eq. (31) over the steady state and canceling the steady state terms we get

$$T'_{f,av} = q_h A_c L_c / H_f a_f. \quad (32)$$

Substituting Eq. (32) into Eq. (30) and rearranging we get

$$q_h = q_{h,ss} \frac{Q'}{Q_{ss}} \left[\frac{1}{1 + m_f C_f s / H_f a_f} \right] \quad (33)$$

Since the heat generation rate in fuel is proportional to the neutron density, Eqs. (27) and (28) can be substituted into Eq. (33) to yield

$$q_h = G_f \gamma_{ss}' \quad (34)$$

$$\text{where } G_f = \frac{C_m / (1 + \tau_f s)(\lambda s + \sum_{m=1}^6 \frac{s\beta_m}{s + \lambda_m})}{\frac{1}{q_{h,ss}} \frac{C_D A_c L_c}{H_f a_f (1 + \tau_f s)(\lambda s + \sum_{m=1}^6 \frac{s\beta_m}{s + \lambda_m})}} \quad (35)$$

and $\tau_f = \frac{m_f C_f}{H_f a_f}$ is the fuel time constant.

The density of two-phase mixture is given by

$$\rho = \gamma \rho_g + (1 - \gamma) \rho_f \quad (36)$$

Perturbing Eq. (36) over the steady state and canceling for steady state condition, we get

$$\gamma' = -\rho' / \rho_{ss} = (\rho_g^2 / \rho_{ss}) \frac{v_{gg} h'}{h_{ss}} \quad (37)$$

The channel average perturbed void fraction can be obtained by integration as

$$\gamma_{ss}' = \frac{1}{L_c} \int_{z=0}^{L_c} \frac{\rho_g^2 v_{gg}}{\rho_{ss} h_{ss}} h' dz, \quad (38)$$

which can be approximated after some algebraic simplification as

$$\gamma_{ss}' = \psi_1 w_{ss}' + \psi_2 q_h, \quad (39)$$

$$\text{where } \psi_1 = \frac{1}{L_c} \frac{v_{gg}}{h_{ss}} \frac{1}{v_{ss}^2} \frac{1}{h_{ss}} \left[\frac{X_1}{r_1} (e^{r_1 L_c} - e^{r_1' L_c}) + \frac{X_2}{r_2} (e^{r_2 L_c} - e^{r_2' L_c}) \right], \quad (40)$$

$$\psi_2 = \frac{1}{L_c} \frac{v_{gg}}{h_{ss}} \frac{1}{v_{ss}^2} \frac{1}{h_{ss}} \left[\frac{Y_1}{r_1} (e^{r_1 L_c} - e^{r_1' L_c}) + \frac{Y_2}{r_2} (e^{r_2 L_c} - e^{r_2' L_c}) \right], \quad (41)$$

$$X_1 = \frac{-q_{h,ss} A}{w_{ss}^2} \left[1 + \left[(e^{-r_1' w} - 1) / \rho_{ss} s \right] (w_{ss} / A)(r_2 + \frac{A s \rho_m}{w_{ss}}) \right] / [(r_1 - r_2) e^{r_1' w}], \quad (42)$$

$$X_2 = \left[(q_{h,ss} / w_{ss}) (e^{-r_2' w} - 1) / \rho_{ss} s \right] - X_1 e^{r_1' w} / e^{r_2' w}, \quad (43)$$

$$Y_1 = \left[\left(\frac{e^{-r_1' w} - 1}{\rho_{ss} s} \right) \left(r_2 + \frac{A s \rho_m}{w_{ss}} \right) + \frac{A}{w_{ss}} \right] / (r_1 - r_2) e^{r_1' w}, \quad (44)$$

$$Y_2 = \left[\frac{e^{-\lambda_2 \tau} - 1}{\rho_m \lambda_2} + Y_1 e^{\lambda_2 \tau} \right] / e^{\lambda_2 \tau} \quad (45)$$

Substituting Eq. (39) into Eq. (34) an expression for the perturbed heat added per unit volume of coolant (\dot{q}'_a) to any channel i for a perturbation of inlet flow rate (w'_m) in the i_m channel can be easily obtained as given by

$$(\dot{q}'_a)_i = \left(\frac{G_j \Psi_1}{1 - G_j \Psi_2} \right)_i (w'_m)_i \quad (46)$$

Coupled multipoint kinetics model

During an out-of-phase instability, neutron diffusion from channel to channel may be an important factor due to change in void fraction among the channels which the point kinetics model does not take into account. This may result in a different \dot{q}'_a for any channel than that calculated using Eq. (46). For this purpose, a coupled multipoint kinetics model was applied in place of simple point kinetics model for the neutron kinetics. The model considers the reactor to contain 'N' no. of subcores which are subcritical, isolated by reflectors and influenced each other only through leakage neutrons number of which is proportional to the average neutron flux over each subcore. Each subcore may contain one channel or group of channels having the same power and resistances.

Taking the model as 'N' bare homogeneous reactors, the coupled multipoint kinetics equation for the i_m subcore is given by

$$\frac{dn_i(t)}{dt} = \frac{k_i(t)(1 - \beta_i) - 1}{l_i} n_i(t) + \sum_{m=1}^6 \lambda_{m,j} C_{m,j}(t) + \sum_{\substack{j=1 \\ j \neq i}}^N \alpha_{ij} \frac{n_j(t)}{l_i} \quad (47)$$

where α_{ij} is the coupling coefficient that determines the reactivity contributed by the interaction of j_m subcore with the i_m subcore. In the analysis, α_{ij} is assumed to be constant which can be estimated from the steady state condition of Eq. (47) as

$$k_{i,ss} = k_{i,ss} - 1 = - \sum_{\substack{j=1 \\ j \neq i}}^N \alpha_{ij} \frac{n_{j,ss}}{n_{i,ss}} \quad (48)$$

For small excess reactivity

$$\rho_{i,ss} = k_{i,ss} - 1 = - \sum_{\substack{j=1 \\ j \neq i}}^N \alpha_{ij} \frac{n_{j,ss}}{n_{i,ss}} \quad (49)$$

Perturbing Eqs. (47) and (26) for the i_m subcore and solving them together as before for the point kinetics equation, the perturbed neutron density in the i_m subcore can be obtained as

$$\frac{n'_i}{n_{i,ss}} = \left[k_i \eta + \sum_{\substack{j=1 \\ j \neq i}}^N \alpha_{ij} \frac{n'_j}{n_{i,ss}} \right] / \Theta_i \quad (50)$$

$$\text{where } \eta = 1 - \sum_{m=1}^6 \frac{s\beta_{m,i}}{s + \lambda_{m,i}}, \quad (51)$$

$$\Theta_i = I_i s + \left(1 - \sum_{\substack{j=1 \\ j \neq i}}^N \alpha_{ij} \frac{n_{j,ss}}{n_{i,ss}}\right) \sum_{m=1}^6 \frac{s\beta_{m,i}}{s + \lambda_{m,i}} + \sum_{\substack{j=1 \\ j \neq i}}^N \alpha_{ij} \frac{n_{j,ss}}{n_{i,ss}}. \quad (52)$$

Similar expressions can be derived to obtain the perturbed neutron density in other subcores which can be substituted into Eq. (50) and simplified to obtain the perturbed heat generation rate in the i_{th} subcore as

$$\left(\frac{Q'}{Q_{ss}}\right)_i = \eta \sum_{j=1}^N X_{ij} k_i' \frac{n_{j,ss}}{n_{i,ss}}, \quad (53)$$

$$\text{where } [X_{ij}]_{N \times N} = [T_{ij}]_{N \times N}^{-1}, \quad (54)$$

$$\text{and } T_{ij} = \begin{cases} \Theta_i & \text{for } i = j \\ -\alpha_{ij} & \text{for } i \neq j \end{cases}. \quad (55)$$

The perturbed heat added per unit volume of coolant for any subcore can be obtained by substituting Eq. (53) into Eq. (33).

Characteristic Equation

For constant inlet subcooling, the equations for perturbed flow rate, enthalpy and pressure drop for single-phase and two-phase regions of the AHWR loop can be expressed as functions of perturbed flow rate in the steam drum (w'_{SD}) alone. Since all parallel paths are connected between the header and the steam drum so

$$(w'_{SD}) = \sum_{i=1}^n (w'_i). \quad (56)$$

Also, the perturbed pressure drop for all parallel paths between the header and the steam drum is the same, i.e.

$$P_H - P_{SD} = \Delta P_{H-SD} = G_1(w'_1) = G_2(w'_2) = \dots = G_i(w'_i) = \dots = G_n(w'_n), \quad (57)$$

where $G(w'_i)$ is the sum of the perturbed pressure drop components in the single-phase and two-phase region of the channel i associated with its inlet and outlet feeders.

Similarly, the perturbed pressure drop between the steam drum and header can be expressed as

$$P_{SD} - P_H = \Delta P_{SD-H} = G_f(w'_{SD}). \quad (58)$$

For the characteristic equation the condition is that the perturbed pressure drop around the closed loop is zero, which can be obtained by adding Eqs. (57) and (58) and rearranging as given by

$$|F_{ij}| = \prod_{i=1}^n \frac{G_i}{G_j} + \sum_{i=1}^n \prod_{j \neq i}^n \frac{G_j}{G_i} = 0. \quad (59)$$

The stability of the system is investigated from the roots of the characteristic equation. If any of the roots is having a positive real part, the system is considered unstable and for zero real part the system is considered to be neutrally stable. The system is considered stable if all the roots have negative real part.

In the AHWR as shown in Fig. 1, both in-phase and out-of-phase oscillations may occur. The out-of-phase mode oscillation has characteristics similar to parallel channel thermohydraulic oscillations with coupled spatial neutron dynamics. But during an in-phase mode of oscillation, oscillations occur in the boiling channels and in the downcomers without any phase difference between them.

From Eq. (57) we can express the ratio of perturbed flow rate oscillation between channels i and j as

$$(w_m)_i / (w_m)_j = (G_j / G_i) = R e^{i\theta} \quad (60)$$

where R is the ratio of amplitude and θ is the phase difference. The nature of oscillation, i.e. in-phase or out-of-phase can be determined by substituting the roots of the characteristic Eq. (59) into Eq. (60).

Results and Discussion

Pure thermohydraulic instability

Before studying the characteristics of nuclear-coupled thermohydraulic oscillations, it is required to study the pure thermohydraulic oscillations of both the in-phase and out-of-phase modes in the AHWR. This investigation will suggest the nature of dependency of the neutronics on the thermal hydraulic behaviour of the system. For this purpose, the above analytical model without neutronic coupling (i.e. $q_a = 0$) was applied. Figure 2 shows a typical flow stability map considering the hottest channels of the AHWR. The analysis considers two parallel boiling channels along with the associated inlet and outlet feeders of the reactor. The stability boundary has been plotted as in the reference (Nayak et al., 1998) on N_{ps} vs. N_{ss} plane. The results indicate that the out-of-phase thermohydraulic oscillations is more likely to occur among the boiling channels than the oscillations of the in-phase mode because of the dampening effect of the extra single-phase friction in the downcomer which stabilises the in-phase mode oscillation. Also it can be observed that the difference in Type-II instability boundary between two modes of oscillation is much larger than that for Type-I instability boundary which is in agreement with the results of Van Bragt and Van der Hagen (1998). However, the difference in the Type-I instability boundary between two modes of oscillation is also significant unlike that observed in the Dodewaard BWR. The frequency of oscillation has been calculated at the threshold point from the imaginary part of the root of the characteristic equation and also shown for both modes of oscillation in the same figure. The frequency of oscillation for Type-II instability is larger compared to that for Type-I instability. This is because the Type-I instability occurs at low power when the flow velocity is smaller under natural circulation conditions than that for the Type-II instability which occurs at much higher power. Hence, the fluid takes longer time to pass through the two-phase region compared to the Type-II oscillation case. In general, it is also found that the frequency of oscillation is very much less for the AHWR channels compared to that predicted for the Dodewaard natural circulation BWR (Van Bragt and Van der Hagen, 1998). This is because the period of oscillation in the AHWR channels is very large due to large two-phase region of the outlet feeder pipes whose length may be several times of the chimney height of the Dodewaard BWR.

Coupled neutronic thermohydraulic instability

Influence of void reactivity coefficient on the stability: Figure 3 shows the effect of C_{α} on the threshold of stability for the in-phase mode of oscillations between two subcores of the reactor considering the point kinetics model for the neutron dynamics. The results indicate that with an increase in negative C_{α} the threshold power increases for Type-II instabilities and decreases that for Type-I instabilities. The stability of the reactor is found to increase with increase in negative C_{α} . Results from previous investigations for vessel type BWRs have shown that the stability of the reactor decreases with increase in negative C_{α} due to the increase in gain of the void reactivity feed back loop (Uehiro, et. al. (1996), Van Bragt and Van der Hagen (1998)). However, the thermohydraulic oscillation frequency for the Type-I and Type-II instabilities in those reactors are much larger than the present system. Addition of neutronic feed back at such low frequency of thermohydraulic oscillations (<0.07 Hz) as observed in the AHWR, stabilises the reactor due to less phase lag between the fuel heat generation rate and channel thermohydraulic oscillations.

Influence of fuel time constant : The effect of fuel time constant on the stability of in-phase mode oscillation for the above case is shown in Fig. 4. The fuel time constant will vary depending on the fuel properties, operational conditions and fuel burn-up. Van der Hagen (1988) has shown that with the use of lumped parameter model it could be as low as 2 s. The fuel time constant in the present analysis has been varied over a wide range from its normal operating value to study its influence on the stability. It can be observed from the above figure that with increase in τ_f the threshold power for Type-II instability decreases and that for Type I instability increases. The stability of the reactor decreases with increase in fuel time constant. Previous studies by March-Leuba and Rey (1993) have shown that changes in fuel time constant have both stabilising and destabilising effects. They found out that the stabilising effect is due to the inherent filtering of the oscillations having frequency greater than 0.1 Hz and the destabilising effect is due to the phase delay to the feed back. For the low frequency thermohydraulic oscillations observed in the AHWR, the phase delay is more significant to destabilise the reactor for an increase in fuel time constant than the filtering effect as observed in the present case.

Effect of radial Power distribution and inlet orificing on the out-of-phase instability : Figure 5 shows the effect of interaction between two subcores having different RPF and inlet orifice pressure loss coefficients on the threshold of out-of-phase mode oscillation. In the analysis, one of the subcores is always considered common and it contains channels of channel Type-3 (i.e. RPF = 1.231 and $K_{\alpha}=0.0$) and the other subcore is considered to be varied with same number of channels having different RPF and inlet orificing coefficient in such a way that its outlet quality almost remains the same as that for the companion subcore. It can be observed that by reducing the RPF and increasing the inlet orifice coefficient in one subcore greatly stabilises the out-of-phase mode of oscillation occurring in the other subcore having channels with higher RPF thereby enhancing the stability of the system.

Study of out-of-phase oscillations using the coupled multipoint kinetics model

As mentioned before, during an out-of-phase mode oscillation neutron diffusion from channel to channel due to variation of void may affect the stability. This effect has been predicted by the coupled multipoint kinetics model. The coupling coefficient which determines the degree of coupling between subcore to subcore because of neutron diffusion was determined and found to be about 3.5 mk considering the reactor core to be divided in to two equal subcores.

Comparison of stability maps between the coupled multipoint kinetics model and modal point kinetics model : In the recent past, the out-of-phase instability is explained as a phenomenon in which the neutron higher modes are excited by the thermal hydraulic feed back effects. The higher modes are all subcritical, which could result in out-of-

phase oscillations depending on the subcriticality of the harmonic mode and the void reactivity feed back. A derivation of the modal point kinetics model governing the higher harmonic modes of oscillations are given in reference (Hashimoto, 1997). It is of interest to compare the stability maps between the coupled multipoint kinetics model and the modal point kinetics model for the out-of-phase oscillations for the AHWR. For this purpose, the subcriticality (i.e. the eigenvalue separation between the fundamental and first harmonic mode) was considered to be twice the coupling coefficient based on the theory of Nishina and Tokashiki (1996). The results are shown in Fig. 6 and it is seen that both the models give practically the same threshold power for stability for the above condition. In fact, the coupling coefficient is an indication of the degree of subcriticality during an out-of-phase instability. The coupled multipoint kinetics model has better advantage over the modal point kinetics model in analysing the out-of-phase instability. Because, when analysing the stability behaviour of a reactor with multiple channels or subcores with different flux distributions, the coupled multipoint kinetics model can handle the problem by considering suitable coupling coefficients. On the otherhand, the modal point kinetics model assign a single value of subcriticality to all the subcores irrespective of their flux distributions.

Decay ratio maps for the AHWR

The contour lines of constant decay ratio for in-phase mode of oscillation at different thermal powers and inlet subcooling are shown in Fig. 7. Also, the constant feed water temperature lines alongwith the constant channel exit quality lines are shown in the same figures. From these maps it is clear that the reactor can have sufficient stability margin with DR less than 0.4 with core inlet subcooling of less than 10 K for operating power of 750 MWth. Also, it is observed that the Type I instability occurs in the reactor at channel exit quality of less than 10%. With increase in channel exit quality at a particular subcooling, the DR increases. Increase of channel inlet subcooling at a particular power also increases the DR. Similar behaviour is also observed for a decrease of feed water temperature at a constant power. With increase in feed water temperature, the subcooling increases, which has destabilising effect since the DR increases.

Conclusions

Analysis was carried out to study the nuclear-coupled density-wave instability behaviour of the AHWR. The following insights are obtained from this study:

- (1) Both in-phase and out-of-phase thermohydraulic instability may occur in the AHWR channels at 7 MPa operating pressure depending on the channel power and core inlet subcooling. The frequency of oscillation of Type-II thermohydraulic instability is larger than that for Type-I instability. The difference of threshold power between in-phase and out-of-phase oscillations for Type-II thermohydraulic instability is larger than that for Type-I instability.
- (2) With increase in negative void reactivity coefficient (C_a), the threshold power for stability increases for Type-II and decreases for Type-I instabilities. The stability of the reactor increases with an increase in negative C_a .
- (3) With increase in fuel time constant (τ_f) the threshold power for stability is reduced for Type-II and increases for Type-I instabilities. The stability of the reactor is reduced with increase in fuel time constant.
- (5) The stability of the reactor increases by reducing the RPF and increasing the inlet orifice loss coefficient of the companion subcore when two subcores interact with each other.
- (6) The coupled multipoint kinetics model predicts the same threshold power for stability as that of a modal point kinetics model if the coupling coefficient is half the eigen value separation between the fundamental and first harmonic mode.

(7) The DR increases with increase in channel exit quality, inlet subcooling and decrease in feed water temperature at a constant power. The reactor can have better stability margin for subcooling of less than 10 K.

Nomenclature

a_f	heat transfer area (m^2)
A	cross sectional area (m^2)
C_{∞}	void reactivity coefficient ($\Delta k/k/\Delta\gamma$)
C_D	Doppler coefficient ($\Delta k/k/\Delta T$)
$C_m(t)$	delayed neutron precursor concentration of group m
C_p	specific heat ($J/kg-K$)
D	hydraulic diameter (m)
f	Darcy friction factor
g	acceleration due to gravity (m/s^2)
h	enthalpy (J/kg)
h_{fg}	latent heat of vapourisation (J/kg)
h_i	heat transfer coefficient (W/m^2K)
$k(t)$	effective multiplication factor
K	loss coefficient
l	prompt neutron life time (s)
L	length of section (m)
m_f	mass of fuel rods (kg)
$n(t)$	neutron density
N_{ps}	$(\psi/wh_p) \quad I$
N_{sa}	$(\Delta h_{sa}/h_p)$
p	pressure (N/m^2)
q_h	heat applied/unit volume of coolant (W/m^3)
s	stability parameter
t	time (s)
T	temperature (K)
v	specific volume (m^3/kg)
v_g, v_l, v_v	(m^3/kg)
w	mass flow rate (kg/s)
z	axial distance (m)

Greek Symbols

α	coupling coefficient
β	delayed neutron fraction
σ	volumetric thermal expansion coefficient (K^{-1})
λ	decay constant of delayed neutron of group m
ψ	power (W)
τ	fluid residence time (s)
τ_f	fuel time constant (s)
Δ	difference
ρ	density (kg/m^3)
γ	void fraction

Subscripts

av	average
c	core
ch	channel
d	downcomer
f	liquid
g	vapour
H	header
in	inlet of section
k	loss due to restriction
sat	saturation
SD	steam drum
sp	single phase
ss	steady state
ss,av	average steady state
sub	subcooling
t	total
tp	two-phase

References

1. Araya, F., Yoshida, K., Hirano, M., Yabushita, Y., 1991. Analysis of neutron flux oscillation event at LaSalle 2. Nucl. Technol. 93, 82-90.
2. Baroczy, C.J., 1966. A systematic correlation for two-phase pressure drop. Chem. Eng. Prog. 62, 232-249.
3. Gialdi, E., Grifoni, S., Parmeggiani, C., Tricoli, C., 1985. Core stability in operating BWR: operational experiences. Prog. Nucl. Energy. 15, 447-459.
4. Hashimoto, K., 1993. Linear modal analysis of out-of-phase instability in Boiling Water Reactor cores. Ann. Nucl. Energy. 20, 789-797.
5. Hashimoto, K., Hotta, A., Takeda, T., 1997. Neutronic model for modal multichannel analysis of out-of-phase instability in BWR cores", Ann. Nucl. Energy, vol. 24, 99-111.
6. March-Leuba, J., 1990. LAPUR benchmark against in-phase and out-of-phase stability tests. NUREG/CR-5605, ORNL/TM-11621.
7. March-Leuba, J., Blakeman, E.D., 1991. A mechanism for out-of-phase instabilities in Boiling Water Reactors, Nucl. Sci. Eng. 107, 173-179.
8. March-Leuba, J., Rey, J.M., 1993. Coupled thermohydraulic-neutronic instabilities in boiling water reactors: a review of the state-of-the-art, Nucl. Eng. Des., vol. 145, 97-111.
9. Muto, S., Yokomizo, Y., Fukahori, T., Ebata, S., 1990. Space dependent analysis of BWR core nuclear thermal hydraulic instability and thermal margin. Nucl. Eng. Des. 120, 227-239.
10. Nayak, A.K., Vijayan, P.K., Saha, D., Venkat Raj, V., Aritomi, M., 1998. Linear analysis of thermohydraulic instabilities of the Advanced Heavy Water Reactor (AHWR). J. Nucl. Sci. Technol. 35, 768-778.
11. Nayak, P.K., Vijayan, D., Saha, V., Venkat Raj and M. Aritomi, 2000. Analytical Study of Nuclear-coupled Density-wave Instability in a Natural Circulation Pressure Tube Type Boiling Water Reactor, Nucl. Eng. Des., Vol. 195, 27-44.
12. Nishina, K., Tokashiki, M., 1996. Verification of more general correspondence between the eigenvalue separation and coupling coefficient. Prog. Nucl. Energy, 30, 277-286.
13. Rao, Y.F., Fukuda, K., Kaneshima, R., 1995. Analytical study of coupled neutronic and thermohydraulic instabilities in a boiling channel. Nucl. Eng. Des. 154, 133-144.
14. Takigawa, Y., Takeuchi, Y., Tsunoyama, S., Ebata, S., Chan, K.C., Tricoli, C., 1987. Coarse limit cycle analysis with three-dimensional transient code TOSDYN-2. Nucl. Technol. 79, 210-218.
15. Takeuchi, Y., Takigawa, Y., Uematsu, H., Ebata, S., Shaung, J.C., Shiralkar, B.S., 1994. TRAGG transient analysis code - three-dimensional kinetics model implementation and application for space dependent analysis. Nucl. Technol. 105, 162-183.
16. Uehiro, M., Rao, Y.F., Fukuda, K., 1996. Linear stability analysis on instabilities of in-phase and out-of-phase modes in Boiling Water Reactors. J. Nucl. Sci. Technol. 33, 628-635.
17. US NRC: Augmented Inspection Team (AIT) report, Report no. 50-373/88008, 1988.
18. Van Bragt, D.D.B., Van der Hagen, T.H.J.J., 1998. Stability of natural circulation Boiling Water Reactors: part II - parametric study of coupled neutronic-thermohydraulic stability. Nucl. Technol. 121, 52-62.
19. Van der Hagen, T.H.J.J., 1988. Experimental and theoretical evidence for a short effective fuel time constant in a Boiling Water Reactor. Nucl. Technol. 83, 171-181.

This paper received the Best Paper award in the INS Annual Conference on 'Power from Thorium: Status, Strategies and Directions' held during June 1-2, 2000 at BARC Training School Hostel, Anushaktinagar, Mumbai.

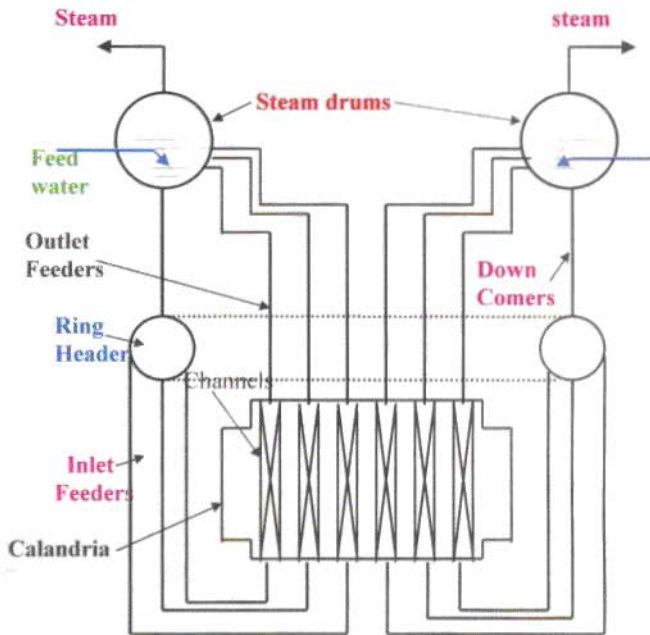


Fig. 1 Schema of AHWR PHT System

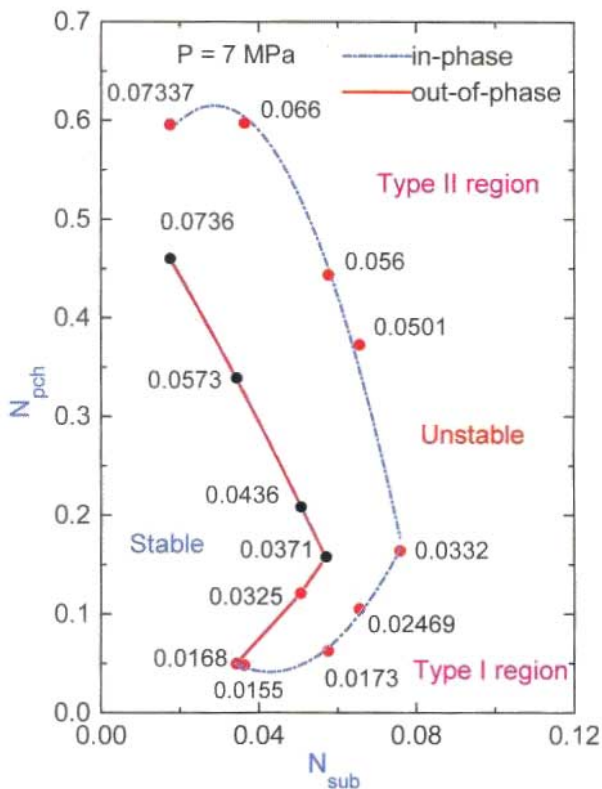


Fig. 2 In-phase and out-of-phase thermohydraulic stability boundary in boiling channels of the AHWR

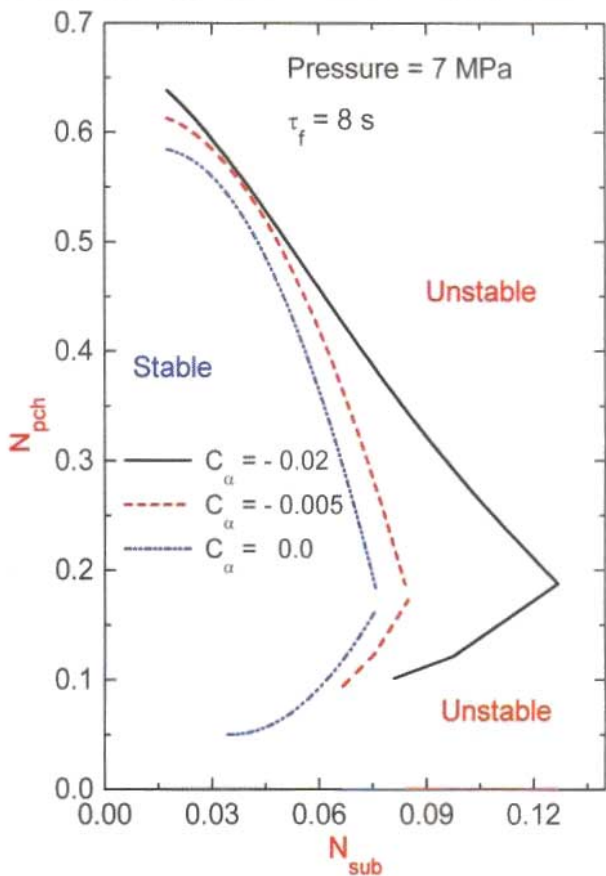


Fig. 3 Effect of void reactivity coefficient on stability

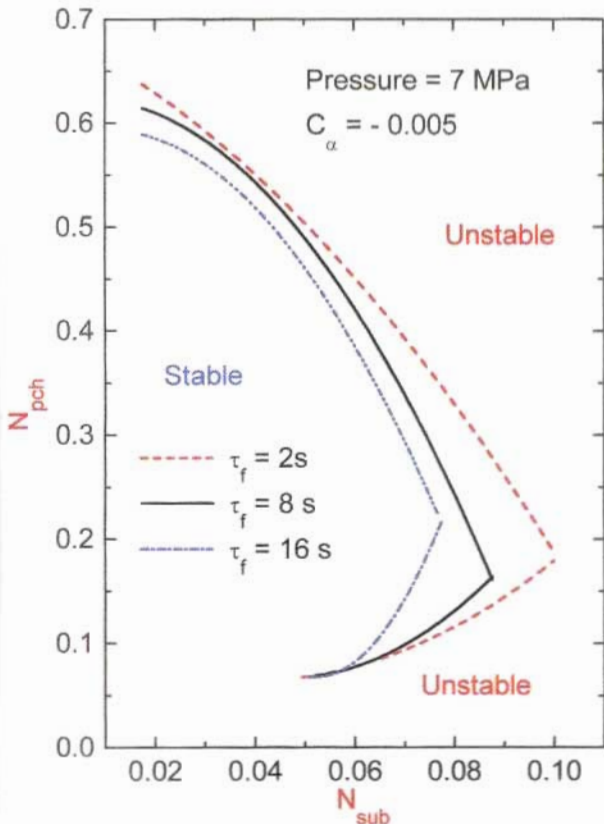


Fig. 4 Effect of fuel time constant on the stability

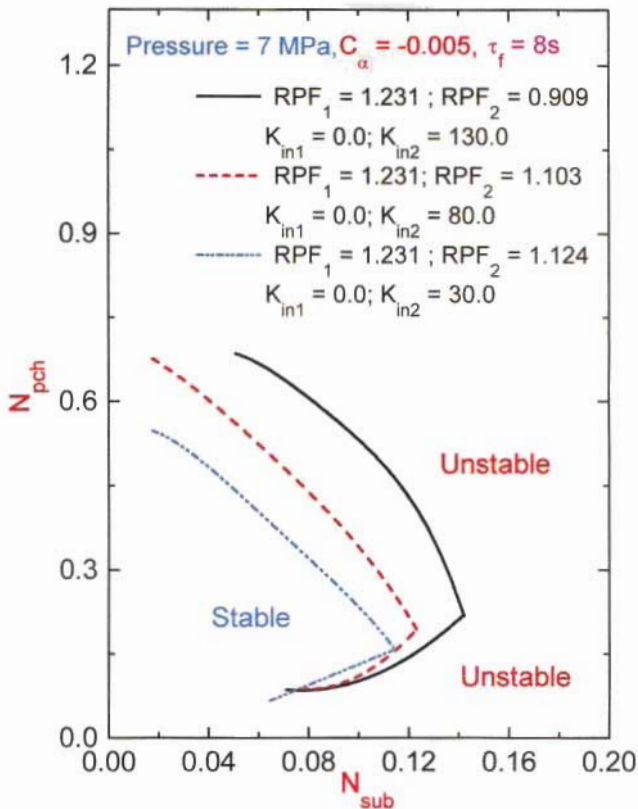


Fig. 5 Effect of radial power factor on stability of out-of-phase mode of oscillation

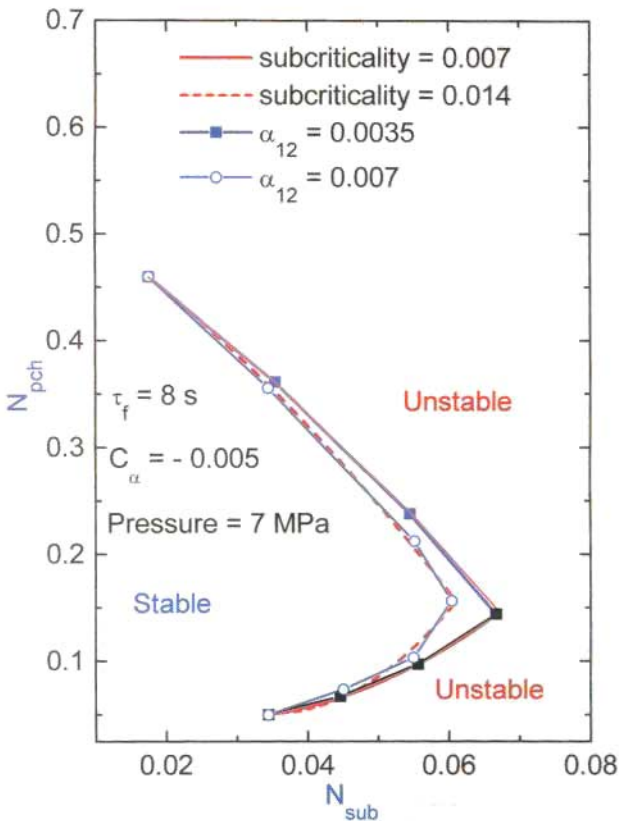


Fig. 6 Comparison of stability maps between coupled multipoint kinetics model and modal point kinetics model for out-of-phase mode of oscillation

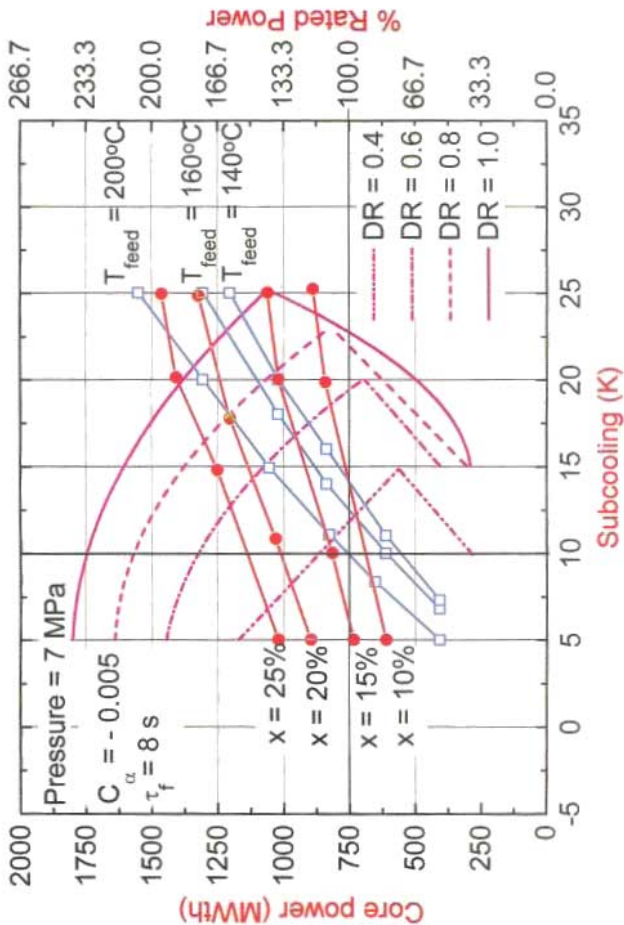


Fig. 7 Decay ratio map of AHWR for in-phase mode of oscillation

About the authors ...

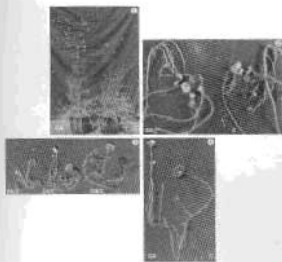
Dr. A.K. Nayak joined the 33rd batch of BARC Training School after graduating in Mechanical Engineering from Regional Engineering College, Rourkela. He obtained his M. Tech from Regional Engineering College, Warangal. Subsequently, he also obtained his Doctorate in Nuclear Engineering from Tokyo Institute of Technology, Tokyo. His current field of interests are single-phase and two-phase natural circulation, thermohydraulic and coupled neutronic-thermohydraulic stability of natural circulation BWRs, spray condensation, gravity separation of steam and water in natural circulation steam drums, scaling of natural circulation systems, etc.



Dr. P.K. Vijayan joined the 20th batch of BARC Training School after graduating in Chemical Engineering from the University of Calicut. He obtained his Ph.D. from I.I.T. Mumbai for his work on natural circulation in a figure-of-eight loop relevant to PHWRs. He has worked in GRS, Munich, for a year on the simulation of natural circulation systems. He has established himself an expert in the area of nuclear reactor thermalhydraulics. Dr. Vijayan's work on single-phase natural circulation loops is frequently cited by researchers as a significant contribution. His current research interests include stability of two-phase natural circulation, scaling of nuclear reactor systems and setting up thermal hydraulic facilities related to AHWR and PHWRs.



Mr D. Saba joined the 15th batch of BARC Training School after graduating in Mechanical Engineering from the University of Calcutta. Subsequently, he obtained his Master's degree in Mechanical Engineering from the same university. Over the period, he has established himself as an expert in the area of thermalhydraulics which plays a key role in the design as well as safe and efficient operation of nuclear power plants. Right from its inception, Mr Saba is deeply involved in the design and development of the Advanced Heavy Water Reactor. He has made exemplary contribution towards a number of international programmes. Recently, he led an international group on pressure drop relationships constituted by IAEA. He worked in Kernforschungszentrum, Karlsruhe (KfK) on reactor safety. At present, he is designated as Head, Thermal Hydraulics Section, RED.



1. Pre-bloom GA, ($10^{-6}M$) treated plants of *Coriopsis tinctoria* at 40 days, showing early flowering and increased flower numbers.
2. GA-induced changes in flower colour in different narrow leaved polypetal cultivars of *Portulaca grandiflora*. *P. grandiflora* cultivars Narrow-Leaf Dull White Polypetal, showing GA-induced Crimson Red and Mosaic flower colours (left side) compared to Dull-White right side control plants.
3. GA-induced change in flower colour in different narrow leaved polypetal cultivars of *Portulaca grandiflora*. The varieties from left to right are Pink, Mosaic and Crimson red, wherein left branches were treated with GA, ($10^{-6}M$), while right side branches sprayed with water, served as control.
4. GA, induced changes in the flower & size vis-a-vis internodal length in *Portulaca grandiflora* cv NL-CR-PyP. Closer view of the plants from the middle cup (GA/C), showing elongated internodes vis-a-vis white flowers on the treated left branch.



Edited and Published by Dr. Vijai Kumar, Head, Library & Information Services Division
 Bhabha Atomic Research Centre, Trombay, Mumbai 400 085, INDIA

Editorial Management : T.C.Balan. Computer graphics & layout : P.A.S. Warriyar. (For private circulation)

Available at URL: <http://www.barc.ernet.in>